SANDIA REPORT

SAND2015-7401
Unlimited Release
Printed August 2015

Analysis of Cavern and Well Stability at the West Hackberry SPR Site Using a Full-Dome Model

Steven R. Sobolik
Geomechanics Department
Sandia National Laboratories
P.O. Box 5800
Albuquerque, New Mexico 87185-0751

Prepared by
Sandia National Laboratories
Albuquerque, New Mexico 87185 and Livermore, California 94550

Sandia National Laboratories is a multi-program laboratory managed and operated by Sandia Corporation, a wholly owned subsidiary of Lockheed Martin Corporation, for the U.S. Department of Energy's National Nuclear Security Administration under contract DE-AC04-94AL85000.

Issued by Sandia National Laboratories, operated for the United States Department of Energy by Sandia Corporation.

Available to DOE and DOE contractors from
U.S. Department of Energy
Office of Scientific and Technical Information
P.O. Box 62
Oak Ridge, TN 37831

Telephone: (865) 576-8401
Facsimile: (865) 576-5728
E-Mail: reports@adonis.osti.gov
Online ordering: http://www.osti.gov/bridge

Available to the public from
U.S. Department of Commerce
National Technical Information Service
5285 Port Royal Rd.
Springfield, VA 22161

Telephone: (800) 553-6847
Facsimile: (703) 605-6900
E-Mail: orders@ntis.fedworld.gov
Online order: http://www.ntis.gov/help/ordermethods.asp?loc=7-4-0#online

SAND2015-7401
Unlimited Release
Printed September 2015

Analysis of Cavern and Well Stability at the West Hackberry SPR Site Using a Full-Dome Model

Steven R. Sobolik
Geomechanics Department
Sandia National Laboratories
P.O. Box 5800
Albuquerque, New Mexico 87185-0751

ABSTRACT

This report presents computational analyses that simulate the structural response of caverns at the Strategic Petroleum Reserve (SPR) West Hackberry site. The cavern field comprises 22 caverns. Five caverns (6, 7, 8, 9, 11) were acquired from industry and have unusual shapes and a history dating back to 1946. The other 17 caverns (101-117) were leached according to SPR standards in the mid-1980s and have tall cylindrical shapes. The history of the caverns and their shapes are simulated in a three-dimensional geomechanics model of the site that predicts deformations, strains, and stresses. Future leaching scenarios corresponding to oil drawdowns using fresh water are also simulated by increasing the volume of the caverns. Cavern pressures are varied in the model to capture operational practices in the field. The results of the finite element model are interpreted to provide information on the current and future status of subsidence, well integrity, and cavern stability.

The most significant results in this report are relevant to Cavern 6. The cavern is shaped like a bowl with a large ceiling span and is in close proximity to Cavern 9. The analyses predict tensile stresses at the edge of the ceiling during repressurization of Cavern 6 following workover conditions. During a workover the cavern is at low pressure to service a well. The wellhead pressures are atmospheric. When the workover is complete, the cavern is repressurized. The resulting elastic stresses are sufficient to cause tension around the edge of the large ceiling span. With time, these stresses relax to a compressive state because of salt creep. However, the potential for salt fracture and propagation exists, particularly towards Cavern 9. With only 200 feet of salt between the caverns, the operational consequences must be examined if the two caverns become connected. A critical time may be during a workover of Cavern 9 in part because of the operational vulnerabilities, but also because dilatant damage is predicted under the ledge that forms the lower lobe in the cavern.

The remaining caverns have no significant issues regarding cavern stability and may be safely enlarged during subsequent oil drawdowns. Predicted well strains and subsidence are significant and consequently future remedial actions may be necessary. These predicted well strains certainly suggest appropriate monitoring through a well-logging program. Subsidence is currently being monitored.

ACKNOWLEDGEMENTS

The author would like to thank Byoung-Yoon Park, Lupe Arguello, Moo Lee, and David Borns for their review and support of this work.

TABLE OF CONTENTS

LIST OF FIGURES

LIST OF TABLES

EXECUTIVE SUMMARY

This report presents computational analyses that simulate the structural response of caverns at the Strategic Petroleum Reserve (SPR) West Hackberry site. The cavern field comprises 22 caverns. These analyses evaluate the geomechanical behavior of the caverns at the West Hackberry SPR site for the current condition of the caverns and their wellbores, the effect of the caverns on surface facilities, and for potential enlargement in the form of drawdowns. The analyses examined the overall performance of the West Hackberry site by evaluating surface subsidence, horizontal surface strains, and axial well strains. Finally, the analyses evaluated the possibility of nonlinear dilatancy behavior of the West Hackberry salt, and its possible ramifications on cavern performance. The following conclusions were obtained from the results of the analyses:

- The transition from JAS3D to Adagio has been completed. The property set used for the M-D model for West Hackberry was reexamined in comparisons between measured and predicted surface subsidence and cavern closure, with the result that higher values of the secondary creep coefficient were required to better match predictions to results.
- The new predictions of surface subsidence compared very well to the historical measured data.
- The new predictions of cavern volume closure compared reasonably well to the cavern volume values derived from cavern pressure data using the CAVEMAN software. The predicted rates of cavern closure during steady state closure (i.e., between workovers) tend to be less than the rates supplied through CAVEMAN, but the predicted change of volume during workovers usually made up the difference. The procedure used by CAVEMAN to calculate cavern volume as a function of wellhead pressure will be examined and compared to the calculation of cavern volume from Adagio will determine if the two processes are consistent; any inconsistencies or potential changes in material creep properties will then be addressed.
- The safety parameters used to evaluate cavern and wellbore integrity (salt dilatant/tension stresses, wellbore axial strain) indicate that caverns WH-6, 8, and 9 have ongoing integrity concerns that have been addressed (e.g., the removal of oil from WH-6), or can be addressed with limits on caverns operations and drawdowns. Some other caverns, including WH-110 and 113, are predicted to experience very localized dilatant stress points at the bottom of the caverns; these points may be merely due to a stress concentration resulting from the mesh construction, or may be indicative of a true condition that due to its location may be of minimal consequence.
- Based on a preliminary assessment of the mechanical behavior of the caverns through five drawdown cycles, there is not expected to be any significant downgrade to the number of available drawdowns for the WH caverns compared to the numbers reported in 2014 (Sobolik et al., 2014), and in fact many of the Phase 2 caverns will probably see an increase in their number of available drawdowns.
- In addition to the new analyses conducted for this report, previous letter reports of analyses concerning WH caverns 6, 8, and 9 have been included in this report for completeness.
- A follow-up report to this work is planned for 2016. The follow-up report will include further examination of the results of these calculations as they pertain to three items: 1) a new assessment of the number of available drawdowns for all the WH caverns; 2) an evaluation

of the methods used to calculate cavern volume closure in both CAVEMAN and Adagio to make sure the methods are reasonably consistent and can be used for effective comparison; and 3) a further evaluation of the plastic strain experienced by the casing materials similar to that performed by Park (2013 & 2014) for the Big Hill site, to provide a more complete understanding of the effect of creep on the WH boreholes. The results in the follow-up report will also be used as input to the West Hackberry well integrity grading matrix used to prioritze wellbore remediation (Roberts et al., 2015).

This page has been intentionally left blank.

1. INTRODUCTION

1.1 BACKGROUND

The U.S. Strategic Petroleum Reserve (SPR), operated by the U.S. Department of Energy (DOE), stores crude oil in solution-mined caverns in the salt dome formations of the Gulf Coast. There are a total of 62 caverns located at four different sites in Texas (Bryan Mound and Big Hill) and Louisiana (Bayou Choctaw and West Hackberry), as shown in Figure 1. Each cavern is constructed and then operated using casings inserted through a wellbore or wellbores that are lined with steel casings cemented in place from the surface to near the top of the cavern.

The SPR sites, as well as most other oil and natural gas storage sites in salt domes along the Gulf Coast, are varied in terms of cavern structure and layout. At West Hackberry (WH), the cavern field includes 22 caverns. Five caverns (6, 7, 8, 9, and 11 – known as the Phase 1 Caverns) were created as early as 1946 and were used for brine storage before the SPR took ownership of them in 1981. Because the Phase 1 caverns were created for brine production, they were built with no particular interest in cavern integrity, resulting in caverns of unusual shapes. The other 17 caverns (101-117, the Phase 2 caverns) were leached according to SPR standards in the mid-1980s and have tall cylindrical shapes.

Since the SPR took ownership of the Phase 1 caverns in 1981, several finite element analyses have been performed to assess the long-term performance and stability of the caverns, each with increasing levels of constitutive model development and technical complexity. Preece and Foley (1984) conducted two-dimensional axisymmetric idealizations and each cavern was simulated independently of the others. The failure function was based on accumulated strain as a function of pressure. While the analyses at that time predicted stability, cavern workover conditions were not simulated. Ehgartner and Sobolik (2002) used a 30-degree wedge to simulate a symmetric 19-cavern field geometry. The caverns in that simulation were modeled as true cylinders. Sobolik and Ehgartner (2009a) conducted a substantially upgraded computational analysis of West Hackberry by using a three-dimensional computational domain that included specific caverns – the Phase 1 caverns plus Caverns 101, 103, 105, 108, 109, 110, and 117 – and the eastern half of the salt dome. The Phase 1 caverns were meshed with geometries based on sonar data measurements, whereas the Phase 2 caverns were modeled as frustums of approximately equal volume, radii and height. For the 2009 analyses, the entire lives of the caverns (construction, brine or oil storage, operating and workover pressures) were modeled individually for each cavern, with average operating pressures and idealized five-year workover schedules applied to each cavern on a rotating basis. Also, the sandstone that surrounds the salt dome was included in the 2009 analysis, providing a realistic far-field stress boundary condition. All of the aforementioned analyses modeled the salt creep behavior using the power law creep model, a simplified creep model that calculates the secondary steady state creep mechanism, a subset of the more complete multi-mechanism deformation (M-D) model of salt creep (Munson & Dawson, 1979, 1982, & 1984). The implementation of the power law creep model included the use of a reduced elastic modulus to simulate the transient response of the salt to pressure changes. The resulting simulations provided satisfactory predictions of long-term creep

behavior, but not of transient response to pressure changes. Beginning in 2010, the 2009 model converted to using an improved implementation of the complete M-D model (Sobolik et al., 2010). This model was then used with the half-dome computational mesh to analyze specific cavern operation concerns regarding West Hackberry Caverns 6, 8, and 9 (Sobolik and Ehgartner, 2012; Sobolik, 2013a; Sobolik and Lord, 2015). (These analyses have been transmitted to the US DOE, and are summarized in Chapter 6 of this report.)

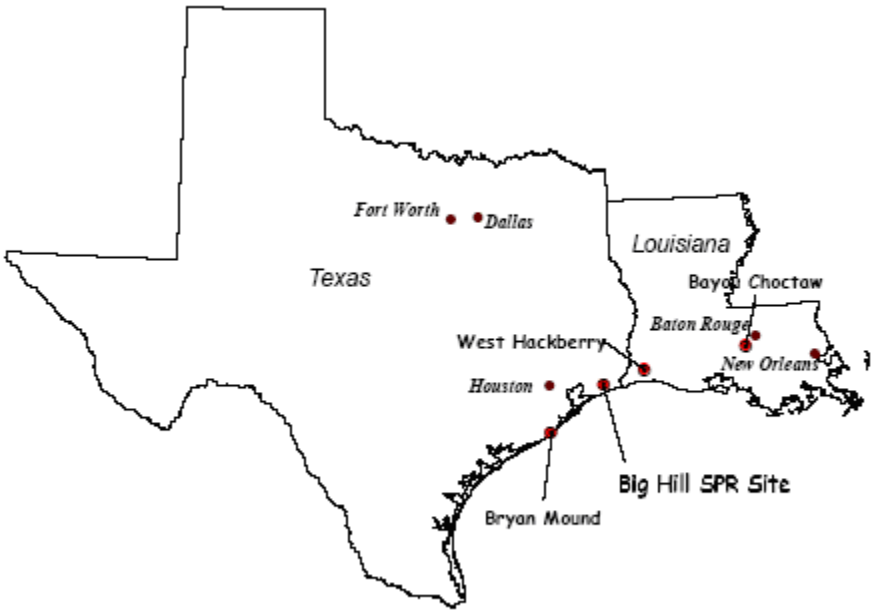

Figure 1: Location of SPR sites.

1.2 OBJECTIVE

This report presents computational analyses that simulate the structural response of caverns at the Strategic Petroleum Reserve (SPR) West Hackberry site. The history of the caverns and their shapes are simulated in a three-dimensional geomechanics model of the site that predicts deformations, strains, and stresses. Future leaching scenarios corresponding to oil drawdowns using fresh water are also simulated by increasing the volume of the caverns. Cavern pressures are varied in the model to capture operational practices in the field. The results of the finite element model are interpreted to provide information on the current and future status of subsidence, well integrity, and cavern stability.

There are several important advances in this new computational simulation of the West Hackberry geomechanical site:

Advancement #1: Transition to Adagio: JAS3D (Blanford et al., 2001), which is a three dimensional iterative solid mechanics code, has been used for the structural analyses for the SPR system since the 1990s. JAS3D is no longer supported by Sandia, and has been replaced by Adagio (SIERRA Team, 2010, 2011; Arguello et al., 2012). Adagio is written for parallel

computing environments, and its solvers allow for scalable solutions of very large problems. The Adagio structure is different from JAS3D. Adagio uses the SIERRA Framework, which allows for coupling with other SIERRA mechanics codes. The existing JAS3D input decks and user subroutines for the SPR works have been converted for use with Adagio. A simulation has been run with Adagio to replicate the simulation using the half-dome model and the M-D creep constitutive model with JAS3D (Sobolik et al., 2010; Sobolik & Ehgartner, 2012); the new results will be compared with the previous JAS3D predictions for purposes of verification.

Advancement #2: Computational mesh enhancement: The West Hackberry model computational mesh has been enhanced to include the entire salt dome, all SPR caverns meshed to axisymmetric geometries based on sonar measurements, and for caverns 6 and 9, leaching layers based on results from the cavern leaching prediction tool SANSMIC (Weber et al., 2014).

Advancement #3: A new baseline set of simulations has been run using the new computational mesh. One important new feature is the use of historical cavern wellhead pressures to develop the evolution of cavern behavior to the present, i.e., late 2014. The historic pressures have been utilized in two ways: one, the actual pressures have been input into the calculations; and two, the actual workover and MIT history has been used, but average operational pressures are used to allow the code to calculate cavern closure based on the amount of fluid at the beginning of the cycle. Other new features of these analyses include: full cavern volume closure histories based on back calculation from wellbore pressures by the cavern pressure monitoring code CAVEMAN (Ballard & Ehgartner, 2000); updated M-D creep parameters based on field cavern closure and surface subsidence data; and a more accurate assessment of available drawdowns for the Phase 2 caverns, based on representation of the caverns in the computational mesh with sonar-based shapes.

Prior to the completion of the new full-dome simulations, continuing issues regarding West Hackberry caverns 6, 8, and 9 required additional analysis with the half-dome model. Because of the cavern geometries and proximity of WH caverns 6, 8, and 9, and the geomechanical issues that arise from them, several workover scenarios were simulated to provide guidance for acceptable limits on workover duration and execution. A chapter of this report is dedicated to documenting these analyses and the resulting recommendations to DOE.

1.3 REPORT ORGANIZATION

This report is organized in the following fashion: Section 2 gives a brief description of the West Hackberry cavern site to show the diversity of cavern geometries. Section 3 describes the half-dome analysis model, and the transition from JAS3D to Adagio. Section 4 describes the full-dome analysis model, including the cavern designs, stratigraphy, material models, material properties, and damage criteria used for the analyses. Section 5 shows the results of the calculations, and identifies issues regarding the validation of the results and potential failure modes for the salt and the casings. Section 6 documents the previous work analyzing the interaction of Caverns 6 and 9, and the recommendations for site operations activities regarding them. Section 7 summarizes the results, and provides concluding remarks. The report concludes with a list of cited references in Section 8.

2. SITE DESCRIPTION

West Hackberry is located in the extreme southwestern corner of Louisiana, some 15 miles from the Louisiana/Texas border to the west and the Gulf of Mexico to the south (Munson, 2006). The geological characteristics related to the West Hackberry site were first described by Whiting (1980). Magorian et al. (1991) utilized the earlier work, together with additional information on dome geology, surrounding stratigraphy, and relevant environmental information, to update the dome characterization. Conversion of the two-dimensional databases from these earlier characterization reports formed the basis for the most recent reexamination by Rautman et al. (2004) using modern three-dimensional methods for representation of the dome and its surroundings. While major aspects of the dome, caprock and surrounding strata defined by the earlier characterizations remain unchanged, the updated three-dimensional models of Rautman et al. (2004) used more refined analysis of the data and produced models of the dome that differed slightly from the earlier models. The three-dimensional models also achieve a level of visualization clarity and graphical manipulation previously impossible.

The West Hackberry dome consists of the more-or-less typical geologic sequence of rocks. With increasing depth below the ground surface, initially there is roughly 1500 feet of soil and unconsolidated gravel, sand, and mud, followed by approximately 400 feet of caprock, consisting of anhydrite and carbonate (a conversion product of anhydrite). Generally, the upper portions of the caprock consist of the anhydrite conversion products of gypsum and dolomite, while the lower portion of the caprock is the initial anhydrite residue from the solution of the original domal material. The caprock is generally lens shaped with the thickest part of the lens over the central portion of the dome, tapering to thin edges toward the periphery of the dome; however, some portions of the caprock, even at the dome edge, are quite thick. In the updated model, the caprock even laps over the dome edge in several locations. The caprock is in contact with the top of the domal salt body. Beneath the caprock, the domal salt body extends to considerable depth, potentially to the original Louann bedded salt source.

Figure 2 shows a plan view of the West Hackberry site (Magorian et al., 1991) with contour lines defining the approximate location of the salt dome's interface with the caprock and surrounding sandstone. The approximate cavern locations are shown in the plan view. An updated geologic perspective of the salt dome and caprock is provided in Figure 3 (Rautman et al., 2004).

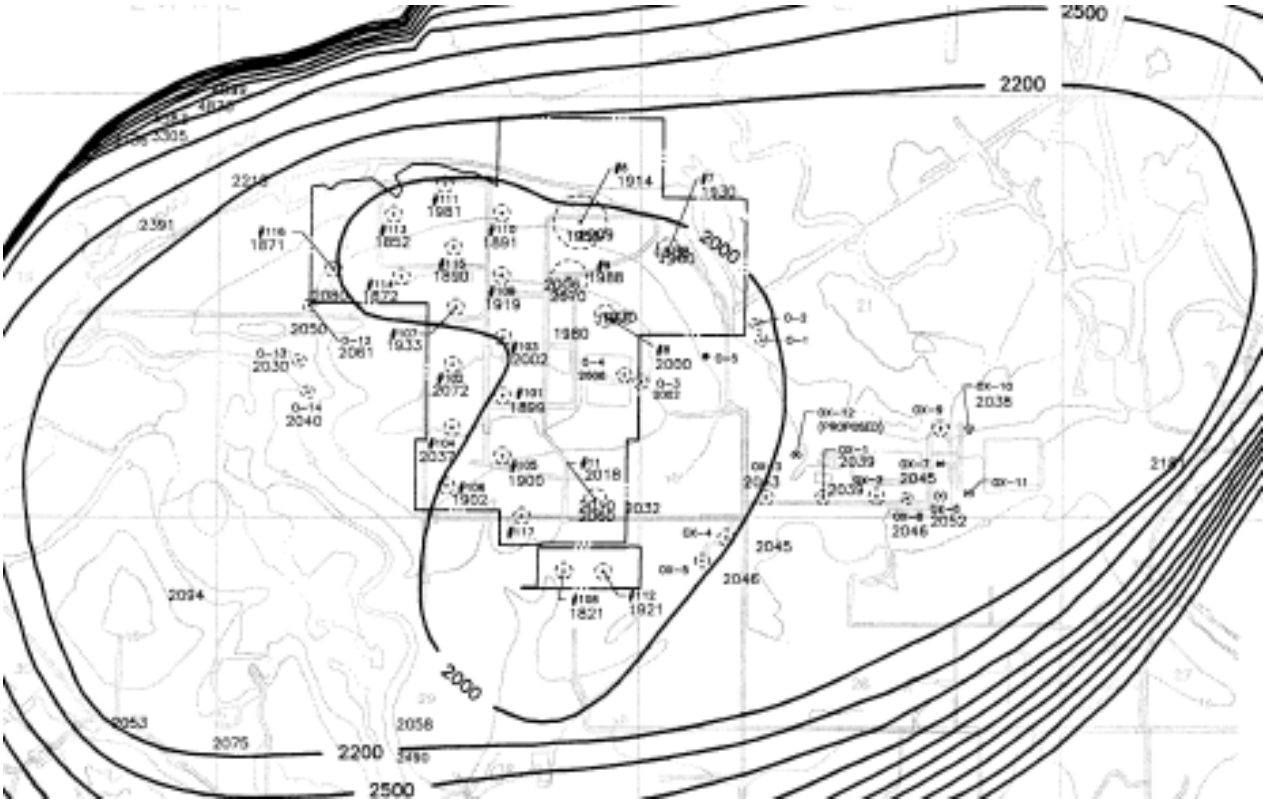

Figure 2: Plan view of the West Hackberry SPR site (Magorian et al., 1991).

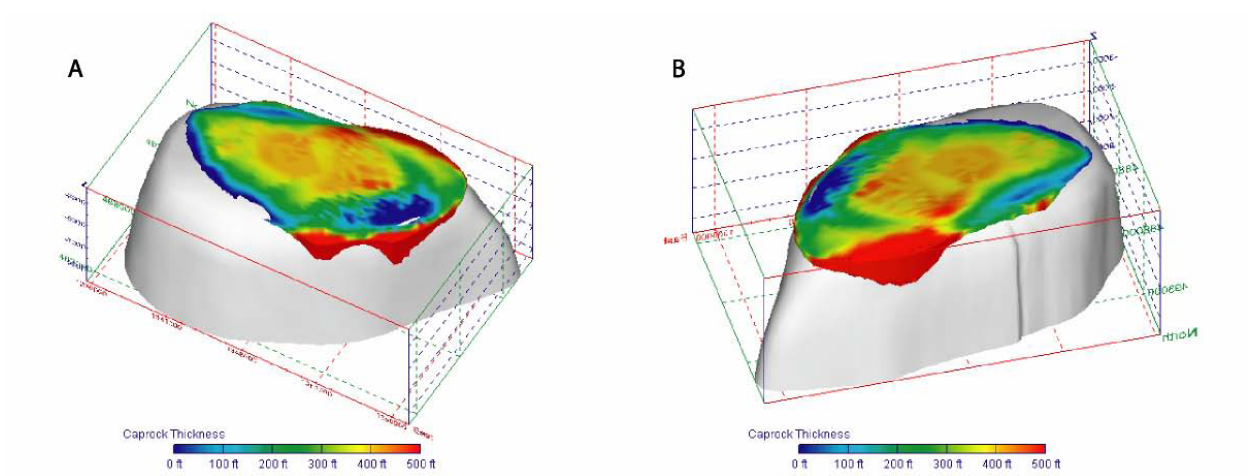

Figure 3: Perspective views of salt dome and caprock (Rautman et al., 2004)

Figure 4 shows the cavern layout at the West Hackberry site (Munson, 2006). Two major shear sections have been identified near the caverns; these extend along the entire distance of the caprock, and for an unknown distance into the salt. These shear zones are not included in the computational model presented in this report. Figure 5 shows cavern geometries based on sonar measurements obtained through 2007 (Rautman and Snider, 2007). Note the enlarged tops and asymmetries of the cavern shapes. In general, caverns in the SPR are intentionally shaped with

larger tops to accommodate future oil drawdowns where the bottom portions of the caverns are preferentially leached, and hence the overall cavern shape becomes more cylindrical, because of raw water injections to remove the oil. Salt properties also result in unpredictable cavern shapes as the insoluble content or dissolution rates of salt can vary spatially. This explains some of the asymmetries found in the cavern shapes. The Phase 1 caverns were acquired through purchase; these caverns have unusual shapes as they were not intentionally leached for product storage, but were used to produce brine. Clearly a variety of shapes are currently found in the SPR and this variety of cavern shapes will continue through future drawdowns.

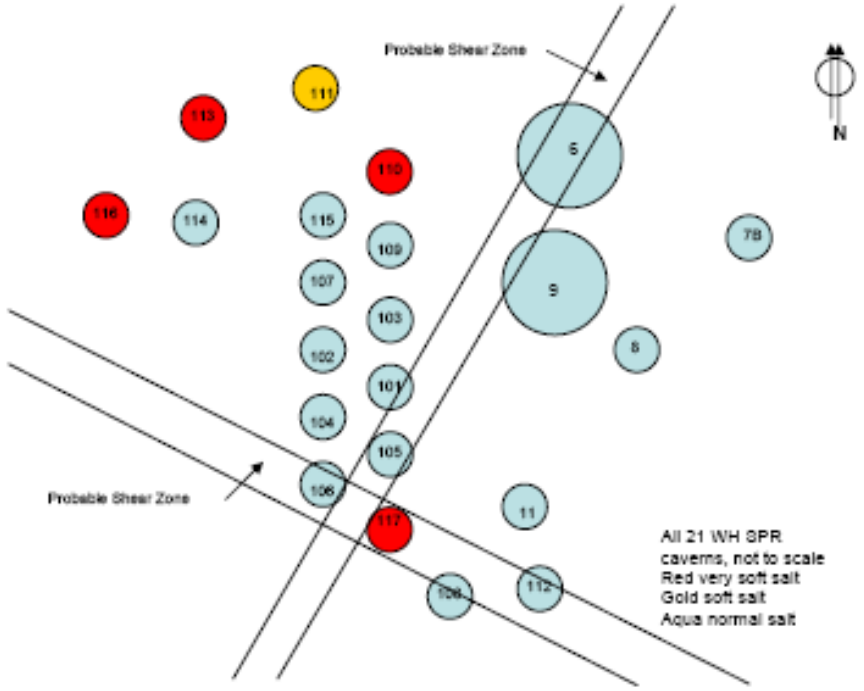

Figure 4. Schematic of the Location of the SPR Caverns at West Hackberry (Munson, 2006)

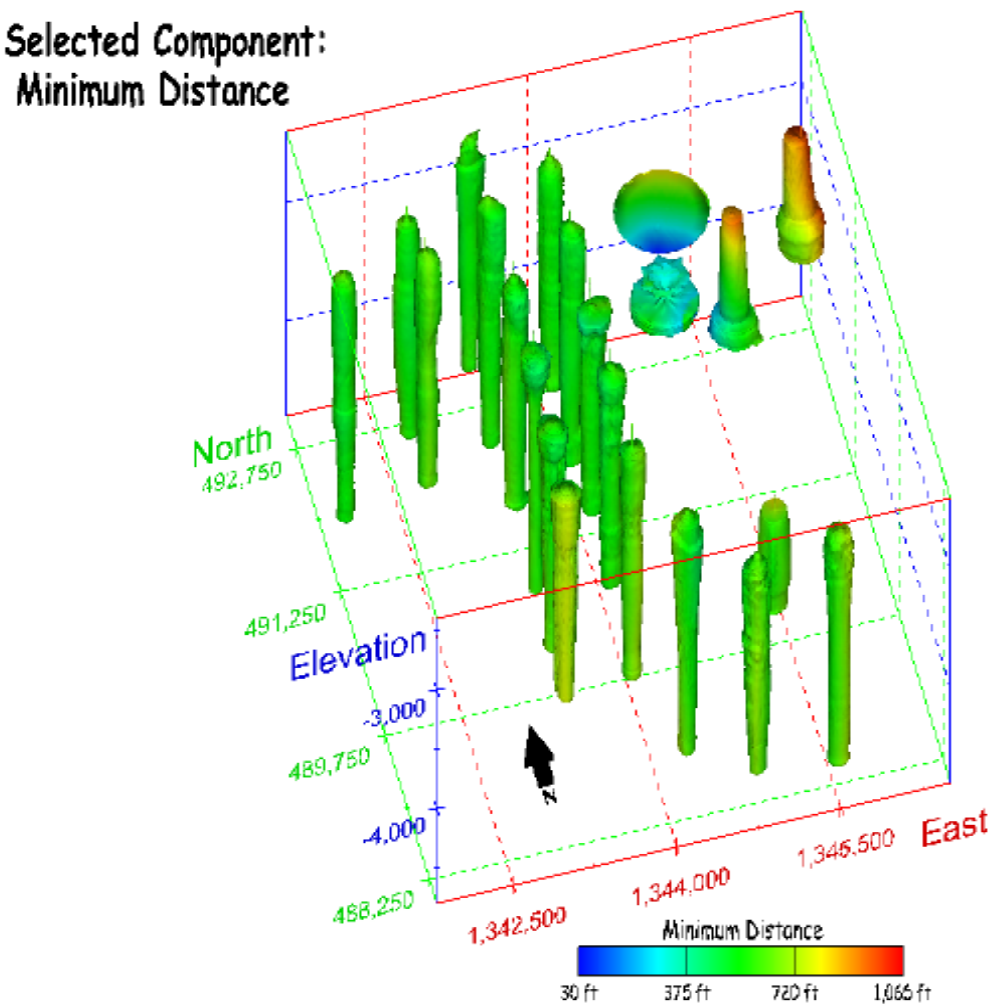

Figure 5. Visualization of the 22 oil-storage caverns at West Hackberry SPR site viewed from the south (Rautman and Snider, 2007).

3. CONVERSION FROM JAS3D TO ADAGIO

For many years, geomechanical analyses performed by Sandia utilized JAS3D, Version 2.0.F (Blanford et al., 2001), a three-dimensional finite element program developed by Sandia, designed to solve large quasi-static nonlinear mechanics problems. JAS3D is no longer supported by Sandia, and has been replaced by Adagio (SIERRA Team, 2010, 2011; Arguello et al., 2012). Adagio is written for parallel computing environments, and its solvers allow for scalable solutions of very large problems. The Adagio structure is different from JAS3D. Adagio uses the SIERRA Framework, which allows for coupling with other SIERRA mechanics codes. The existing JAS3D input decks and user subroutines for the SPR works have been converted for use with Adagio. A simulation has been run with Adagio to replicate the simulations using the half-dome model and the M-D creep constitutive model with JAS3D (Sobolik et al., 2010; Sobolik & Ehgartner, 2012). This section briefly describes the SIERRA solid mechanics code Adagio; the formulation of the M-D creep model; the West Hackberry half-dome model as used in several analyses (Sobolik and Ehgartner, 2012; Sobolik, 2013a; Sobolik and Lord, 2015); and new results obtained from Adagio that are compared with the previous JAS3D predictions for purposes of verification.

3.1 CODE DESCRIPTIONS

For many years, geomechanical analyses performed by Sandia utilized JAS3D, Version 2.0.F (Blanford et al., 2001), a three-dimensional finite element program developed by Sandia, designed to solve large quasi-static nonlinear mechanics problems. Several constitutive material models are incorporated into the program, including models that account for elasticity, viscoelasticity, several types of hardening plasticity, strain rate dependent behavior, damage, creep, and incompressibility. The continuum mechanics modeled by JAS3D are based on two fundamental governing equations. The kinematics are based on the conservation of momentum equation, which can be solved either for quasi-static or dynamic conditions (a quasi-static procedure was used for the SPR analyses). The stress-strain relationships are posed in terms of the conventional Cauchy stress. JAS3D has been ideal for simulations of processes occurring over many years, for computational meshes consisting of millions of elements, and for modeling salt behavior with either the power law creep model or the multi-mechanism deformation model. In addition, the capability of running JAS3D in parallel mode, allowing for the use of 32 CPU nodes for calculations, decreased CPU time substantially and allowed for parametric studies using large computational meshes.

The development of the SIERRA Mechanics code suite has been funded by the Department of Energy (DOE) Advanced Simulation and Computing (ASC) program for more than ten years (Edwards and Stewart, 2001). The goal is development of massively parallel multi-physics capabilities to support the Sandia engineering sciences mission. SIERRA Mechanics was designed and developed from its inception to run on the latest, most sophisticated, massively parallel computing hardware. It has the capability to span the hardware range from a single workstation to computer systems with thousands of processors. The foundation of SIERRA Mechanics is the SIERRA toolkit, which provides finite element application-code services such as: (1) mesh and field data management, both parallel and distributed; (2) transfer operators for

mapping field variables from one mechanics application to another; (3) a solution controller for code coupling; and (4) included third party libraries (e.g., solver libraries, communications package, etc.). The SIERRA Mechanics code suite is comprised of application codes that address specific physics regimes. The two SIERRA Mechanics codes that are used as the launching point for fully integrated Thermal Mechanical (TM) coupling, with adaptive solution control, in a repository-setting are the thermal-fluid mechanics code Aria (Notz, et al., 2007) and Adagio (SIERRA Team, 2010, 2011; Arguello et al., 2012). The solid mechanics portion of the TM coupling is handled by Adagio. It solves quasi-static, large deformation, large strain behavior of nonlinear solids in three dimensions. Adagio has Sandia-developed (i.e., proprietary) technology for solving solid mechanics problems, that involves matrix-free iterative solution algorithms for efficient solution of extremely large and highly nonlinear problems. This advanced technology is especially well-suited for scalable implementation on massively parallel computers. During the past few years, the material models in JAS3D that are most important to geomechanical applications, such as salt creep models (power law creep model, and the multi-mechanism deformation (M-D) model), crushable foam models, and the Sandia GeoModel/Kayenta porous material model, have been implemented in the suite of models in Adagio, with most of these models having completed verification and validation procedures.

The previous JAS3D input decks and user subroutines for the SPR works have been converted for use with Adagio. Previously, the original full-dome analytical results for the SPR Bryan Mound site (Sobolik and Ehgartner, 2009b) using JAS3D and the power law creep model were replicated with Adagio; the resulting predictions were a nearly perfect match with the JAS3D predictions (Sobolik, 2013b). A simulation has been run with Adagio to replicate the simulation using the WH half-dome model and the M-D creep constitutive model with JAS3D (Sobolik et al., 2010; Sobolik & Ehgartner, 2012); the following discussion compares the results with the previous JAS3D predictions for purposes of verification. The resulting Adagio predictions with the M-D model matched the JAS3D predictions acceptably well, but not with the near perfection that was experienced with the Bryan Mound/power law creep model. The difference in results is likely due to the implementation of the integration technique for the M-D model that was introduced in JAS3D (Sobolik et al., 2010); the same integration technique was implemented for the M-D model in Adagio, but was altered to configure with the different overall integration and convergence mechanisms in Adagio.

3.2 M-D MODEL DESCRIPTION

The multi-mechanism deformation (M-D) model of salt creep (Munson & Dawson, 1979, 1982, & 1984) is currently being used for modeling salt creep behavior. The M-D model is a rigorous mathematical description of both transient and steady-state creep phenomena, and provides a realistic model of the transient behavior of salt under pressure change conditions such as a workover. This constitutive model considers three well-recognized fundamental features of a creeping material: a steady-state creep rate, a transient strain limit, and both a work-hardening and recovery time rate of change (*i.e.* curvature). Because of the highly non-linear nature of the curvature of the transient strain response, this model has been difficult to integrate in a fully three-dimensional calculation for a model with hundreds of thousands of elements. Many published papers exist presenting two-dimensional calculations using the M-D model, but three-dimensional, large-scale simulations have been more difficult due to the model's high

nonlinearity. Sobolik et al. (2010) documents the integration algorithm enhancements of the M-D model that allow it to be utilized for large-scale three dimensional calculations.

The following discussion of the M-D model was provided by Jim Bean for inclusion in Sobolik et al. (2010). The MD model mathematically represents the primary and secondary creep behavior of salt due to dislocations under relatively low temperatures (compared to the melting temperature) and low to moderate stresses which are typical of mining and storage cavern operations. Three micromechanical mechanisms, determined from deformation mechanism maps (Munson, 1979), are represented in the model: 1) a dislocation climb mechanism active at high temperatures and low stresses, 2) an empirically observed mechanism active at low temperatures and low stresses, and 3) a dislocation slip mechanism active at high stresses. These creep mechanisms are assumed to act such that the total steady state creep rate $\dot{\varepsilon}_s$ can be written as the sum of the individual mechanism strain rates.

$$\dot{\varepsilon}_s = \sum_{i=1}^{3} \dot{\varepsilon}_{s_i} \tag{1}$$

The influence of temperature on the creep strain rate is included through an Arrhenius term. The steady state creep strain rates for the first and second mechanisms are identical in form and are implemented using a power law model while the third mechanism (dislocation slip) is represented using an Eyring type model.

$$\dot{\varepsilon}_{s_1} = A_1 \left(\frac{\sigma_{eq}}{G} \right)^{n_1} e^{\frac{-Q_1}{RT}} \tag{2}$$

$$\dot{\varepsilon}_{s_2} = A_2 \left(\frac{\sigma_{eq}}{G} \right)^{n_2} e^{\frac{-Q_2}{RT}} \tag{3}$$

$$\dot{\varepsilon}_{s_3} = \left(B_1 e^{-Q_1/RT} + B_2 e^{-Q_2/RT} \right) \sinh\left[q \left(\frac{\sigma_{eq} - \sigma_0}{G} \right) \right] H\left(\sigma_{eq} - \sigma_0\right) \tag{4}$$

where:

σ_{eq}	equivalent stress
T	temperature (absolute)
G	shear modulus
A_1, A_2, B_1, B_2	structure factors
Q_1, Q_2	activation energies
R	universal gas constant
q	activation volume
σ_0	stress limit
H	Heaviside function with argument $(\sigma_{eq} - \sigma_0)$

From the definition of the Heaviside function, the third mechanism is only active when the equivalent stress exceeds the specified value of the stress limit σ_0. The equivalent stress appearing in these equations is taken to be the Tresca stress (Munson, et al., 1989). The Tresca stress can be written in terms of the maximum and minimum principal stresses σ_1 and σ_3 respectively ($\sigma_1 \geq \sigma_2 \geq \sigma_3$). Alternatively, the Tresca stress may be written as a function of the Lode angle ψ and the second invariant J_2 of the deviatoric stress tensor **s** (whose components are s_{ij}).

$$\sigma_{eq} = \sigma_1 - \sigma_3 = 2\cos\psi\sqrt{J_2} \tag{5}$$

The Lode angle is dependent on both the second and third invariant J_3 of the deviatoric stress tensor s_{ij}.

$$\psi = \frac{1}{3}\sin^{-1}\left[\frac{-3\sqrt{3}J_3}{2J_2^{3/2}}\right] \qquad -\frac{\pi}{6} \leq \psi \leq \frac{\pi}{6} \tag{6}$$

$$J_2 = \frac{1}{2}s_{ij}s_{ji} \tag{7}$$

$$J_3 = \frac{1}{3}s_{ij}s_{jk}s_{ki} \tag{8}$$

The kinetic equation used in the MD model is given by Equation 9 where F is a function which accounts for transient creep effects and $\dot{\varepsilon}_s$ is the steady state dislocation creep strain rate defined by Equation 1.

$$\dot{\varepsilon}_{eq} = F\dot{\varepsilon}_s \tag{9}$$

The function F has three branches: a work hardening branch ($F > 1$), an equilibrium branch ($F = 1$), and a recovery branch ($F < 1$).

$$F = \begin{cases} \exp\left[\Delta\left(1-\dfrac{\zeta}{\varepsilon_t^f}\right)^2\right] & \zeta < \varepsilon_t^f \quad \text{Transient Branch} \\ 1 & \zeta = \varepsilon_t^f \quad \text{Equilibrium Branch} \\ \exp\left[-\delta\left(1-\dfrac{\zeta}{\varepsilon_t^f}\right)^2\right] & \zeta > \varepsilon_t^f \quad \text{Recovery Branch} \end{cases} \tag{10}$$

The choice of the particular branch depends on the transient strain limit ε_t^f and the internal variable ζ . The transient strain limit is defined by Equation 11 where K_0, c, and m are material parameters, T is the absolute temperature, and G is the shear modulus.

$$\varepsilon_t^f = K_0 e^{cT}\left(\frac{\sigma_{eq}}{G}\right)^m \tag{11}$$

The internal variable ζ , appearing in the calculation of the function F, is obtained by integration of the evolution equation

$$\dot{\zeta} = (F-1)\dot{s} \tag{12}$$

Δ and δ , appearing in Equation 10, are the work hardening and recovery parameters and are given by Equations 13 and 14 respectively. In these equations α , β , α_r , and β_r are material parameters. Typically the recovery parameter δ is taken to be constant (i.e. $\delta = \alpha_r$).

$$\Delta = \alpha + \beta \log\left(\frac{\sigma_{eq}}{\mu}\right) \tag{13}$$

$$\delta = \alpha_r + \beta_r \log\left(\frac{\sigma_{eq}}{\mu}\right) \tag{14}$$

If only the steady state creep response is of interest then the transient and recovery branches may be effectively turned off by setting $\alpha = 0$, $\beta = 0$, $\alpha_\gamma = 0$, $\beta_\gamma = 0$. The MD model can be further simplified to that of a power law creep model by setting the appropriate structure factors and activation energies to zero.

For three dimensional states of stress the components of the creep strain rate tensor are generalized (Fossum et al., 1988) as

$$\dot{\varepsilon}_{ij} = \dot{\varepsilon}_{eq}\frac{\partial \sigma_{eq}}{\partial \sigma_{ij}} \tag{15}$$

Using the Tresca stress (Eq. 5) as the equivalent stress in this form means the creep strains are purely deviatoric ($\dot{\varepsilon}_{ij} = \dot{\varepsilon}_{ij}$ since $\dot{\varepsilon}_{kk} = 0$) and that all volume change is elastic as defined though the bulk modulus K (i.e. $\varepsilon_{kk} = \sigma_{kk} / 3K$). Therefore Equation 15 becomes

$$\dot{\varepsilon}_{ij} = \dot{\varepsilon}_{eq} \frac{\partial \sigma_{eq}}{\partial \sigma_{ij}} = \dot{\varepsilon}_{eq} N_{ij} \tag{16}$$

Including the bulk and shear moduli, which are both assumed constant, there are a total of 19 parameters used to define the MD model.

3.3 HALF-DOME MODEL DESCRIPTION

Sobolik and Ehgartner (2009a) conducted a computational analysis of West Hackberry by using a three-dimensional computational domain that included specific caverns – the Phase 1 caverns plus Caverns 101, 103, 105, 108, 109, 110, and 117 – and the eastern half of the salt dome, with a vertical symmetry plane through six WH caverns (110, 109, 103, 101, 105, and 117). Originally, the salt creep behavior was modeled using the power law creep model, a simplified creep model that calculates the secondary steady state creep mechanism, a subset of the more complete multi-mechanism deformation (M-D) model of salt creep (Munson & Dawson, 1979, 1982, & 1984). Beginning in 2010, the 2009 model converted to using an improved implementation of the complete M-D model (Sobolik et al., 2010). This model was then used with the half-dome computational mesh to analyze specific cavern operation concerns regarding West Hackberry Caverns 6, 8, and 9 (Sobolik and Ehgartner, 2012; Sobolik, 2013a; Sobolik and Lord, 2015).

The mesh for the half-dome computational model is illustrated in Figures 6 and 7. Figure 6 shows the entire mesh used for these calculations, and Figure 7 shows the same view with the overburden and caprock removed to expose the salt formation. The Phase 1 caverns were meshed with geometries based on sonar data measurements, whereas the Phase 2 caverns were modeled as frustums of approximately equal volume, radii and height. Four material blocks are used in the model to describe the stratigraphic layers: the overburden, caprock, salt dome and sandstone surrounding the salt dome. The overburden is made of sand, and the caprock layer is made of gypsum or limestone.

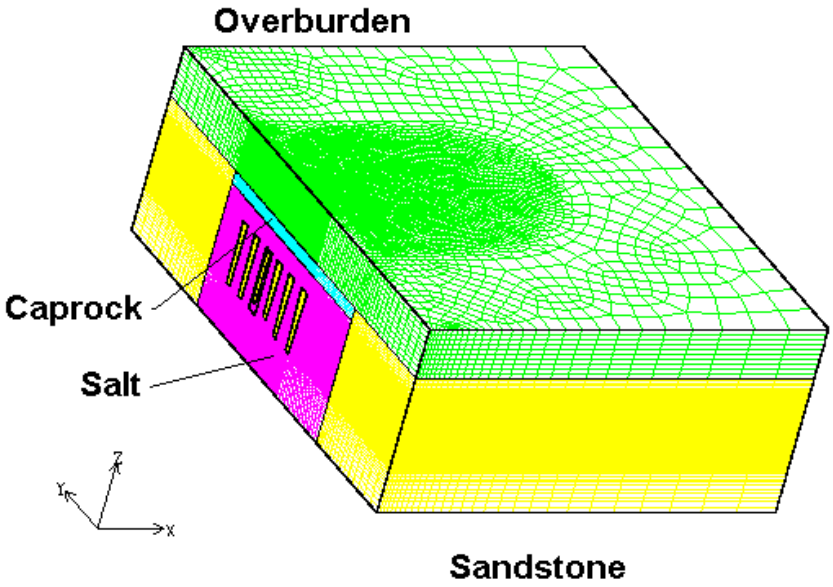

Figure 6. Computational mesh used for the West Hackberry half dome calculations (2009-2014).

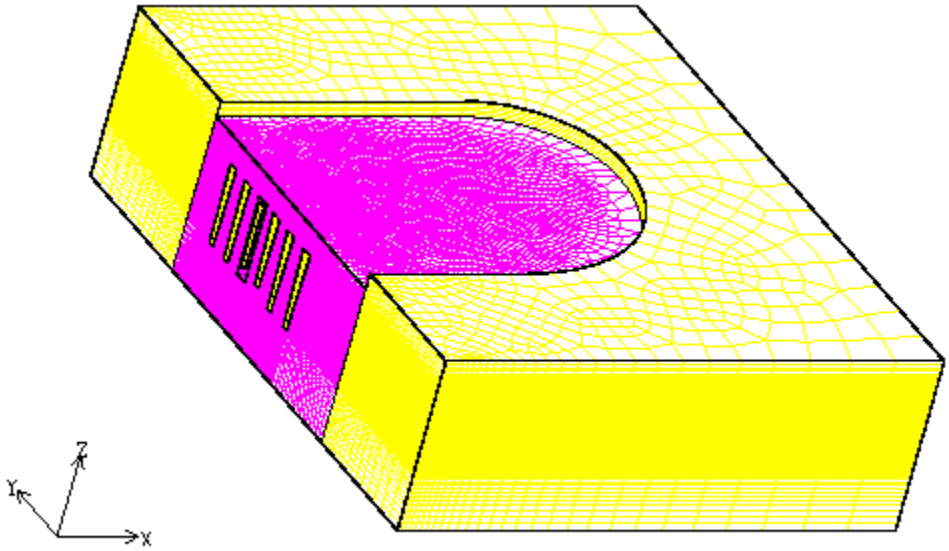

Figure 7. Computational mesh showing the salt formation and surrounding sandstone.

Figure 8 shows three views of the layout of the meshed caverns used for the half-dome calculations, which includes the six Phase-1 half caverns, plus full cavern representations for 108 and the Phase 1 caverns (6, 7, 8, 9, and 11). The figures show the caverns at their original volumes plus five additional extraction layers. The salt extraction layers, or onion skins, represent the proposed additional salt leaching operations to grow the existing West Hackberry caverns. Simulated leaching operations were initiated at the analysis time of September 2008, with each subsequent leaching at five-year intervals afterward.

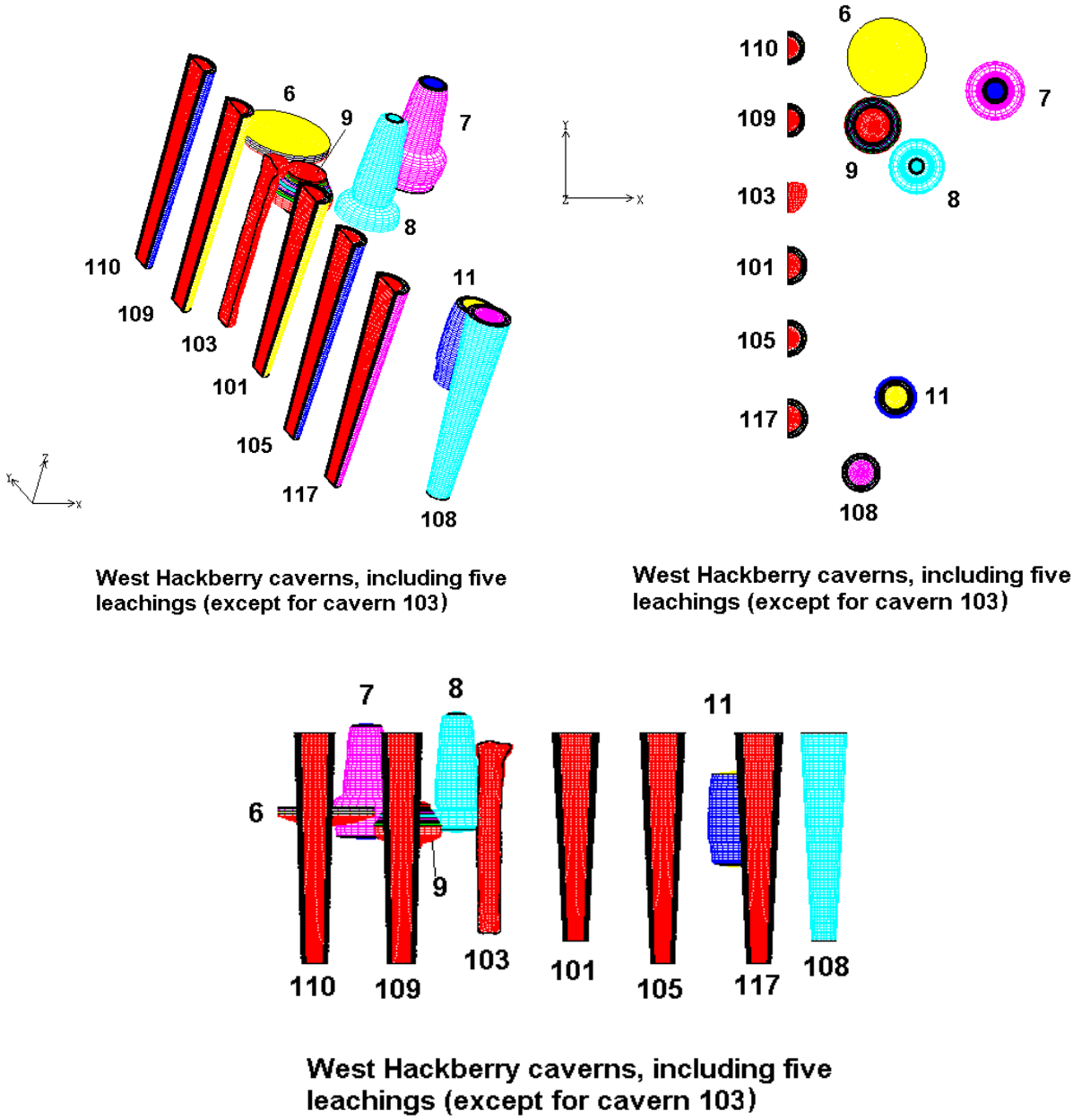

Figure 8. West Hackberry caverns included in the 2009 computational mesh (3 views).

3.4 ADAGIO RESULTS

To compare the results of the two calculations, several different values were checked for the Adagio run. First, the initial stress and temperature states were confirmed to have been reproduced exactly as for the JAS3D run. Second, the resulting predictions of surface subsidence and cavern closure were compared with the JAS3D results to confirm they were sufficiently equivalent. The predicted cavern performance values were expected to be nearly equivalent but

not exactly equal due to the different numerical integration and convergence techniques and measures used in Adagio, and also due to a modification of the mesh for Cavern 6. The results from the two codes were extensively compared and found to produce results that are very similar in behavior, but not exact in their numerical results; the following discussion summarizes this conclusion with a few plots of important parameters used for analysis of SPR site performance.

Two simulations were performed using the half-dome model with Adagio. The first simulation used the exact M-D material properties, and all the other input values and user subroutines, as the JAS3D version. The resulting predictions from this run were found to underpredict the surface subsidence and cavern closure of the original calculations. Therefore, a second simulation was performed multiplying the secondary creep coefficient A2 (Equation 3) by a factor of 2. Figures 9 and 10 plot the surface subsidence over the WH caverns, comparing the measured values to the JAS3D and Adagio second simulation results. The results from the second Adagio simulations are very good. Figures 11 and 12 show the difference between the JAS3D predictions of surface subsidence and the first and second Adagio predictions, respectively, with positive values reflecting that JAS3D predicts the greater value. The second Adagio run produces values that are very reasonable compared to both the measured data and the JAS3D predictions.

Figures 13 and 14 show the predicted cavern volume closure (by percent of the original volume) for the JAS3D and second Adagio simulations. The two sets of predictions are reasonably close to each other. Figures 15 and 16 show the difference between the JAS3D predictions of percentage cavern volume closure and the first and second Adagio predictions, respectively, with positive values reflecting that JAS3D predicts the greater value. Once again, the first Adagio run, using the same M-D properties as the JAS3D run, underpredicts the overall cavern closure for all caverns, whereas the second Adagio run produces predictions much closer to those for JAS3D. The differences in predicted values are related to the different integration algorithms in Adagio and JAS3D, as well as the difference in implementation of the enhanced M-D integration technique. This is unusual, in that nearly all the other material models used in Adagio have been validated against previous models using JAS3D, with no or negligible differences between the codes. The power law creep model was verified by the Bryan Mound simulations. It has long been known that the transient creep component of the M-D model (Equations 9 through 12) is very difficult to implement in a finite element code due to its intrinsic numerical instability; the enhanced integration technique described in Sobolik et al. (2010) fixed many of the problems in implementing the M-D model. The primary conclusion from the results of the transition from JAS3D to Adagio is that the property set used for the M-D model for West Hackberry will need to be reexamined in comparisons between measured and predicted surface subsidence and cavern closure, with the likelihood that higher values of the secondary creep coefficient will be required to match predictions to results.

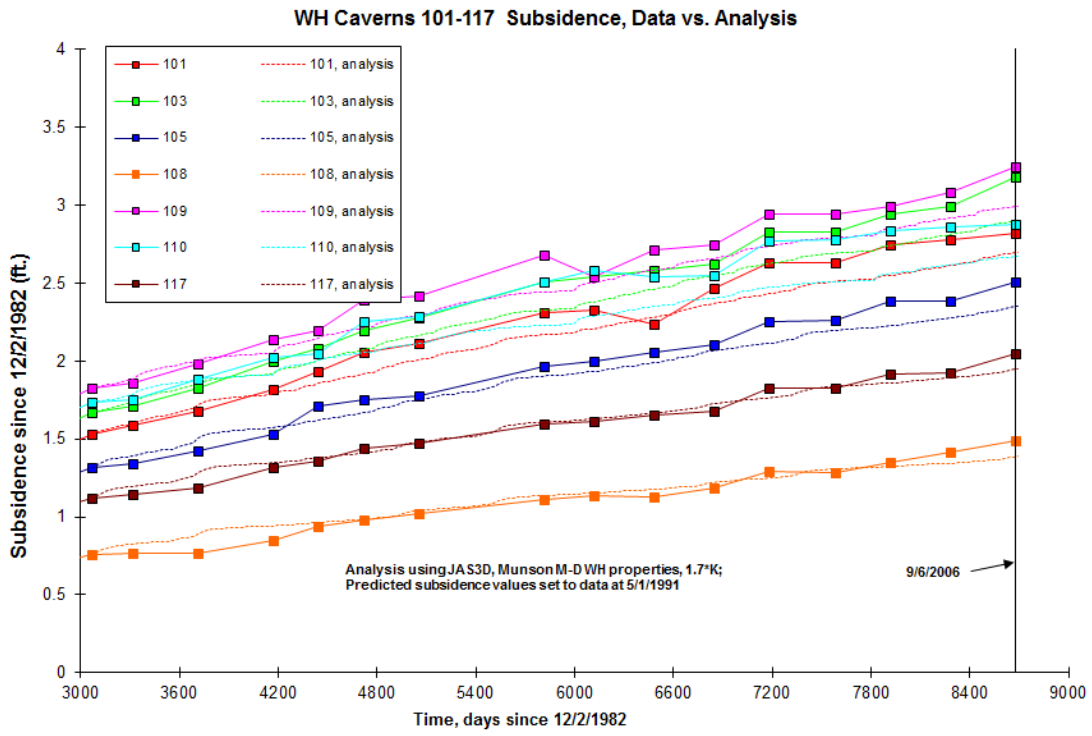

Figure 9. Surface subsidence above West Hackberry caverns, JAS3D predictions vs. measurements.

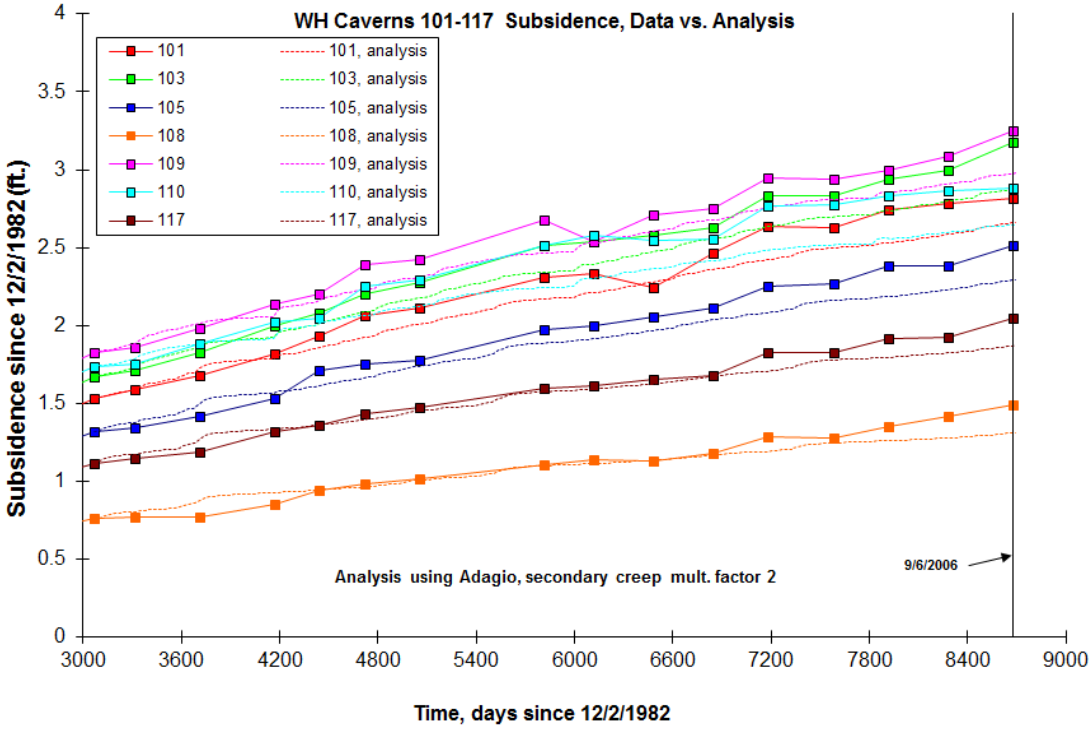

Figure 10. Surface subsidence above West Hackberry caverns, Adagio predictions with additional secondary creep multiplication factor of 2 vs. measurements.

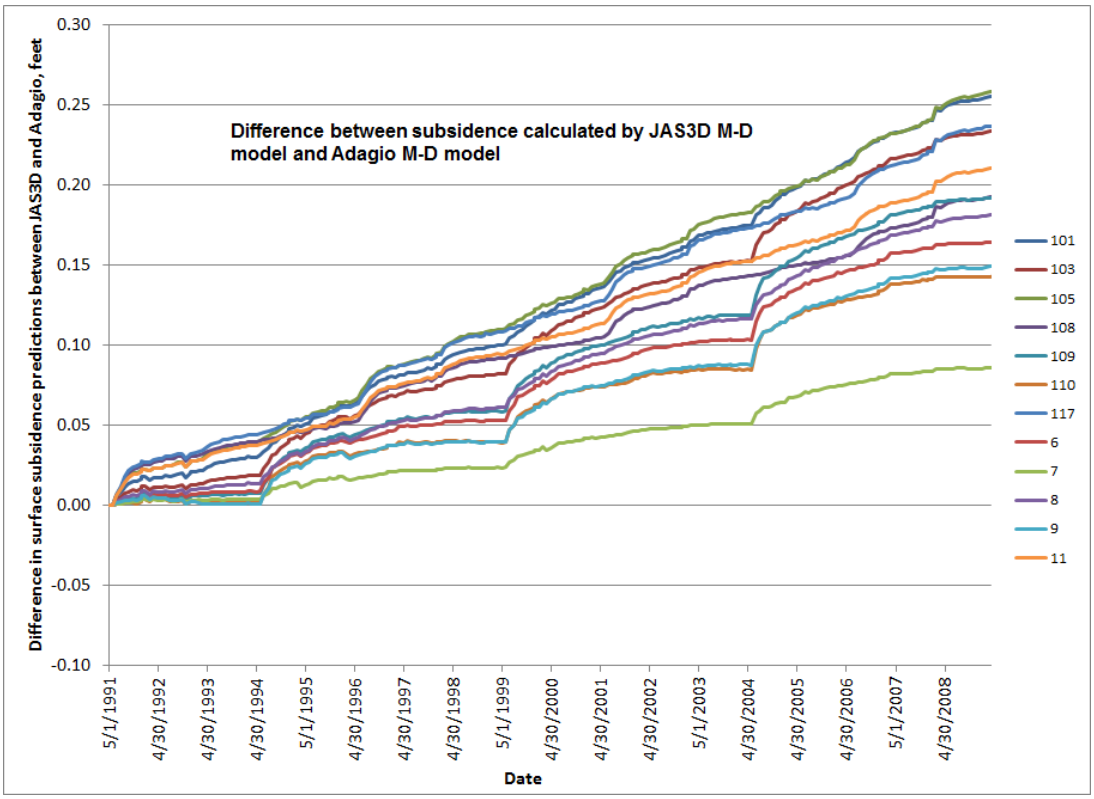

Figure 11. Difference in predictions of surface subsidence (JAS3D – Adagio), using M-D property set of Sobolik & Ehgartner (2012).

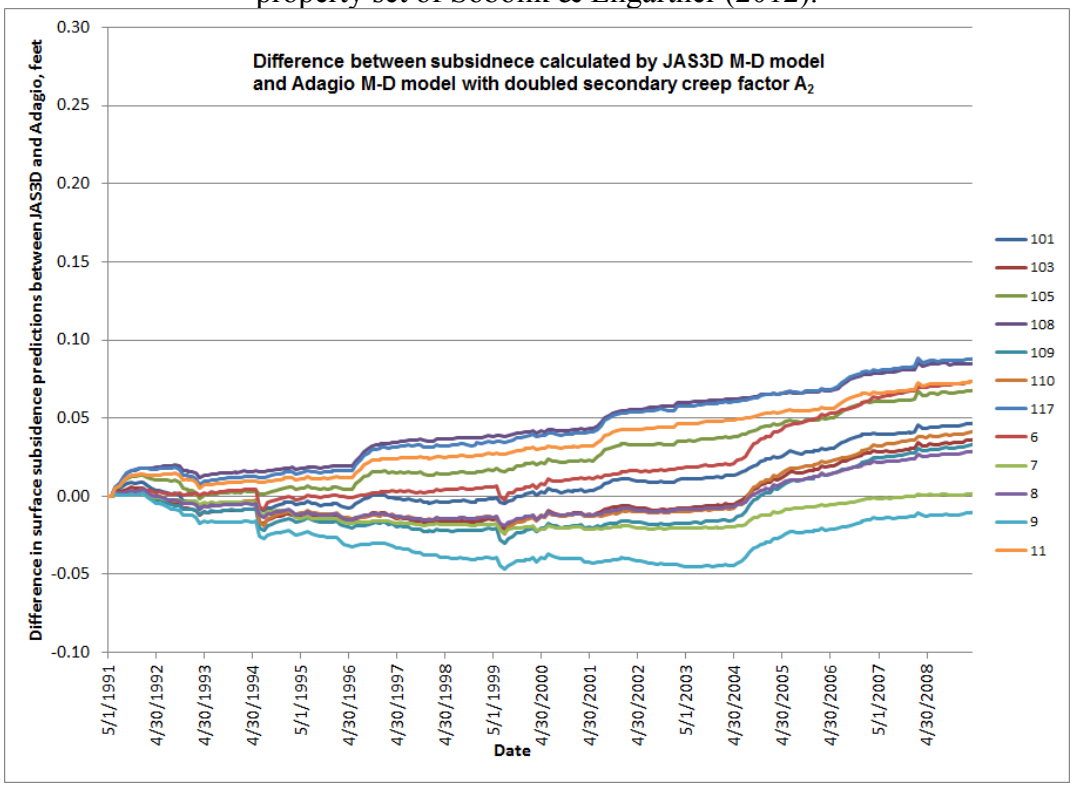

Figure 12. Difference in predictions of surface subsidence (JAS3D – Adagio), Adagio predictions with additional secondary creep multiplication factor of 2.

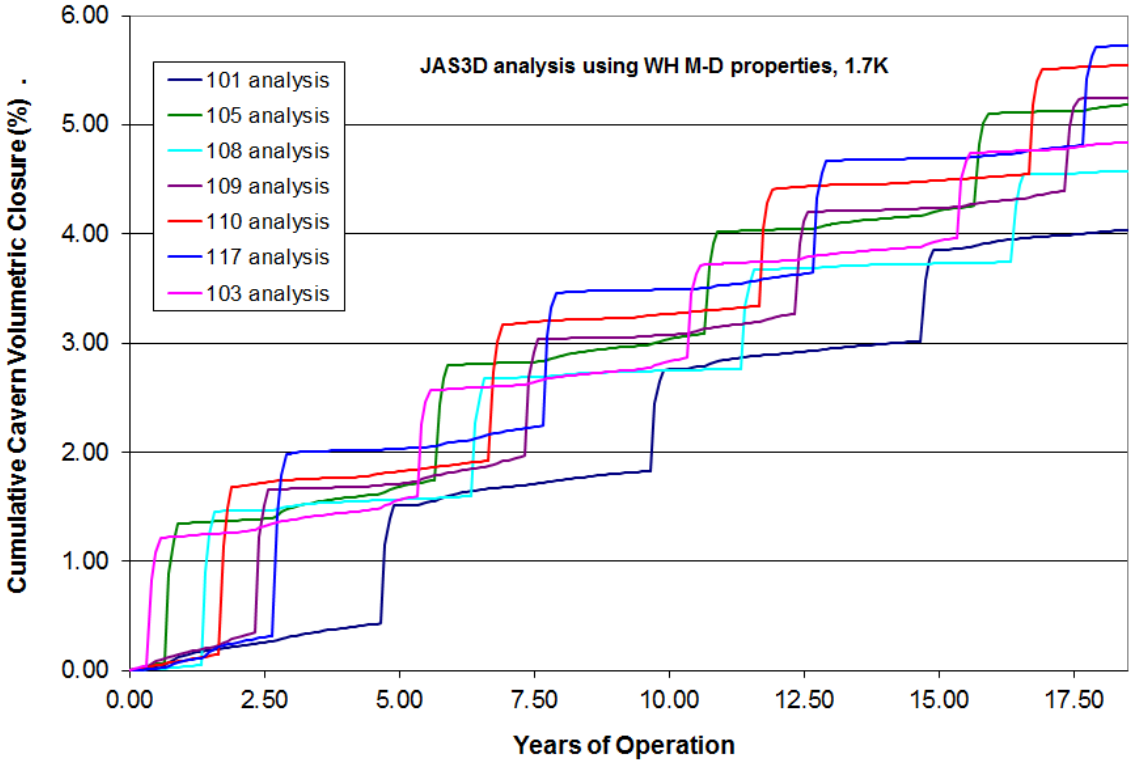

Figure 13. Cavern volume closure above West Hackberry caverns, JAS3D predictions.

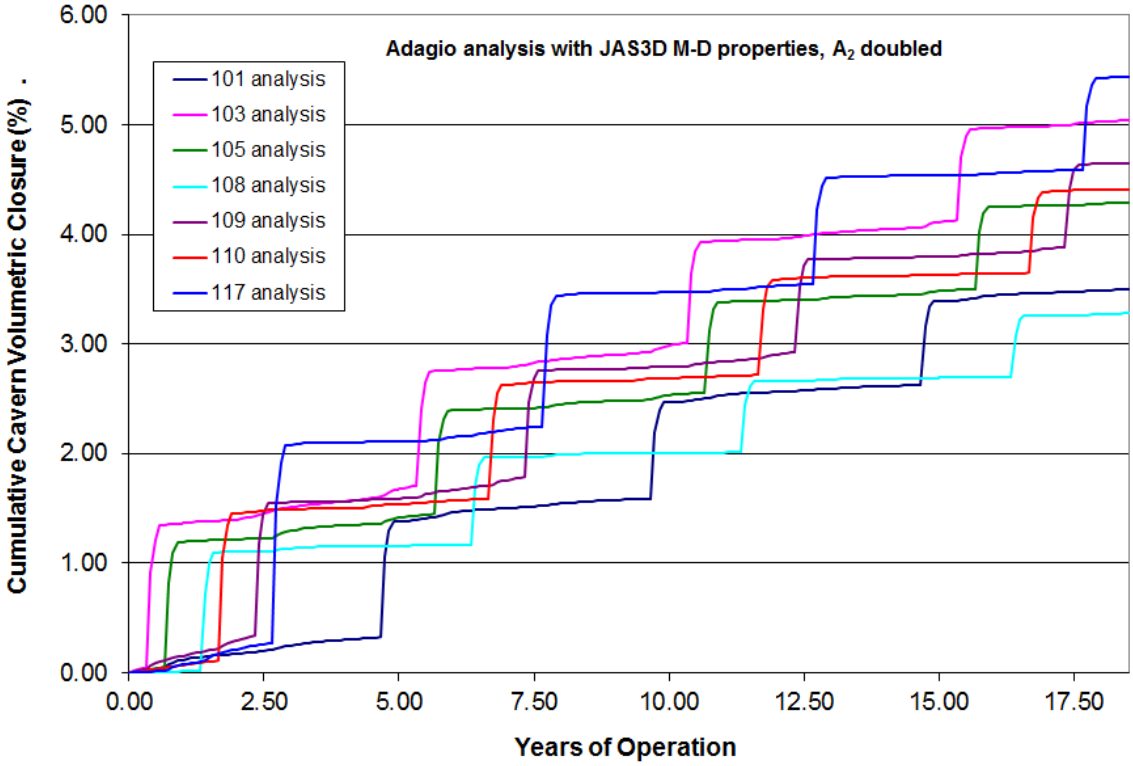

Figure 14. Cavern volume closure above West Hackberry caverns, Adagio predictions with additional secondary creep multiplication factor of 2.

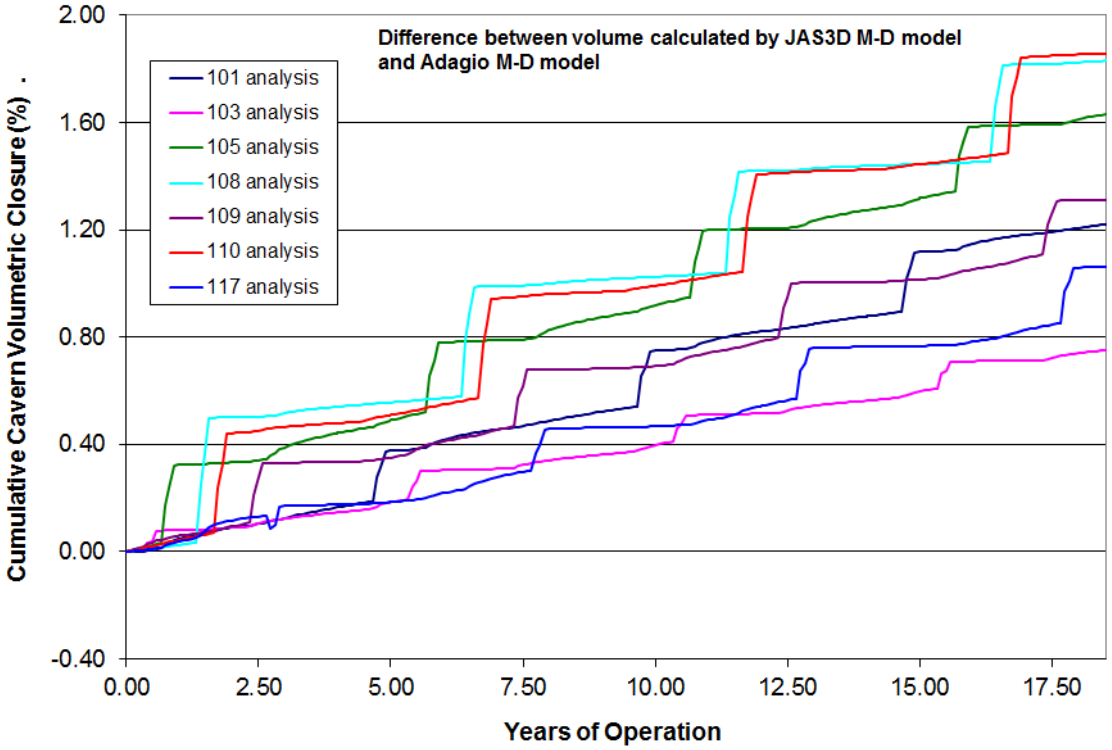

Figure 15. Difference in predictions of cavern volume closure (JAS3D – Adagio), using M-D property set of Sobolik & Ehgartner (2012).

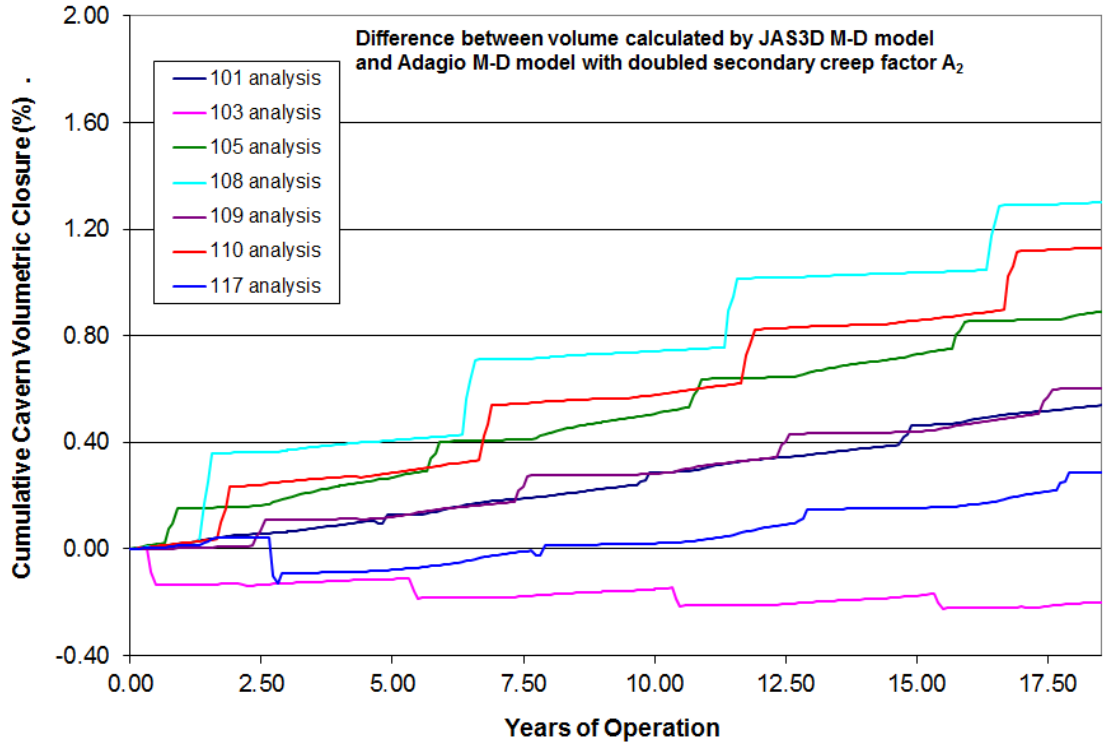

Figure 16. Difference in predictions of cavern volume closure (JAS3D – Adagio), Adagio predictions with additional secondary creep multiplication factor of 2.

4. FULL-DOME ANALYSIS MODEL

4.1 MODEL DESCRIPTION

The new full-dome computational model of the West Hackberry site has several enhancements over the previous analytical models. The intent of these enhancements is to compute stresses and strains using more accurate geometries of the salt dome and the caverns and their subsequent leaches, implement the M-D salt constitutive model with cavern-specific creep properties, and compare the use of time-averaged wellhead pressure histories against actual pressure histories for the purposes of understanding sympathetic behavior of adjacent caverns during workover operations. Each of these enhancements is described in detail in this section. The analytical model follows the same general time history as the 2009 analyses. The five caverns known as Phase 1 – Caverns 6, 7, 8, 9, and 11 – were created as early as 1946 and were used for brining and brine storage before the SPR took ownership of them in 1981. After that time, the seventeen Phase 2 storage caverns were created over an eight-year period. The simulation begins in 1945 with a one-year stress equilibration calculation. The analysis then simulates the creation of the Phase 1 caverns leached to full size over some period of time and filled with brine until 1981, and then filled with oil. The caverns are "created" by immediately removing the cavern material from the mesh by the element death option in Adagio, and at the same time applying a pressure boundary condition in the cavern that changes linearly from in situ salt pressure to cavern fluid pressure of the period of cavern creation. The analysis then simulates the creation of the post-1981 caverns and subsequent filling with oil. Where actual wellhead oil pressure histories are available, they are used explicitly or as a time-averaged function based on that history; otherwise, an average operating pressure with three-month workovers on five-year cycles is assumed. Drawdown, or leaching, operations to create additional volume are simulated periodically for a total of five drawdowns for all 22 caverns in five-year intervals beginning in 2018, and are done in a similar manner as the cavern creation.

In order to perform a cavern stability analysis that investigates damage in salt, the analytical tools ideally need to be able to perform the following functions: 1) calculate the changes in the in situ stress field and deformations surrounding the well casings and caverns over a long period of time resulting from the creep deformation of the salt; 2) include criteria by which tensile failure or shear damage of the salt can be determined and located; 3) have the ability to reduce the time step of the analysis to discretize short-time events such as changes in cavern pressure because of workovers; and 4) allow post-processing to be able to identify high strain and failure regions and compute cavern volume changes. The computational models utilized the finite element code Adagio (ideal for simulations of processes occurring over many years), the M-D creep model for salt, and the full-dome computational mesh and model.

4.2 STRATIGRAPHY AND COMPUTATIONAL MESH

The mesh for the computational model is illustrated in Figures 17 and 18. Figure 17 shows the entire mesh used for these calculations, and Figure 18 shows the same view with the overburden and caprock removed to expose the salt formation. The mesh comprises 5,990,870 nodes and 5,953,952 elements. Four material blocks are used in the model to describe the stratigraphic

layers: the overburden, caprock, salt dome and sandstone surrounding the salt dome. The overburden is made of sand, and the caprock layer is made of gypsum and limestone. The overburden layer is 1600 feet thick, and the caprock is 400 feet thick in the central portion of the dome. In an attempt to include the downward contour of the top of the salt dome at its outer perimeter, an outer ring of caprock has a total thickness of 800 feet. Figure 19 superimposes the geometry of the West Hackbery dome obtained from seismic measurements onto the geometry created for the computational mesh, which was constructed by vertically extruding two palnar outlines of the salt dome boundary. The 22 SPR caverns are included in the mesh, as are the three current Sempra natural gas storage caverns just to the west of the SPR site and three proposed cavern sites. (For these calculations the three Sempra caverns were assigned a variable cavern pressure equal to between 0.8 and 1.0 of the lithostatic pressure at the top of the cavern.)

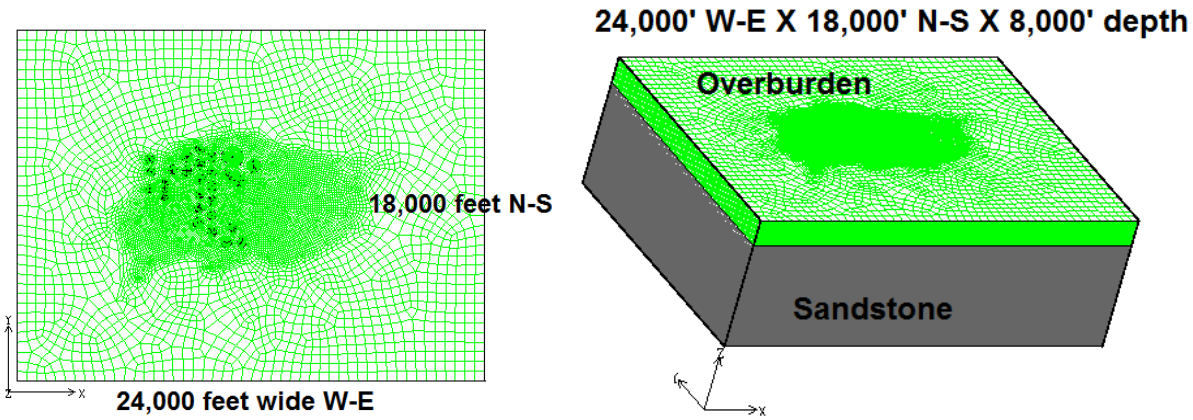

Figure 17. Computational mesh for the full-dome West Hackberry model.

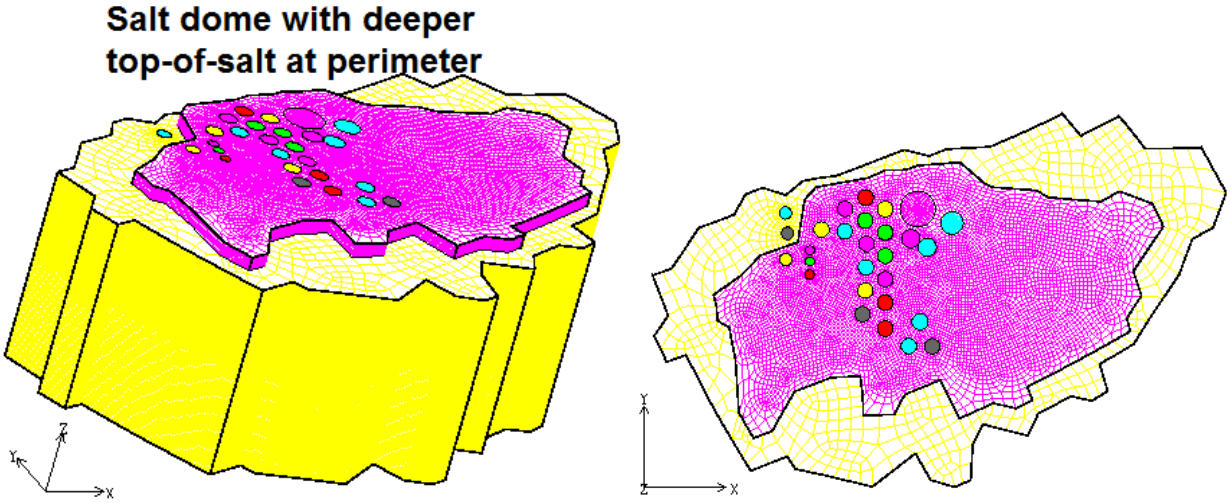

Figure 18. Computational mesh showing the salt dome and cavern locations.

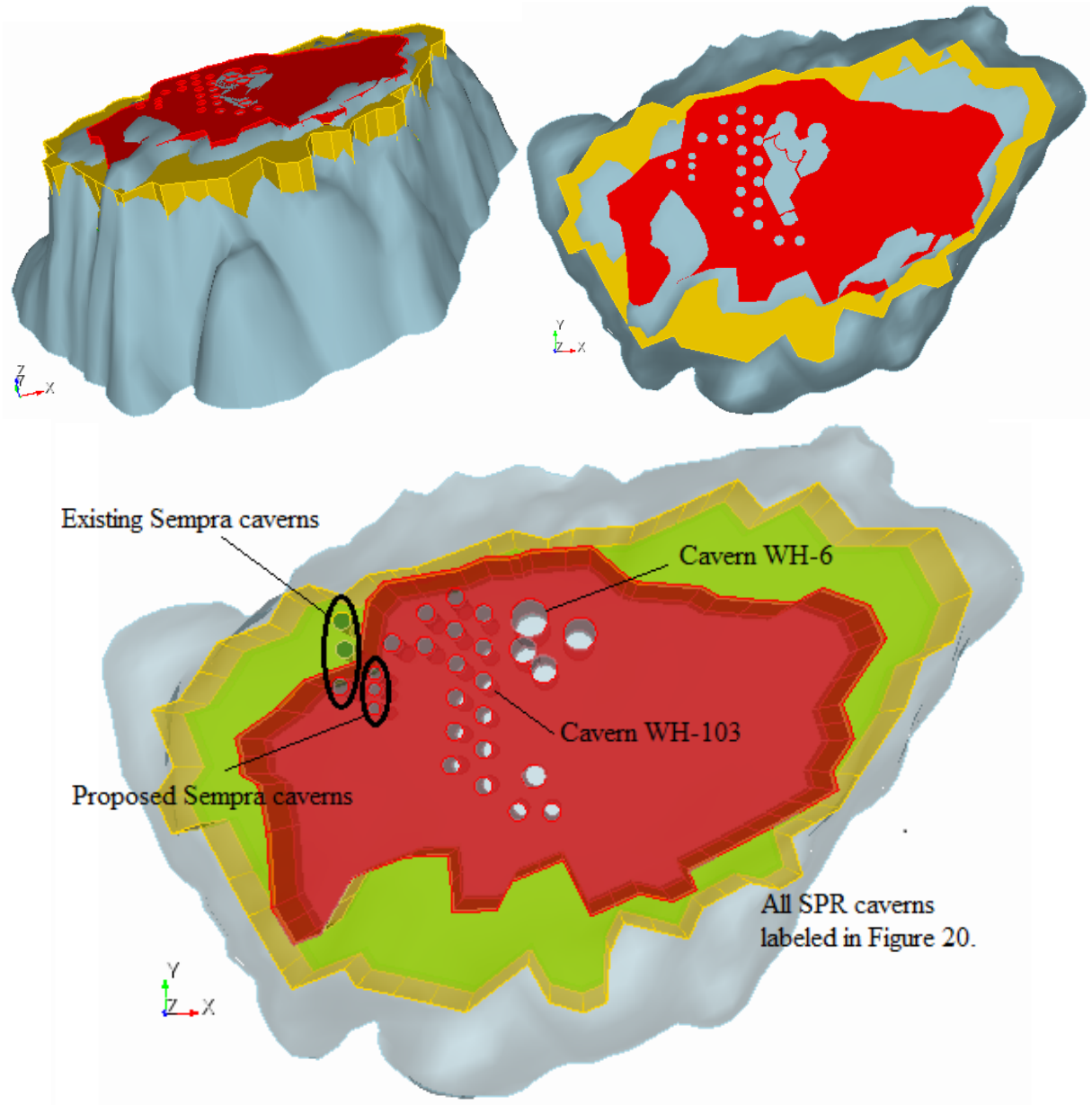

Figure 19. Comparison of the salt dome geometry obtained from seismic measurements (grey) to the constructed salt dome for the West Hackberry geomechanical mesh (red and yellow).

The post-1981 caverns were typically constructed on 750-feet center-to-center spacings. Table 1 lists the cavern coordinates, top-of-cavern depths, and initial heights and volumes used in the analysis. The coordinates are based on Louisiana field coordinates, and converted to mesh coordinates with Cavern 103 at the origin, and coordinate axes aligned with compass directions (X-axis for W-E, Y-axis for N-S). Figure 20 shows three views of the layout of the meshed caverns used for these calculations. The meshes for 22 SPR caverns include both their original geometries plus up to five additional extraction layers; because of meshing problems created due to their close proximity, WH-8 was limited to 4 extraction layers, and WH-9 was limited to three. The salt extraction layers, or onion skins, represent proposed additional salt leaching operations to grow the existing West Hackberry caverns, each of which would increase the

volume of the cavern by approximately 15% (somewhat less for some of the Phase 1 caverns due to their unusual geometries and concerns). For this analysis, the first leaching operation was scheduled for September 2018, with each subsequent leaching at five-year intervals afterward.

Table 1: Cavern coordinates, depths, heights, and construction dates used in West Hackberry computational analyses.

Cavern	Coordinates*		Depth to Ceiling, feet	Init. Height, feet	Init. Volume, MMB	Begin Construct	End Construct	Begin Oil Storage
	X, feet	Y, feet						
Phase 2 caverns								
101	-12.665	-748.739	2557	1872	10.6	5/1/1981	12/1/1983	12/1/1983
102	-618.767	-366.944	2622	2029	6.0	2/1/1982	12/1/1984	11/30/1984
103	0	0	2667	1686	10.3	5/1/1981	1/1/1984	1/1/1984
104	-638.778	-1115.417	2630	1864	10.5	5/1/1981	1/1/1984	1/1/1984
105	-22.083	-1499.731	2640	1915	9.9	1/1/1981	1/1/1984	1/1/1984
106	-724.913	-1867.503	2557	1716	10.9	1/1/1984	12/1/1987	12/1/1987
107	-599.715	384.384	2610	1915	11.4	7/1/1981	8/1/1984	8/1/1984
108	756.	-2890.	2598	1795	11.8	2/1/1982	12/1/1984	12/1/1984
109	8.878	750.074	2584	2010	11.5	3/1/1984	11/1/1985	11/1/1985
110	23.11	1499.328	2610	1904	11.6	2/1/1982	3/1/1985	3/1/1985
111	-625.531	1867.335	2625	1957	9.0	2/1/1982	4/1/1988	4/1/1988
112	1507.28	-2900.041	2564	1909	11.4	9/1/1983	1/1/1987	1/1/1987
113	-1279.829	1508.091	2840	1814	11.4	7/1/1982	6/1/1985	6/1/1985
114	-1299.626	790.594	2576	1949	10.9	9/1/1982	9/1/1985	9/1/1985
115	-638.850	1136.594	2537	2086	11.1	3/1/1984	6/1/1987	6/1/1987
116	-2038.007	846.701	2657	2017	10.6	7/1/1982	9/1/1985	9/1/1985
117	257.024	-2314.750	2565	1989	11.7	6/1/1985	9/1/1988	9/1/1988
Phase 1 caverns								
6	1042	1504	3230	160	8.7	1/1/1946	1/1/1947	1/1/1981
7	2140.46	1054.86	2520	1000	12.8	1/1/1946	1/1/1947	1/1/1981
8	1348	275.58	2420	1040	11.2	1/1/1946	1/1/1947	1/1/1981
9	818	548	3180	440	9.4	1/1/1947	1/1/1948	1/1/1981
11	1113.49	-2110.067	2940	820	9.1	1/1/1962	1/1/1963	1/1/1981

* Based on Louisiana field coordinates and converted to mesh coordinates with Cavern 103 at the origin (X-axis aligned along W-E, Y-axis aligned along N-S)

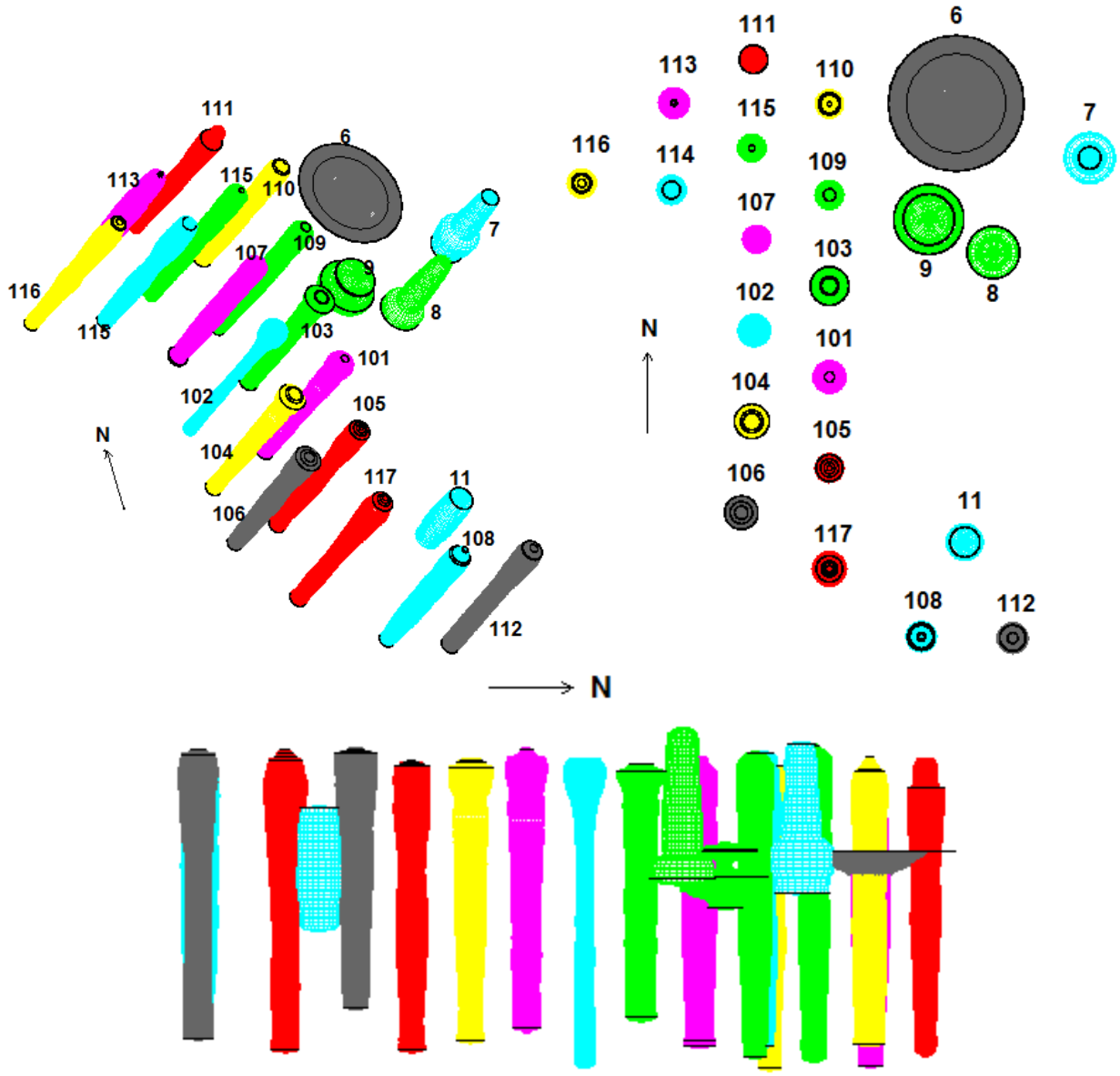

Figure 20. West Hackberry caverns included in the computational mesh (3 views).

WH Caverns 6 and 9 represent a significant challenge, both from a modeling standpoint and from an actual operational aspect as the cavern sizes increase along with the potential for adverse interactions. The meshes for these caverns are shown in Figure 21; the dimensions and relative locations of the caverns are shown to scale. The large rim around the bowl-like WH-6 was discovered from sonar and strapping data from the early 1980s. The 2009 computational analyses determined that the upper and lower surfaces of the rim came into contact and essentially "closed" sometime in the mid-to-late 1990s; an analysis of the pressure and oil-brine interface data from WH-9 indicate the same conclusion happening in the early-to-mid 1990s (Sobolik & Ehgartner, 2009a). The inclusion of the open WH-6 rim in the computational simulations creates numerical instability in the calculation due to the initiation of contact algorithms when the top and bottom surfaces come into contact. The primary effects of the rim on any results of the calculations tend to be related to the behavior of the salt between WH-6 and

9, and not on any other caverns or on the overall subsidence of the site. Therefore, for the analyses presented in this report, the WH-6 rim volume and element are not removed per element death as for the other caverns, but instead represented by salt with a smaller elastic modulus to allow it to deform more. The option to perform future calculations with the rim removed remains in the model.

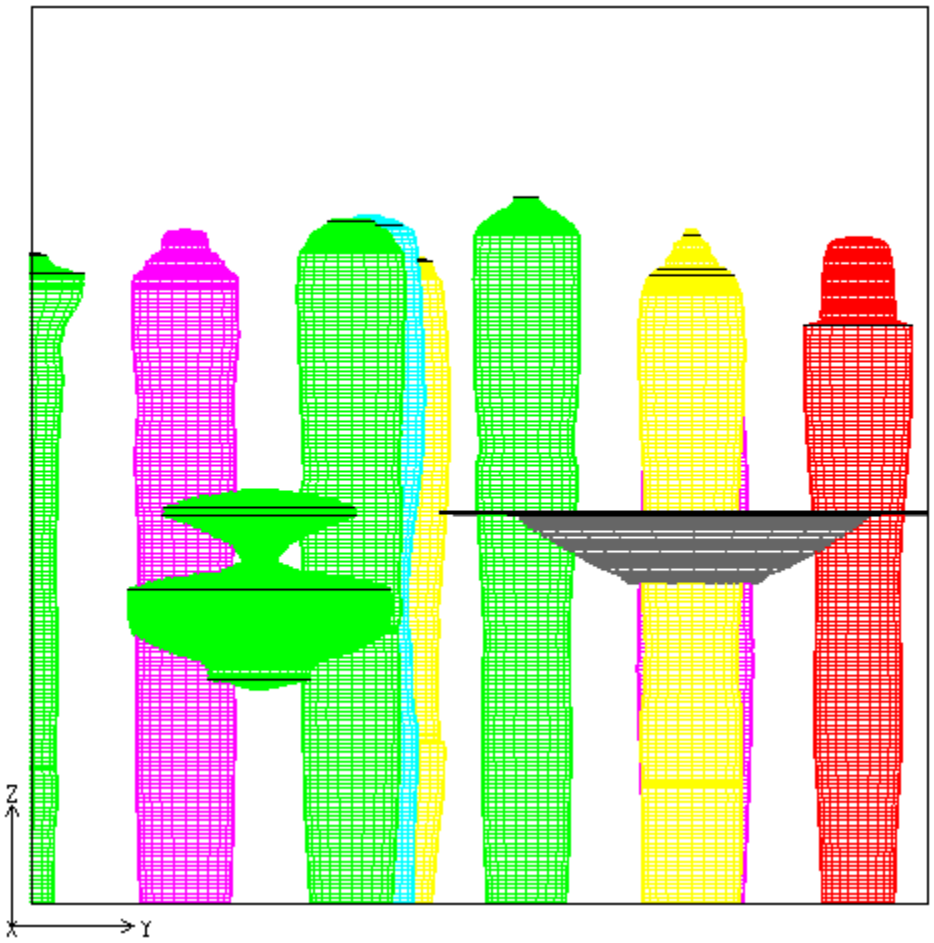

Figure 21. Proximity of Caverns 6 (grey) and 9 (green).

4.3 USE OF CAVERN PRESSURE HISTORIES

In all of Sandia's previous geomechanical analyses of West Hackberry and the other SPR sites, approximated values for wellhead pressure (and thus, cavern pressure) based on general operating conditions have been used in the model. Both JAS3D and Adagio (because they are purely mechanical codes) require the specification of a pressure boundary condition on the inside of the cavern walls. The codes then predict cavern closure due to creep, but the cavern pressure does not automatically change in the simulation. The historical wellhead pressure data for the cavern WH-101 are shown in Figure 22. The typical operating pressure range for the cavern is about 900-975 psi. As the cavern volume closes due to creep, the pressure increases for a period of time until some fluid is bled off at the wellhead; this bleed-off typically happens about every 90 days. Workover periods are observed to occur during those times when the wellhead pressure is near zero; mechanical integrity tests are represented by pressures significantly higher than 100 psi. For previous SPR geomechanical analyses, this type of pressure history was represented by a constant wellhead operating pressure, with three-month workover period of zero pressure occurring every five years.

For this new geomechanical model for West Hackberry, it was decided to model the historical cavern pressure as closely as possible during the times when historical data are available. One of the reasons for doing this was to develop a better understanding of the creep behavior of caverns when an adjacent cavern is operated in workover mode. Examination of cavern wellhead pressure data indicate that when one cavern is in workover, the pressurization rate of adjacent caverns will increase (Checkai et al., 2014). This can be explained by Equations 2, 3, and 4 of the M-D creep model, which pose strain rate as a function of the equivalent stress, which is itself a measure of the magnitude of deviatoric stress. This deviatoric stress increases in the vicinity of a cavern when the fluid pressure is dropped to levels significantly less than the in situ stress. In previous SPR models, this increase in the pressurization rate has been obserbed as an increase in the cavern volume closure rate during a workover. One of the goals of the new model is to use it to develop a predictive capability for monitoring pressurization rate changes in adjacent caverns, so as to help determine if leakage is occurring during these operations.

Two methods for inputing the historical wellhead pressures will be examined in these analyses. The first method, referred to as the "actual pressure" method, reads the historical wellhead pressures "as is", with some minor modification for mechanical integrity test pressures (these are nitrogen pressures at the wellhead, with the resulting cavern pressure only slightly different than under normal oil wellhead pressures). Because the increased pressures are already "pre-programmed" into the analysis by using the measured values, the resulting predicted cavern volume closure will be affected. Therefore, a second method was used, called the "average pressure" method, for which a constant pressure was applied during normal operations much like the previous SPR calculations used, but the historical workover schedule was applied. The average historical pressure for each cavern was taken as an average value of all days with a pressure higher than 700 psi; all days less than 700 psi were assumed to be workover condiions with 0 psi at the wellhead. Figure 23 compares the actual and average pressure histories for WH-101 that were used in these analyses; similar pressure histories were used for the other 21 caverns. For times outside the time range of available data, an average pressure schedule with 90-day workovers every five years (much like the earlier SPR analyses) was applied.

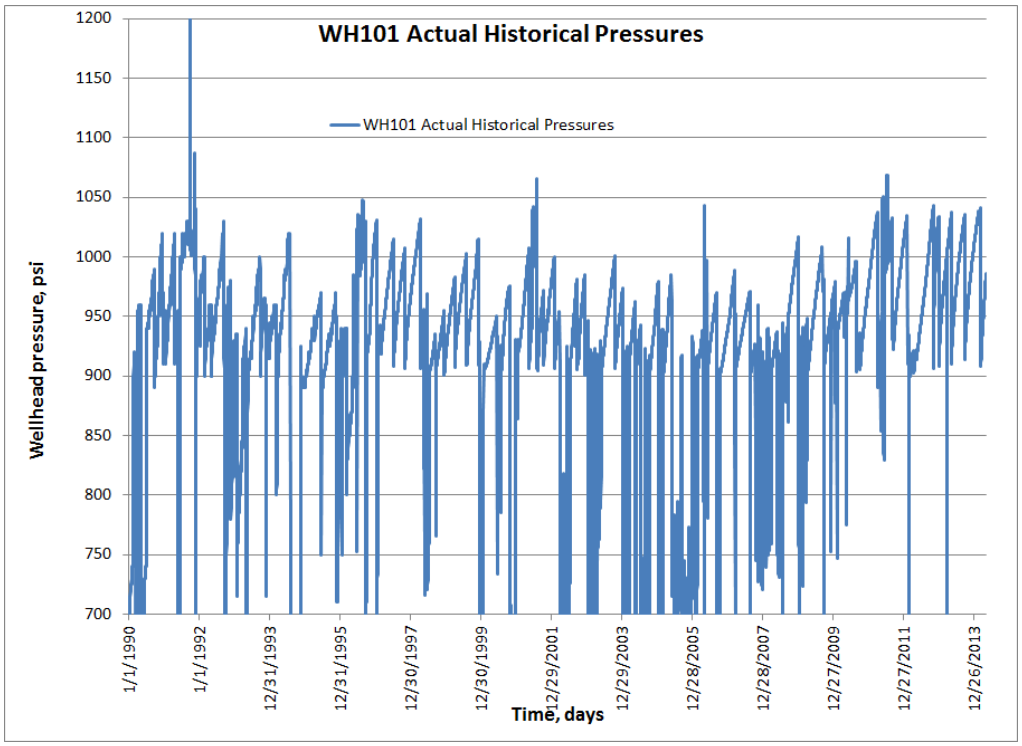

Figure 22. Historical wellhead pressures for WH-101.

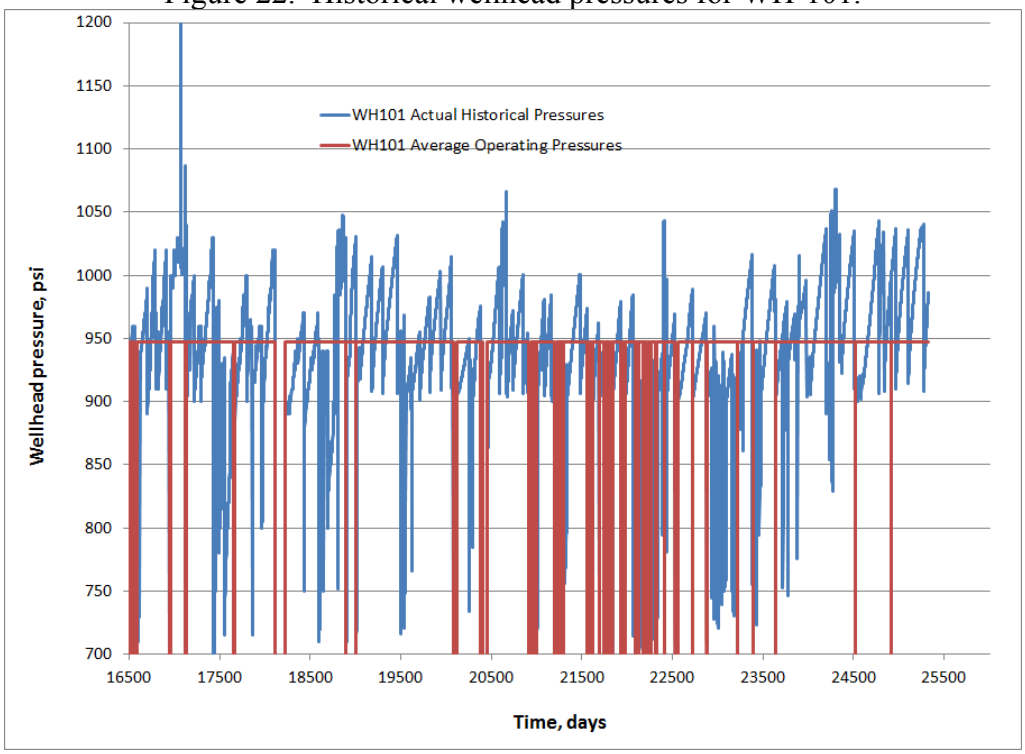

Figure 23. Comparison of actual historical wellhead pressures and average operating pressures used in the calculations for WH-101.

4.4 MATERIAL PROPERTIES

The classic M-D material properties for West Hackberry salt were first published in Munson (1998); these properties are listed in Table 2. This property set, with one minor change, was used for several JAS3D and Adagio analyses of West Hackberry behavior using the half-dome model described in Section 3 (Sobolik et al., 2010; Sobolik and Ehgartner, 2012; Sobolik, 2013a; Sobolik and Lord, 2015). They were also used for the Adagio calculations used to evaluate the transition from JAS3D to Adagio, also described in Section 3. The predicted values for cavern volume closure and surface subsidence from Adagio were slightly less than they were from JAS3D.

Table 2. M-D Model mechanical properties published for West Hackberry salt in Munson (1998)

Property	West Hackberry, soft salt properties
Density, lb/ft^3	144 (2300 kg/m^3)
Elastic modulus, lb/ft^2	648 $\times 10^6$ (31.0 GPa)
Shear modulus G, lb/ft^2	259 $\times 10^6$ (12.4 GPa)
Poisson's ratio	0.25
Primary Creep Constant A_1, sec^{-1}	9.81 $\times 10^{22}$
Exponent n_1	5.5
Q_1, cal/mol	25000
Secondary Creep Constant A_2, sec^{-1}	1.13 $\times 10^{13}$
Exponent n_2	5.0
Q_2, cal/mol	10000
B_1, sec^{-1}	7.121$\times 10^6$
B_2, sec^{-1}	3.55$\times 10^{-2}$
σ_0, , lb/ft^2	429 $\times 10^3$ (20.57 MPa)
q	5335
m	3.0
K_0	6.275$\times 10^5$
c (1/R) (0.009198/1.8)	0.00511
α	-17.37
β	-7.738
δ	0.58
K_f, Multiplication factor for K_0 in Equation 11 (i.e., K_0 used in analysis = ($K_{0,\ Munson}$) * (K_f)	18.2

Because of the discrepancy between the predicted cavern closure and surface subsidence for the between JAS3D and Adagio for the half-dome model, it was decided to run an intial simulation using the M-D properties in Table 2, and comparing the resulting predictions to West Hackberry field data. Cavern volume closure as a function of time is not a directly measured quantity; volumes of specific fluid exchanges from oil removal, pressure bleed-offs, workover, and so on are recorded, but the day-to-day volume closure due to creep cannot be monitored. However, oil wellhead pressure is recorded daily, and cavern volume closure can be estimated based on the creep properties of salt around a particular cavern, the basic cavern geometry, the volumes of oil and brine in the cavern, and the compressibilities of those fluids as a function of temperature and pressure. The cavern pressure monitoring code CAVEMAN (Ballard & Ehgartner, 2000) was

used the estimate the cavern volume closure as a function of time for all 22 caverns. CAVEMAN uses the wellhead pressure to calculate an average cavern pressure for each cavern. It also used the oil-brine interface depth to calculate the percentages of the cavern contining oil and brine, and the temperature of the fluids to calculate their compressibilities. The daily rate of change of the difference between the average cavern pressure and the in situ salt pressure at the mid-heights of the oil and brine-filled parts of the cavern, along with the compressibilties of the fluids, are used to calculate a daily rate of change in volume. The code makes additional assumptions for the dates with no pressure data, pressure data indicating a workover or mechanical integrity test, and the days immediately following a fresh-water drawdown when resdiaul leaching may still be occurring. CAVEMAN also uses documented fluid exchanges to periodically reference volume loss to a known number. Because of the number of simplifying assumptions that go into the estimates for cavern volume closure as calculated by CAVEMAN, the accuracy of such calculations is difficult to measure. However, the total volume loss over a long period of time should be a useful metric to evaluate the effectiveness of a given M-D property set to model the West Hackberry salt creep behavior.

Figures 24 through 26 compare the cumulative cavern volume closure derived from CAVEMAN from wellhead pressure data (solid lines) to the same values predicted by the geomechanical calculations using Adagio, the full-dome mesh, the M-D properties in Table 2, and the actual wellhead pressure histories (dashed lines). Figure 24 plots these values for the Phase 1 caverns (6, 7, 8, 9, and 11); Figure 25 for the Phase 2 caverns on the east side of the site (101, 103, 105, 108, 109, 110, 112, and 117); and Figure 26 for the Phase 2 caverns on the west side (102, 104, 106, 107, 111, 113, 114, 115, and 116). For both the CAVEMAN and Adagio values, the long time periods with relatively straight slopes in the plots represent period of normal operating conditions (these will be referred to as “steady-state” periods), whereas the sudden jumps in cavern closure represent periods (usually workovers) when the wellhead pressure was much lower than normal. Two obvious trends can be obseved from these plots. One, the slopes of the steady-state periods for the measured and predicted values are significantly different, with the measured values nearly always having a larger slope indicating a larger steady-state volume closure rate. This behavior would indicate that the secondary creep coefficient A_2 in Table 2 is not high enough, and should be increased by some factor for nearly all the caverns. The primary creep coefficient, A_1, may also need to be increased, but for the stress and temperature regimes where the SPR caverns are located the secondary creep tends to dominate the primary creep. Two, the overall volume closure over 25 years tends to be greater than the Adagio predictions indicate. Increasing the secondary creep coefficient will certainly increase the overall predicted cavern closure. The magnitude of the sudden increases in cavern closure at workovers is a function of both primary and secondary creep, but also of the transient creep phenomenon, which is governed by the factor K_0 in Equation 11. The magnitude of these “jumps” is higher for the predictions that the data for some caverns, and lower for the others.

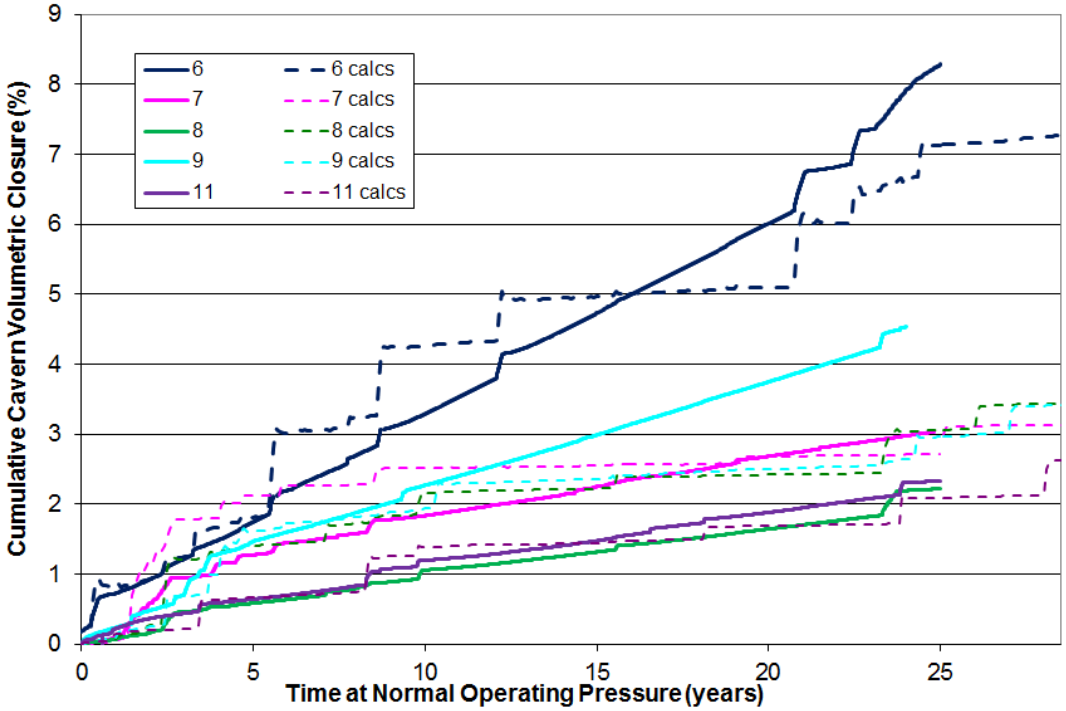

Figure 24. Comparison between measured, predicted (M-D properties from Table 2) cumulative cavern volume closure since 1/1/1990 for West Hackberry Phase 1 caverns.

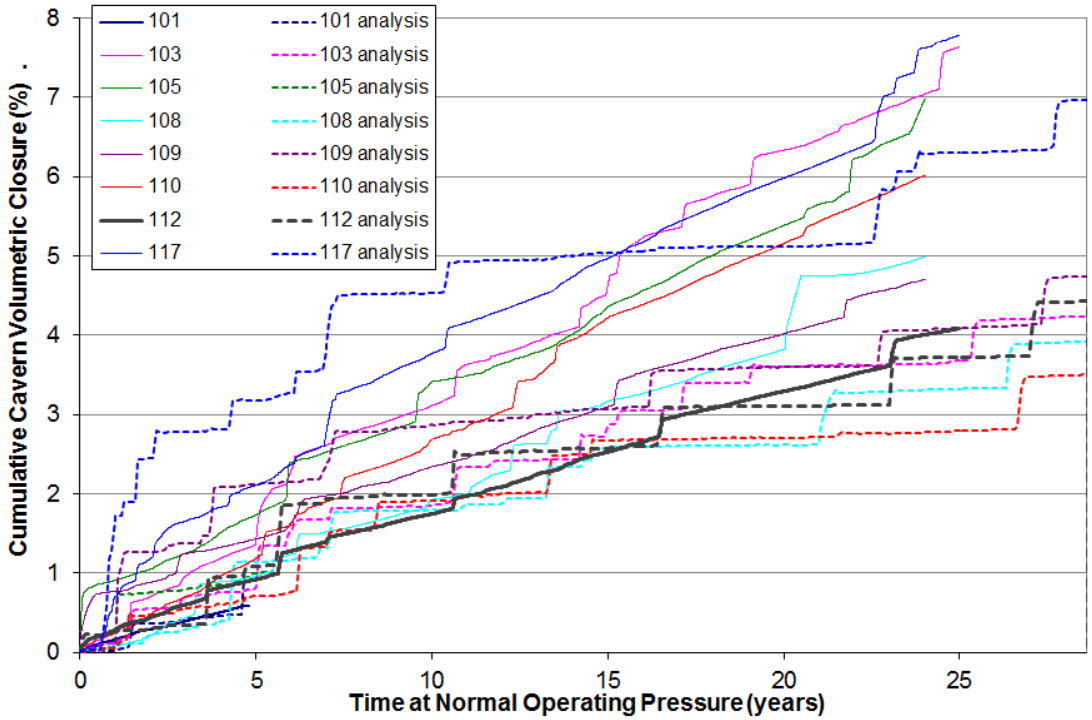

Figure 25. Comparison between measured, predicted (M-D properties from Table 2) cumulative cavern volume closure since 1/1/1990 for West Hackberry Phase 2 caverns, east side.

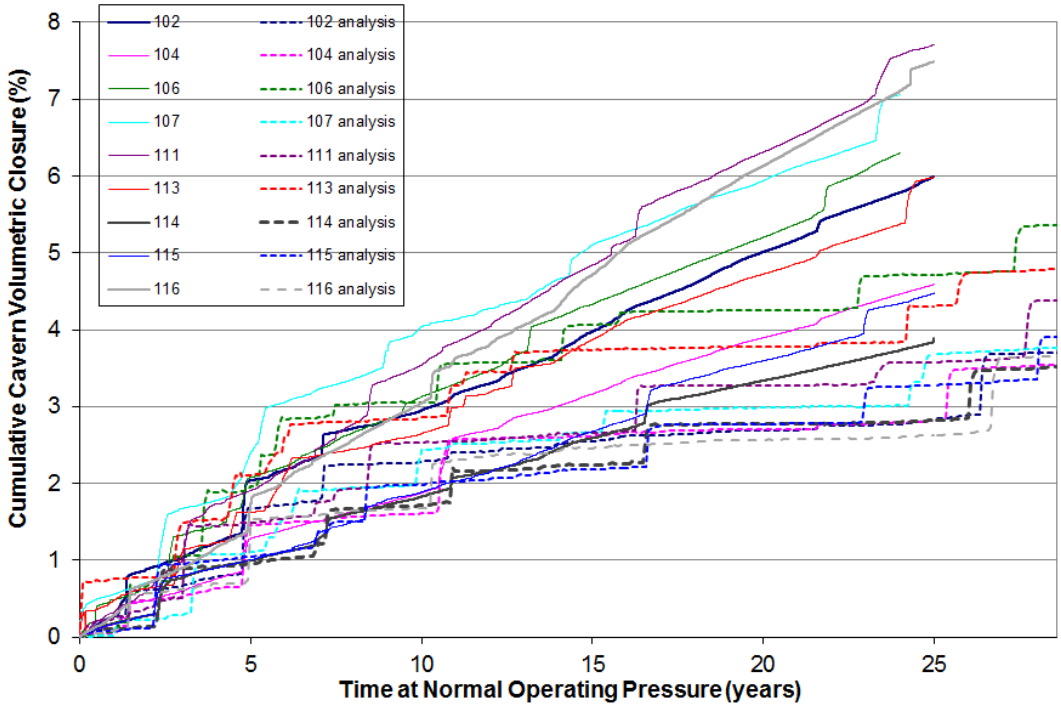

Figure 26. Comparison between measured, predicted (M-D properties from Table 2) cumulative cavern volume closure since 1/1/1990 for West Hackberry Phase 2 caverns, west side.

The other metric used for evaluating the M-D property set is surface subsidence, which is measured at all the wellheads and many monuments across the site. Subsidence measurements at West Hackberry have been documented by many reports over the years (most recently Moriarty, 2014; Sobolik and Lord, 2015), and provide a meaningful measurement of salt behavior below the surface and its effect on surface facilities. Figure 27 through 29 compare the measured versus predicted subsidence for the Phase 1, Phase 2 east side, and Phase 2 west side caverns, respectively. The predictions tend to match the measured values fairly well through about 2002, then diverge from and underpredict the measurements thereafter. Again, the lower predictions indicate that the values for A_2 are too low.

In order to achieve predicted volume closure and surface subsidence that matches more closely the CAVEMAN derived volume closure values and measured surface subsidence, it was decided to apply a multiplication factor to the secondary creep coefficient A2. The cavern volume closure was used as the metric from which to derive multiplication factors, using the difference between least-square fit slopes to determine the factor. In addition, because of the variability of the discrepancies for each cavern, it was decided to apply individual factors to the region surrounding each cavern, as well as to the overall salt dome. Table 3 lists the secondary creep multiplication factors derived for each cavern and for the overall salt dome. These factors are used in the calculations present in Chapter 5 in this report.

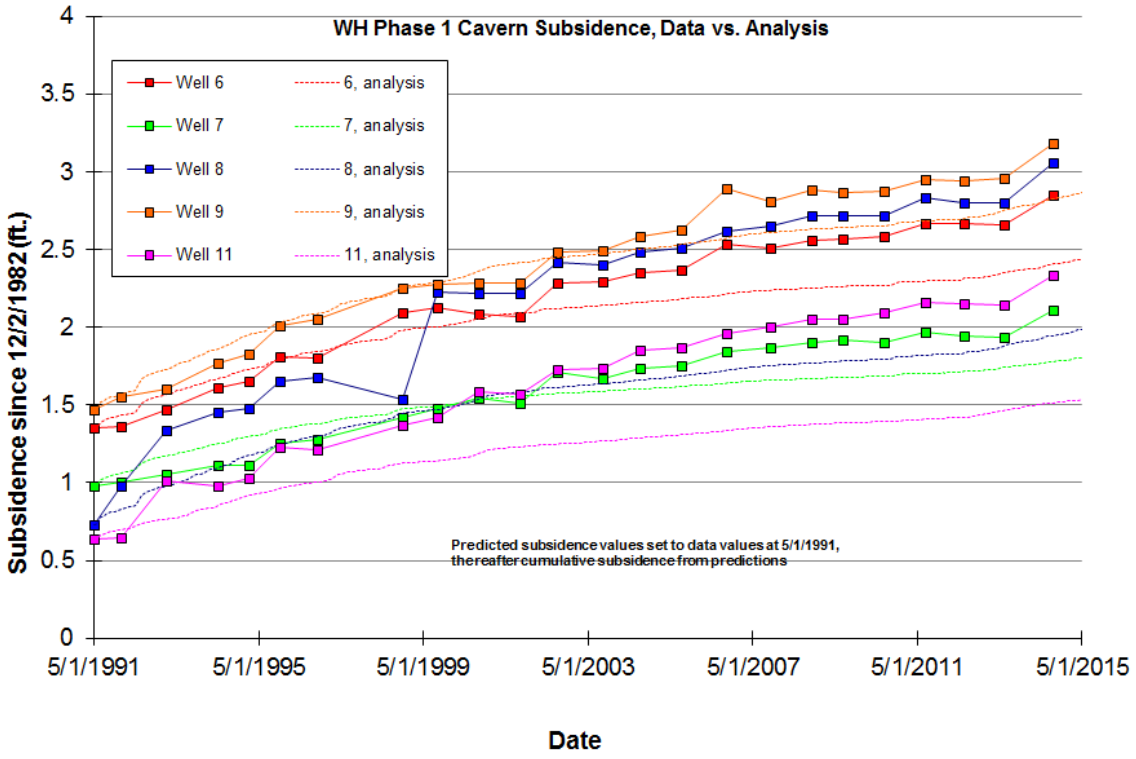

Figure 27. Comparison between measured, predicted (M-D properties from Table 2) surface subsidence since 12/2/1982 for West Hackberry Phase 1 caverns.

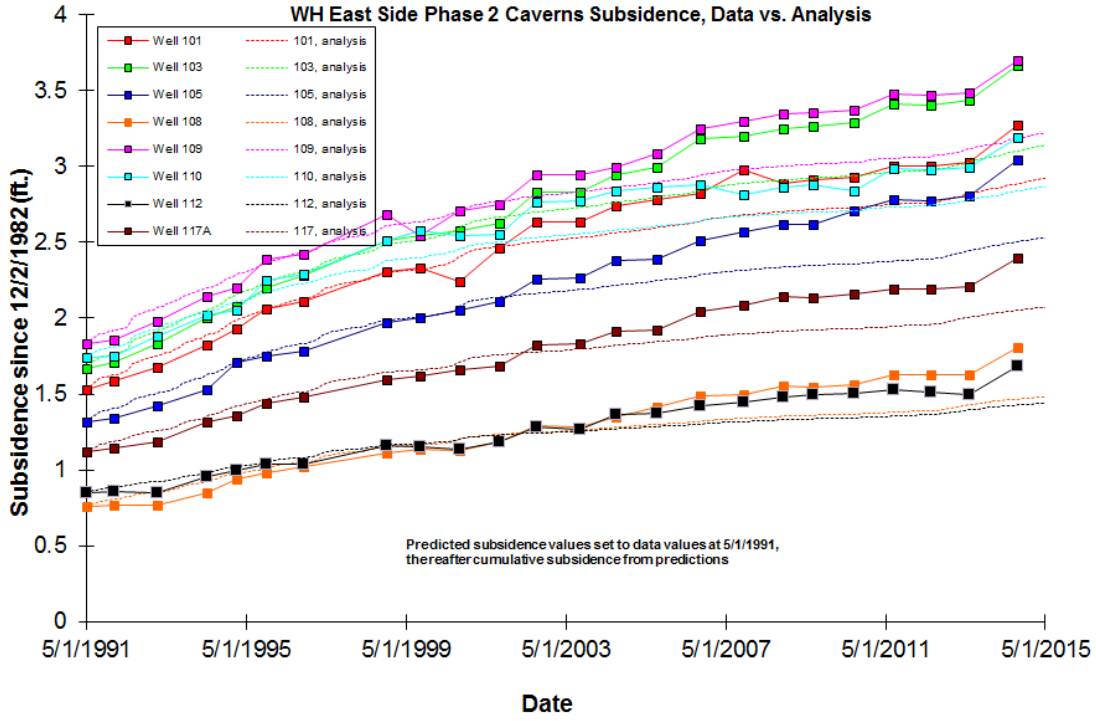

Figure 28. Comparison between measured, predicted (M-D properties from Table 2) surface subsidence since 12/2/1982 for West Hackberry Phase 2 caverns, east side.

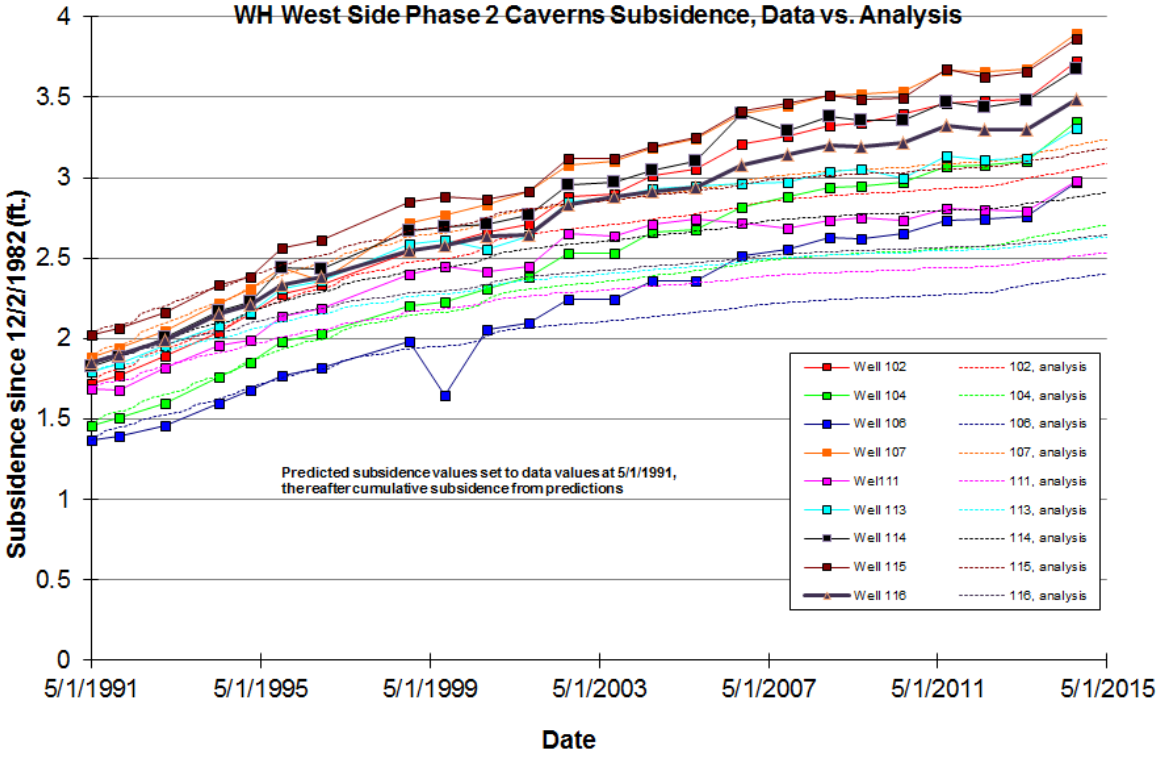

Figure 29. Comparison between measured, predicted (M-D properties from Table 2) surface subsidence since 12/2/1982 for West Hackberry Phase 2 caverns, west side.

Table 3. Multiplication factors applied to the A2 values listed in Table 2.

Cavern	A_2 multiplication factor	Cavern	A_2 multiplication factor
101	1.44	112	1.21
102	2.44	113	1.77
103	2.08	114	1.43
104	1.79	115	1.51
105	2.79	116	3.20
106	1.48	117	1.73
107	2.24	6	1.44
108	1.73	7	1.67
109	1.46	8	0.89
110	2.35	9	1.96
111	2.42	11	1.21
WH Salt	1.80		

The surface overburden layer, which is mostly comprised of sand and sandstone, is considered isotropic and elastic, and has no assumed failure criteria. The caprock layer, consisting of gypsum and limestone, is also assumed to be elastic. These properties have been used for all the West Hackberry analyses. The sandstone surrounding the salt dome is assumed to be elastic

(Lama and Vutukuri, 1978). Mechanical properties of each of these geologic materials used in the present analysis are listed in Table 4.

Table 4: Material properties of other geologic materials.

Parameters	Units	Overburden	Caprock	Sandstone
Density	lbm/ft^3	117.	156.	133.6
Young's Modulus	lb/ft^2	2.09×10^6	146×10^6	153×10^6
Poisson's Ratio		0.33	0.29	0.33

4.5 SALT DAMAGE CRITERION

The salt damage factor (analogous to a safety factor) has been developed from a dilatant damage criterion based on a linear function of the hydrostatic pressure (Van Sambeek et al., 1993). Dilatancy is considered as the onset of damage to rock resulting in significant increases in permeability. Dilatant damage in salt typically occurs at a stress state where a rock reaches its minimum volume, or dilation limit, at which point microfracturing increases the volume. Dilatant criteria typically relate two stress invariants: the mean stress invariant I_1 (equal to three times the average normal stress) and the square root of the stress deviator invariant J_2, or $\sqrt{J_2}$ (a measure of the overall deviatoric or dilatant shear stress). (By convention, tensile normal stresses are positive, and compressive normal stresses are negative, hence the sign nomenclature in the following equations.) The dilatant criterion chosen here is the equation typically used from Van Sambeek et al. (1993),

$$\sqrt{J_2} = -0.27 I_1 . \tag{17}$$

The Van Sambeek damage criterion defines a linear relationship between I_1 and $\sqrt{J_2}$, and such linear relationships have been established from many suites of laboratory tests on WIPP, SPR, and other salt samples. This criterion was applied during post-processing of the analyses. A damage factor (safety factor) index was created (SF_{VS}) by normalizing I_1 by the given criterion:

$$SF_{VS} = \frac{-0.27 I_1}{\sqrt{J_2}} \tag{18}$$

Several earlier publications define that the Van Sambeek damage factor SF_{VS} indicates damage when $SF_{VS}<1$, and failure when $SF_{VS}<0.6$. In previous studies, values of $SF_{VS}<1.5$ have been categorized as cautionary because of unknown localized heterogeneities in the salt that cannot be captured in these finite element calculations. This report will use these damage thresholds.

5. RESULTS

The historical performance of the West Hackberry caverns, and their predicted future performance, will be evaluated on the basis of several design factors: cavern volume closure, surface subsidence, dilatant and tensile stress damage to the salt surrounding the caverns, and axial well strain in the caprock. These performance factors will provide metrics to determine the long-term geomechanical performance of the caverns, and also the number of available drawdowns to expand the storage capacity of the caverns. All of the results in this section use the M-D properties listed in Table 2, with the secondary creep coefficient for each cavern region and the salt dome in general increased by the multiplication factors listed in Table 3. Results from both the calculations using the actual pressure history and the averaged pressure history will be compared in evaluating the predictions for cavern volume closure and surface subsidence. Because the results using the actual pressure histories matched the available data better, the results from those calculations will be used to assess the additional performance factors. However, the use of the averaged pressure history provides interesting information that will be used to refine future analyses and develop a predictive capability for pressure changes in adjacent caverns during workovers.

5.1 CAVERN VOLUME CLOSURE

The volume of the caverns decreases as the salts creeps. The figures in this section compare the predicted cavern volume closure (as a precentage normlaized by initla cavern volume) and that back-calculated from measured wellhead pressure data using CAVEMAN. Predicted cavern closure up to the present, and into the future, depends upon the timing of workover operations, during which the caverns undergo their greatest deformation, and of future cavern expansion (leaching) operations. Figures 30 and 31 show the predicted and measured cumulative cavern closure for the Phase 1 caverns for the actual and averaged pressure simulations, respectively; these figures can also be compared with Figure 24 that had the original M-D peroperties and the actual pressure history. In a similar fashion, Figures 32 and 33 present the cavern closure for the Phase 2 east side caverns (and may be compared with Figure 25), and Figures 34 and 35 present for the Phase 2 west side caverns (compare to Figure 26). All of these figures show the amount of cavern closure from 1990 through 2014.

First, a general analysis of the closure behavior of the caverns is important. Table 5 summarizes the results in Figures 30 through 35 by listing the measured and predicted cumulative cavern closure from 1990 through 2013 for each of the caverns. Caverns 6, 103, 105, 107, 111, 116, and 117 exhibit the highest percentage cavern closure. These caverns are spread out over different areas of the site, so it is difficult to find any correlation between location and magnitude of closure. The Phase 1 caverns, with the exception of WH-6, tend to experience lower closure than the Phase 2 caverns, likely due to their relatively shallow bases; the greater difference between oil and in situ pressure at greater depths result in greater closure at the bottom of caverns. WH-6 closure is markedly higher than the other Phase 1 caverns due to its large-diameter ceiling, which has deflected nearly 12 feet over the oil storage life of the cavern. There does not seem to be any corrleation among the Phase 2 caverns between initial volume, depth of bottom of cavern, or location with the amount of cavern closure.

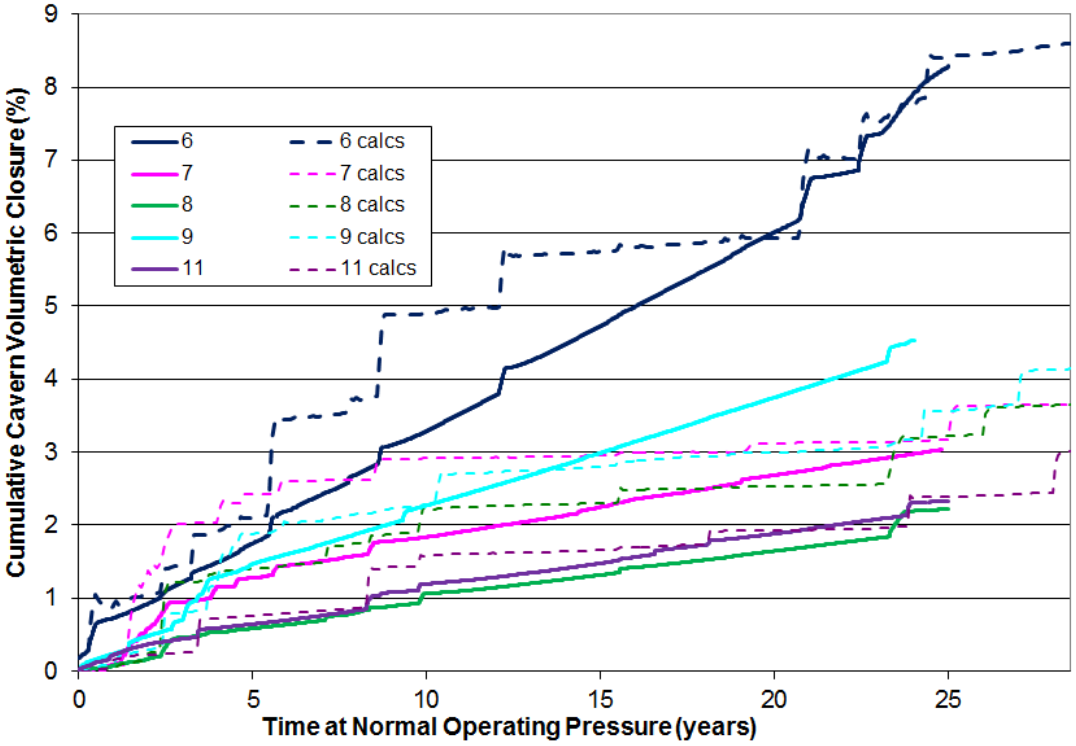

Figure 30. Comparison between measured, predicted (actual pressure history) cumulative cavern volume closure since 1/1/1990 for West Hackberry Phase 1 caverns.

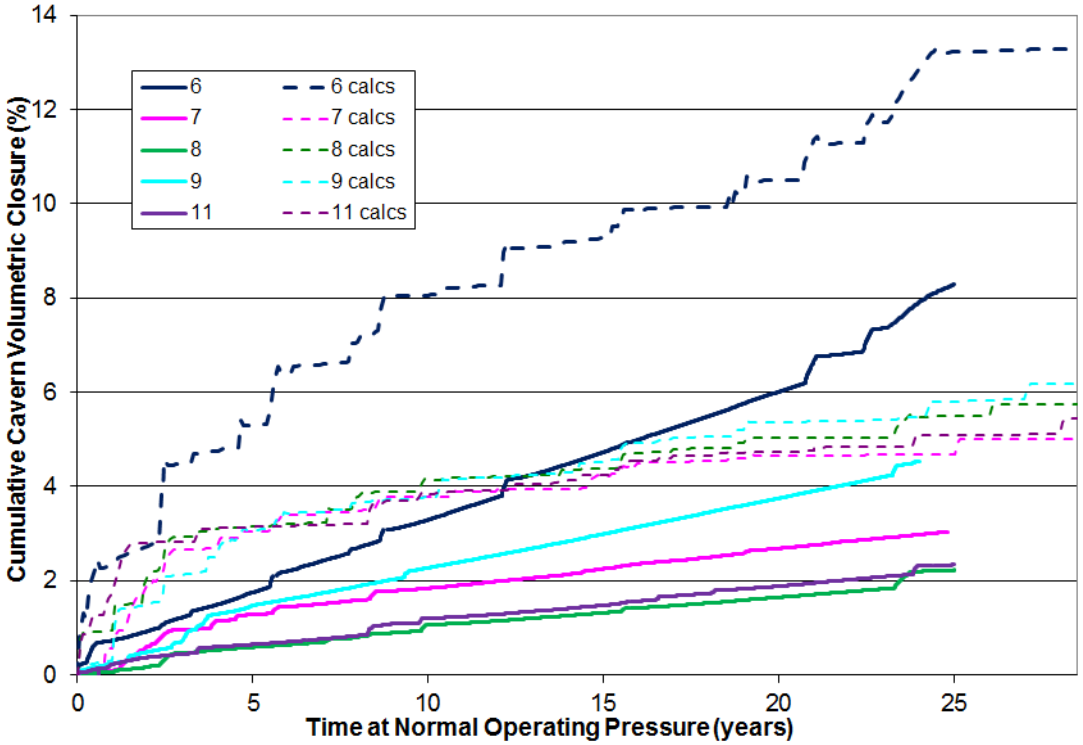

Figure 31. Comparison between measured, predicted (average pressure history) cumulative cavern volume closure since 1/1/1990 for West Hackberry Phase 1 caverns.

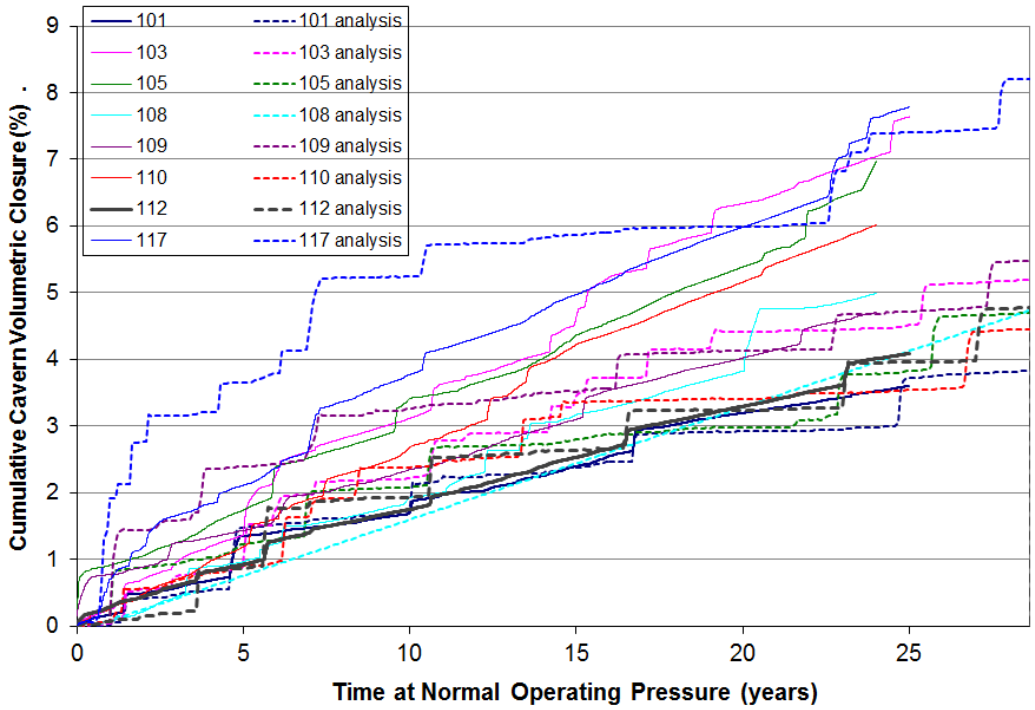

Figure 32. Comparison between measured, predicted (actual pressure history) cumulative cavern volume closure since 1/1/1990 for West Hackberry Phase 2 caverns, east side.

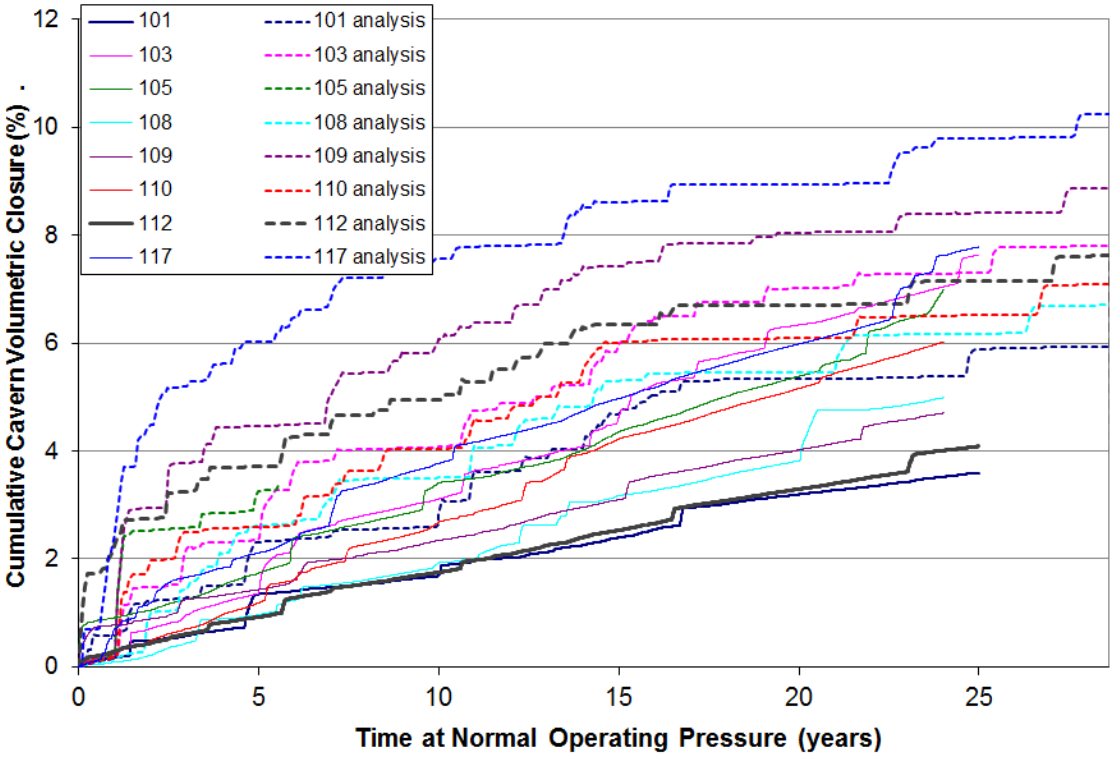

Figure 33. Comparison between measured, predicted (average pressure history) cumulative cavern volume closure since 1/1/1990 for West Hackberry Phase 2 caverns, east side.

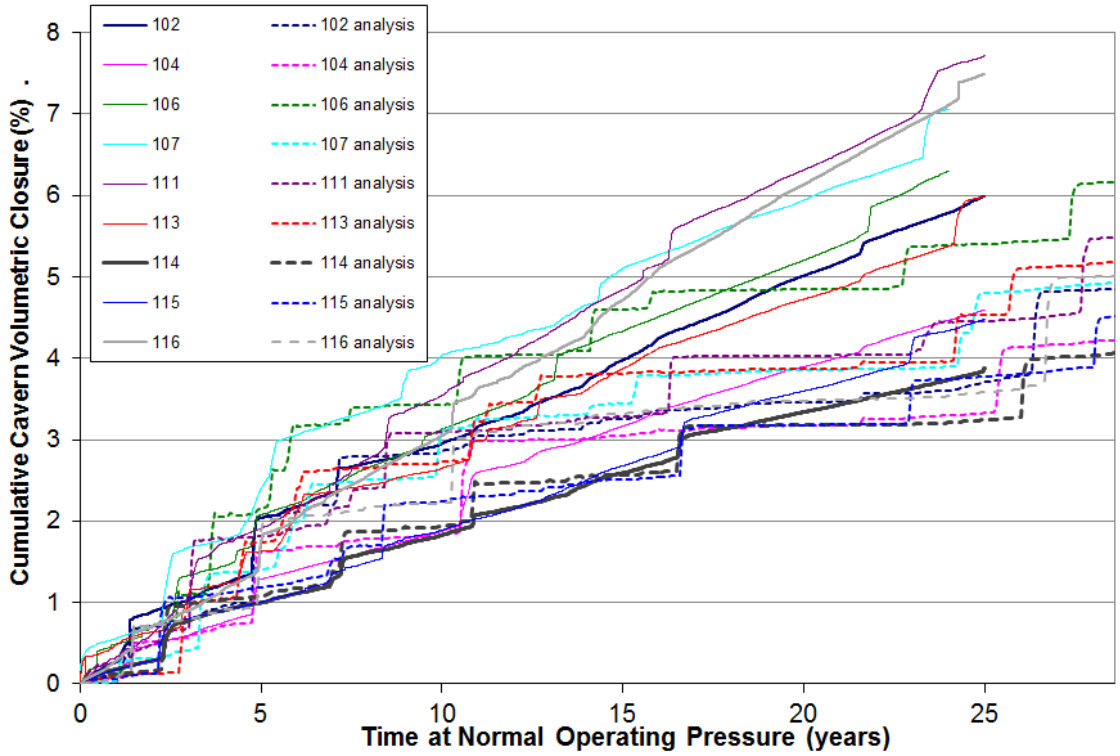

Figure 34. Comparison between measured, predicted (actual pressure history) cumulative cavern volume closure since 1/1/1990 for West Hackberry Phase 2 caverns, west side.

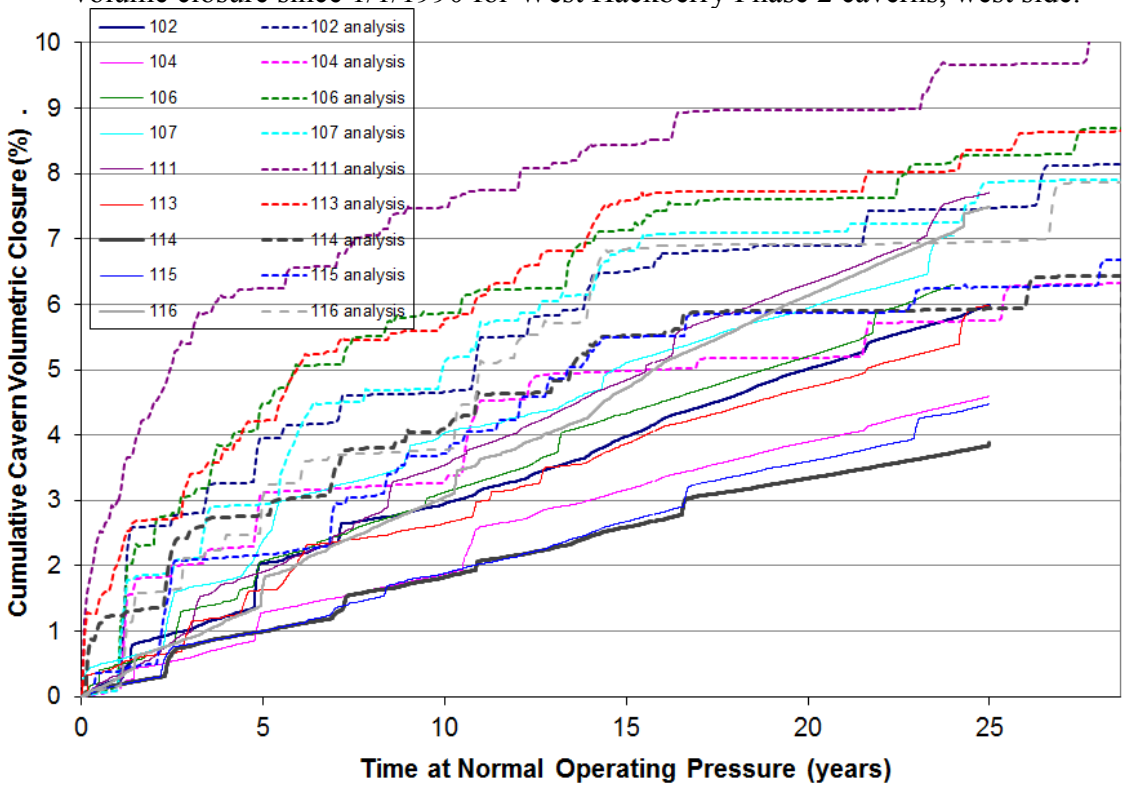

Figure 35. Comparison between measured, predicted (average pressure history) cumulative cavern volume closure since 1/1/1990 for West Hackberry Phase 2 caverns, west side.

Table 5. Total percentage cavern volume closure, 1990-2013, measured and predicted.

WH Cavern	Data (CAVEMAN)	Actual Pressures	Average Pressures	WH Cavern	Data (CAVEMAN)	Actual Pressures	Average Pressures
101	3.5	3.0	5.4	112	4.0	4.0	7.2
102	7.0	5.8	7.5	113	5.4	4.5	8.0
103	7.0	4.5	7.3	114	3.7	3.2	5.9
104	4.5	3.3	5.8	115	4.3	3.8	6.3
105	7.0	3.8	7.8	116	7.1	3.6	6.9
106	6.3	5.4	8.3	117	7.6	7.4	9.8
107	7.0	5.8	7.3	6	7.9	7.8	12.9
108	5.0	4.1	6.2	7	3.0	3.2	4.5
109	4.7	4.7	8.4	8	2.2	3.2	5.5
110	6.0	3.5	6.5	9	4.5	3.2	5.5
111	7.6	4.5	9.7	11	2.3	2.4	5.1

For the comparison between measured (CAVEMAN) and predicted values, two immediate observations can be made. First, the slopes of the steady-state periods between workovers are still significantly different between measurements and predictions. The calculations with the averaged pressure histories exhibit somewhat closer behavior to the measured closure data than do the predictions using the actual pressure histories, but the pressurization rates still differ substantially. This observation suggests that an increase of the magnitudes of the secondary creep coefficients may not be sufficient to match the measured closure rates. This result leads to at least one of the following conclusions: one, other M-D parameters, such as the primary creep coefficient A1, or the primary and secondary creep exponents n1 and n2, may also need to be modified to provide a better match to the measured results; and two, the method used in CAVEMAN to back-calculate the cavern volume closure may itself need to be reexamined to determine its correctness. The second observation is that the predictions using the actual pressure histories tend to underpredict the overall cavern closures, whereas the results using the averaged pressure histories tend to overpredict the cavern closures, and the difference between the predictions are substantial. This large difference in predicted results was not expected, and may be caused by several phenomena, including the pre-orientation of the cavern volumes in the actual pressure calculations to close less due to the actual presure increases, and the "zeroing out" of wellhead pressures below 700 psi for periods in the vicinity of workovers or other periods of lower wellhead pressure. The cumulative differences of the predictions with the actual pressures with the CAVEMAN values are significantly less than those using the averaged pressures; this is not proof that one waty is better than the other, but it does indicate which simulation will be used to examine other cavern performance criteria.

5.2 SURFACE SUBSIDENCE

The issue of surface subsidence is an important design and operations factor for surface facilities, especially for those located in flood prone areas, but subsidence also results in horizontal ground strains that can damage buildings, pipelines, and other infrastrusture. The SPR is currently over 30 years old and the life of the SPR may extend another 30 years depending upon a number of factors, including oil consumption, import dependency, and geopolitical instability. Expected subsidence during a 100-year life of an SPR site on the order of up to ten feet is possible. Therefore, a reliable prediction of surface subsidence can be very valuable for site management. The plots in Figures 36 through 41 that compare surface subsidences measured since 5/1/1991 to predicted values for both the calculations with the actual and averaged pressure histories. Much like in the previous section, Figures 36 and 37 show the predicted and measured surface subsidence above the Phase 1 caverns for the actual and averaged pressure simulations, respectively, and can be compared with Figure 27; Figures 38 and 39 present the subsidence over the Phase 2 east side caverns (and may be compared with Figure 28), and Figures 40 and 41 present for the Phase 2 west side caverns (compare to Figure 29). Similar to the predictions for the cavern volume closure, the simulations using the actual pressure histories still tend to underpredict the surface subsidence, whereas the simulations using the averaged pressure histories tend to overpredict it, particularly after 2006. Both sets of calculations exhibit a decrease in the rate of subsidence starting about 2006, whereas the data exhibit little if any significant change in their rate. The relative stability of the measured subsidence rate has previously been reported, as shown in Figure 42 (Moriarty, 2014). It is unknown why both sets of simulations predict this change in subsidence rate when the measurement do not, and the historical cavern pressures are being used; there may be other factors, such as regional subsidence, inelastic mechanics of the overburden, or uncaptured creep behavior, that are not adequately addressed in the model. Another interesting observationis that the predictions for subsidence over the Phase 1 and Phase 2 east side caverns seem match the data better than those for the Phase 2 west side caverns; this may be due to the estimate used for the pressure history of the Sempra caverns. Figure 43 plots the predicted cumulative surface subsidence since 5/1/1991, using the actual pressure history results. The center of the “bulls-eye” appears over Cavern 103, in the middle of the cavern field, which demonstrates that the predictions indicate no unusual influence of the Phase 1 caverns on the surface subsidence footprint. This conclusion agrees with the results of the surface subsidence measurements taken over the past 25 years. (This is different than the Bryan Mound site, in which the data indicate an inordinate influence on subsidence of the abandoned cavern BM-3 (Sobolik & Ehgartner, 2009), which the reported analyses confirm.)

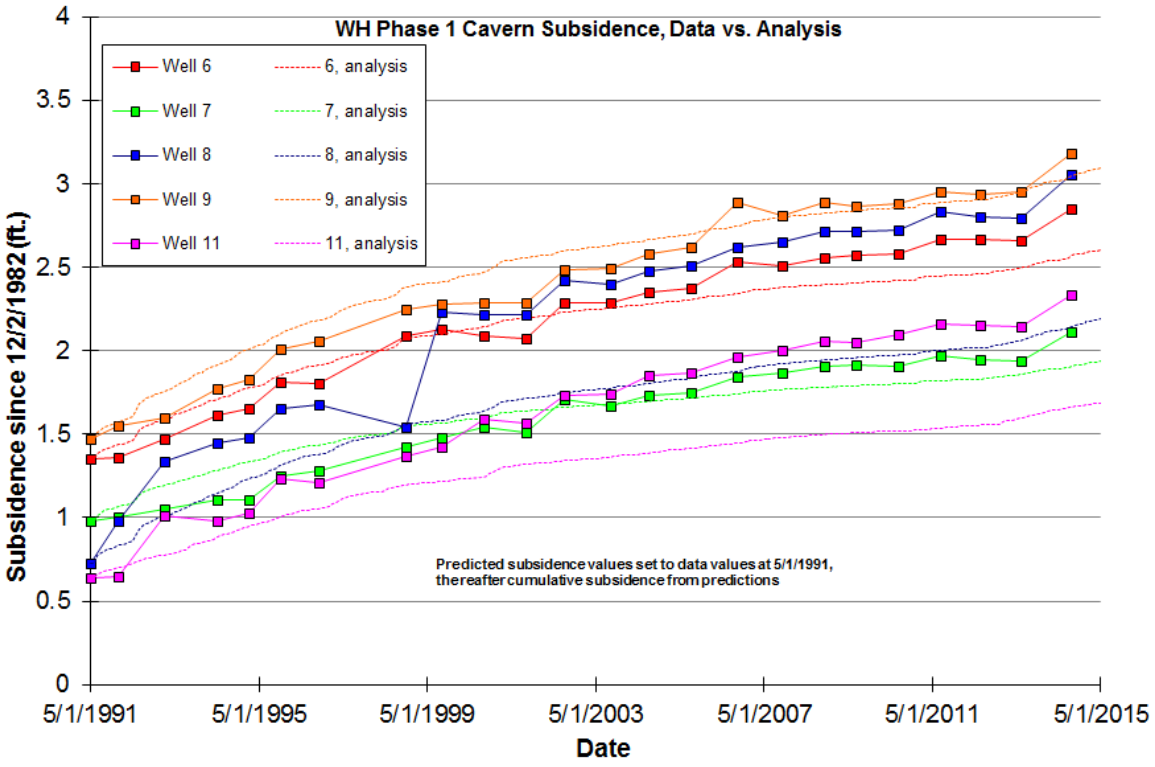

Figure 36. Comparison between measured, predicted (actual pressure histories) surface subsidence since 12/2/1982 for West Hackberry Phase 1 caverns.

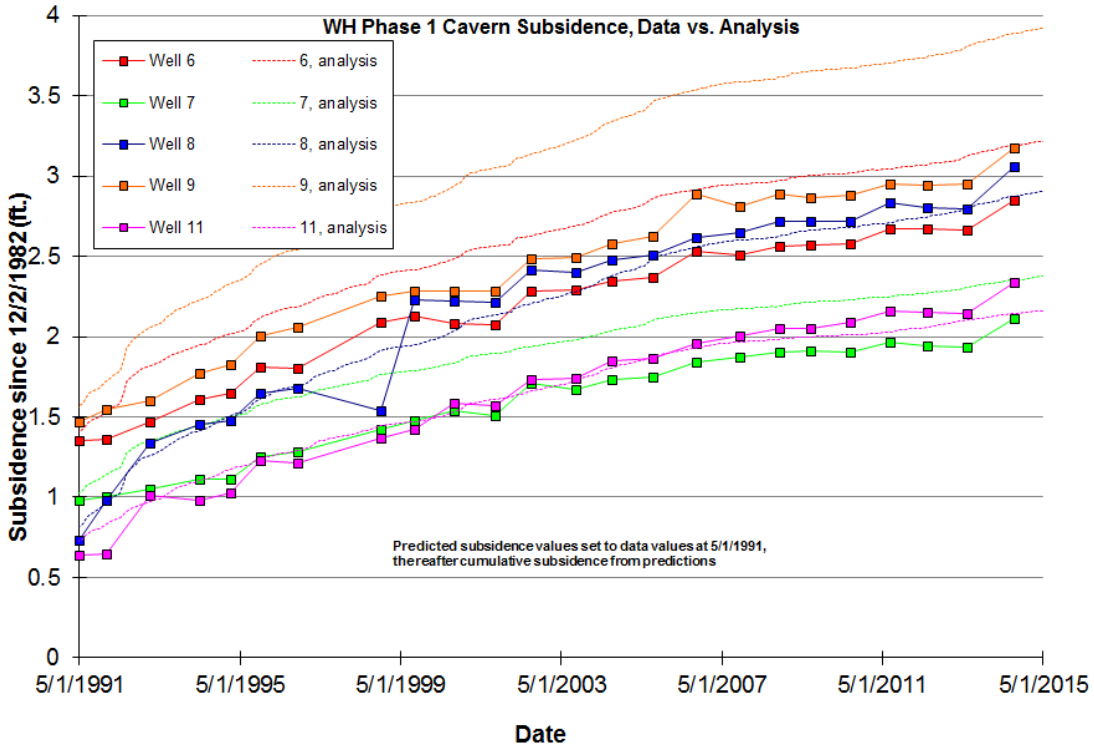

Figure 37. Comparison between measured, predicted (average pressure histories) surface subsidence since 12/2/1982 for West Hackberry Phase 1 caverns.

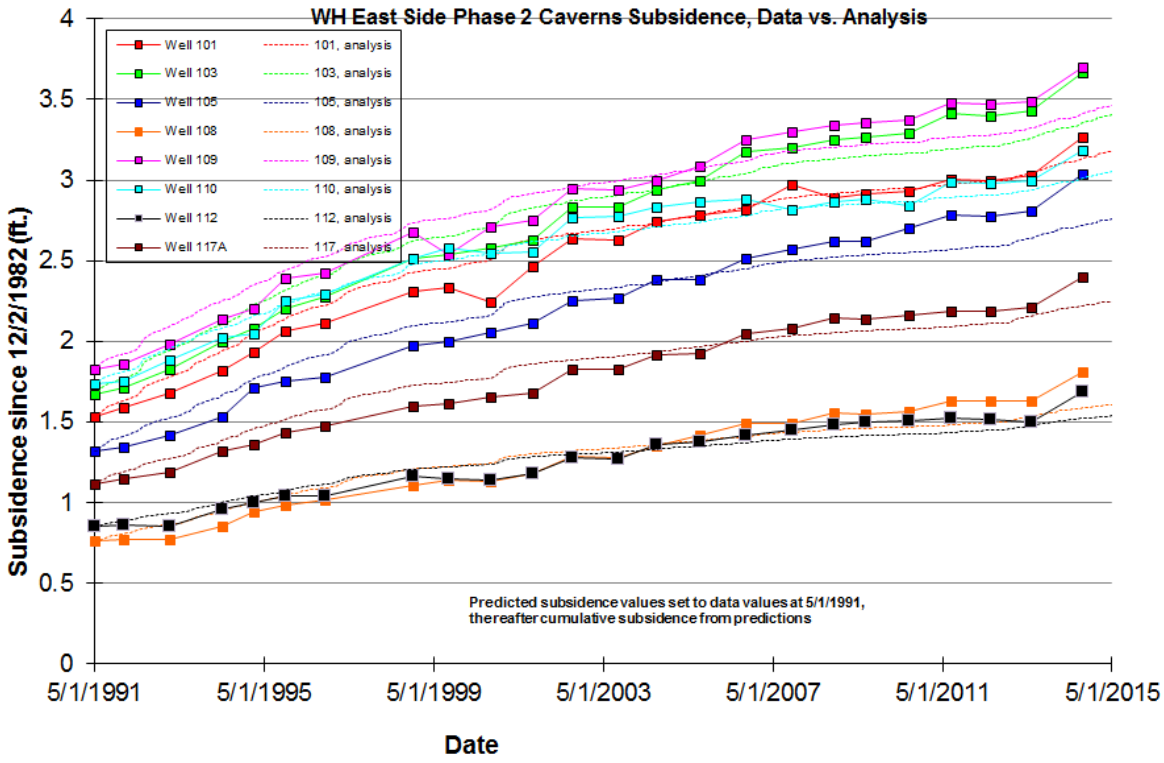

Figure 38. Comparison between measured, predicted (actual pressure histories) surface subsidence since 12/2/1982 for West Hackberry Phase 2 caverns, east side.

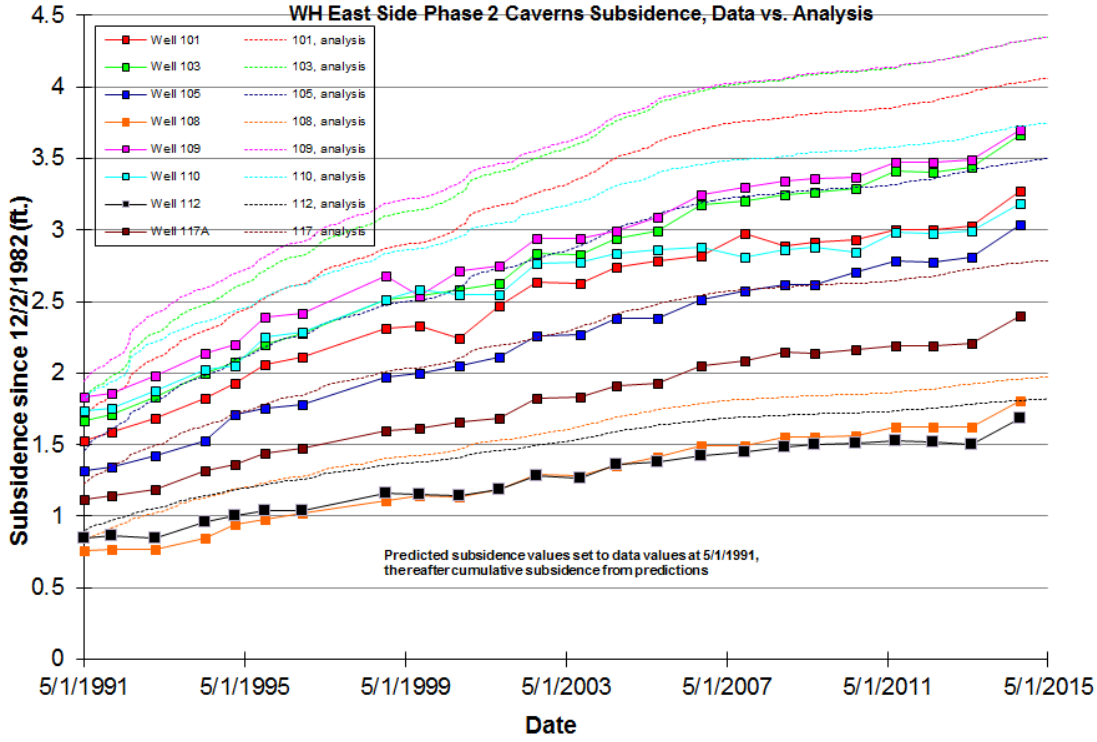

Figure 39. Comparison between measured, predicted (average pressure histories) surface subsidence since 12/2/1982 for West Hackberry Phase 2 caverns, east side.

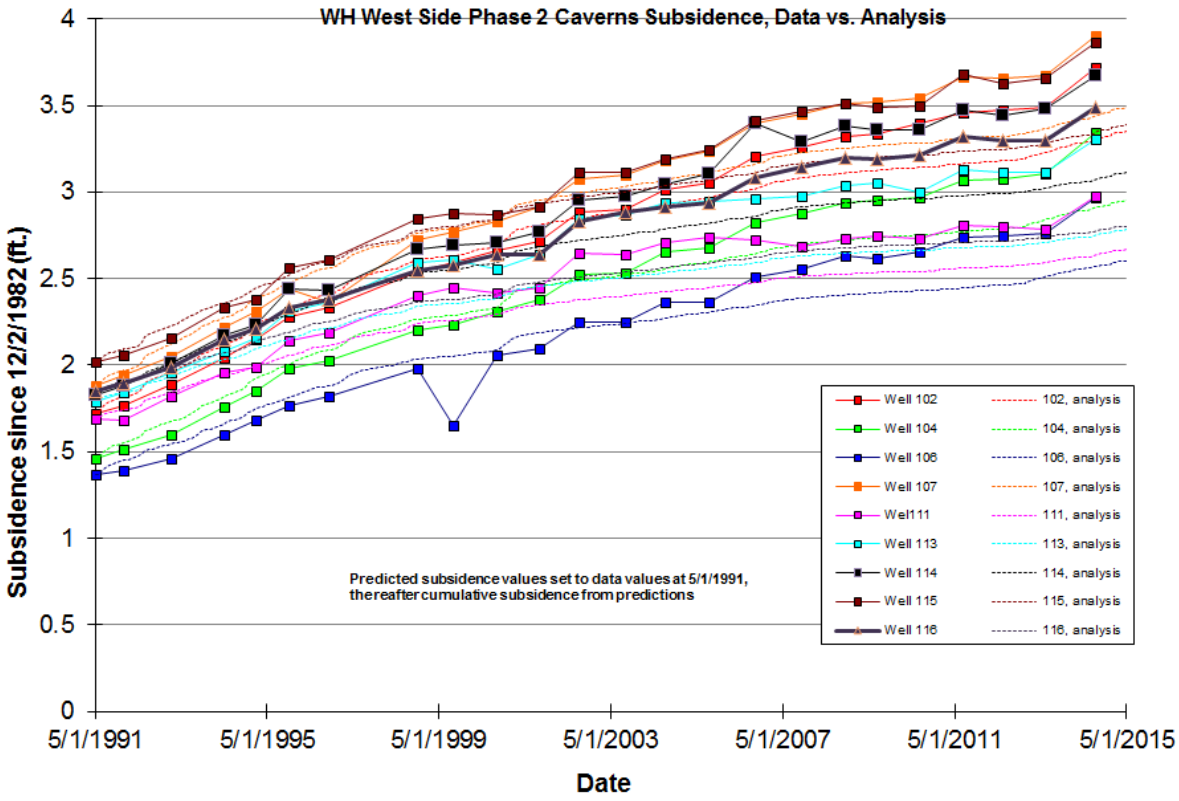

Figure 40. Comparison between measured, predicted (actual pressure histories) surface subsidence since 12/2/1982 for West Hackberry Phase 2 caverns, west side.

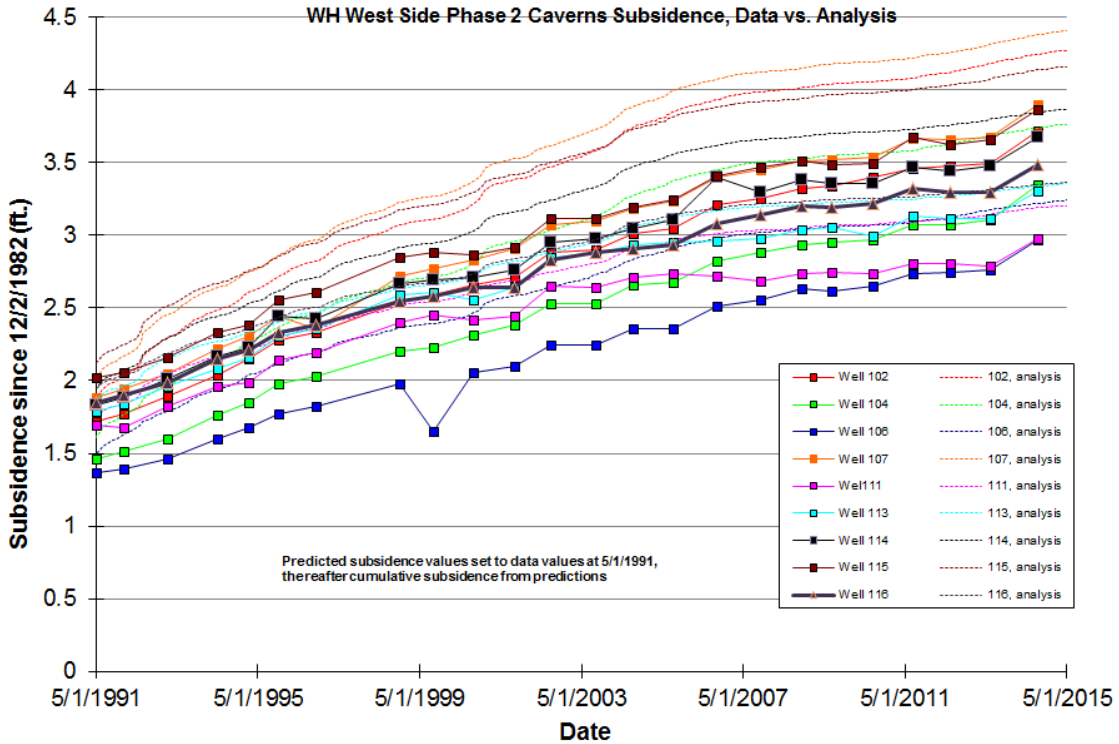

Figure 41. Comparison between measured, predicted (average pressure histories) surface subsidence since 12/2/1982 for West Hackberry Phase 2 caverns, west side.

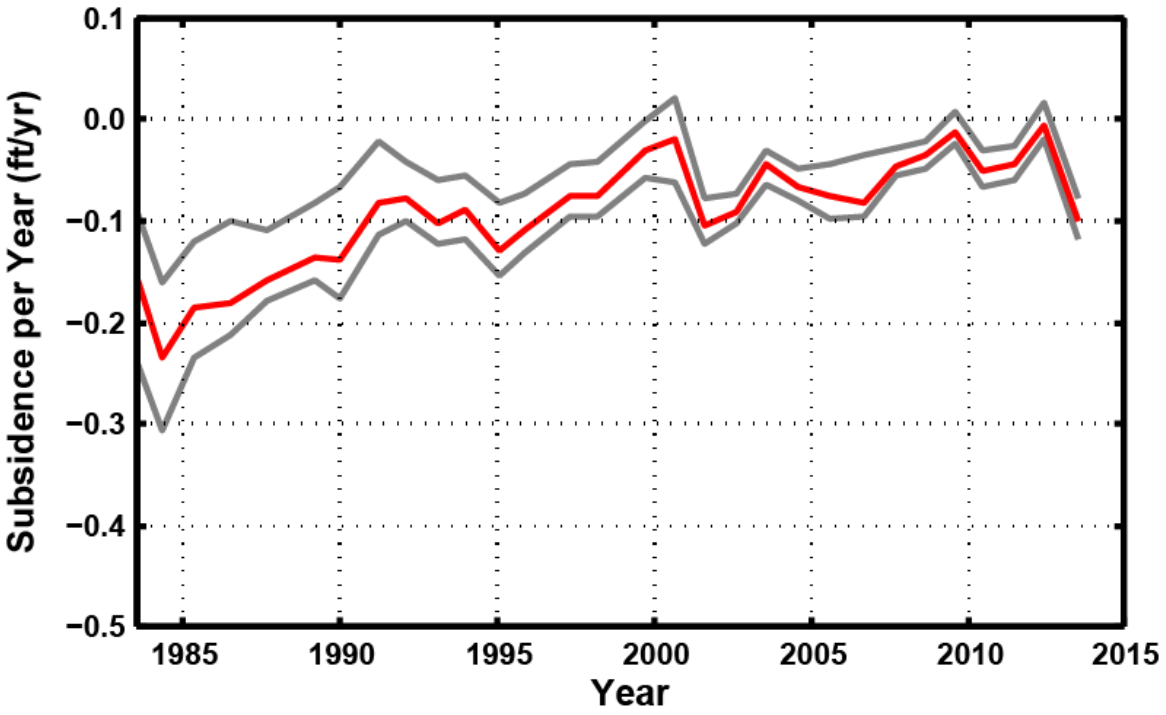

Figure 42. West Hackberry median subsidence rate periods (red) with the 10th and 90th percentiles (grey) measured biennially (Moriarty, 2014).

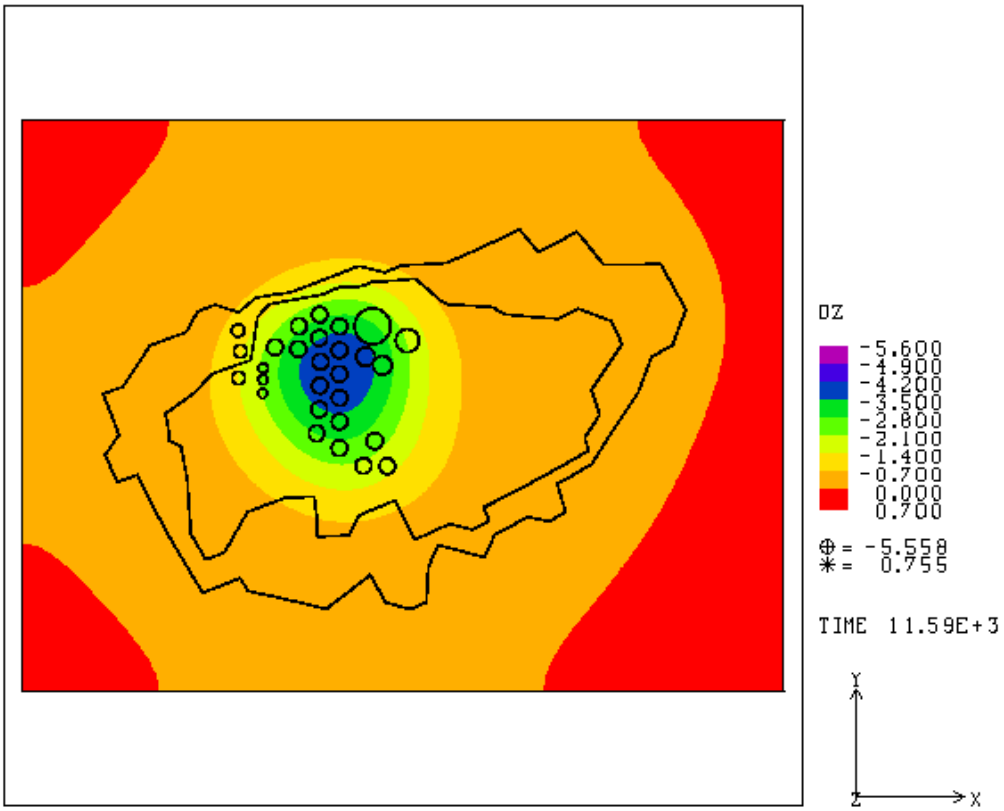

Figure 43. Contour plot of predicted cumulative surface subsidence between 5/1/1991 and 8/22/2014, simulation with actual pressure history.

The cumulative differences in surface subsidence between the measurements and each of the simulations are nearly equal. Because of the very good subsidence match for the east side caverns from the actual pressure history calculations, and also the overall better match for cavern volume closure, the results from the simulation using actual wellehad pressures will be used for the remainder of the analysis of overall cavern behavior.

Figures 44 through 46 show the predicted surface subsidence rate at the three most recent time intervals over which subsidence data were acquired. The predicted maximum subsidence rate varies between 0.03 and 0.08 feet/year, very similar to the rates derived from the measured subsidence. The location of the maximum subsidence rate varies somewhat – between caverns 9 and 109 in 2011-12, just to the east of cavern 101 in 2012-13, and just to the east of cavern 103 in 2013-14. These movements reflect the result from workovers and other pressure-changing activities in those caverns over time.

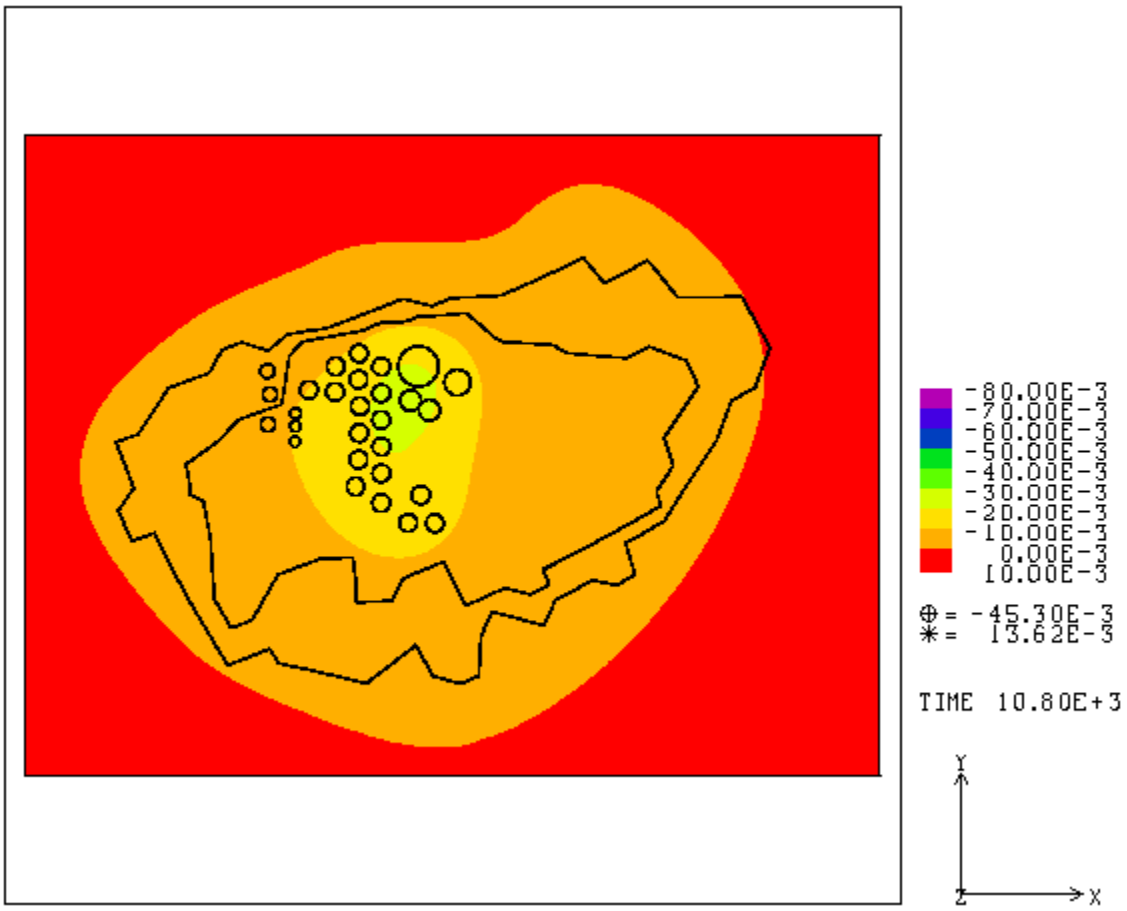

Figure 44. Predicted subsidence rate, in feet/year, betweenJune 2011 and June 2012.

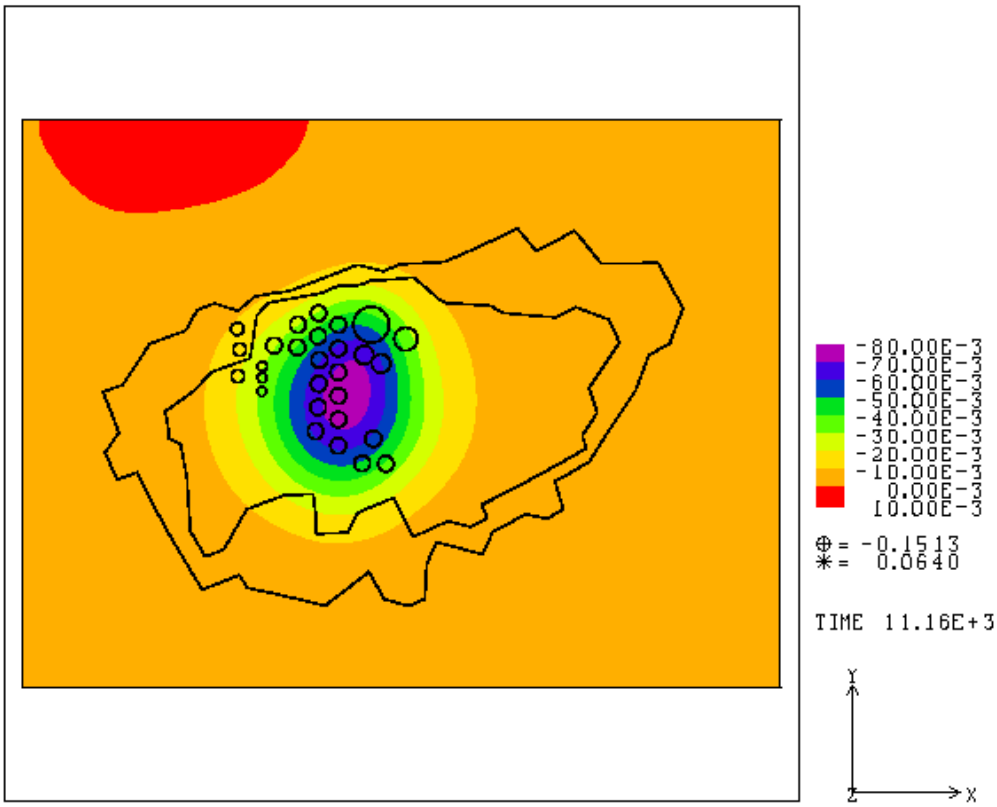

Figure 45. Predicted subsidence rate, in feet/year, betweenJune 2012 and August 2013.

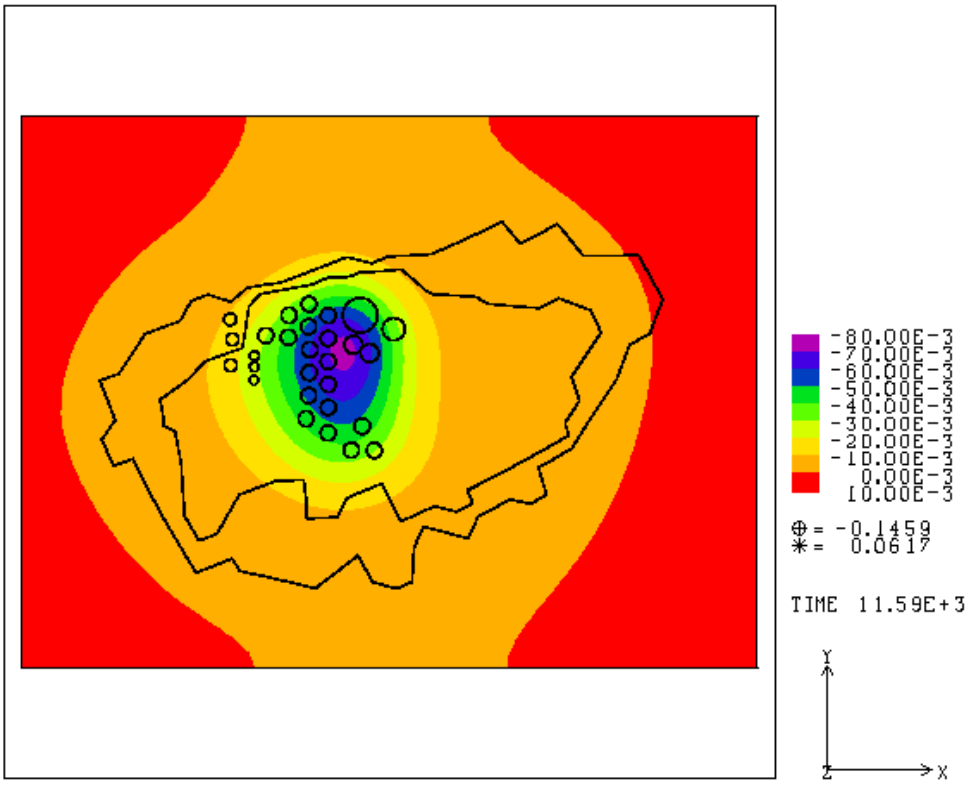

Figure 46. Predicted subsidence rate, in feet/year, between August 2013 and August 2014.

Figures 47 through 49 show the predicted surface displacement with the assumed workover and cavern expansion cycles out to the year 2044 (when the facility is approximately 60 years old). The predictions indicate surface subsidence of an additional three feet between 2014 and 2044, to a maximum of nearly 7 feet since 1991. Because the surface structures at the wellhead are at elevations between 4 and 18 feet above sea level, the predicted subsidence may cause some of the wellheads to sink below sea level by the 2030s.

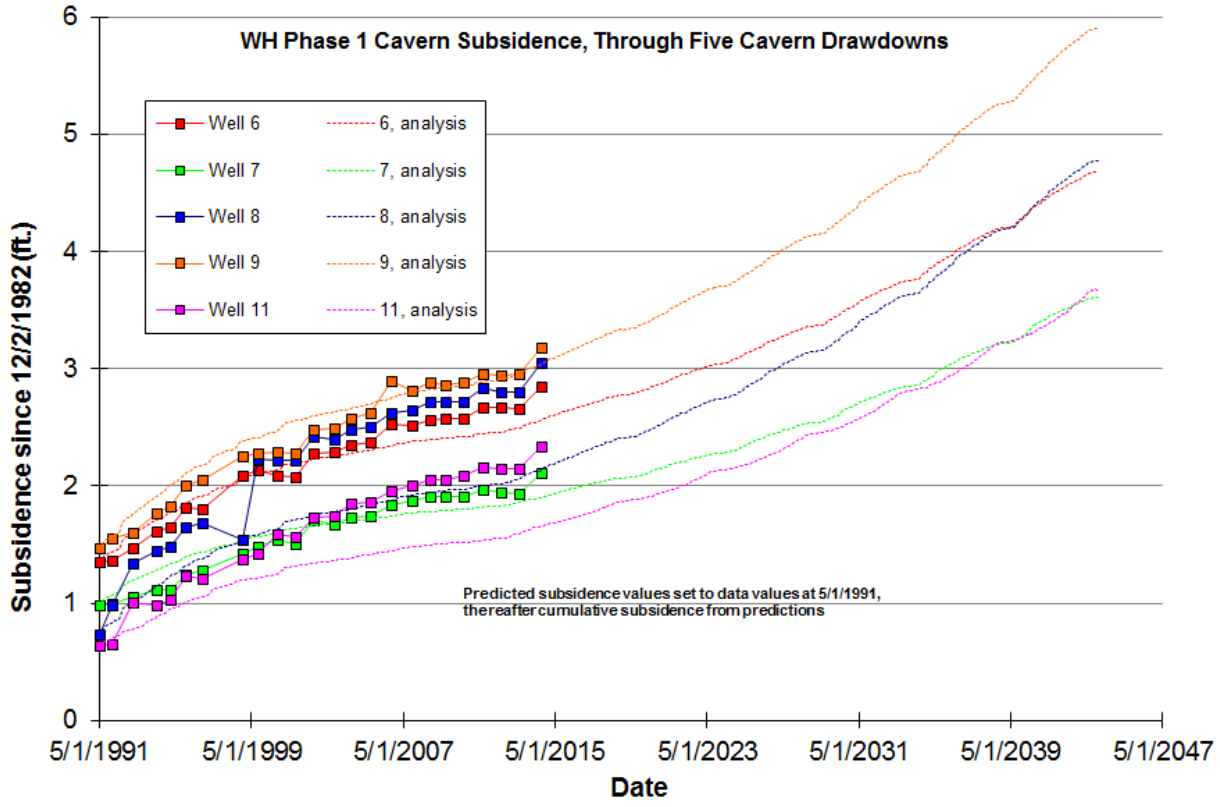

Figure 47. Predicted subsidence over the Phase 1 caverns through 5 cavern drawdowns, to 2044.

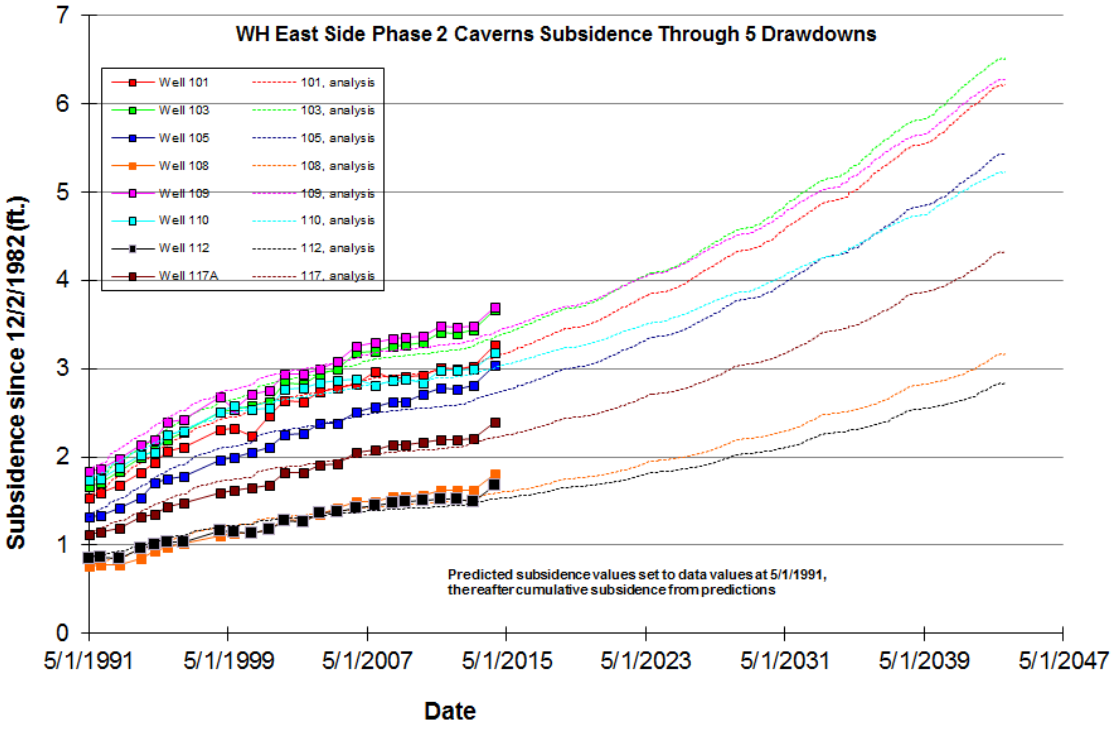

Figure 48. Predicted subsidence over the Phase 2 east side caverns through 5 cavern drawdowns, to 2044.

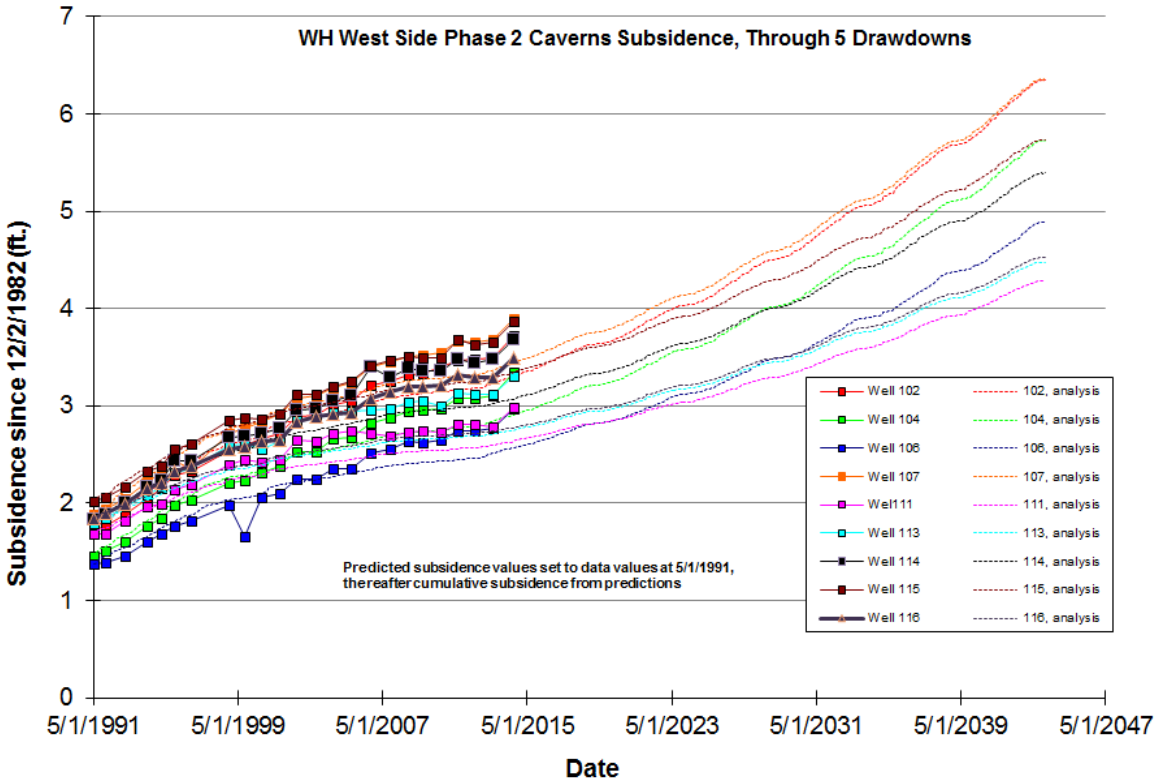

Figure 49. Predicted subsidence over the Phase 2 west side caverns through 5 cavern drawdowns, to 2044.

Structural damage on the surface is typically caused by large accumulated surface strains caused by surface subsidence. These strains can cause distortion, damage, and failure of buildings, pipelines, roads, bridges, and other infrastructure. Surface strains will accumulate in structures over time, which increases the possibility of damage in older facilities. Typically, subsidence strains tend to be compressive in the central portion of the subsided area and become tensile in nature for areas farther removed. Some guidance and solutions are available to evaluate the predicted surface strains. These criteria vary from country to country, possibly because of different building codes and structural materials. Some examples of allowable strains are presented by Peng (1985). The criteria vary in some countries depending on application. For purposes of this report, the allowable strain is taken to be 1 millistrain for both compression and tension. Criteria for shear strains have not been found, perhaps because they are less important. In practice, allowable strain limits for a structure are design specific and should be examined on a case-by-case basis.

The horizontal surface strains are related to the subsidence above the caverns. Typically, the region above the caverns undergo compressive horizontal stresses at the surface as the geologic units sag, but at some distance away from the cavern field the horizontal strains become tensile as the surface rises up to its original elevation. Figure 50 shows the maximum compressive and tensile strains at the surface as a function of time. This figure shows that the 1-millistrain threshold for compressive strains could be exceeded by the year 2015. The tensile strains do not exceed the threshold, but are also significant. A better understanding of the effects of these strains can be gained by looking at contour plots of strain at the surface over the salt dome. Figure 51 shows the predicted minimum horizontal principal strains at the surface at August 2014. By convention, negative strains are compressive, and positive strains are tensile. The minimum principal strains (i.e., maximum compressive strains) are centered above Cavern 109, and become steadily less compressive radially from that point. A similar plot of the maximum horizontal principal strains on the surface in August 2014 is shown in Figure 52. Tensile horizontal strains occur around the perimeter of the SPR cavern field, including the areas over some of the Phase 1 caverns and caverns 112 and 117. Figures 53 and 54 show the west-east and north-south directional strains, respectively. As would be expected, high tensile strains in the east-west direction are located on the east and west sides of the SPR footprint, and similarly the highest north-south strains are on the north and south sides. Most importantly, tensile surface strains are not expected to exceed 1 millistrain due to normal operations and five drawdown cycles through the year 2043. The most significant long-term concern for structure and infrastructure stability on the surface from subsidence will be due to compressive strains in the center of the SPR footprint.

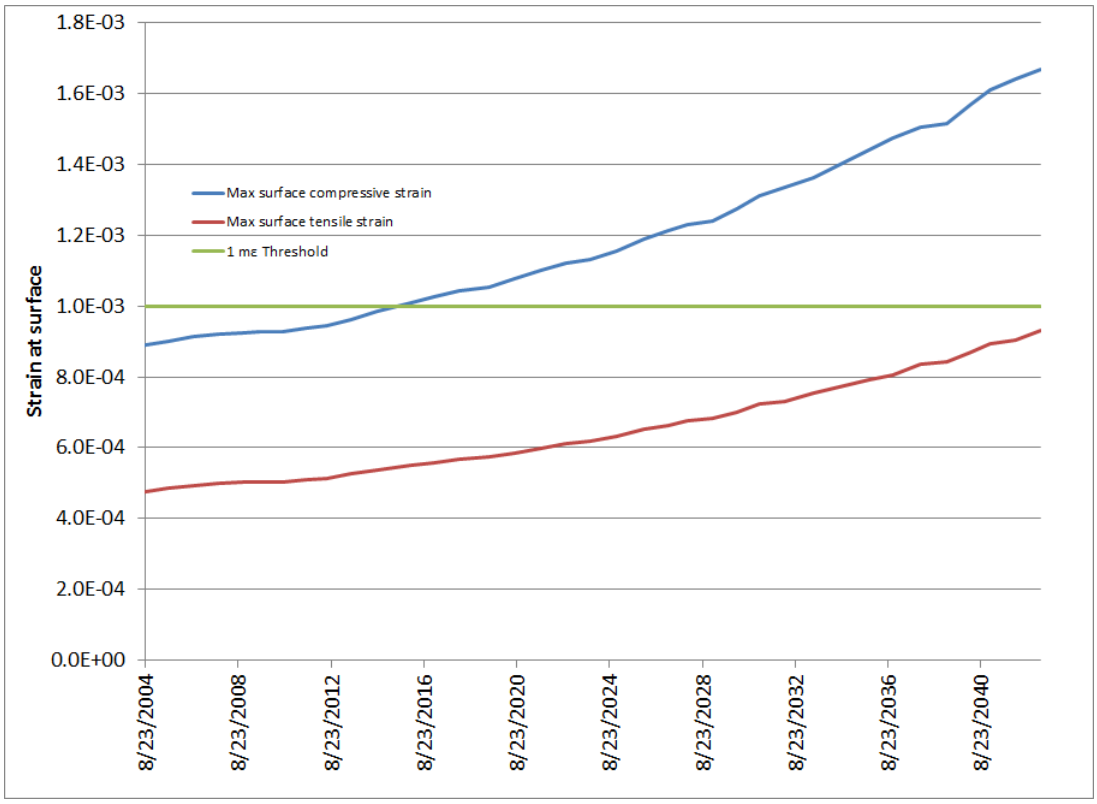

Figure 50. Predicted maximum horizontal compressive and tensile strains as a function of time.

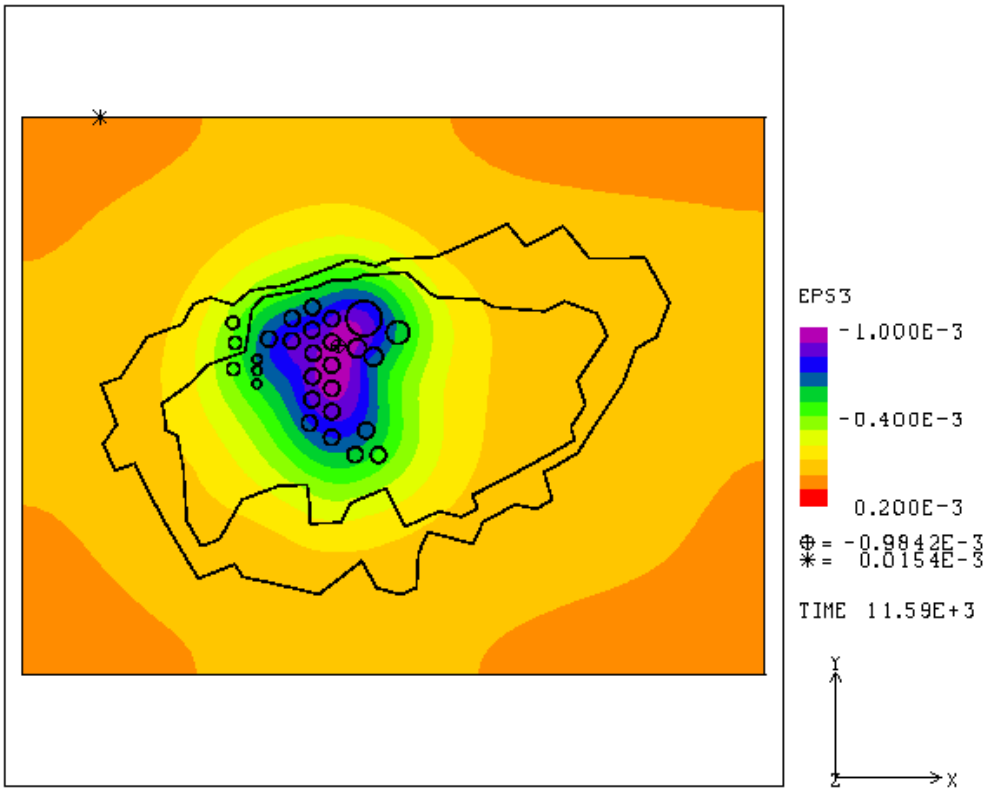

Figure 51. Minimum horizontal principal strains at the surface (negative strains in compression).

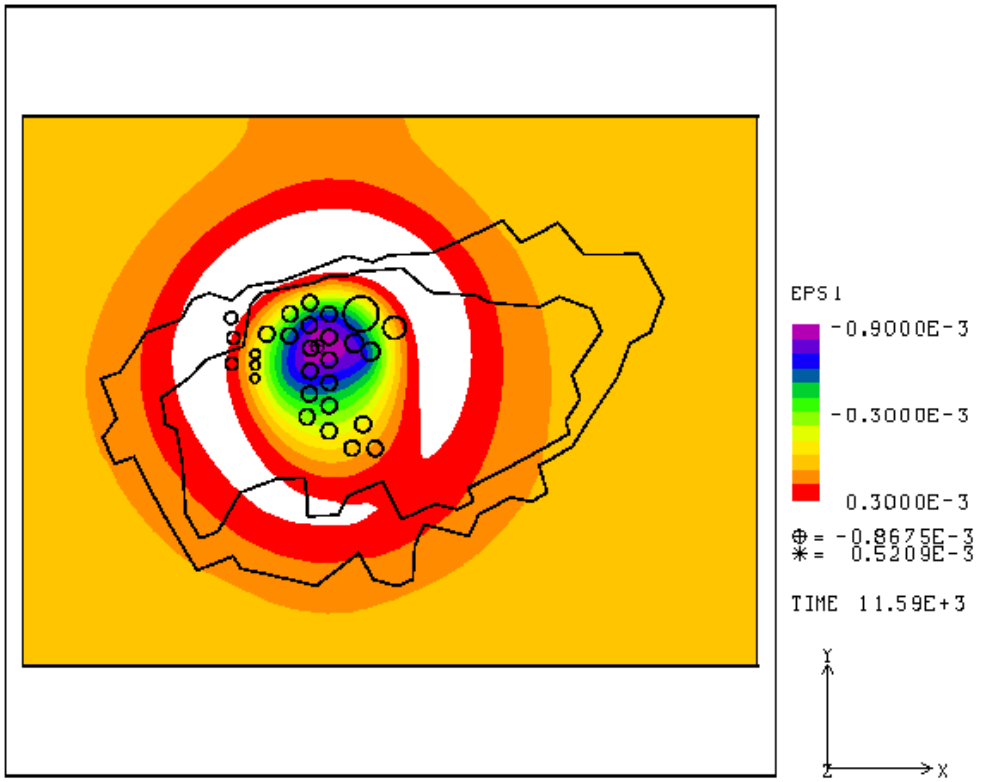

Figure 52. Maximum horizontal principal strains at the surface (positive strains in tension).

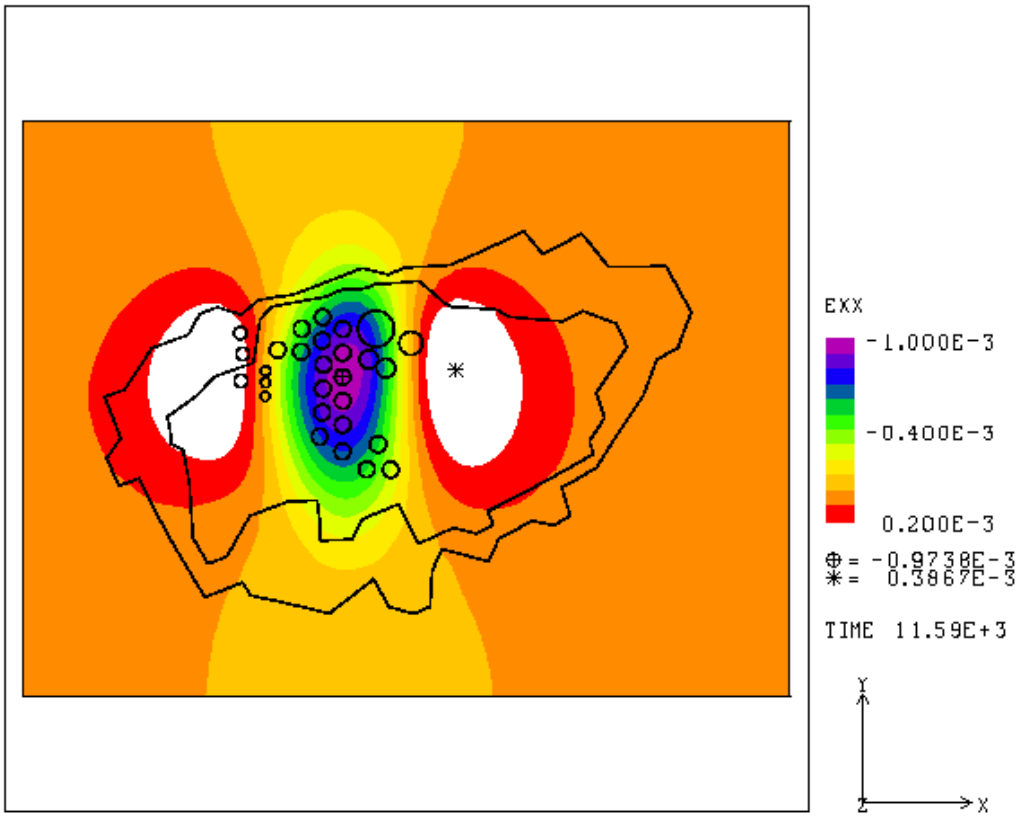

Figure 53. West-east directional strains at the surface (negative strains in compression).

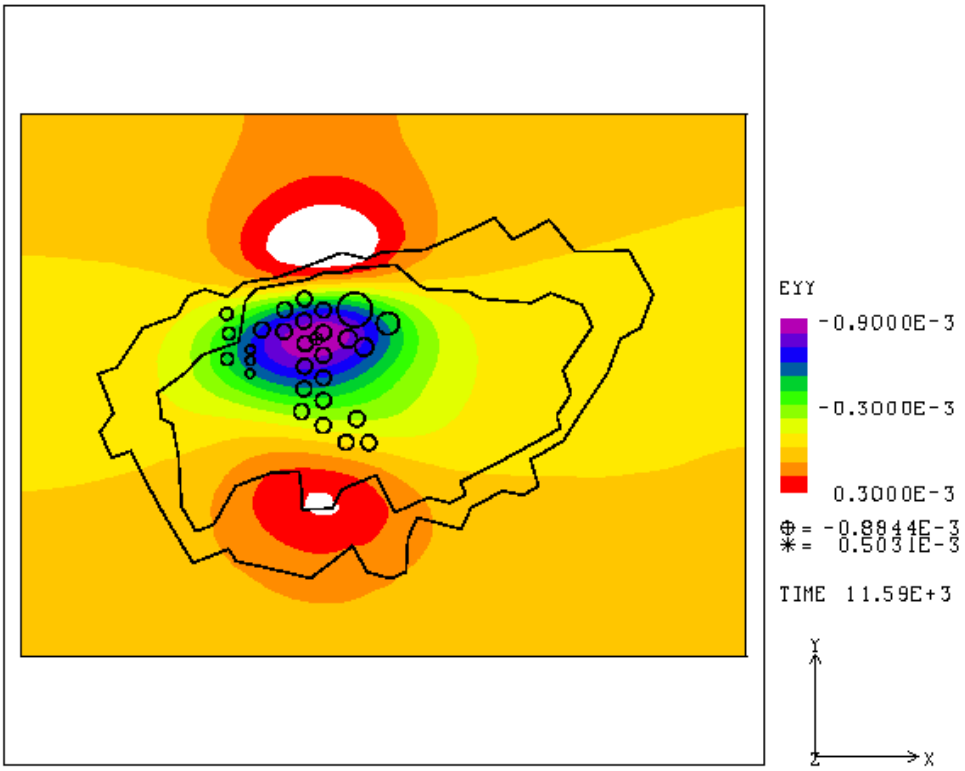

Figure 54. North-south direction strains at the surface (positive strains in tension).

5.3 DILATANT AND TENSILE STRESS DAMAGE NEAR CAVERNS

There are two ways in which the salt surrounding the caverns can be damaged: by dilatant damage resulting from microfracturing that increases permeability and the potential for crack propagation, and by tensile stresses which cause salt fracture and crack propagation. A quick way to evaluate the potential for damage is by the use of history plots of the extreme values of damage factor and maximum principal stress in the salt surrounding the cavern through each of the five leaching operations. Figure 55 shows the minimum value of the Van Sambeek dilatant damage factor (Equation 18) surrounding each of the five Phase 1 caverns as a function of time through the present time. The lowest values of damage factor occur during workover operation periods. Two caverns, WH-6 and WH-9, have several time periods where the value of the safety factor is less than 1; in fact, WH-9 would appear to be in very serious condition, because the minimum damage factor is nearly always zero. A closer examination of the location of the extreme value provides more insight. Figure 56 is a cutaway contour plot of Caverns 8 and 9. In this plot, safety factor values less than 1 are shown in red. Nearly all the region around and between WH-8 and WH-9 have safety factor values over 2, which implies that there are no dilatant damage concerns. However, the top of the lower lobe of WH-9, at its closest approach to WH-8, has one element that consistently has tensile and high shear stress values such that its calculated damage safety factor is nearly zero. The cause of this stress concentration is certainly due to the combination of two effects: the geometry of the sharp corner in the mesh at the location, and thin web between WH-8 and WH-9 at this point. No locations around WH-8 experiences low safety factor values; only the top corner of the top lobe of WH-9 also experiences safety factor values that oscillate between 0.4 and 2 around the entire perimeter.

These results would certainly raise concerns about cavern expansion for both WH-8 and WH-9. The internal ledge of WH-9, which has been predicted in previous analyses (Sobolik 2013a; also references in Section 6) to be a potential location for high shear and thus low damage safety factor, is predicted to have less severe conditions that do not attain dilatant damage conditions (although do still come close). The reason for this improved behavior prediction is probably due to the way in which the closed rim of WH-6 was modeled, so there will not be any suggestion that the ledge of WH-9 is no longer of concern until some additional analyses are performed in the future.

Figure 57 shows the predicted damage safety factor for the entire West Hackberry cavern field at the elevation of the ceiling of WH-6. As noted in Section 4.2, for this analysis the rim of WH-6, which is believed to have closed in the late 1990s or early 2000s, is modeled as intact but weakened to reflect the reality of rim closure. The instances of low safety factor for WH-6 shown in Figure 55 occur during WH-6 workovers, and in Figure 57 are shown to be around the circumference of the bowl of WH-6, where the rim has re-closed. This prediction matches the predictions from earlier analyses, that the repressurization of WH-6 after a workover would put tensile stresses (which automatically make the value for safety factor zero) around the perimeter of the cavern, either at the outside of an open rim or at the perimeter of a bowl with a closed rim. Because the oil has been removed from WH-6, and is not likely to be restored in that cavern, the future operations of the cavern will probably be redesigned to maintain a high constant pressure with very few workovers in the future.

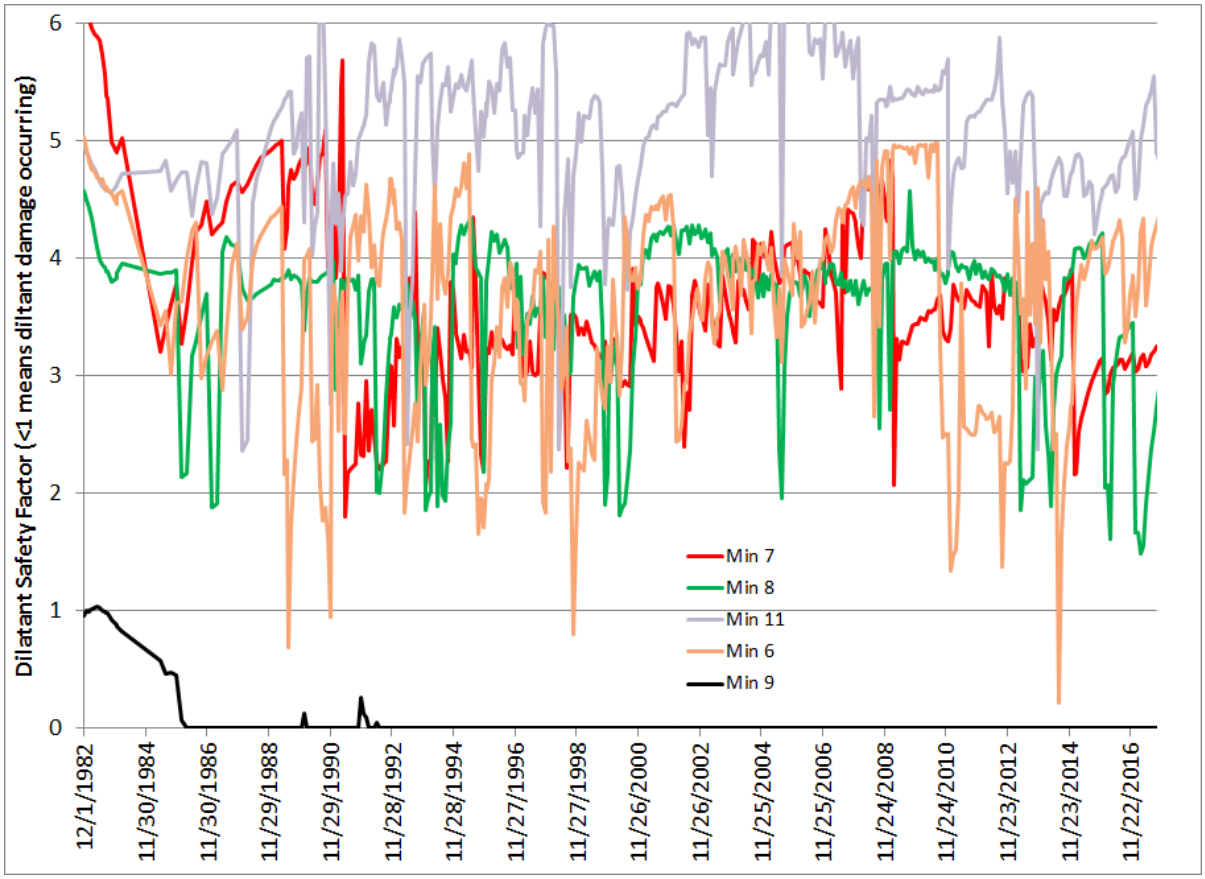

Figure 55. Minimum value of the damage safety factor surrounding each Phase 1 cavern.

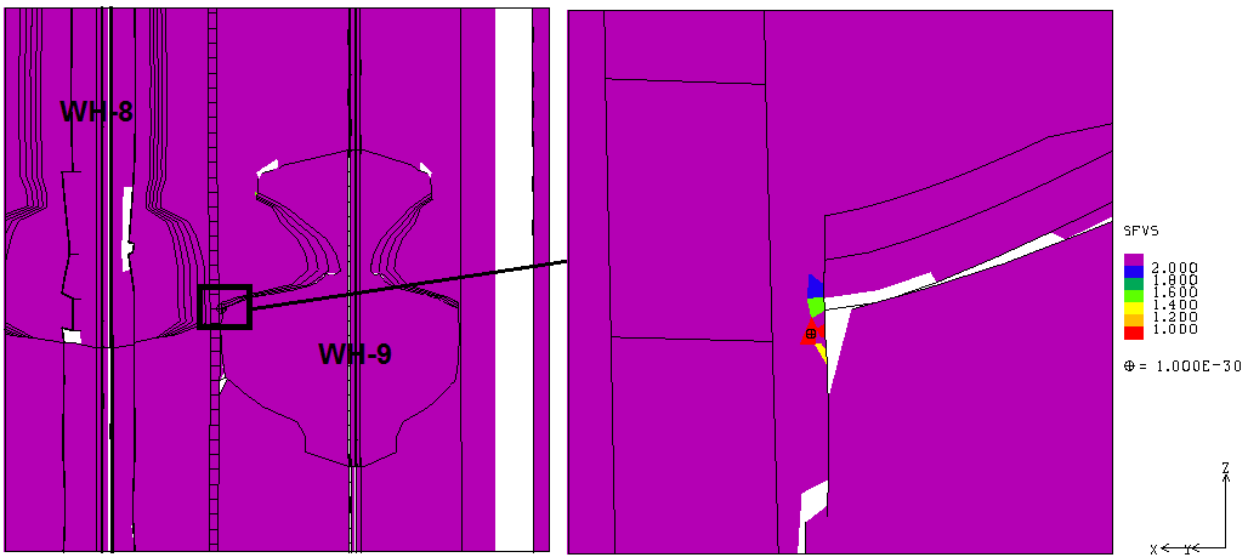

Figure 56. Contour plot of damage safety factor, cross-section of Caverns 8 and 9.

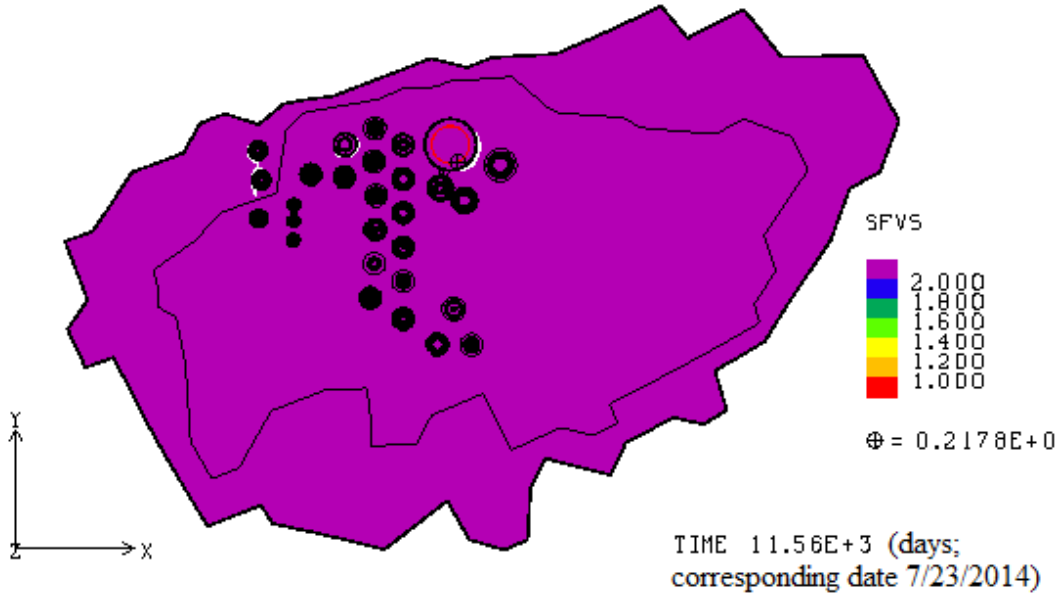

Figure 57. Contour plot of damage safety factor, cross-section at elevation of WH-6 ceiling.

Figure 58 shows the minimum value of the dilatant damage safety factor surrounding each of the Phase 2 east side caverns through the present time, and Figure 59 does the same for the Phase 2 west side caverns. From these figures, WH-110 and WH-113 would appear to have significant issues. However, as shown in Figure 60, the location of the minimum value of safety factor is at the bottom of the cavern for WH-110 (and WH-113 has the same prediction). No other locations around these caverns experience dilatant damage conditions. These results indicate that the Phase 2 caverns should not have experienced any large-scale dilatant damage that would cause cracking, with the possible exceptions being at sharp geometry locations where stress concentrations can occur. Figure 61 highlights caverns that are predicted to occasionally experience safety factor values less than 1 somewhere on their cavern walls through five drawdown cycles. These results will be examined more closely in FY2016 to address the number of allowable drawdowns for each cavern.

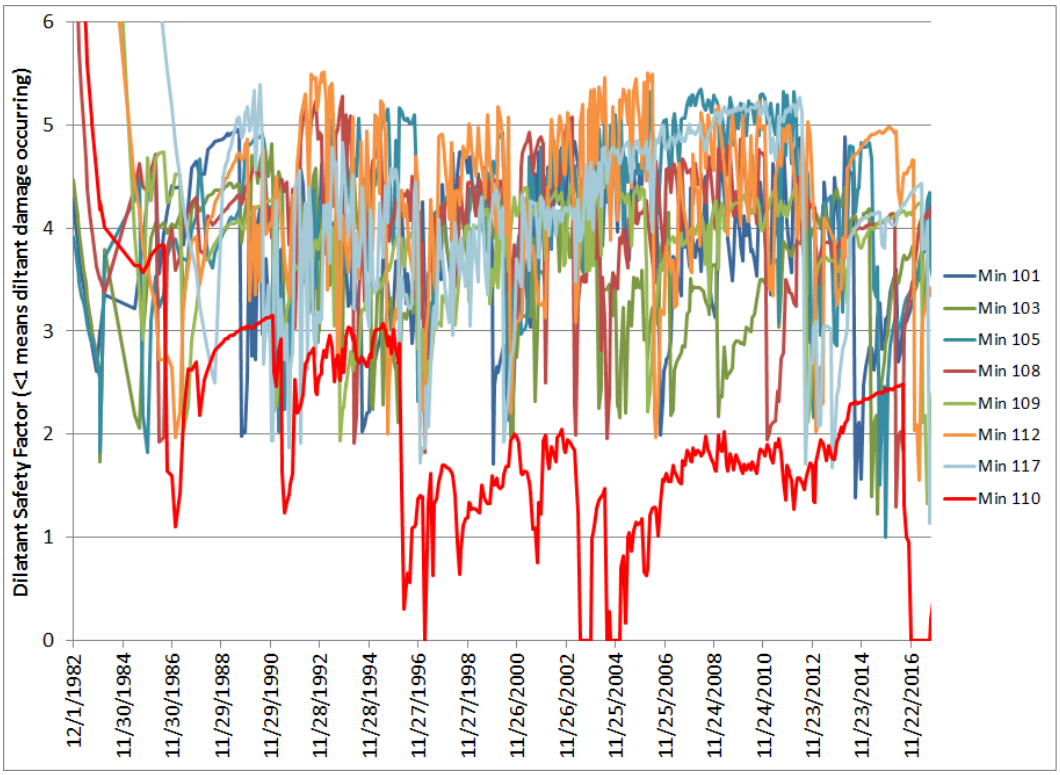

Figure 58. Minimum value of the damage safety factor surrounding each Phase 2 east side cavern.

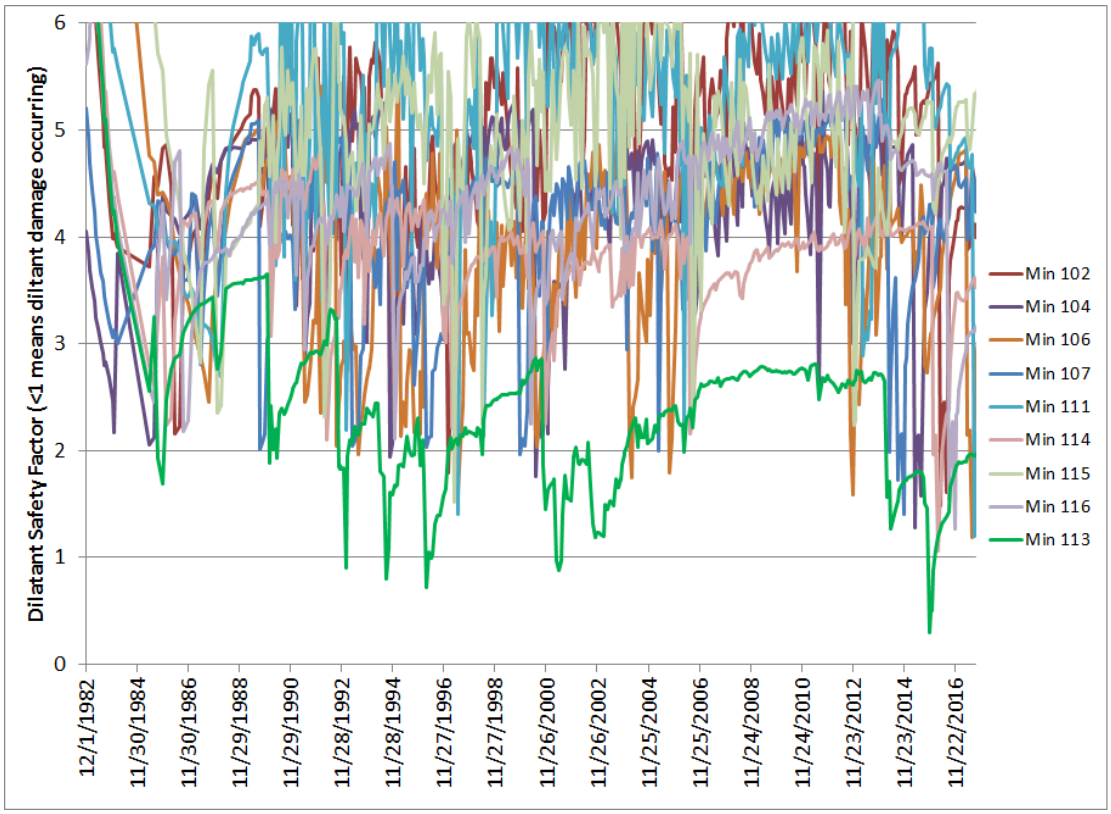

Figure 59. Minimum value of the damage safety factor surrounding each Phase 2 west side cavern.

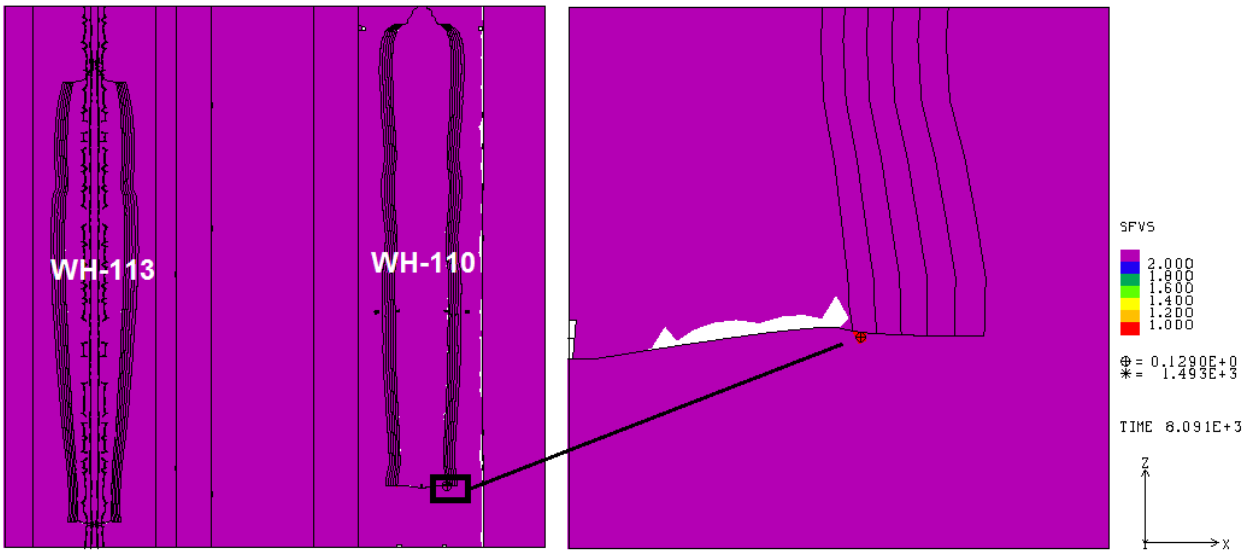

Figure 60. Contour plot of damage safety factor at floor of WH-110.

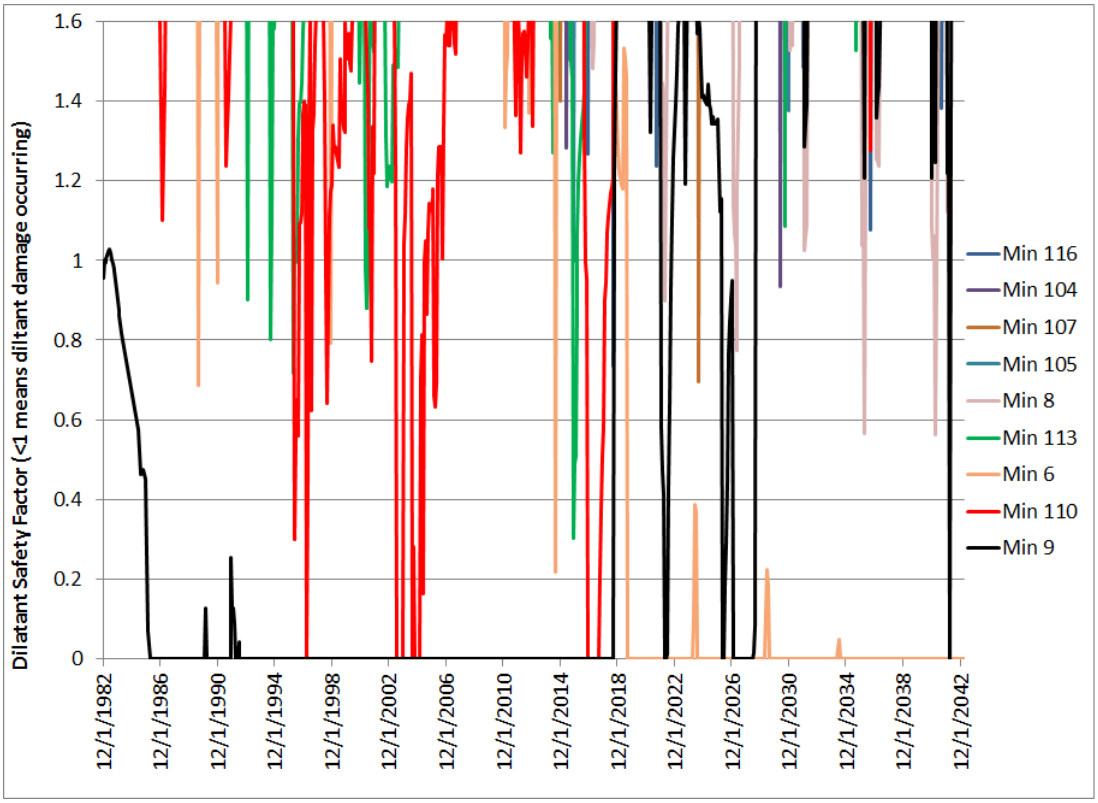

Figure 61. WH caverns with minimum value of the damage safety factor less than 1 (indicating onset on dilatant damage) through 2043.

Figure 62 shows the maximum value of the maximum principal stress around the each West Hackberry caverns as a function of time through 2014. These plots represent the maximum value of maximum principal stress in the cavern wall for each cavern, as well as a cylinder of salt

around the cavern extending up to the salt/caprock interface. The important observation to make with Figure 62 is to identify caverns where a positive value of stress, therefore tensile stress, may occur around a cavern. As was the case for the damage safety factor, four caverns are predicted to have experience tensile stress as some point around the cavern – 6, 9, 110, and 113. The locations of and causes for the tensile stresses are identical to those for the undesired safety factor values. Figure 63 plots the same information through five drawdown cycles for any cavern that is predicted to experience tensile stress. Two additional caverns are added to the list: WH-8, which has several instance as the number of drawdowns increase; and WH-107, which has just one instant immediately after the first workover after its first drawdown. These results will be evaluated more closely for the determination of the number of available drawdowns for each cavern.

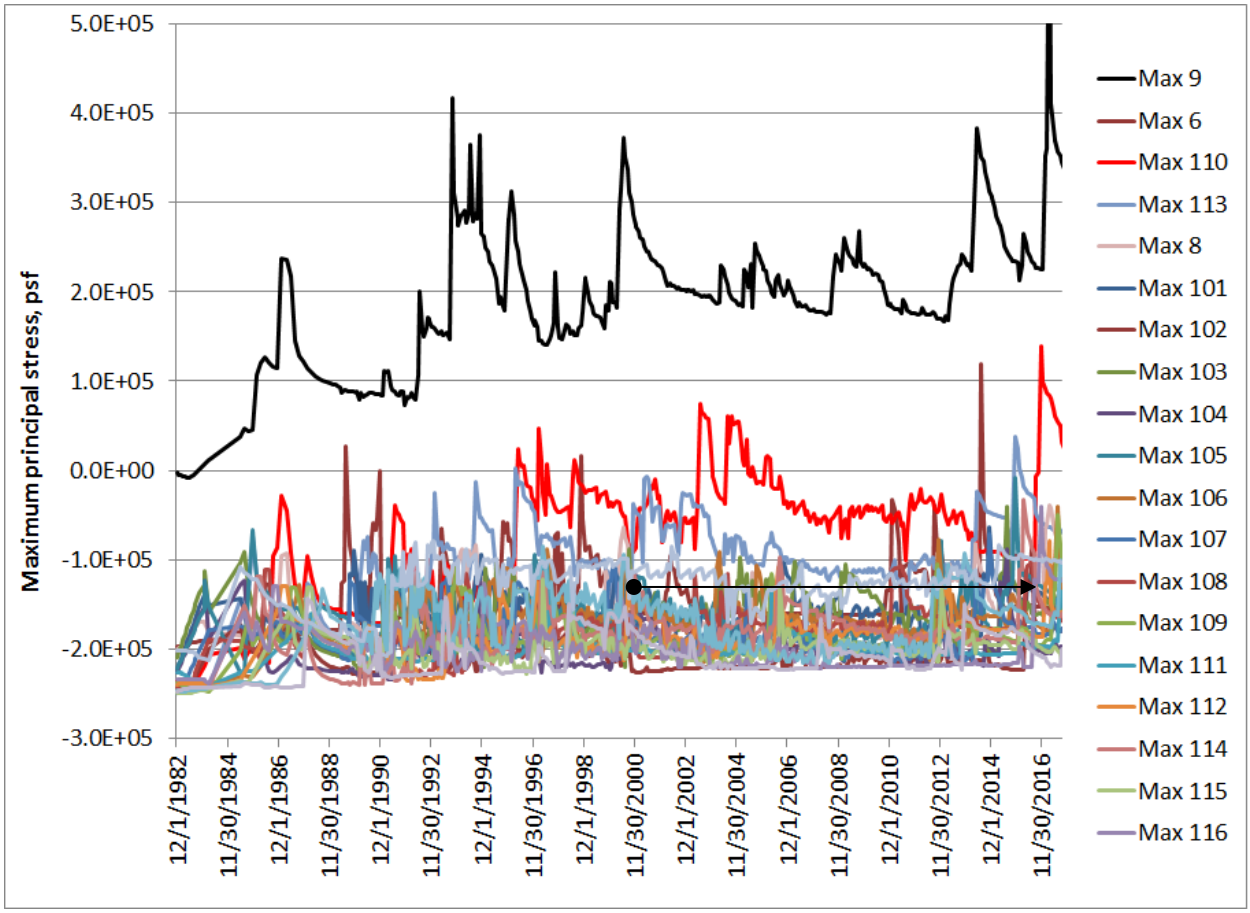

Figure 62. Maximum value of the maximum principal stress surrounding each West Hackberry cavern.

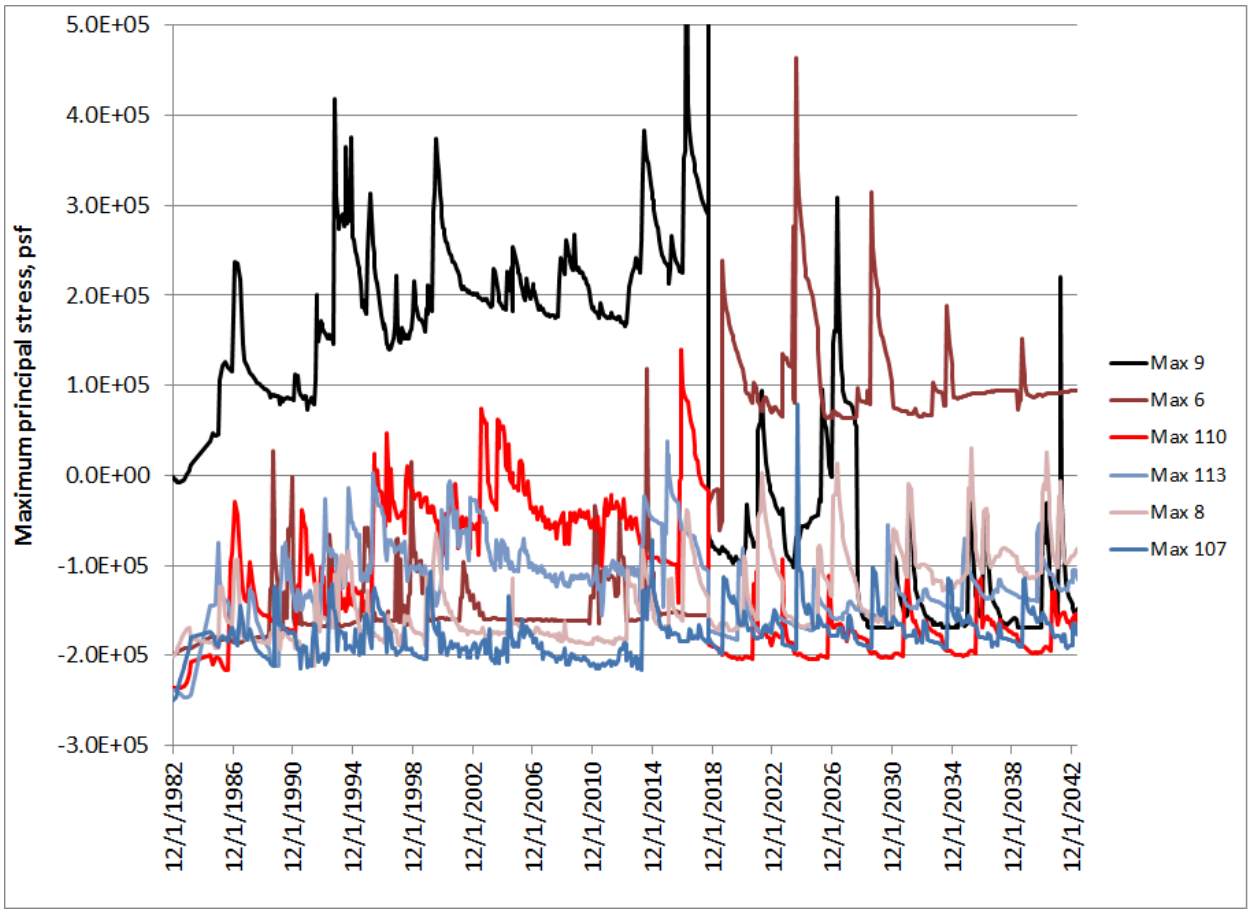

Figure 63. WH caverns predicted to experience some tensile stress through 5 drawdown cycles, as noted by the maximum value of the maximum principal stress surrounding each cavern.

5.4 AXIAL WELL STRAIN

The physical presence of wells and surface structures are not included in the finite element model, but the potential for ground deformation to damage these structures can be conservatively estimated by assuming that they will deform according to the predicted ground strains. At well locations, subsidence will primarily induce elongation of the axis of the well. Under these conditions, the cemented annulus of the wells may crack forming a horizontal tensile fracture that may extend around the wellbore. This fracture may not result in vertical fluid migration along the casing, but could permit horizontal infiltration into ground waters. This condition may be a well vulnerability, especially in the caprock, where acidic ground waters may gain access to the steel casing and corrode it. More extensive damage could heavily fracture the cement which could result in a loss of well integrity in that leakage could occur from the cavern along the outside of the casing. Such leakage could result in flow to the surrounding environment, resulting in loss of product. For the purposes of this report, the strain at which cement experiences the onset of cracking due to tension is assumed to be 0.2 millistrains. This would be typical of cement with a compressive strength in the range from 2500 to 5000 psi (Thorton and Lew, 1983). It should also be noted that vertical well strain reduces the collapse resistance of the steel casings. For casing steels, the threshold strain at which plastic deformation begins is typically

about 1.6 millistrains. The strain value is not an indication of imminent failure, but rather where the steel begins plastic deformation which makes the casing more susceptible to actual tensile failure, shear failure, or casing collapse. Additionally, recent laboratory experiments indicate the casings may experience leakage at their threaded connections long before failure of the main casing sections themselves (Gerstle et al., 2014). For SPR experience, Park (2013 & 2014) calculated in situ value for total plastic strain of steel casings at the time of failure for the Big Hill site, based on a combination of multi-arm caliper readings and geomechanical analyses; these values were typically higher than 1.6 millistrains, with one estimate of the equivalent plastic strain at failure being 7.9 millistrains. For the purposes of this report, a threshold value of strain for the steel casing of 1.6 millistrains has been chosen, in order to use the results to plan borehole remediation activities.

Figures 64 and 65 show the predicted average vertical strain in the salt along the casing location over the entire length of the boreholes between the top of salt and the casing shoe for each of the caverns. These strains are baselined to the strain accumulated since 6/1/1985, when nearly all the caverns and their boreholes had been constructed. It is assumed that these salt strains are directly transferred to the cement and steel casings. Figure 64 shows the predicted strains through approximately the present time, and Figure 65 forecasts these strains through five drawdown cycles. Figure 64 shows that average casing strain over the casing length in salt exceeds the 1.6-millistrain threshold value for four caverns – WH-6, 106, 112, and 9 – and is nearly at the threshold value for WH-11. Figure 65 shows that over five drawdown cycles, at least half the caverns are expected to experience an average strain over 1.6 millistrains. An examination of the locations of the caverns in relation to amount of accumulated strain indicates a tendency for the caverns on the periphery of the field to have greater vertical strains than those in the middle of the field, although salt variability, cavern geometry and depth of ceiling, and cavern pressure histories also affect the strain accumulation. The reason for this tendency is probably due to the bowl-shaped subsidence depression of the site, which results in less bending of the casings in the middle of the cavern field and more horizontal strain bending in the transition zone between the middle and the outside of the subsidence bowl.

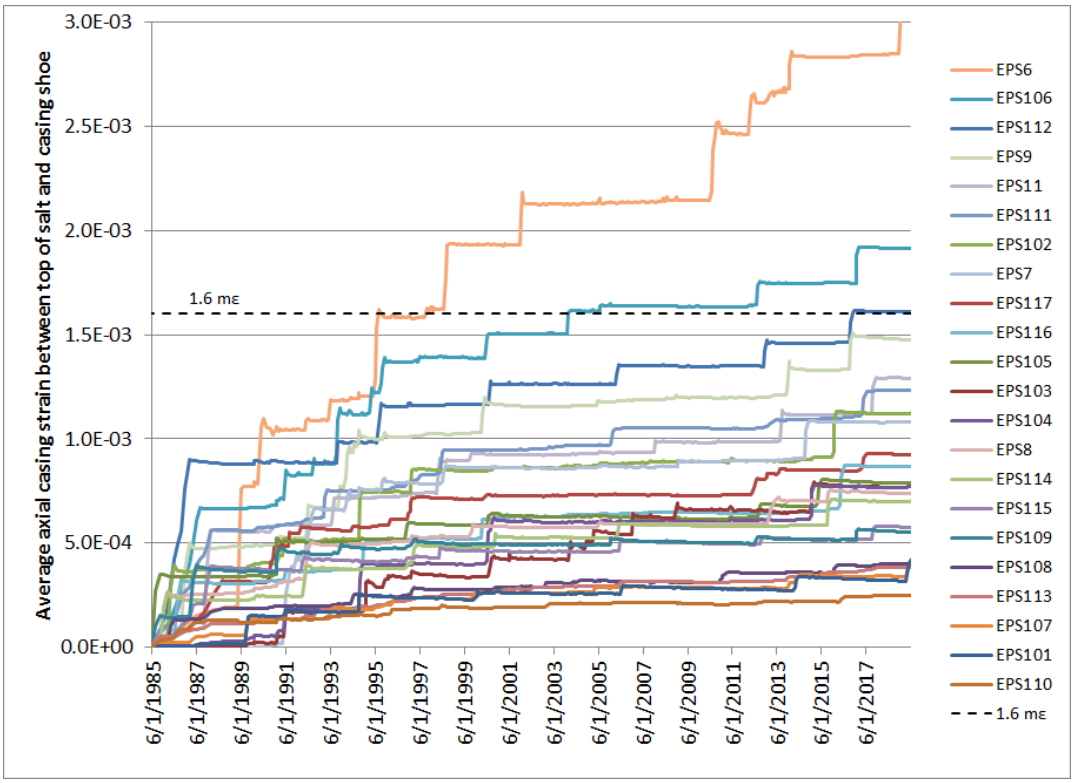

Figure 64. Average axial casing strain between top of salt and casing shoe, measured from 6/1/1985.

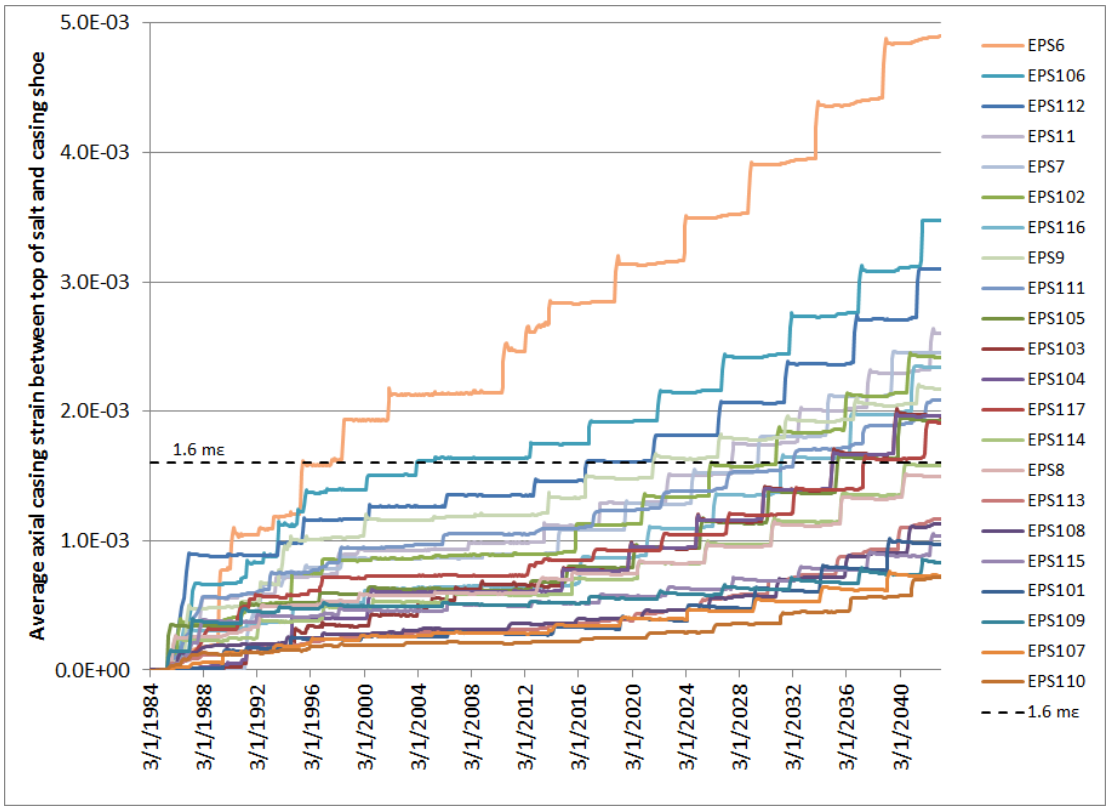

Figure 65. Average axial casing strain between top of salt and casing shoe, measured from 6/1/1985, out through five drawdown cycles.

Of course, the average strain across the length of casing in the salt is not the same as localized strain along the length of the boreholes. Figures 66 through 77 show the predicted strain along the lengths of the boreholes for caverns WH-101 through 107, and WH-6, 7, 8, 9, and 11, respectively. The strains are calculated from a baseline date of June 1, 1985, to try to be reasonably close to the time when all the casings have been installed in the formation. The first curve for each figure shows the casing strain for August 2004, with subsequent curves plotted through August 2014. For nearly all the caverns, the maximum predicted strain is predicted to occur at the top of the cavern near the casing shoe; caverns 101, 105, 106, 107, and all the undisplayed caverns 108-117 display this behavior. The region of high stain for these caverns (i.e., predicted strain exceeding 1.6 millistrains) typically extends to between 50 and 120 feet above the casing shoe. Caverns 102, 103, and 104 display a curious feature, in that the maximum strain occurs somewhat above the casing shoe. This behavior is best explained by their "flat" ceilings for which there is a substantial reduction in cavern radius immediately beneath the ceiling (these geometries can be examined in Figure 20). WH-106 is also somewhat of an aberration in that high strain for that borehole are predicted to occur up to 230 feet above the shoe. The most curious feature of all shown in these figures is that the location for the maximum strain above WH-6 is between 1/3-1/2 of the distance from the cavern shoe to the top of salt. This is perhaps the posterchild example of the effect of the flat ceiling, as the geometry of the ceiling causes the maximum stresses and strains above the cavern to occur well above the bottom of the borehole. The remaining Phase 1 caverns behave more like their Phase 2 counterparts, although the region of high strains extends significantly higher for them. Note that in general there is little change in the casing strain between 2004 and 2014, indicating that much of the strain in the casings occurred early in the caverns' histories as the formation responded to cavern construction and initial storage. However, there are large changes in the strain for WH-6 over the past ten years due to workovers in that cavern and the resulting strain on the casing. The other Phase 1 caverns, and WH-103, also exhibit greater strain accumulation over the past 10 years than the other caverns. One of the major conclusions from the predictions shown here is that, with the exception of WH-6, the primary region of concern for the effects of axial strain on the borehole casings is the 50 to 250 feet above the casing shoe.

In addition to axial strain, accumulated volumetric plastic strain is an important measure of the effect of creep on casing integrity. A follow-on report to these analyses is planned for 2016; its primary concern will be the evaluation of available drawdowns for the West Hackberry caverns. As part of that report, a more detailed examination of the predicted plastic strain on the casings, and their relation to measured casing deformation from multi-arm calipers, will be performed.

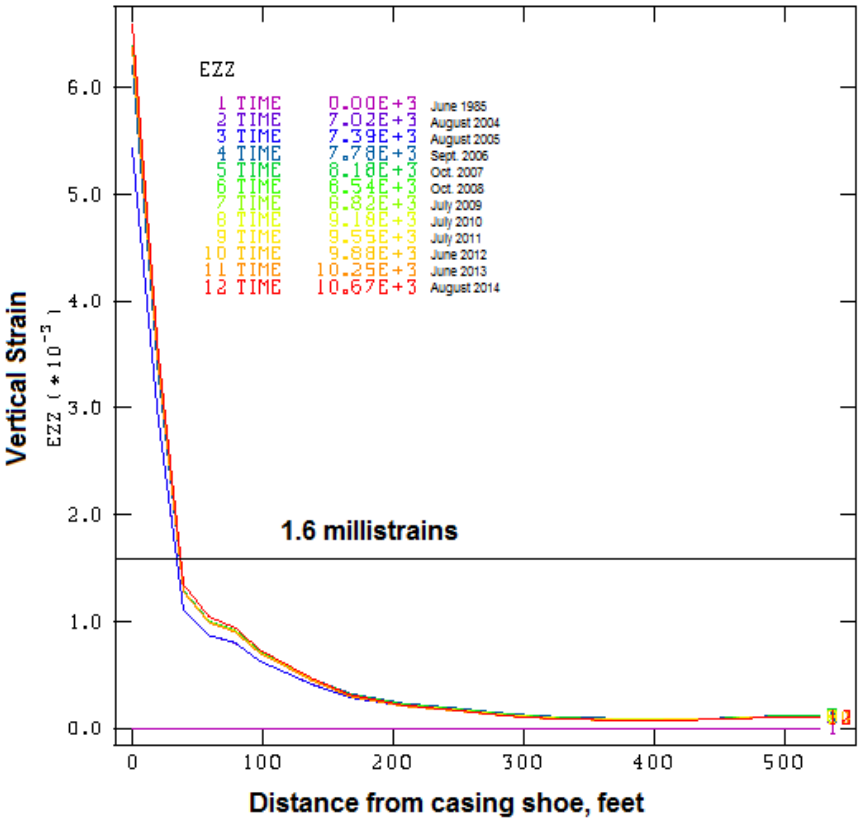

Figure 66. Axial (vertical) strain along borehole casing, WH-101.

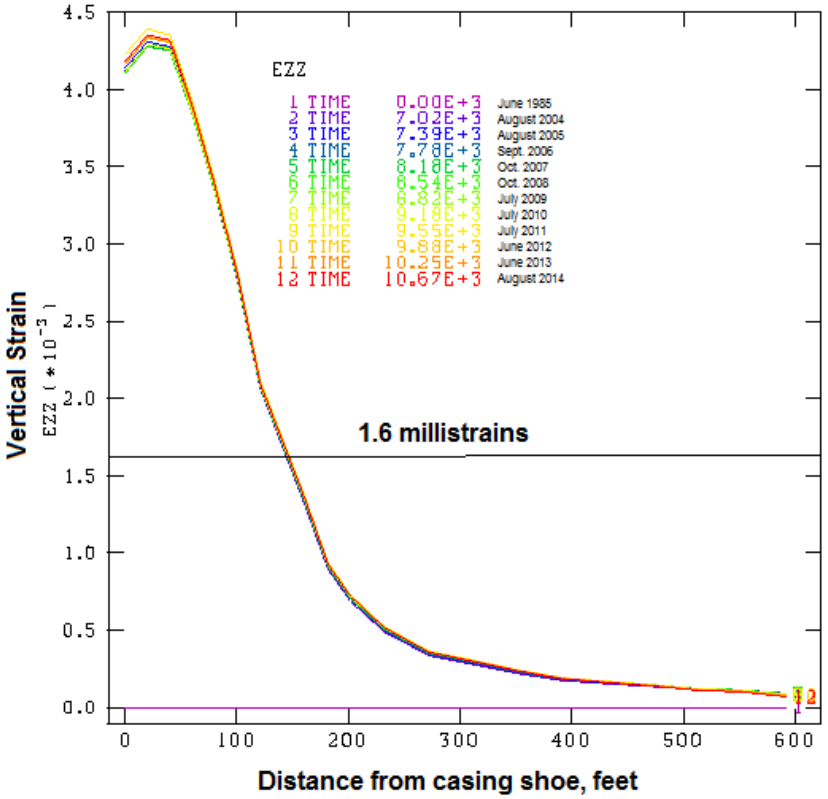

Figure 67. Axial (vertical) strain along borehole casing, WH-102.

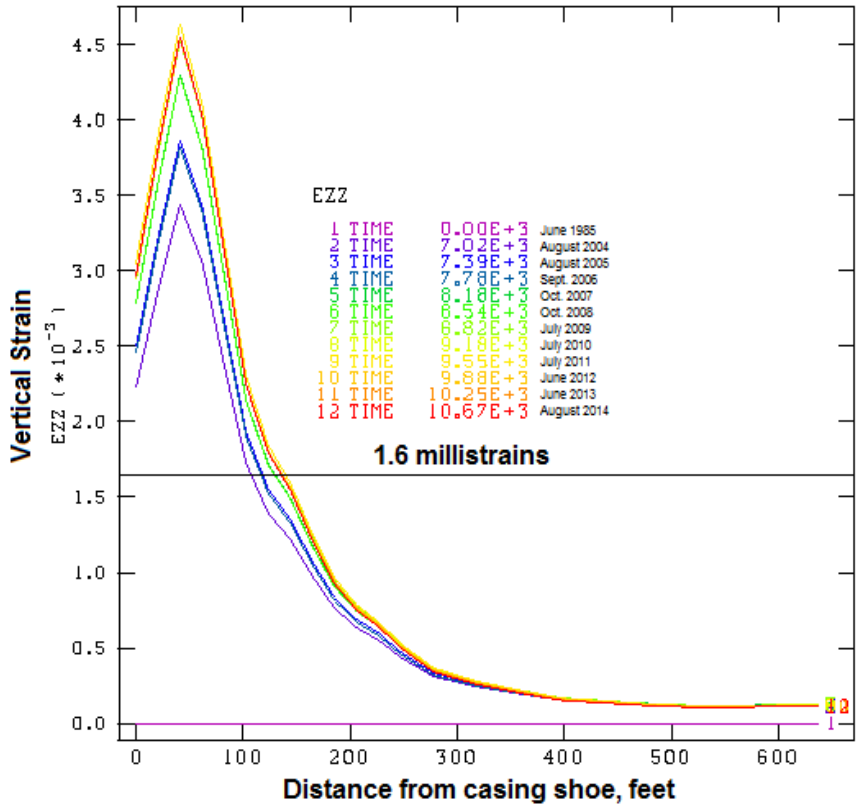

Figure 68. Axial (vertical) strain along borehole casing, WH-103.

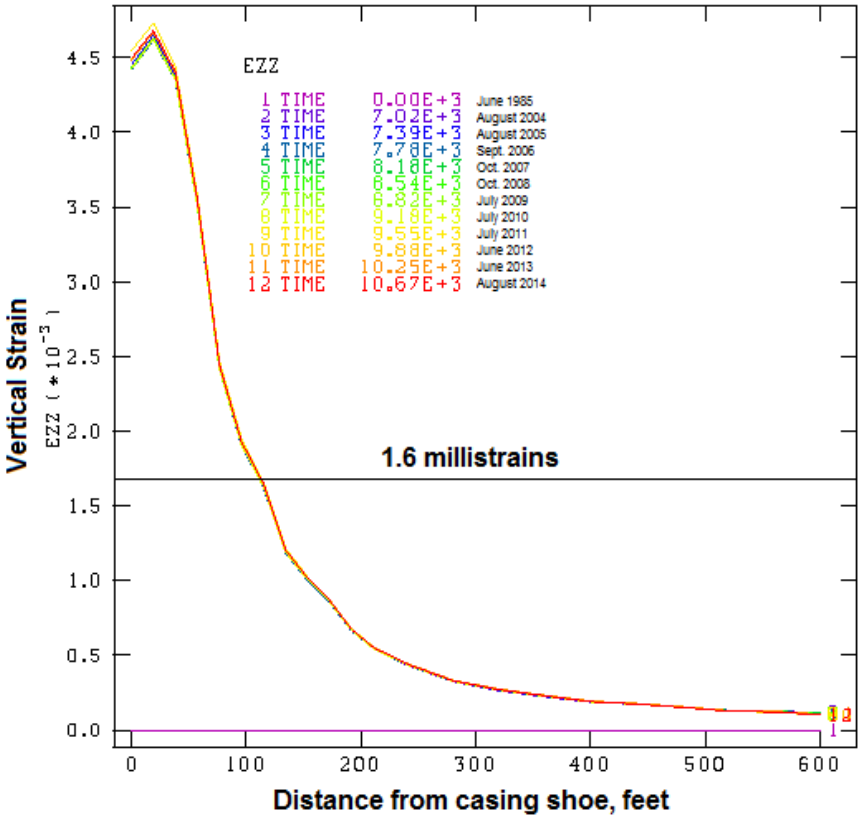

Figure 69. Axial (vertical) strain along borehole casing, WH-104.

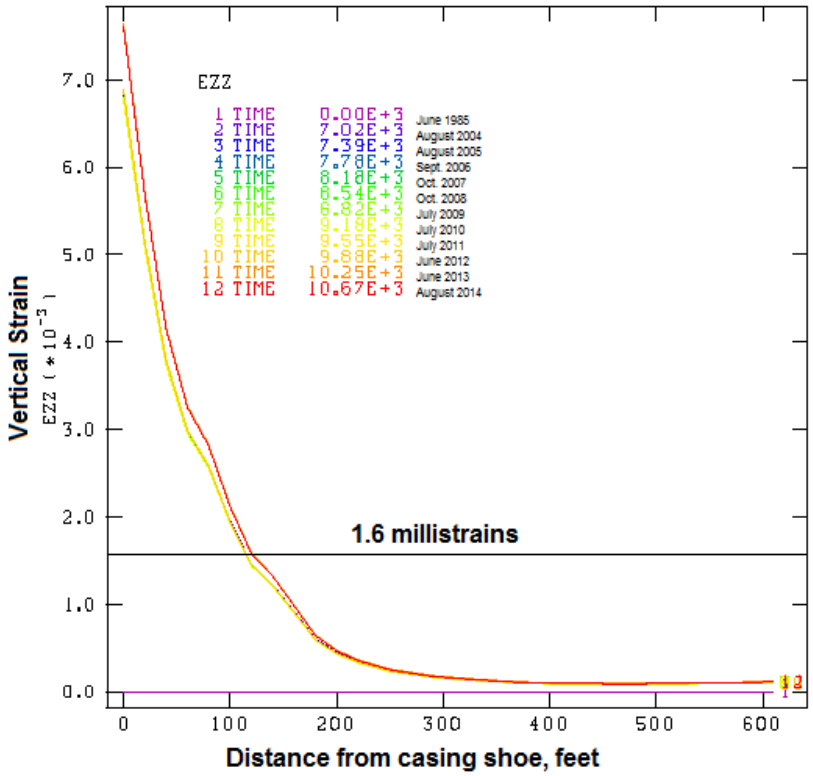

Figure 70. Axial (vertical) strain along borehole casing, WH-105.

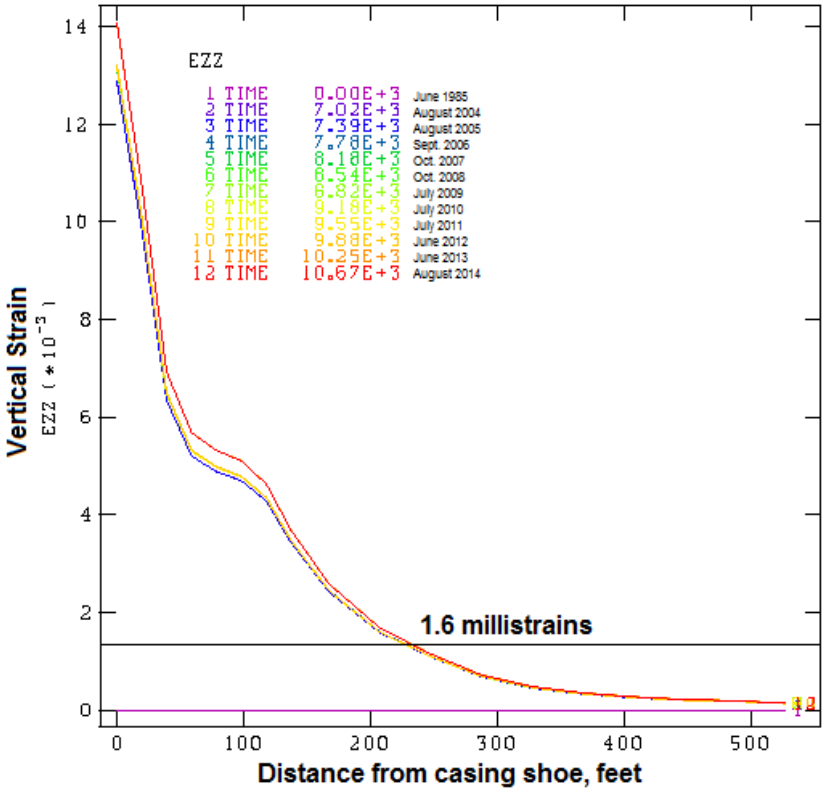

Figure 71. Axial (vertical) strain along borehole casing, WH-106.

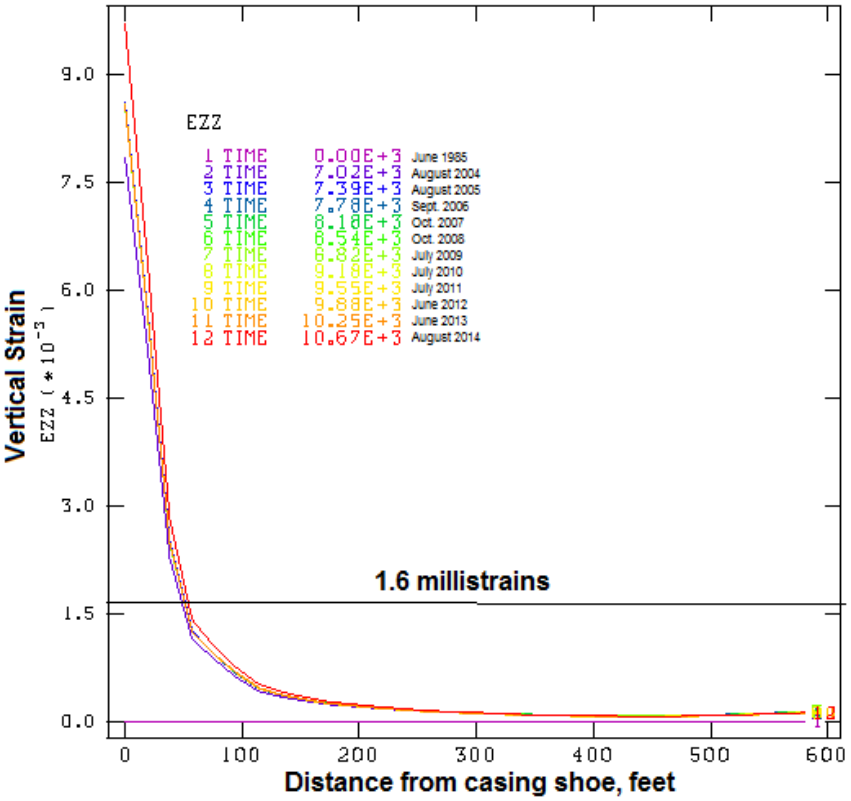

Figure 72. Axial (vertical) strain along borehole casing, WH-107.

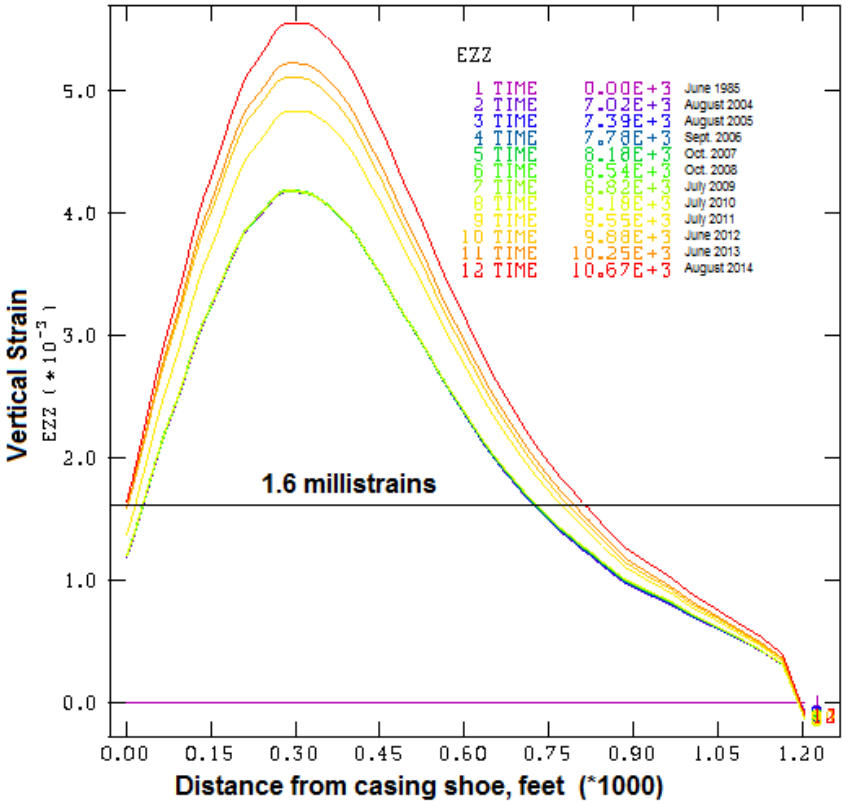

Figure 73. Axial (vertical) strain along borehole casing, WH-6.

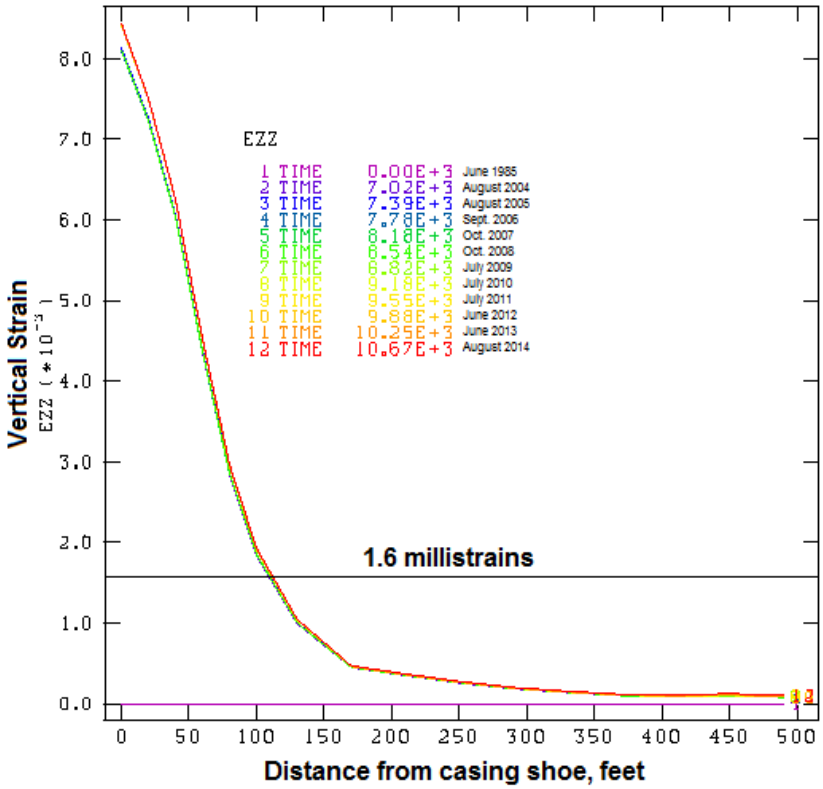

Figure 74. Axial (vertical) strain along borehole casing, WH-7.

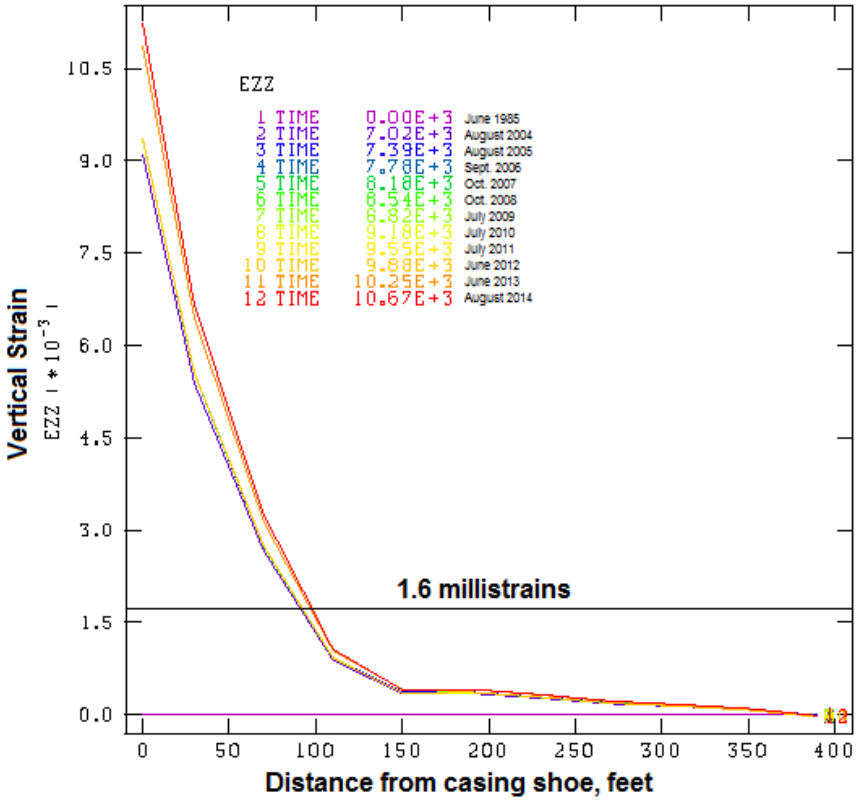

Figure 75. Axial (vertical) strain along borehole casing, WH-8.

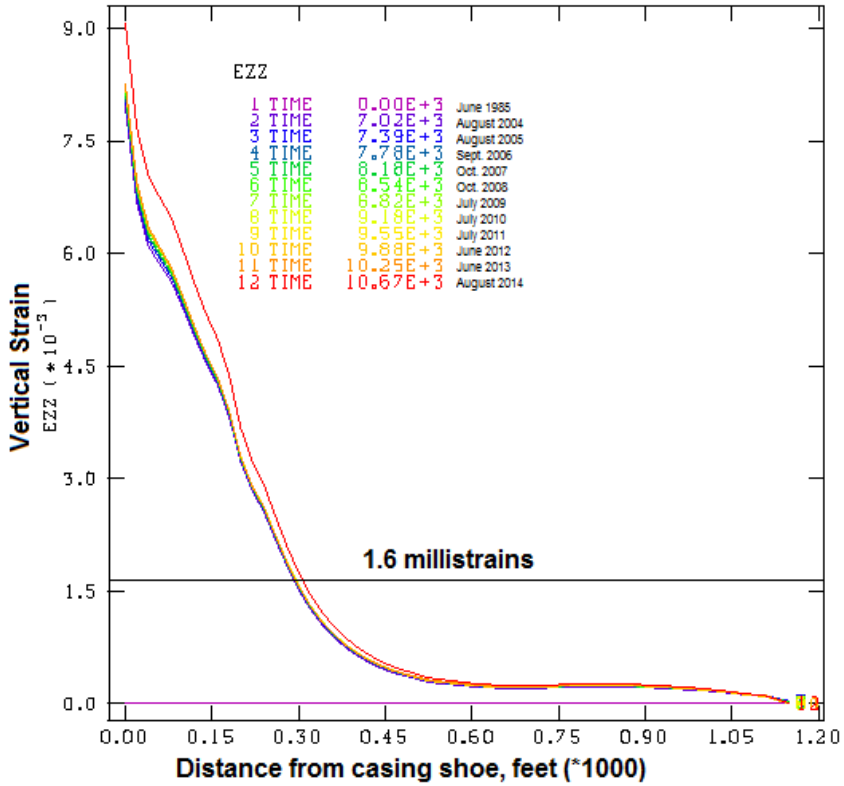

Figure 76. Axial (vertical) strain along borehole casing, WH-9.

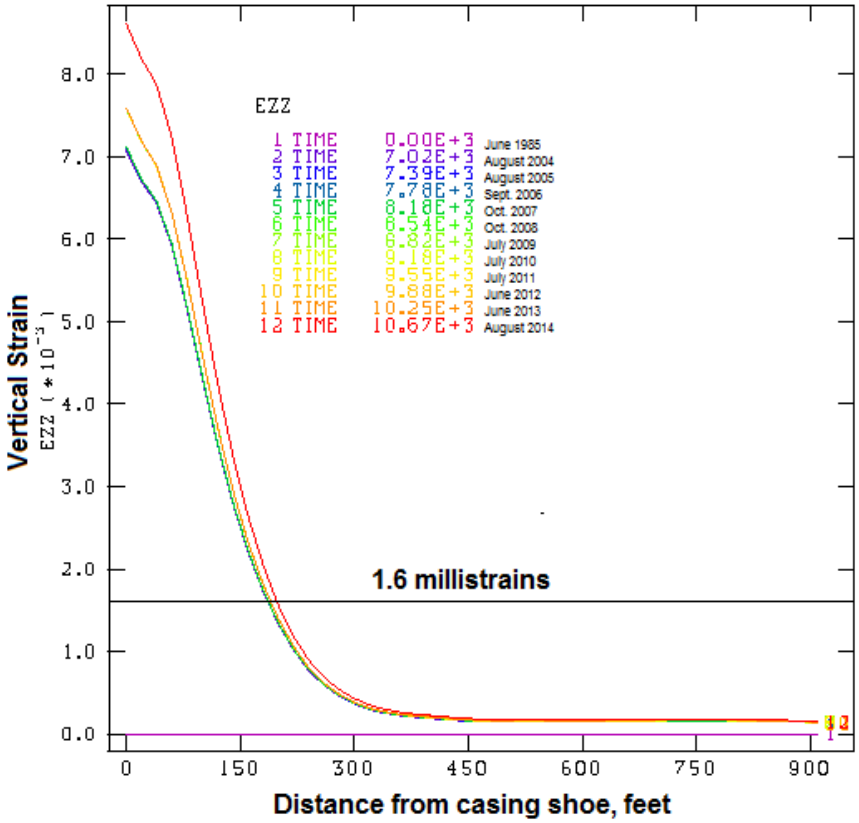

Figure 77. Axial (vertical) strain along borehole casing, WH-11.

5.5 PRELIMINARY DISCUSSION OF AVAILABLE DRAWDOWNS

The U.S. Strategic Petroleum Reserve (SPR) management has for a long time wanted to know how many full drawdowns are available for current SPR caverns while maintaining system integrity. The number of drawdowns for a particular cavern has in the past been characterized by the pillar-to-diameter ratio (P/D) of adjacent caverns. Two recent studies (Rudeen and Lord, 2013; Lord et al., 2013) calculated the P/D ratios for all adjacent cavern pairs throughout the SPR using several different formulas based on specific geometric properties of the caverns. In addition, the collection of SPR geomechanical analyses of the past several years have applied geomechanical conditions such as generation of dilatant and/or tensile stresses to the salt surrounding each cavern to further instruct the evaluation of available drawdowns. Several meetings were held in 2014 to develop a technical baseline to calculate the number of drawdowns for each cavern (Sobolik et al., 2014). From those meeting, several definitions and criteria were established:

1. What is an available drawdown? To answer this, the following definitions were discussed and agreed upon:
   - Full Drawdown (DD) = 90% of the oil removed from a cavern with raw water
   - Partial Drawdown (PD) is defined by the change to the radius of the cavern where raw water was injected: $\frac{\hat{a}\hat{}\dagger r_{PD}}{\hat{a}\hat{}\dagger r_{DD}}$ at the maximum value of radius. (We later discussed that partial drawdowns would have to be logged and counted, and a mechanism to track downloads should be established.)
   - Available Drawdown: A cavern has an available drawdown if after that full drawdown, the long-term stability of the cavern, the cavern field, or the oil quality are not compromised.

2. What criteria are to be used to impose a limit on drawdowns? In these discussions, it was decided that for either a P/D condition or a geomechanical analysis to limit a drawdown, it must create a condition within the cavern that can potentially create failure. To answer this question, we had a long discussion on the three ways that a cavern may "fail":
   - Loss of cavern integrity such that oil escapes to another cavern, oil escapes to a caprock or anhydrite conduit to the environment, or the cavern collapses thus creating a sinkhole above (BC-7) or at the side (Bayou Corne) of a salt dome.
   - Loss of access to stored oil due to irreparable damage to casing, irreparable damage to hanging strings, or sufficient sagging of the roof to below the oil/brine interface.
   - Loss of casing integrity such that oil escapes to another cavern or oil escapes to a caprock or anhydrite conduit to the environment.

3. What process, then, should be used to determine the number of available drawdowns for a given cavern? This five-step process was developed in the 2014 meetings (Sobolik et al., 2014):
   - Step 1: Using the industry standard of keeping the P/D > 1, the drawdown limit is initially assigned the number of drawdowns before the SOCON-defined 2D P/D becomes less than 1.0.

- Step 2: The drawdown limit based on the 3D P/D ratio defined in Lord, Rudeen et al. (2009), which represents a more physically meaningful description of the pillar thickness between caverns, is compared to the 2D P/D limit.
- Step 3: The drawdown limit based on full-scale geomechanical model predictions are also compared to the 2D P/D limit. If the limits based on the 3D P/D and the geomechanical analyses are both at least at large as the 2D P/D, the 3D P/D limit is used as the best estimate for the drawdown limit. If the geomechanical analysis additionally fits certain criteria described below, and if its drawdown limit is the highest of the three, then the geomechanical limit is used as the best estimate.
- Step 4: If, after all these steps, the drawdown limit is equal to zero, the best estimate is assigned a value of 1, with comments describing the anticipated technical issues during a drawdown of that cavern. This step results from the fact that the oil must at some point be withdrawn from all the caverns.
- Step 5: Regardless of P/D or geomechanics calculations, an absolute maximum limit of 5 drawdowns has been defined, to allow for increased knowledge and experience to better inform this process in the future.

For all of the SPR sites, large dome-scale geomechanical analyses have been performed including representations for all the caverns. All of these analyses have included drawdown or leach layers for all the Phase 1 and Phase 2 caverns with the exception of BM-5. For only one of the published analyses (Bryan Mound; Sobolik and Ehgartner, 2009b) have all the caverns been meshed according to the geometries obtained by sonars. A second model, West Hackberry (Sobolik and Ehgartner, 2009a) has sonar-based geometries for the Phase 1 caverns, and frustums for the Phase 2 caverns. The published Big Hill and Bayou Choctaw models include cylinder and frustum representations for the caverns. (All models are currently being updated with sonar-based geometries for all caverns, and their results will eventually be used to update the tables below.) In general, when assessing the potential for cavern stability problems, the following events/processes are the most critical:

- Large ΔP events such as workovers; dilatant and tensile stress conditions occur during large values of ΔP, but are driven by large values of rate of pressure change dP/dt; these events may cause salt falls and cracking.
- Length of time that the caverns are held in workover; strain rate is a function of ΔP, and most vertical strain on casings occurs during the enhanced creep resulting from a workover.
- Other phenomena which can cause casing strain, such as Big Hill caprock/salt interface.

The overriding observation from the geomechanical analyses (most of the cited Park and Sobolik references) is that the drawdown process itself rarely induces stress conditions (i.e., shear stress levels that create dilatant salt damage, tensile normal stresses that create fractures in the salt, or excessive vertical strains on the borehole casings) that cause instability issues. This is because the drawdown process uses fresh water injected at pressures not significantly different from the normal operating pressures of the cavern; therefore, the large pressure differential that causes increased cavern creep, and that can create the conditions listed above, is not present during drawdown. Therefore, for this reason as well as for ease of numerical computation, drawdown processes are modeled in the geomechanical analyses as instantaneous removal of a specified "onion layer" of material around the cavern.

Stability problems related to a drawdown would be expected to occur during a workover following the drawdown. The wellhead pressure during a workover is zero, creating the maximum pressure differential condition for a cavern, and as the cavern volume expands from leaching and the pillar thickness decreases, the potential for undesired stress conditions increases during workovers. Nearly all of the Phase 2 & 3 caverns, because of their cylindrical construction and designed spacing, are expected to be capable of having several drawdowns in their lifetime. Many of the Phase 1 caverns, however, have cavern geometry issues which will limit their available drawdowns to one or two.

The results of the geomechanical analyses are used to establish a limit to available drawdowns in the following manner. If at any time, and for any duration, during a simulated five-year period after a drawdown, which will include one workover, the maximum principal stress achieves a tensile condition, or the dilatant damage factor achieves a value less than 1.0, then that particular drawdown would be disallowed (i.e., if this condition occurs after the 3rd drawdown, then the limit due to geomechanics would be two drawdowns). This criterion is very conservative regarding the dilatant stress condition because achieving a short-term state of dilatant stress is not a distinct threshold for failure. In addition, the failure due to dilatant stress may be merely a salt fall, which is not necessarily a condition that would cause environmental or operational problems. Similarly, a tensile stress would likely result in a crack in the salt, but may not necessarily be a limiting condition depending on the severity of the crack.

Step 3 listed above stated that geomechanical analyses may be used as the overriding values for the best estimate for the drawdown limit if they fit certain criteria. The criteria are as follows: if the specific caverns have been meshed according to the sonar geometry (either an axisymmetric representation of the geometry, or the actual sonar-measured geometry), and additional drawdown layers are built into the cavern's mesh and removed in simulated leaching processes. The cavern geometry caveat is important, because the bumps and sharp corners are the locations of stress concentrations, and thus are the most likely locales for dilatant or tensile stresses.

Using the steps listed above, a best estimate for the available drawdowns for each cavern was been determined in 2014. These best estimates for the West Hackberry Site as they were designated in May 2014 are listed in Table 6. In the comments column of Table 6, the choice of the overriding limit used for the best estimate (P/D or geomechanics – GM) is listed, along with applicable references documenting the P/D ratio calculations and geomechanical analyses.

Table 6. Number of Available Drawdowns West Hackberry (from Sobolik et al., 2014)

Cavern	Basis				Best Estimate Basis (P/D or GM), Comments, Reference
	2D P/D < 1	3D P/D < 1	Geomechanics (through 2014)	Best Estimate	
WH101	3	3	5	3	P/D; Rudeen & Lord, 2013; Sobolik & Ehgartner, 2009b*
WH102	3	3	5	3	P/D; Rudeen & Lord, 2013; Based on S&E, 2009b
WH103	2	4	5	4	P/D; Rudeen & Lord, 2013; Sobolik & Ehgartner, 2009b*
WH104	3	3	5	3	P/D; Rudeen & Lord, 2013; Based on S&E, 2009b
WH105	2	2	5	2	P/D; Rudeen & Lord, 2013; Sobolik & Ehgartner, 2009b*
WH106	4	4	5	4	P/D; Rudeen & Lord, 2013; Based on S&E, 2009b
WH107	2	5	5	5	P/D; Rudeen & Lord, 2013; Based on S&E, 2009b
WH108	4	4	5	4	P/D; Rudeen & Lord, 2013; Sobolik & Ehgartner, 2009b*
WH109	2	4	5	4	P/D; Rudeen & Lord, 2013; Sobolik & Ehgartner, 2009b*
WH110	1	5	5	5	P/D; Rudeen & Lord, 2013; Sobolik & Ehgartner, 2009b*
WH111	5	5	5	5	P/D; Rudeen & Lord, 2013; Based on S&E, 2009b
WH112	4	4	5	4	P/D; Rudeen & Lord, 2013; Based on S&E, 2009b
WH113	4	4	5	4	P/D; Rudeen & Lord, 2013; Based on S&E, 2009b
WH114	4	4	5	4	P/D; Rudeen & Lord, 2013; Based on S&E, 2009b
WH115	4	5	5	5	P/D; Rudeen & Lord, 2013; Based on S&E, 2009b
WH116	4	5	5	5	P/D; Rudeen & Lord, 2013; Based on S&E, 2009b
WH117	5	5	5	5	P/D; Rudeen & Lord, 2013; Sobolik & Ehgartner, 2009b*
WH6	0	0	1	1	GM; Yellow, Lord et al 2013; Sobolik & Ehgartner, 2009b, Sobolik, 2013
WH7	0	0	5	5	GM; Green, Lord et al 2013; Sobolik & Ehgartner, 2009b
WH8	0	0	2	2	GM; Green, Lord et al 2013; Sobolik & Ehgartner, 2009b
WH9	0	0	1	1	GM; Yellow, Lord et al 2013; Sobolik & Ehgartner, 2009b, Sobolik, 2013
WH11	5	5	5	5	GM; R&L, 2013; S&E, 2009b

Legend: * - Results not published in Sobolik & Ehgartner (S&E), 2009b, but from same analytical calculations. Based on S&E, 2009b – Calculations in S&E 2009b were performed with mesh that includes eastern half of dome. WH caverns in western half are also spaced on 750' center-to-center grid as in eastern dome, so similar results are expected.

The values in Table 6 must be updated by the results from the analysis in this report. The figures for dilatant and tensile stresses in Section 5.3 show that WH-6 and WH-9 continue to have issues regarding the development of dilatant and tensile stresses. WH-6 has been emptied of oil through brine exchange, and in not expected to be used for oil stroage in the future. The occurrence of a very limited region of large dilatant stress for WH-110 and WH-113 requires further evaluations to determine its true impact on drawdown capability. An extensive reexamination of the drawdown values in Table 6 based on the analyses in this report, and for all the SPR caverns in Sobolik et al. (2014) based on their most recent geomechanical analyses, is planned for 2016. However, from a preliminary examintion of the predicted dilatant and tensile stress behavior, there will be very few (perhaps none) and limited downgrades to the number of available drawdowns based on geomechanical concerns for the caverns as listed in Table 6.

6. ADDITIONAL DISCUSSION OF CAVERNS 6 AND 9

Between the West Hackberry half-dome analyses of 2009 (Sobolik & Ehgartner, 2009a) and this report, there have been several interim analyses performed on the interaction between WH caverns 6, 8, and 9, whose results have been transmitted to DOE through letters. These letters are included in this section for more formal documentation. The letters included here include the following:

- Section 6.1: Sobolik, S.R., 2013. *Preliminary Recommendations Regarding the Maximum Length of Workover of West Hackberry Cavern 8 on Cavern 9 during Cavern 6 Oil Removal Process.* Letter Report to Robert Myers, DOE-SPR, July 25, 2013.
- Section 6.2: Sobolik, S.R., 2014. *Recommendations Regarding the Maximum Length of Workovers of West Hackberry Caverns 6, 8, and 9 during Cavern 6 Oil Removal Process.* Letter Report to Lionel Gele, DOE-SPR, January 15, 2014.
- Section 6.3: Sobolik, S.R., D.L. Lord, and B.L. Roberts, 2014. *Recommendations Regarding the Sonars to be Performed on West Hackberry Cavern 6 for Evaluation of Final Oil Removal*, Letter to Lionel Gele, DOE-SPR, September 30, 2014.
- Section 6.4: Sobolik, S.R., B.L. Roberts, and P. Weber, 2014. *Sandia Analysis of West Hackberry Cavern 6 – Remaining Oil Volume and Leaching Options*, Letter to Paul Malphurs, DOE-SPR, December 15, 2014.
- Section 6.5: Sobolik, S.R. and B.L. Roberts, 2014. *Update of Sandia Analysis of West Hackberry Cavern 6 – Remaining Oil Volume and Leaching Options*, Letter to Paul Malphurs, DOE-SPR, December 18, 2014.
- Section 6.6: Sobolik, S.R., 2015. *Sandia Analysis of the Safe Operation Capability of West Hackberry Caverns 8 and 9 from a Geomechanical Perspective*, Letter to Paul Malphurs, DOE-SPR, April 22, 2015.

6.1 *PRELIMINARY RECOMMENDATIONS REGARDING THE MAXIMUM LENGTH OF WORKOVER OF WEST HACKBERRY CAVERN 8 ON CAVERN 9 DURING CAVERN 6 OIL REMOVAL PROCESS*

This letter serves as an update to the milestone to evaluate the impact of long duration depressurization of West Hackberry Cavern 8 on Cavern 9, in particular while Cavern 6 is undergoing oil removal. The driving concern for this task is that Cavern 8 required borehole diagnostic (well 8A) and remediation (wells 8 and 8B) work that may require it to be depressurized for significantly greater than three months, which is the typical maximum workover period. This concern is augmented because of the close proximity of Cavern 8 to Cavern 9, and the reduced pressure in nearby Cavern 6 during its oil removal process. Although the previous geomechanical analyses performed by Sandia have been helpful to understand the interaction between these three caverns during workovers, they did not capture the unusual sequence of activities involving these caverns that have occurred in the past 2-3 years and will continue well into 2014. Therefore, it was decided to perform additional modeling calculations simulating recent and scheduled workover activities to determine the effect of an extended Cavern 8 workover on Cavern 9.

The requirement to perform these new calculations has unfortunately occurred during the time when, out of necessity, the West Hackberry geomechanical model has had to transition from the use of the Sandia code JAS3D to the upgraded Sandia-designed code ADAGIO. This transition was made necessary because of the recent decision by the Computational Mechanics groups at Sandia to discontinue support and implementation of JAS3D on its servers in favor of the newer ADAGIO code. In other words, for reasons beyond our control, JAS3D is no longer available for use. On the positive side, ADAGIO does provide potential new benefits for future analytical purposes, such as the capability to model coupled thermal-hydrological-mechanical behavior with other codes in the Sierra computational domain, of which ADAGIO is a thermal-mechanical simulation program. In addition, the West Hackberry geomechanical model is also being transitioned from using the previous half-dome computational mesh to a mesh containing the full dome, and all caverns built with axisymmetric geometries based on sonar data. Beginning in late May 2013, two sets of calculations were initiated: one with the original half-dome mesh to produce results that may be compared with previous JAS3D calculations for the purpose of validation; and the other with the full dome, whose number of elements is six times as great as the previous half dome mesh, resulting in much longer simulation CPU times. For both sets of calculations, after the "base-case" results were obtained, the next step was to run two or three simulations beginning from a simulation time just prior to the 2010 WH-6 workover to include actual pressure histories in Caverns 6, 8, and 9 up to the beginning of the WH-8 workover, then different potential workover schedules to evaluate the effect of workover length on WH-9.

Unfortunately, there have been several problems getting the calculations to completion. Many of the problems have involved the lack of availability of the CPU nodes on the high-performance computer Redsky where the parallelized calculations must be performed, resulting from power outages, the resulting repair to processing and memory units, and high-priority computing by some of the defense groups. Other problems are related to the transition to the new code, some unexpected numerical convergence issues using the M-D model, and the numerical instability generated by the geometry of the rim of WH-6 when it closes during simulated workovers. Also,

some of the early results, particularly predicted surface subsidence, have had some noticeable disagreement with the JAS3D predictions (which was not the case for the transition of the Bryan Mound model from JAS3D to ADAGIO (Sobolik, 2013), for which the results were nearly identical).

While these computational issues will be resolved over the next few weeks or months, it is apparent that there is a need for a more immediate evaluation of the effect of the WH-8 workover on WH-9. The workover on WH-8 began on April 11, 2013, to perform diagnostic work on well 8A, and remediation work on wells 8 and 8B; the wellhead pressure reached 0 psi on April 16, 2013. The date of this memo, July 25, 2013, reflects 100 days of zero wellhead pressure, which is about the usual maximum workover period. The WH-8 workover is currently scheduled to end on September 14, 2013. A complete schedule of the actual workovers since 9/28/2010, and the workovers on WH-8 and WH-9 as currently scheduled, is given in Table 1, along with measured or expected wellhead pressures. While working toward resolving the computational issues, a preliminary evaluation of the WH-8 workover issue has been performed using the results from the 2010 calculations using the half-dome model. Normally, an evaluation of cavern and wellbore stability would examine three key performance indicators: axial wellbore strain, cavern closure, and dilatant stress in the salt surrounding the cavern. Previous analyses have shown that the axial wellbore strains for both WH-8 and WH-9 are predicted to be well below the standard 1.6 millistrain plastic threshold through 2014, so this indicator does not appear to be a concern. However, because of the hourglass shape of WH-9, and the concentration of deviatoric, possible dilatant stress conditions in the ledge at the cavern's mid-depth, the indicators of salt behavior must be examined. Therefore, predictions for the effect on WH-9 during a normal workover on WH-8 will be shown for a 90-day workover, by presenting the predicted effects on dilatant stress in the salt, and cavern closure for WH-9. Then, these results will be extrapolated for a 150-day period using the trends observed over 90 days. These predictions were obtained during a time when WH-6 was fully pressurized in the model, and not at its current reduced wellhead pressure during oil removal. This discrepancy will be addressed as well.

Figure 1 shows the cavern closure rate for Caverns 6, 8, and 9 using the JAS3D calculations and a regular 5-year workover cycle. The large changes in volume closure during workovers; however, it can be seen that a workover on either Cavern 6 or Cavern 8 increases the closure rate of Cavern 9. (Similar cavern interactions on WH-6 and WH-8 can also be observed when WH-9 is in workover mode.) The cavern closure rate for WH-9, which is another way of measuring the cavern pressurization rate due to cavern creep, can increase by as much as a factor of 10 when CWH-6 is undergoing a workover, and a factor of 4 during a WH-8 workover. Presumably, the corresponding measured changes in pressurization rates for WH-9 should be by roughly the same factors. However, note that during a nearby workover, and after that workover, a steady decrease in the pressurization rate (slope) occurs after the initial perturbation, and that over the long term the workovers on nearby caverns do not have a significant influence on the normal creep closure of WH-9.

Table 1. Actual and scheduled workovers on WH Caverns 6, 8, and 9.

Date	Duration, days	Description	Cavern 6 WHP (avg.)	Cavern 8 WHP (avg.)	Cavern 9 WHP (avg.)
9/28/2010	5	**Begin WH-6 actual WO**	**oil, 900 psi head**	oil, 925 psi head	oil, 925 psi head
10/3/2010	103	**WH-6 actual WO**	**0 psi head**	oil, 925 psi head	oil, 925 psi head
1/14/2011	3	**WH-6 Re-pressurize, actual WO**	**0 psi head**	oil, 925 psi head	oil, 925 psi head
1/17/2011	14	**Re-pressurize, actual WO**	**700 psi head**	oil, 925 psi head	oil, 925 psi head
1/31/2011	39	**WH-6 wellhead pressure**	**850 psi head**	oil, 925 psi head	oil, 925 psi head
3/11/2011	440	**WH-6 higher pressure**	**1070 psi head**	oil, 925 psi head	oil, 925 psi head
5/24/2012	4	**Begin WH-6 actual WO**	**1070 psi head**	oil, 925 psi head	oil, 925 psi head
5/28/2012	83	**WH-6 actual WO**	**0 psi head**	oil, 925 psi head	oil, 925 psi head
8/19/2012	2	**WH-6 Re-pressurize, actual WO**	**0 psi head**	oil, 925 psi head	oil, 925 psi head
8/21/2012	2	**WH-6 Re-pressurize, actual WO**	**325 psi head**	oil, 925 psi head	oil, 925 psi head
8/23/2012	3	**WH-6, Hold until 8/26**	**650 psi head**	oil, 925 psi head	oil, 925 psi head
8/26/2012	3	**WH-6 Re-pressurize, actual WO**	**650 psi head**	oil, 925 psi head	oil, 925 psi head
8/29/2012	12	**WH-6, Hold until 9/10**	**850 psi head**	oil, 925 psi head	oil, 925 psi head
9/10/2012	144	**WH-6 wellhead pressure**	**919 psi head**	oil, 925 psi head	oil, 925 psi head
2/1/2013	69	**Begin WH-6 oil removal**	**530 psi avg head**	oil, 925 psi head	oil, 925 psi head
4/11/2013	5	**Begin actual WH-8 WO**	**530 psi avg head**	**oil, 925 psi head**	oil, 925 psi head
4/16/2013	90	**WH-8 actual WO**	**530 psi avg head**	**0 psi head**	oil, 925 psi head
7/15/2013	7	**End of 90-day WH-8 WO**	**530 psi avg head**	**0 psi head**	oil, 925 psi head
7/22/2013	54	**End of WH-8 repress (90-day WO)**	**530 psi avg head**	**0 psi head**	oil, 925 psi head
9/22/2013	122	**End of WH-8 WO**	**530 psi avg head**	**oil, 925 psi head**	oil, 925 psi head
1/22/2014	5	**Sched: Begin WH-9 WO**	**530 psi avg head**	oil, 925 psi head	**oil, 925 psi head**
1/27/2014	27	**Sched: WH-9 WO**	**530 psi avg head**	oil, 925 psi head	**0 psi head**
2/25/2014	21	**Sched: Begin Diagnostic WO WH-6**	**0 psi head**	oil, 925 psi head	**0 psi head**
3/18/2014	67	**Sched: End Diagnostic WO WH-6**	**530 psi avg head**	oil, 925 psi head	**0 psi head**
5/24/2014		**Sched: End WH-9 WO**	**530 psi avg head**	oil, 925 psi head	**oil, 925 psi head**

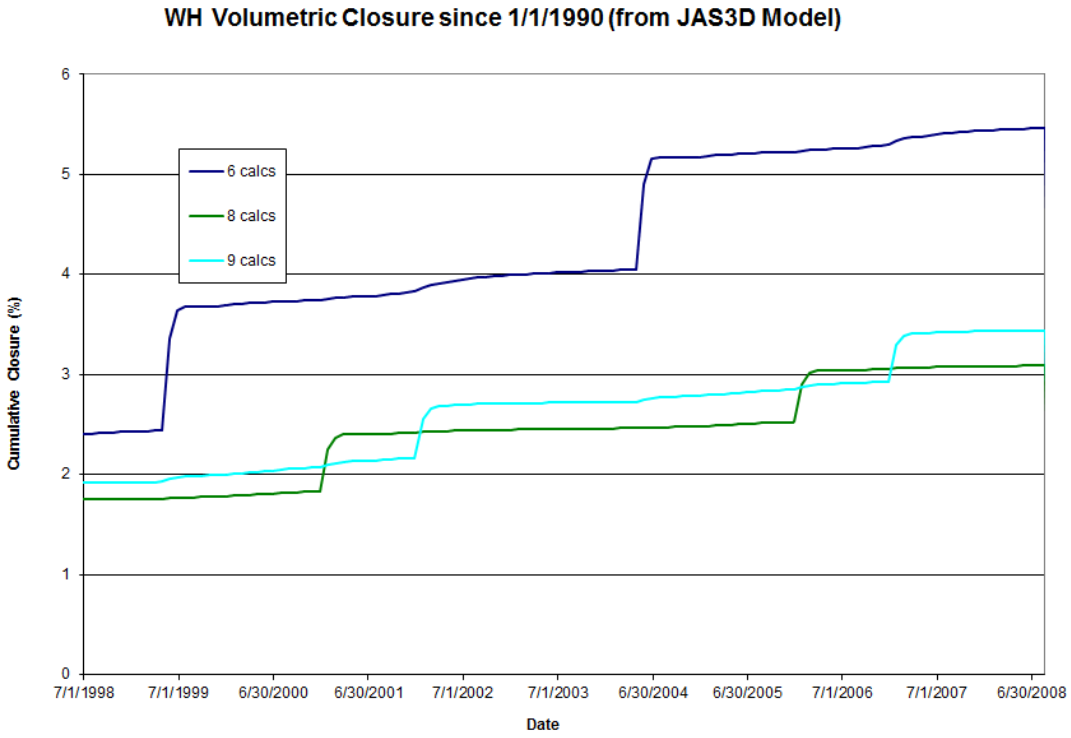

Fig. 1. Predicted cavern closure for Caverns 6, 8, and 9, JAS3D predictions.

Figure 2 shows the predicted minimum damage factor in the salt around WH-9 calculated for the time period after the September 2010-January 2011 workover of WH-6. The damage factor indicates when deviatoric stresses in the salt reach a state where microfracturing would begin, causing an increase in permeability of the salt and a greater potential for actual fracturing; a value less than 1 indicates the onset of microfracturing, and a value of 1.5 has been chosen as a "safety factor" value to maintain. For WH-9, the area of concern has been the ledge; previous analyses indicate that a fast repressurization would create damage factors less than 1 in the ledge. Remember that at the end of the WH-6 workover, the wellhead pressure for WH-6 was increased gradually over a period of 17 days to avoid a large stress perturbation that would induce dilatant stress in the ledge of WH-9. Two additional workovers followed in the simulation: a workover on WH-9 about 45 days after WH-6 reached normal operating pressure, and a workover on WH-8 nearly a year later. Note that the perturbation induced by the workover in WH-8 creates an inconsequential change in the predicted minimum damage factor. This result would indicate that a WH-8 workover alone would not cause dilatant damage around WH-9. However, the current situation includes the complication of the oil removal process from WH-6, during which the pressures in that cavern are around 400 psi less than usual. Because the pressure differential between WH-6 and WH-9 is around 400 psi, and also because there was a two-month interval between the beginning of oil removal from WH-6 and the WH-8 workover, allowing time for the stresses around WH-9 to adjust to the WH-6 perturbation, it does not seem likely that the combination of the effects from the two caverns will create conditions that would dramatically change the damage factor for the worse. Additionally, as pressures in both WH-6 and WH-8 are held steady during their respective procedures, the stresses around WH-9 are able to readjust and equilibrate, reducing the dilatant stresses over time. This would indicate that, so long as there

are no large pressure perturbations in WH-6, the workover in WH-8 may continue until its scheduled September end date with no expected damage to WH-9.

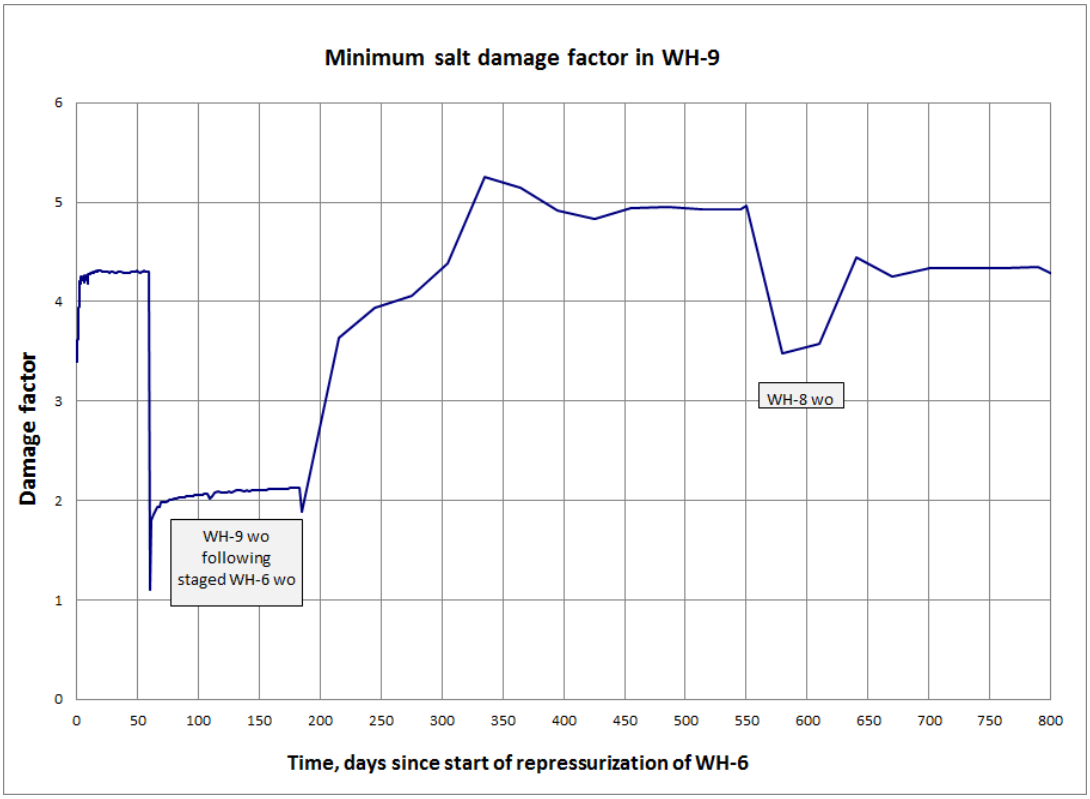

Fig. 2. Minimum dilatant damage factor around WH-9, JAS3D predictions.

Conclusions

An evaluation of the effect of the current WH-8 workover on the integrity of WH-9, using the results of previous geomechanical analyses, indicate that it is unlikely that a 5-month workover period will have detrimental effects on WH-9. This conclusion is caveated by the assumption that the oil removal operations in WH-6 experience no large pressure perturbations while WH-8 is pressured down. The remaining primary concern about the duration of the WH-8 workover is the lost volume due to higher creep under low cavern pressure conditions. A more rigorous geomechanical computational analysis is currently underway, but it is not proceeding as quickly as desired due to several issues regarding computer resource availability, transition to a new numerical code and its own numerical and logistical issues, and other model enhancements which still require some debugging. Once the computational problems have been resolved, a more detailed analysis of the WH-8 workover will be completed. The completion of the WH-8 workover analysis will act as a prologue to the analysis of the coincident WH-9 and WH-6 workovers scheduled for early 2014.

References

- Sobolik, S.R., 2013. *Verification of the Transition from JAS3D to ADAGIO for the Bryan Mound Geomechanical Model.* Letter Report to Robert Myers, DOE-SPR, March 21, 2013, Sandia National Laboratories, Albuquerque, New Mexico.

6.2 *RECOMMENDATIONS REGARDING THE MAXIMUM LENGTH OF WORKOVERS OF WEST HACKBERRY CAVERNS 6, 8, AND 9 DURING CAVERN 6 OIL REMOVAL PROCESS*

This letter serves as completion to the milestone to evaluate the impact of long duration depressurizations of West Hackberry Caverns 6, 8 and 9, in particular while Cavern 6 is undergoing oil removal. There are several driving concerns for the analyses described in this letter. There have been long standing concerns about the stability of both caverns WH-6 and WH-9 due to the large diameters, unusual geometries, and close proximity to each other (Sobolik, 2012). Because of these concerns, DOE made the decision to remove the oil from WH-6 for the opportunity to inspect the current geometry and condition of the cavern before making a decision on its long-term status. The oil removal from WH-6 began in February 2013. In addition, Cavern 8 required borehole diagnostic (well 8A) and remediation (wells 8 and 8B) work that required it to be depressurized for significantly greater than three months, which is the typical maximum workover period. This concern was augmented because of the close proximity of Cavern 8 to Cavern 9, and the reduced pressure in nearby Cavern 6 during its oil removal process. Although the previous geomechanical analyses performed by Sandia have been helpful to understand the interaction between these three caverns during workovers, they did not capture the unusual sequence of activities involving these caverns that have occurred in the past 2-3 years and will continue well into 2014. Therefore, it was decided to perform additional modeling calculations simulating recent and scheduled workover activities to determine the effect of extended simultaneous workover activities on Caverns 6, 8, and 9.

The purposes of the analyses described in this letter are to evaluate the stability of West Hackberry Caverns 6, 8, and 9, given the workover schedule described later in this letter (most importantly, a 4-month workover on WH-9 beginning in late January 2014, with a concurrent 3-week workover in WH-6 beginning in late February), and to provide recommendations for maximum duration, depressurization and repressurization schedules, and maximum pressure differential for these caverns. Cavern stability can be described by two components: one, the stability of the cavern walls themselves, and the pillars between caverns, due to the pressure changes during cavern operations; and two, the stability of the wellbore casings during those operations. Based on our discussions at SNL Project Review during the first week of December, the following five items are required to satisfy the requirements of the milestone:

1. Predictions for damage factors and maximum principal stresses that the workover scenario above would impose around the cavern walls for WH-6, 8, and 9. (These results were presented at the SNL Project Review in Albuquerque on December 4, 2013, and included in this letter.)
2. Predictions of the casing strains that the workover scenario above would impose on the wellbores for WH-6/8/9, and identification of any wellbores which may experience strains above accepted thresholds during the time period. This item would also include casing strain histories at several depth locations along each wellbore.
3. Based on the results obtained for Items 1 and 2, a general assessment of borehole impact pertaining to workovers on WH 6/8/9, with SNL recommendations on maximum total workover length and/or cumulative length of several workovers before accepted strain thresholds are exceeded.

4. SNL recommendations for depressurization and repressurization schedules for WH-6 and WH-9.
5. SNL recommendations for the maximum differential pressure between WH-6 and WH-9.

Based on the results of previous calculations with JAS3D (Sobolik and Ehgartner, 2009), and recent calculations with Adagio that employ the given workover schedule, responses for these items are included in this letter. A complete schedule of the actual workovers on Caverns 6, 8, and 9 since 9/28/2010, and the workovers on WH-6 and WH-9 as currently scheduled, is given in Table 1, along with average measured or expected wellhead pressures. For the new Adagio calculations, the depressurization and repressurization of WH-9 were both modeled to occur over a five-day period, to minimize the effect of pressure change on the creep strain rate, thus minimizing the potential for damage to the cavern salt. The 2014 workover on WH-6 was also simulated with 5-day de/re-pressurization schedules.

Table 1. Actual and scheduled workovers on WH Caverns 6, 8, and 9.

Date	Duration, days	Description	Cavern 6 WHP (avg.)	Cavern 8 WHP (avg.)	Cavern 9 WHP (avg.)
9/28/2010	5	Begin WH-6 actual workover	900 psi	925 psi	925 psi
10/3/2010	103	WH-6 actual workover	0 psi	925 psi	925 psi
1/14/2011	3	WH-6 Re-pressurize, actual workover	0 psi	925 psi	925 psi
1/17/2011	14	Re-pressurize, actual workover	700 psi	925 psi	925 psi
1/31/2011	39	WH-6 wellhead pressure	850 psi	925 psi	925 psi
3/11/2011	440	WH-6 higher pressure	1070 psi	925 psi	925 psi
5/24/2012	4	Begin WH-6 actual workover	1070 psi	925 psi	925 psi
5/28/2012	83	WH-6 actual workover	0 psi	925 psi	925 psi
8/19/2012	2	WH-6 Re-pressurize, actual workover	0 psi	925 psi	925 psi
8/21/2012	2	WH-6 Re-pressurize, actual workover	325 psi	925 psi	925 psi
8/23/2012	3	WH-6, Hold until 8/26	650 psi	925 psi	925 psi
8/26/2012	3	WH-6 Re-pressurize, actual workover	650 psi	925 psi	925 psi
8/29/2012	12	WH-6, Hold until 9/10	850 psi	925 psi	925 psi
9/10/2012	144	WH-6 wellhead pressure	919 psi	925 psi	925 psi
2/1/2013	69	Begin WH-6 oil removal	530 psi	925 psi	925 psi
Date	Duration, days	Description	Cavern 6 WHP (avg.)	Cavern 8 WHP (avg.)	Cavern 9 WHP (avg.)
4/11/2013	5	Begin actual WH-8 workover (depressure)	530 psi	925 psi	925 psi
4/16/2013	149	WH-8 actual workover	530 psi	0 psi	925 psi
9/22/2013	122	End of WH-8 workover	530 psi	925 psi	925 psi
1/22/2014	5	Sched: Begin WH-9 workover (depressure)	530 psi	925 psi	925 psi
1/27/2014	27	Sched: WH-9 workover (115 days total)	530 psi	925 psi	0 psi
2/25/2014	21	Sched: Begin Diagnostic workover WH-6	0 psi	925 psi	0 psi
3/18/2014	67	Sched: End Diagnostic workover WH-6	530 psi	925 psi	0 psi
5/24/2014		Sched: End WH-9 workover	530 psi	925 psi	925 psi

Item 1: Stability of cavern walls and pillars during scheduled workovers

The damage factor indicates when deviatoric stresses in the salt reach a state where microfracturing would begin, causing an increase in permeability of the salt and a greater potential for actual fracturing; a value less than 1 indicates the onset of microfracturing, and a value of 1.5 has been chosen as a "safety factor" value to maintain. For WH-9, the area of concern has been the ledge; previous analyses indicate that a fast repressurization would create damage factors less than 1 in the ledge.

Figure 1 shows the predicted minimum damage factors around Caverns 6, 8, and 9 using the workover schedule in Table 1 and the Adagio calculations based on that schedule. Figure 2 is a contour plot of the damage factor in the pillar between WH-6 and WH-9 on 2/25/2014, the scheduled beginning of the workover on WH-6. Several observations can be made from these figures. First, in Figure 1 the minimum damage factor never falls below 1.5 for WH-8. Second, during the proposed workover for WH-9 in 2014, the minimum damage factor around WH-9 decreases to about 1.2 for the duration. The location of the minimum damage factor for WH-9 is in the ledge of the cavern, as shown in Figure 2. Figure 1 shows that the three-week workover on WH-6, scheduled to happen during the workover on WH-9, has almost no effect on the ledge in WH-9. Two minima in damage factor to WH-6 are observed during this three-week workover, and better perspective is gained from looking at the spatial distribution of damage factor in Figure 2. Note that the predicted damage factors in the pillar between WH-6 and WH-9 illustrated in Figure 2 on 2/25/2014 are well above the safety threshold. The location for the minimum damage factor for WH-6 is at the circumference of the main bowl of the cavern, where the rim begins. Moreover, the duration and areal extent of the low damage values on WH-6 are small, and at the times when the pressure change in the cavern commences; as a result, any damage to the cavern wall around WH-6 will be very localized and of minimal concern to the nearby caverns.

Figure 3 shows a time series of the predicted maximum principal stress in the salt around Caverns 6, 8, and 9. Tensile stresses are positive in this plot, and because salt has very little tensile strength, the preference is to avoid tensile stresses. Again, the workover on WH-9 does not produce tensile stresses in the ledge, and the workover on nearby WH-6 has no effect on those stresses. Figure 4 is a contour plot of maximum principal stress in the pillar between the two caverns on 2/25/2014 (similar to Figure 2), and similar conclusions may be drawn: the pillar between the caverns is not adversely affected by the coincident workovers, and region around the circumference of the bowl of WH-6 is only of minimal concern. Based on these results, the planned coincident workovers on WH-6 and should not impact cavern stability for those caverns or for WH-8.

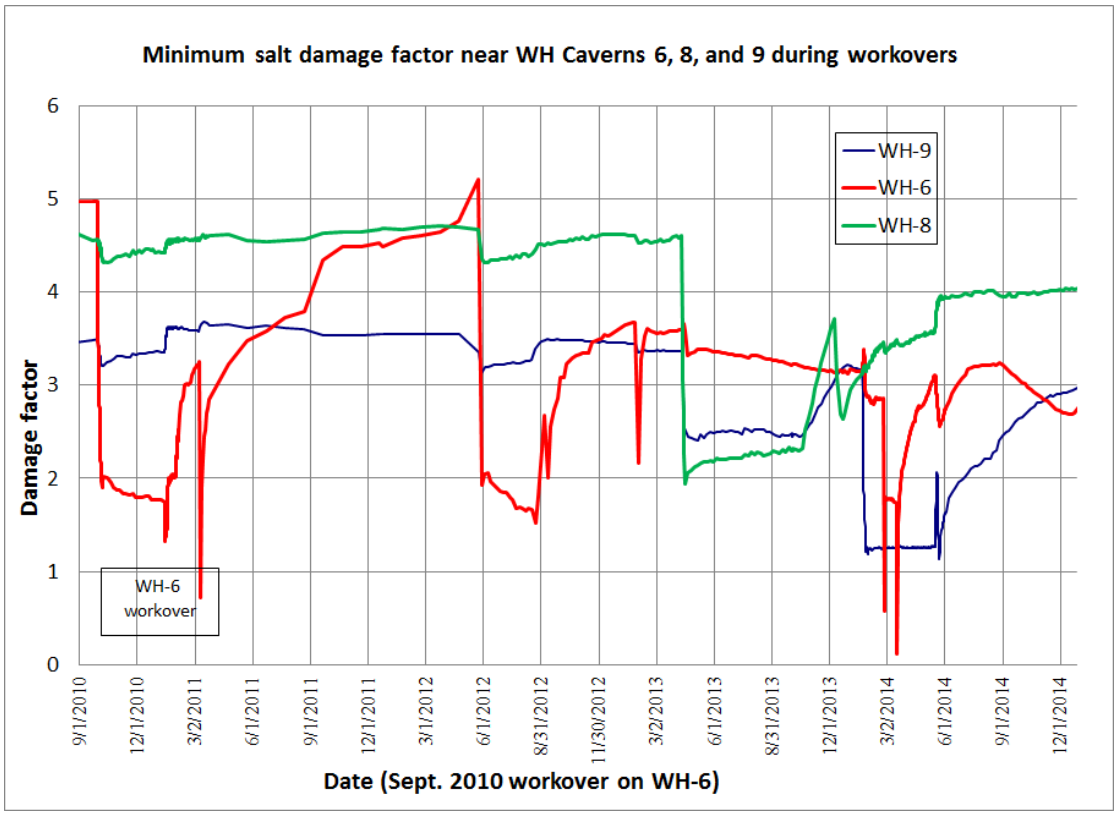

Fig. 1. Predicted minimum dilatant damage factor around WH caverns 6, 8, and 9.

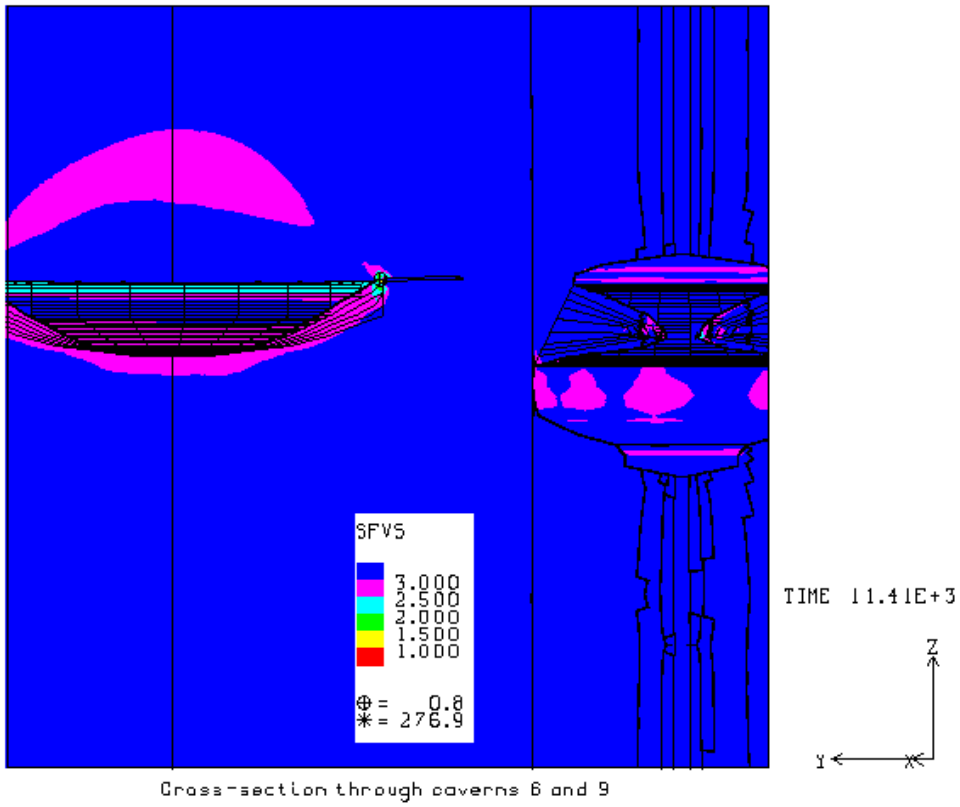

Fig. 2. Dilatant damage factor between WH-6 and WH-9 on 2/25/2014, beginning of WH-6 workover during WH-9 workover.

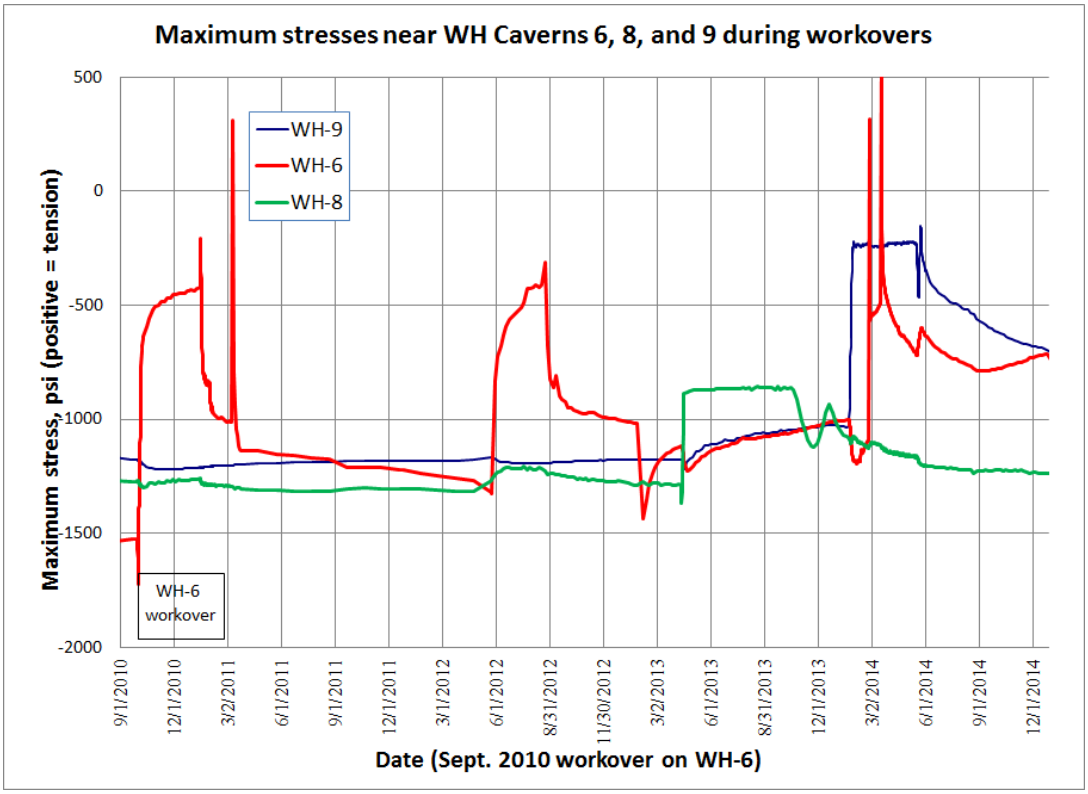

Fig. 3. Predicted maximum principal stress around WH caverns 6, 8, and 9.

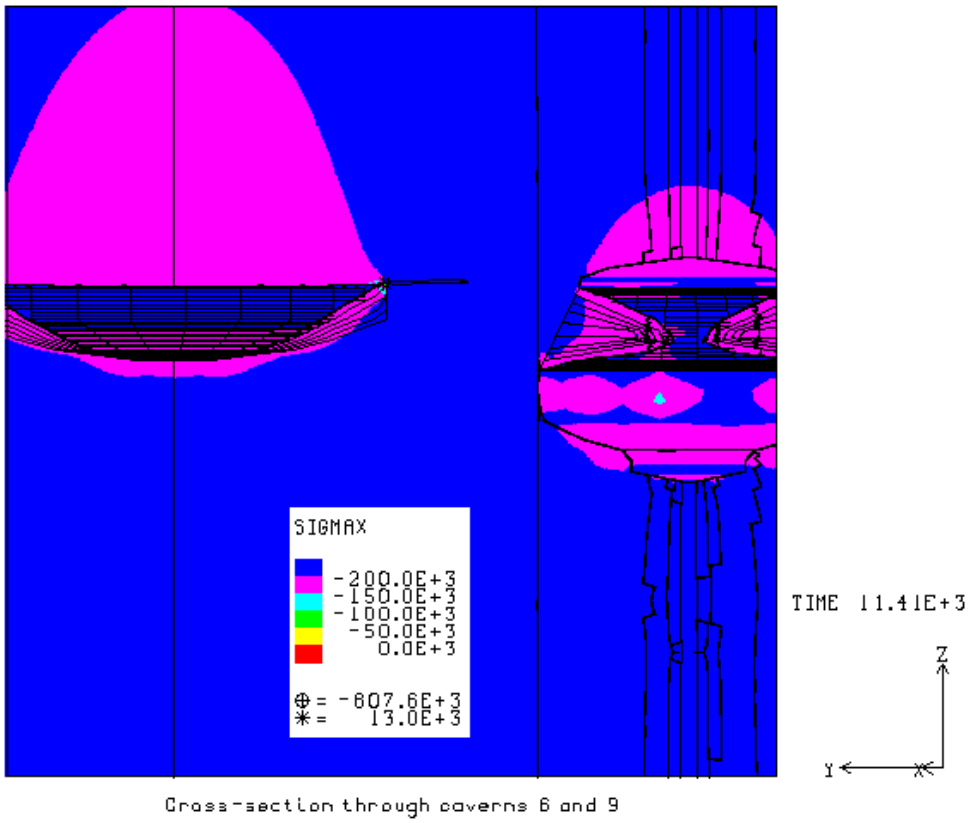

Fig. 4. Predicted maximum principal stress between WH-6 and WH-9 on 2/25/2014, beginning of WH-6 workover during WH-9 workover.

Item 2: Stability of wellbore casings during scheduled workovers

As the caverns close due to creep, vertical strain is created along the borehole casings. The majority of the strain that is accumulated in the casing occurs during workovers, when the wellhead pressure is zero and the resulting lower cavern pressure allows creep closure to occur at a much faster rate than at normal operating conditions. In previous analyses, a prediction of 1.6 millistrains (mϵ) has been used as a limiting threshold value for strain accumulation. The 1.6-millistrain threshold indicates the point at which plastic deformation of the steel will occur; however, it does not indicate the point of failure for the steel (i.e., the point at which the casing is breeched and fluid may flow outside the casing). The failure strain for the casing steel itself will be at a higher strain than 1.6 mϵ, but failure for the threaded joints will likely occur at a lower strain than the material itself. Because there is not a readily established strain value to use to determine the onset of steel casing failure, an absolute limit of 1.6 millistrains for any location along the borehole during a single workover will be used in this letter to determine the maximum duration of workover activities. The need to establish a threshold value for strain is addressed later in this letter.

Figures 5 and 6 show the vertical strain on the casings for WH-6, 8, and 9, accumulated since January 24, 2009, at specific points along the casing; Figure 5 displays six years from 2009- 105, while Figure 6 is a zoom of the period April 2013 – June 2014. For WH-6 in Figure 5, two monitoring points are selected, one at the cavern ceiling (3230 feet depth) and one at the maximum strain location (2884 feet depth – about 340' above the ceiling). For WH-8 and WH-9, the maximum strain location is at the ceiling. The plotted time period in Figure 5 includes the late-2010 and mid-2012 workovers on WH-6, the 5-month workover on WH-8 in 2013, and the scheduled workovers on 2014 for WH-6 and 9. Figure 7 shows the strain as a function of distance from the ceiling of WH-9, at different points in time.

The 2014 workover (commence 1/22/2014) for WH-9 is currently planned for 120 days; the event was modeled for 100 days at zero wellhead pressure, with 5-day depressurization and repressurization periods. Figures 5 and 6 indicate that the strain rate in the casing decreases over time during a workover: a total accumulation of 0.44 mϵ during the initial 5-day depressurization period, ending with a strain rate of 0.14 mϵ/day; an additional 0.31 mϵ after ten days of zero wellhead pressure, closing with a strain rate of 0.02 mϵ/day; an additional 0.77 mϵ, 0.005 mϵ/day at the end of 90 days; and finally another 0.11 mϵ, 0.005 mϵ/day during the last 20 days, totaling 1.63 mϵ over the 100 days. After the cavern is repressurized, a small amount of strain, 0.14 mϵ, is predicted to be recovered. These strains are predicted to occur near the cavern ceiling; the amount of strain is predicted to decrease as a function of distance above the cavern, as shown in Figure 6. The calculations predict that the 110-day workover on WH-9 will add an additional 1.6 millistrains to the bottom of the borehole, and at least 1 millistrain to the bottom 140' of borehole. The results from the earlier JAS3D calculations predicted a very similar strain rate for WH-9 when under workover.

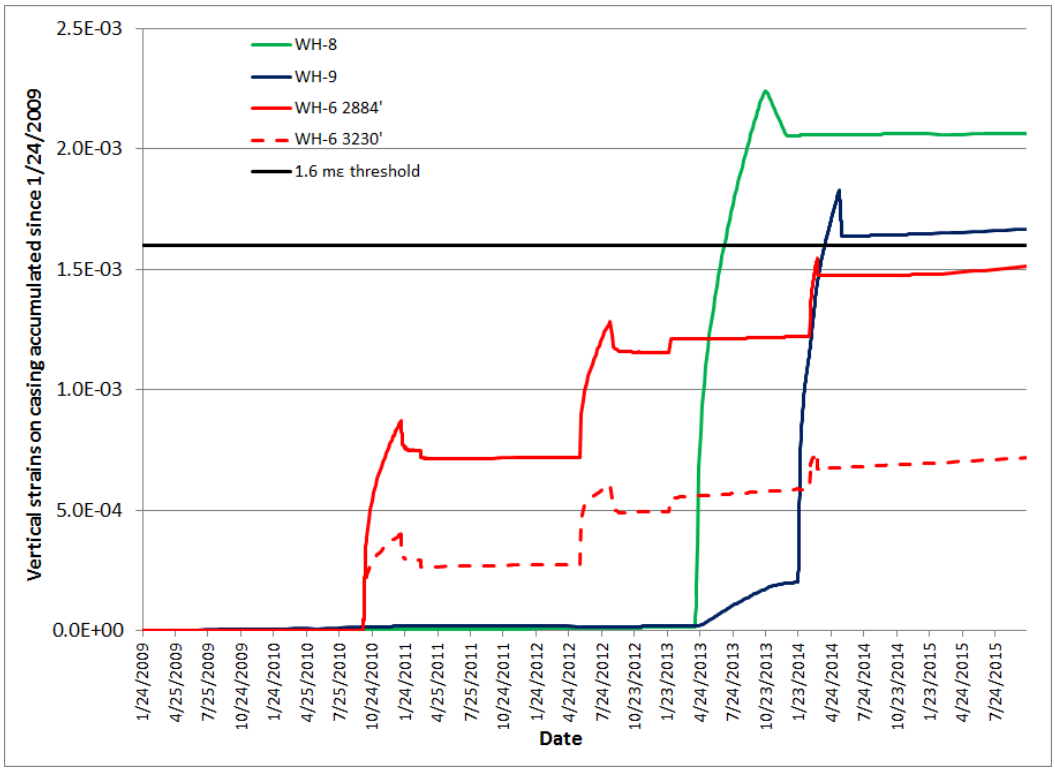

Figure 5. Predicted vertical casing strain for WH Caverns 6, 8, and 9 during scheduled workovers (2009-2014).

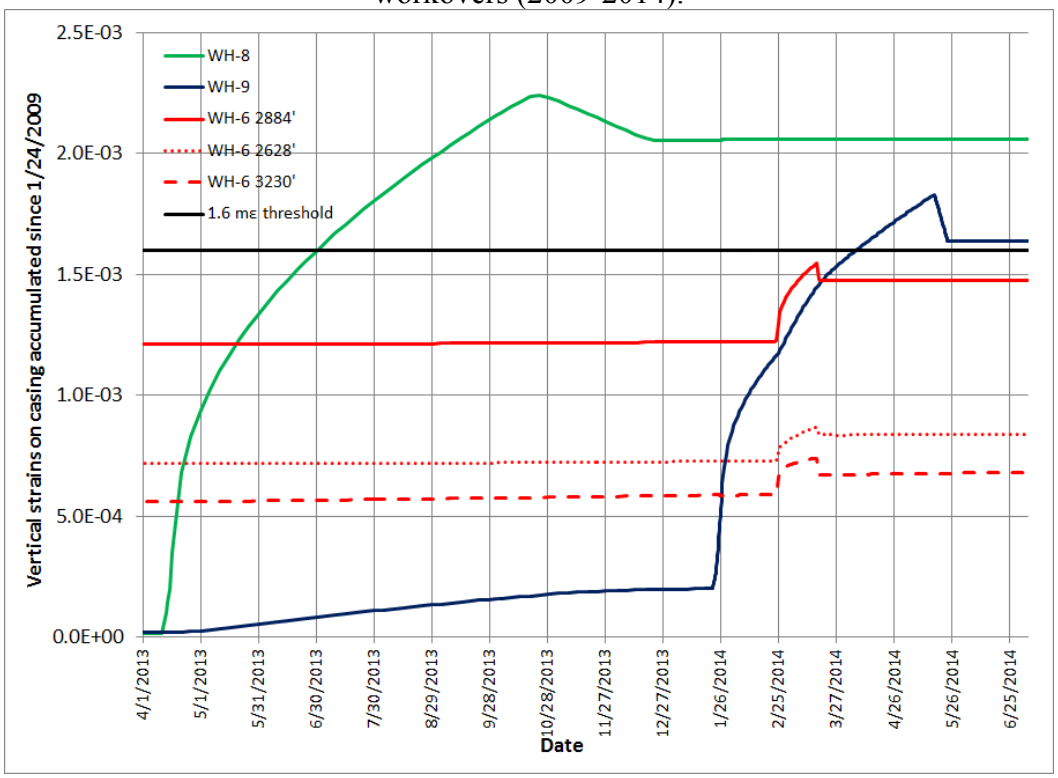

Figure 6. Predicted vertical casing strain for WH Caverns 6, 8, and 9 during scheduled 2014 workovers.

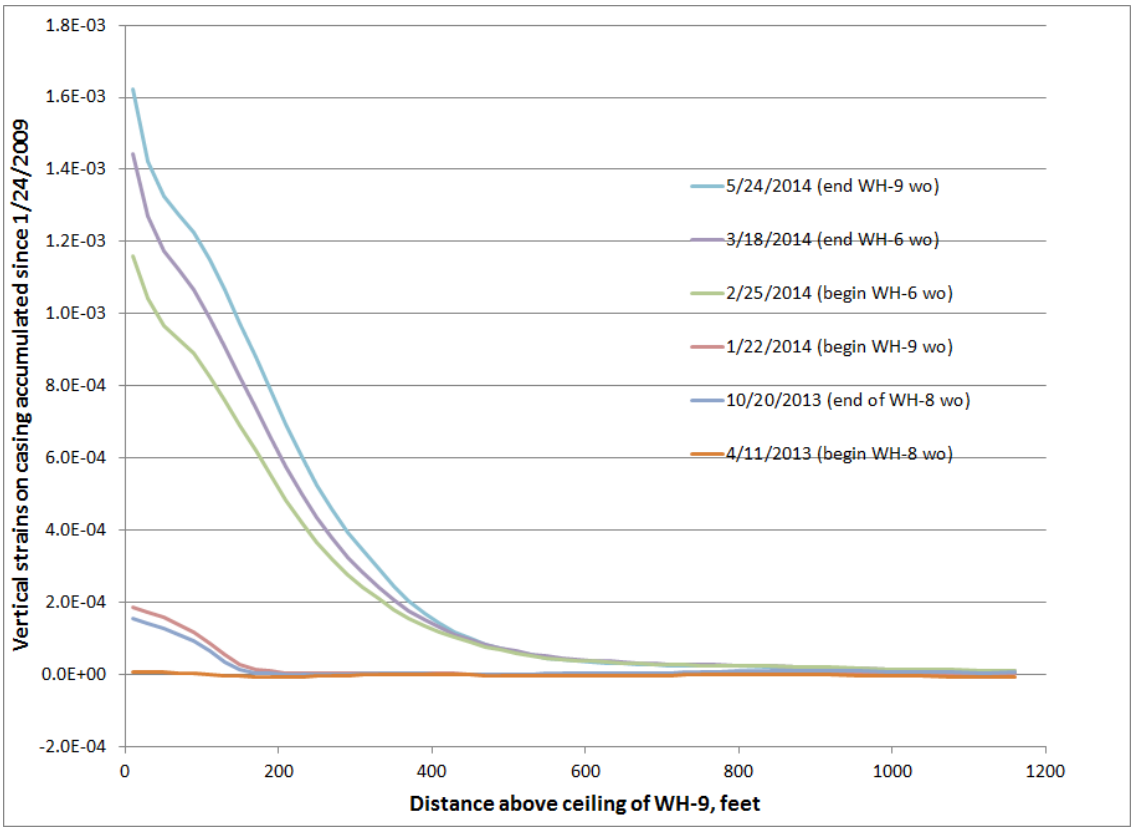

Figure 7. Predicted casing strain for WH-9 as a function of distance above the cavern ceiling.

Several observations can be made from Figures 5, 6 and 7:

- The three-week workover on WH-6 scheduled in February 2014 at the same time as the workover on WH-9 (and also while WH-8 is fully pressurized) appears to increase the strain rate for WH-9 from 0.010 mϵ/day to 0.015 mϵ/day. For the three-week duration of the planned WH-6 workover, this is not a significant increase.
- However, when WH-8 and WH-6 were at reduced pressure at the same time (April-September 2013), there is a noticeable effect on the casing for WH-9. The five-month workover on WH-8 added about 0.2 millistrains to the WH-9 casing.
- The five-month workover on WH-8 might have induced as much as 2 millistrains on the bottom of the borehole.
- The maximum strains for WH-8 and WH-9 occur at the bottom of the boreholes, whereas for WH-6 the maximum strain occurs roughly midway between the top of salt and top of cavern. (This discrepancy in the location of maximum strain might be explained by cavern ceiling geometries used in the models (flat vs. domal), and requires further evaluation.)

Item 3: SNL recommendations for the general assessment of borehole impact pertaining to workovers on WH 6/8/9

The predicted accumulated strains for WH Caverns 6, 8, and 9 (and also WH-7) come close to or exceed the 1.6-millistrain plastic deformation threshold during a workover lasting the standard 90 days or slightly longer. These values are significantly higher than for the Phase 2 caverns at West Hackberry, which typically should accumulate about 0.5 millistrains during their

workovers. This discrepancy is due to the unusual geometries and proximity of the caverns. As casing strain accumulates through multiple workovers, all three of these caverns are more likely to develop casing problems after 2-3 workovers, and are thus candidates for prioritized remediation. Therefore, it is important not only to set a limit of the duration of a single workover, but also to evaluate the effect of multiple workovers on accumulated strain in a particular casing. To complete this evaluation requires knowledge of the history of each borehole: the date of installation of the casing, the number and length of workovers since installation, casing shoe depth, etc.

Under Item 2, it was stated that the maximum strains for WH-8 and WH-9 are predicted to be located just above the ceiling. (Remember that the computational model does not explicitly include the casings, thus predicted strains in the salt are assumed to occur in the casings as well.) The cemented casings in SPR salt cavern boreholes do not typically extend all the way to the ceiling; in fact, casing shoe distances above the ceiling vary substantially in the WH caverns. For example, the WH-9 shoes are 500-700 feet above the ceiling, while for WH-8 they are only 30 feet above the ceiling. Therefore, using the large strains at the bottom of the borehole as an indicator of casing damage might be overly conservative for WH-9. It is also unclear how completely that strain experienced by the surrounding salt is imparted through layers of cement and steel liners to the innermost steel casing.

Therefore, to provide the appropriate extent of recommendations regarding the impact of workovers of WH-6, 8, and 9 on the boreholes, there are several outstanding issues:

1. Established threshold strain for failure of casing;
2. History of individual casings, including installation date and number/duration of workovers, to estimate strain accumulated to date;
3. Actual location of casing in the borehole and its correspondence to predicted strain;
4. Transmission of strain from salt to innermost casing.

The following comments are listed in two parts. The first is a list of recommendations that can be made right now, given the analytical results and available information. The second part is an issue that requires recommendations, but for which SNL does not yet have sufficient information to complete.

SNL makes the following recommendations for WH-6, 8, and 9, using 1.6 millistrains as an absolute limit for a single workover:

- The maximum total workover length (i.e., duration of zero wellhead pressure) for WH Caverns 6, 8, and 9, should be 90 days, to keep the accumulated strain during a single workover to less than 1.6 millistrains. This recommendation will be modified later based on gathering information regarding the amount of time these casings have already been in workover mode, as described below.
- Because individual workovers for WH-6, 8, and 9 can apply excessive strains to their casings, it is recommended that cavern pressure monitoring during and immediately after a workover should be intensified to detect the potential development of any leaks.
- WH-6 and 8 should not be depressurized at the same time, as the combination induces additional strain on the casings for WH-9.

- The planned workover for the inspection of all three boreholes for WH-9 is currently scheduled for 120 days, with an assumption that the cavern will be at zero wellhead pressure for 110 days. Because of the high strain rate at the beginning of a workover cycle, it is probably better (and thus recommended) to complete all three borehole inspections for WH-9 during the same workover than to break the work into two workovers. However, if rig availability necessitates interrupting the WH-9 workover, the question arises if there is a minimum time limit that must elapse before the second workover can be performed. Based on the results shown here, a longer elapsed time favors the cavern integrity by allowing the salt stresses to equilibrate back to pre-workover levels, thus minimizing dilatancy potential. However, the casing strain rates for WH-6 in figure 5 for the 2010 and 2013 workovers show a somewhat smaller initial strain rate during depressurization for the second workover. Using WH-6 as a predictor for WH-9, the potentially smaller casing strain rate may be more important than the potential for dilatancy in the cavern's ledge; therefore, the recommendation is that the second workover may occur as soon as the rig is available, provided that depressurization is performed slowly.
- Because of the length of time required to empty oil out of WH-6, and also budgetary considerations, the workovers on WH-6 and 9 might be delayed because of workover rig and funding availability. This potential delay will not be a problem as long as the wellhead at WH-6 is pressurized sufficiently to maintain a normal operating pressure at cavern depth (see recommendations below regarding pressure differential).

As of today, the schedule for WH-6 and 9 is as follows: 1) Completion of oil removal from WH-6 in April 2014; 2) Immediately begin workover and remediation of all three boreholes on WH-9, and perform concurrent workover and diagnostics on WH-6; 3) The contract for the workover rigs is scheduled to end in July 2014, and the WH-9 work might not be complete before the loss of the rig. Based on the above statements, the following scenarios are recommended for the conduct of the workovers:

1. If oil removal in WH-6 is completed by April, then the following scenarios are recommended:
    - If there is enough time to complete remediation of all three boreholes in WH-9, then perform concurrent work on WH-6 and WH-9, with the stipulation that WH-6 should be repressurized slowly when its work is finished.
    - If there is not enough time to complete remediation of all three boreholes in WH-9 before rig availability is lost, then the workover and diagnostics on WH-6 should be performed, then WH-6 repressurized. The WH-9 workover can be conducted when rig availability returns (estimated in January 2015).
2. If the oil removal is completed in May or June, then the WH-6 workover and diagnostics can be completed immediately, after which WH-6 should be repressurized, and then the WH-9 workover can be conducted when rig availability returns (estimated in January 2015).

The following issue regarding the effect on borehole casings will be addressed later in FY14:

- Boreholes for caverns WH-6, 8, and 9 have already developed significant strain due to previous workovers in their lifetime. It is likely that most or all of these casings have already accumulated more than 1.6 millistrains in some portion of their lengths. Because the 1.6 mε threshold does not necessarily equal (and is actually probably less than) the failure strain for

the casing, it is unknown how to develop a recommendation for total accumulated duration of workover time. In the near term, SNL will perform a combination of data mining, literature searches, and internal meetings to develop a specific recommendation for the maximum accumulated workover time for these caverns.

Item 4: SNL recommendations for depressurization and repressurization schedules for WH-6 and WH-9

Because of the unusual geometries and proximity of WH-6 and WH-9, SNL has recently recommended that depressurization and repressurization of these caverns occur over several days to minimize the creep strain rate due to stress change. (WH-8 does not have the geometry issues of WH-6 and WH-9, and may undergo typical de/re-pressurization procedures.) The primary driver for longer pressure change cycles is cavern integrity, as abrupt stress changes can induce dilatant stress conditions in the cavern wall. (Casing strain is not a driver for evaluating the duration of pressure change operations; it makes little difference during depressurization, and no discernible negative impact during repressurization.) For the late-2010 workover on WH-6, DOE employed a 5-day depressurization period (equivalent to a pressure drop rate of 7.5 psi/hr), and a stepped repressurization process for which the wellhead pressure was raised to 700 psi over 3 days (9.7 psi/hr), then up to 850 psi at 0.4 psi/hr over an additional 14 days. The change in repressurization rate at 700 psi wellhead pressure was recommended because it was after that corresponding cavern pressure that the cavern wall stresses trended toward undesirable levels.

Based on these observations, SNL makes the following recommendations:

- For WH-6, the recommended minimum duration for depressurization to zero wellhead pressure is 5 days (or maximum rate of 7.5 psi/hr); for repressurization, a minimum of 3 days at 9.7 psi/hr to raise the wellhead oil pressure (or, after oil removal, the wellhead brine pressure to 215 psi – see discussion below), followed by a minimum period of 14 days at 0.4 psi/hr to the minimum normal operating pressure of 850 psi (or wellhead brine pressure to 365 psi).
- For WH-9, the recommended minimum duration for depressurization and repressurization is 5 days (7.5 psi/hr).

When the oil removal from WH-6 is complete, there will need to be a different "normal operating range" for wellhead pressure, as the borehole and most of the cavern will be filled with brine, not oil. It will be important to maintain the same pressure at the cavern ceiling during brine storage as it was during oil storage. Using 0.37 lb/ft^3 as the density of oil, and 0.52 lb/ft^3 as the density of brine, and 3230 feet as the depth of the ceiling of WH-6, the wellhead pressure P under brine that would correspond to a 900-psi wellhead pressure with oil can be calculated by:

$$900 + (0.37)3230 = P + (0.52)3230;\ P=415.5\ \text{psi}.$$

Therefore, such a conversion will be required once the oil has been removed from WH-6.

Item 5: SNL recommendations for the maximum differential pressure between WH-6 and WH-9

From a cavern integrity perspective, there are two predominant cavern features that give concern. One is the outer rim around WH-6, which was detected in sonar measurements from circa 1980. The current condition of that outer rim – whether it is still open and containing oil, it is partially or totally closed, or if it has grown larger – is currently unknown; the planned 2014 workover will hopefully provide new information on the rim's status. If a new fracture were to extend radially from the rim, it may possibly intersect WH-9 and result in significant communication between the two caverns. The other concern is the ledge in WH-9 between the upper and lower lobes; its geometry results in a stress concentration region which may result in salt falls or a conduit to nearby caverns, particularly WH-6. These features have thus far governed our approach to pressure maintenance for these caverns. The riskiest time periods are during depressurization and repressurization, when the stress and strain rates are highest and most likely to induce tensile or dilatant conditions in these features. This concern is addressed by extending the duration of pressure change, as described in Item 4. The next time periods of concern are the workover periods themselves, when one cavern is at zero wellhead pressure and the other at normal operating pressure. Because the tops of the caverns are at nearly the same depth (3230' for WH-6, 3180' for WH-9), the difference in cavern pressures at the ceiling is approximately the difference in oil wellhead pressure during normal oil storage operations. When one of the caverns is in workover, the stresses around the nearby cavern are altered. Fortunately, the current and previous calculations show that the effect of one cavern's workover, in itself, directs the other cavern toward less desirable stress conditions but does not drive it into unsafe stress conditions. In particular, Figures 1 and 3 indicate that the predicted minimum dilatant damage factor and maximum stress around WH-9 during its workover are unaffected when WH-6 is depressurized; the stress fields are affected, but not enough to adversely impact WH-9 at its ledge. Therefore, from a cavern integrity standpoint, there is no need to specify a maximum wellhead (or cavern ceiling) pressure differential between WH-6 and WH-9, so long as pressure change operations are performed slowly, and there is no indication of communication or fluid loss between the caverns (i.e. WH-6 and 9 can be depressurized either separately or together, given appropriately slow depressurization and repressurization processes).

However, the plots in Figures 5 through 7 indicate that casing strain for one of these caverns is significantly affected when it is under workover, and under certain conditions can affect the strain in a nearby cavern. Based on the results presented here, the recommendation under Item 3 is reiterated: WH-6 and 8 should not be depressurized at the same time, as the combination induces additional strain on the casings for WH-9.

Conclusions – Summary of Recommendations

Here is a summary of SNL's recommendations regarding workovers for WH Caverns 6, 8, and 9 (see detailed discussion of these recommendations in the main text):

- The recommended maximum total workover length (i.e., duration of zero wellhead pressure) for a single workover for WH Caverns 6, 8, and 9, is 90 days. A recommendation regarding the maximum total accumulated workover duration from multiple workovers will be forthcoming later in FY14.
- It is preferable to complete all three borehole inspections for WH-9 during the same workover (which is currently scheduled for 120 days) than to break the work into two workovers.
- If rig availability necessitates interrupting the WH-9 workover, the primary recommendation is that the workover wait until the rig is available in January 2015. If, however, the workover is initiated and then interrupted, the second workover may occur as soon as the rig is available, provided that depressurization of WH-9 is performed slowly.
- A potential delay of the workovers on WH-6 and 9 because of workover rig and funding availability will not be a problem as long as the wellhead at WH-6 is pressurized sufficiently to maintain a normal operating pressure at cavern depth.
- Cavern pressure monitoring during and immediately after a workover on WH-6, 8, or 9 should be intensified to detect the potential development of any leaks.
- WH-6 and 8 should not be depressurized at the same time, as the combination induces additional strain on the casings for WH-9.
- For WH-6, the recommended minimum duration for depressurization to zero wellhead pressure is 5 days (or maximum rate of 7.5 psi/hr); for repressurization, a minimum of 3 days at maximum rate 9.7 psi/hr to raise the wellhead oil pressure to 700 psi (or, after oil removal, the wellhead brine pressure to 215 psi), followed by a minimum period of 14 days at 0.4 psi/hr_to the minimum normal operating pressure of 850 psi (or wellhead brine pressure to 365 psi).
- For WH-9, the recommended minimum duration for depressurization and repressurization is 5 days (maximum rate of 7.5 psi/hr).
- From a cavern and pillar integrity standpoint, there is no need to specify a maximum wellhead (or cavern ceiling) pressure differential between WH-6 and WH-9, so long as pressure change operations are performed slowly per recommended rates, and there is no indication of communication or fluid loss between the caverns.

References

- Sobolik, S.R., 2012. *Sandia Technical Recommendations for Continued Operation of West Hackberry Cavern 6.* Letter Report to Robert Myers, DOE-SPR, November 20, 2012, Sandia National Laboratories, Albuquerque, New Mexico.
- Sobolik, S.R., 2013. *Preliminary Recommendations Regarding the Maximum Length of Workover of West Hackberry Cavern 8 on Cavern 9 during Cavern 6 Oil Removal Process.* Letter Report to Robert Myers, DOE-SPR, July 25, 2013, Sandia National Laboratories, Albuquerque, New Mexico.

6.3 *RECOMMENDATIONS REGARDING THE SONARS TO BE PERFORMED ON WEST HACKBERRY CAVERN 6 FOR EVALUATION OF FINAL OIL REMOVAL*

This letter provides Sandia's recommendations regarding the upcoming sonars to be performed on West Hackberry Cavern 6 for evaluation of the final oil removal from that cavern. Currently, two sonars for WH-6 by competing vendors are scheduled to be completed by October 31, 2014. There are two questions for which Sandia has been asked for its recommendation or position:

1. At what depth should the hanging string be cut to perform the sonars and to allow for subsequent cavern operations?
2. What is the essential information Sandia requires from the sonars?

Sandia's answers to these questions may be summarized by the following statements; these answers are described in detail in the remainder of the letter:

1. Based on discussions held between DOE, Fluor, and Sabine Storage staff, a consensus seems to have been established that the hanging string may be cut to a depth 10 feet below the roof of WH-6, and that depth would be sufficient for obtaining roof and perimeter sonar measurements and maintain the pipe beneath the oil/brine interface. Sandia has no technical information to contradict this consensus, and so long as this cut depth is sufficient to allow for good sonar examination of the roof around WH-6B, agrees with this depth.
2. The sonars need to provide information to verify/disprove the geomechanical predictions of the cavern roof geometry, and thus the amount of oil remaining in the cavern, and also provide an initial condition of the borehole chimney for future leaching operations used to recover oil. Therefore, the following information needs must be addressed:
    a. The geomechanical simulations predict that the roof near the bottom of WH-6B may be only 3 inches beneath the oil/brine interface. This small distance may be difficult to accurately measure, but if so, it can be used to confirm the roof curvature and estimate the roof geometry above the OBI. However, if a large bump is detected beneath the OBI, it can disprove this prediction. These data will also be used to assess the current geomechanical simulation estimate of the remaining oil in the cavern, which has been recalculated to be 105,000 barrels (with a "factor of safety" maximum estimate of 170,000 barrels).
    b. The sonars will attempt to detect the rim (or "wing") geometry at the perimeter of the cavern bowl. Based on geomechanical simulation, cavern volume and OBI data, and engineering judgment, it is assumed that the rim closed several years ago; if by some chance it does exist, it is likely located above the OBI and will not be seen by the sonars.
    c. One proposed method of accessing and removing the remaining oil in the cavern involves installing a 4-1/2" hanging string ~100' feet below the 7" casing (cut ~10' below the roof) to support a leaching operation. Before any leaching occurs, it is important to have some idea of the current geometry of the chimney of WH-6B between the roof and the casing shoe. Sonar data should be obtained to establish this initial condition.

Hanging String Cutting Depth

There are two concerns for determining the depth at which to cut the hanging string. The first concern is that it allows for the sonar to capture the required data as described below. The second concern is that the new length can support further operations to include oil skimming from a gas injection operation or raw water injection from a leaching operation. In addition, the actual depth of the cavern's roof at WH-6B must be known to provide a total depth at which to cut. Each concern is discussed below.

The two sonars for WH-6 will necessarily be shot from the 6B borehole in the current configuration, which enters the cavern off-center in the NE quadrant. There are several sets of desired data from these sonars: the chimney geometry from the casing shoe down to where it opens up into the roof; the roof itself, including where it may be below the oil/brine interface in the vicinity of the bottom of WH-6B; and back into the rim, if it exists. Assuming 10-foot stations, it is also desired to see the walls at every station, and some upward shots at several stations for a more complete perspective and perhaps use the multiple angles for verification. There have been several recent discussions between DOE (Bob Murray, Lionel Gele) and Sabine Storage (John Kyle and Harry Allison) staff defining the method and schedule for performing these sonars. During these discussions, the proposed cut depth has been at 10 feet beneath the cavern roof. They determined that this depth would be close enough to horizontal to provide a good look toward the rim, and also allow for vertical shots at the roof to define its geometry. They were not as optimistic about getting good readings of the chimney through the hanging string.

For the purposes of future oil removal and leaching, a cut at 10 feet below the cavern roof would keep the hanging string below the oil/brine interface and prevent oil from entering the brine string. For oil removal using nitrogen, the gas injection would require a setting depth that would allow oil skimming to begin after some number of barrels gas were injected. At 90,000 bbl/ft strapping near the roof, the string should be set a few feet below the cavern-average OBI depth. For leaching, the cut would determine the raw water injection depth. A brine withdrawal string would then have to be placed inside the current 7-inch string. Paula Weber at Sandia has performed some SANSMIC simulations where the cut was at 3210 feet, which is up in the chimney (compare with about 3250 feet depth for the roof). For a cut of 10 feet below the roof, there is less control over the leach zone injecting that far into the open cavern. We know raw water jets penetrate maybe 50-75 feet in Phase II and III caverns with 100MBD leach rate. How deep the jet will penetrate and mix in WH-6, which is infinitely wide and will have a 7-inch x 4 – inch annular space, is a bigger unknown.

Based on these competing concerns, Sandia supports setting the maximum cut depth at 10 feet below the roof, as this will allow for good sonar data acquisition in the cavern and for future oil removal using gas injection. Whether to cut the string higher is primarily a function of what decision is made regarding leaching to access trapped oil.

Geomechanical Analysis

The sonars proposed for WH-6 are meant to help answer two basic questions: 1) How much oil is left in WH-6? 2) What is the location of the oil, so that plans can be made to remove it? In order for the sonars to be useful, they must help verify two predictions from the geomechanical analyses: the geometry of the roof sag, and the amount of oil trapped by the roof sag.

Regarding the first geomechanical prediction – what is the geometry of the roof sag – Figure 1 plots the predicted roof subsidence at several dates. The simulations predict as much as 11 feet of roof subsidence near the center of the cavern. The roof depression is nearly axisymmetric, but slightly biased in the direction of nearby WH-9; that is, the point of maximum subsidence is about 30 feet off-center of WH-6 on a line pointed toward the center of WH-9. The location of wellbore WH-6B where it intersects the ceiling is shown in the figure. The difference in elevation between the 6B entry point and the point of maximum sag is about 0.25 feet (3 inches). If the assumption is that the oil/brine interface is at the point where WH-6B intersects the cavern roof, this means that only 3 inches of roof should be visible beneath the OBI. It is unknown if the sonar can detect that small difference accurately; if so, it would provide a means to estimate the shape of the roof above the OBI. If the sonar detects a much larger "bump" than 3 inches, it may indicate a steeper inclination of the roof than what is predicted, thus implying a larger amount of trapped oil than predicted.

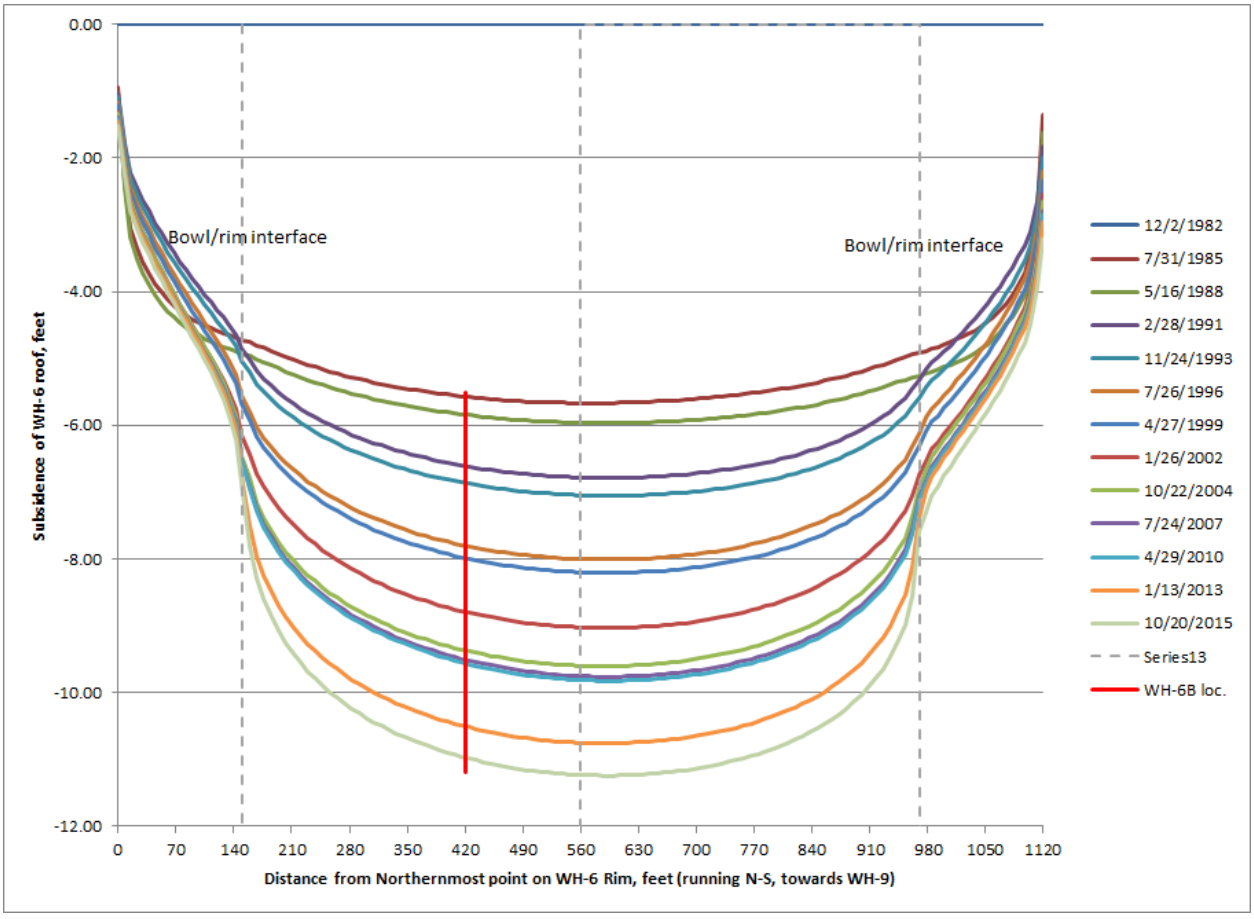

Figure 1: Predicted roof geometry of WH-6 from geomechanical calculations.

Regarding the second prediction – the amount of oil trapped by the roof sag – Sobolik (2012) included a crude upper-limit estimate of as much as 1.3 MMB of oil that might be left in the cavern due to roof sag. Of that amount, 1.0 MMB would have been in the rim (or "wing") section and 300K barrels in the bowl section. This number was based on the possibility that the

rim might have never closed. However, the geomechanical calculations predicted that it should have closed, and the common opinion on the project is that is probably did close at some point. In addition, Sobolik and Ehgartner (2009; SAND2009-2194) present data logs of Cavern 6 taken in the years 1983 to 1992. These logs were used to determine they might confirm the "lost oil" scenario regarding continued existence of the rim around the cavern. Figure 2 shows the measured changes in oil volume and interface depth beginning in 1983. From Cavern 6 data logs, oil volume starts out constant then it reduces by 1 MMB. During this volume reduction, caused by the inward deformation of the cavern by the creeping salt, one would expect the depth to the oil/brine interface to start out constant and then move upward. In fact, the interface drops this entire time period between 10 and 20 feet. This phenomenon can be explained by the rim of Cavern 6 which is predicted to close during this time period – on the order of 10 feet in agreement with the data. After 1992, the cavern exhibits expected or typical behavior – a continued decrease in oil volume (0.5 MMB) accompanied by a rising interface. Figure 3 shows the measured oil volume and the measured wellhead pressure for Cavern 6. These data support the results from the geomechanical calculations that the rim of Cavern 6 has likely closed, resulting in the period of the drop in elevation of the interface depth and the possible entrapment of oil in the pinched rim or in the cavern regions above the ceiling access points.

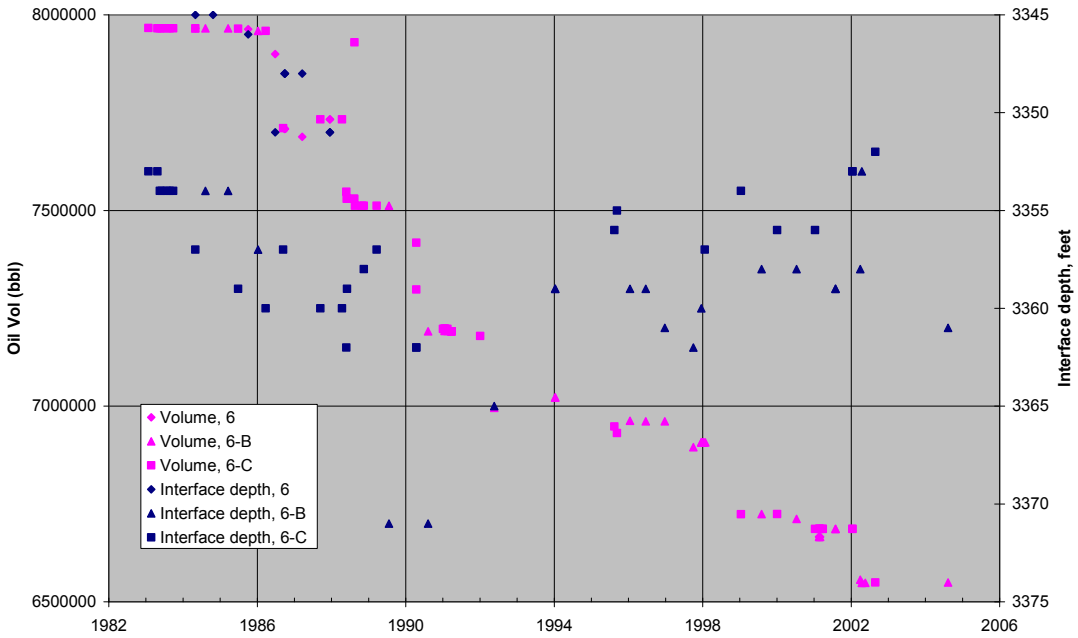

Figure 2. Measured oil volume and interface depth in Cavern 6 (Sobolik and Ehgartner, 2009).

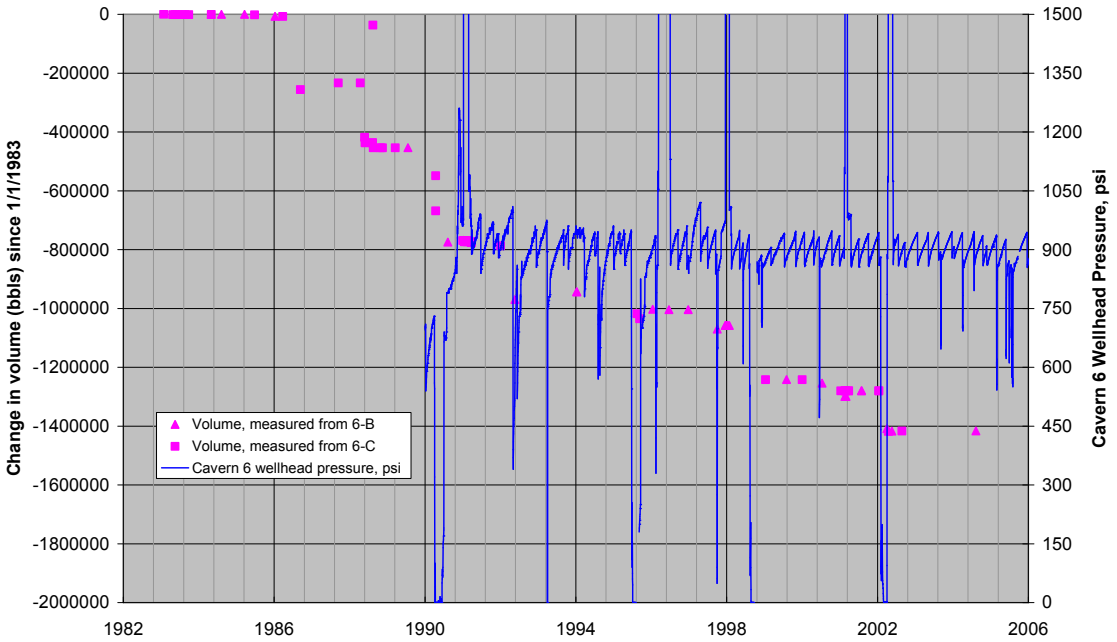

Figure 3. Measured oil volume and wellhead oil pressure in Cavern 6 (Sobolik and Ehgartner, 2009).

Based on the assumption that the rim has closed, and the predicted roof sag shown in Figure 1, new estimates of the trapped oil volume in Cavern 6 have been calculated. Figure 4 shows the areas on which these estimates are based. The area hatched in green is the cross-sectional area of oil-filled volume predicted to be in the cavern. When this area is integrated around the cavern (using an axisymmetric integration), the predicted volume of oil is 103K barrels. This volume is based on the assumption that the OBI interface is at the point where WH-6B intersects the cavern roof, and that the flat roof geometry as shown by the 1980 sonar is the true original geometry on the cavern. Because of our uncertain knowledge of the actual roof geometry, a potential maximum oil volume has been calculated based on area formed by a straight line between the maximum sag point and the top of the outer perimeter of the cavern (the gray region in Figure 4). This volume is estimated to be 170K barrels. Based on our current knowledge of the conditions of Cavern 6, the estimated amount of oil still contained in the cavern is between 103 and 170 thousand barrels.

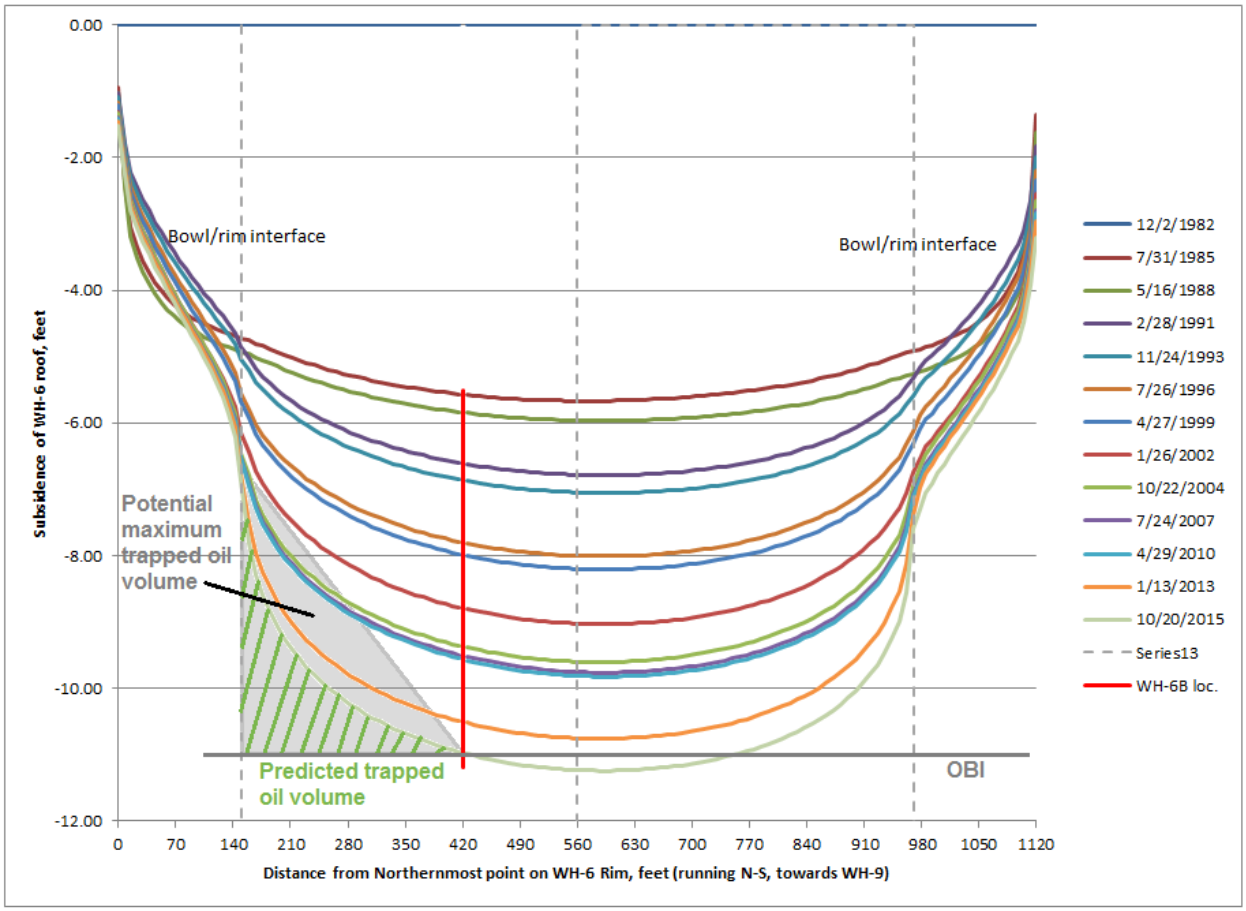

Figure 4. Predicted and potential maximum volumes of trapped oil in WH-6.

References

- Sobolik, S.R. and B.L. Ehgartner, 2009. *Analysis of Cavern Stability at the West Hackberry SPR Site.* SAND2009-2194, Sandia National Laboratories, Albuquerque, New Mexico.
- Sobolik, S.R., 2012. *Sandia Technical Recommendations for Continued Operation of West Hackberry Cavern 6.* Letter Report to Robert Myers, DOE-SPR, November 20, 2012, Sandia National Laboratories, Albuquerque, New Mexico.

6.4 *SANDIA ANALYSIS OF WEST HACKBERRY CAVERN 6 – REMAINING OIL VOLUME AND LEACHING OPTIONS*

This letter serves as a formal response to several questions regarding the remaining oil in West Hackberry Cavern 6. DOE and Fluor are in the process of developing the plan to remove any remaining oil in WH-6 cavern, which may include making changes to the cavern roof geometry and/or the casing in wellbore 6B. The plan will also address the future maintenance of the cavern after the remaining oil has been removed. The plan is scheduled for completion by the end of December 2014. DOE has asked for information regarding four technical questions to assist them in completing this plan:

1. Use the latest sonar data, along with geomechanical predictions, to update the estimate of oil remaining in WH-6, which based on geomechanical analyses is currently 100 to 170 thousand barrels (MB).
2. Use the latest sonar data along with previous sonar data to confirm the depth of roof sag since ~1980.
3. During a roof leaching process, the brine strings will likely have to be pulled. Because there is now a brine gradient rather than an oil gradient in the borehole, are there any technical issues with lowering the cavern to a brine gradient long enough to change strings?
4. DOE has been discussing "doming" the roof of WH-6 to add structural stability. How much doming is required to get any structural benefit? Specifically, we would look at a few scenarios to develop some idea about levels of this structural benefit.

Sandia's answers to these questions may be summarized by the following statements; these answers are described in detail in the remainder of the letter:

3. Based on strapping calculations from the Sonarwire sonar data, the volume of WH-6 located above the bottom of the 6B borehole is approximately 523 MB. However, there are several significant uncertainties regarding that volume, including: how much of this volume is actually oil; are the far-radius data points reflections from the actual cavern roof, or the oil-brine interface (OBI); what is the accuracy of the far-radius data points; and are the interpreted regions of oil the only oil in the cavern. Additional correspondence with Sonarwire (specifically, Sean McCool) is required to develop a more definitive answer.
4. Based on 1981 and 2014 sonar data, the amount of roof sag in WH-6 over that period of time is calculated to be 12 feet.
5. Based on using previous geomechanical analyses and comparing the expected conditions for a brine string change in WH-6, the only technical issues with lowering the cavern to a brine gradient for changing strings are the current standard operation procedures for WH-6: repressurize the cavern at the recommended slow rate, and keep low pressure time as short as possible.
6. The only leaching operation that should be considered from well 6B is an operation to remove enough salt to access and remove as much remaining oil as possible. There would be geomechanical consequences from the creation of an asymmetric hump by leaching from 6B, and a specific geomechanical analysis would need to be performed on such a geometry to evaluate those consequences. There are potential long-term integrity gains from an axisymmetric leach from Well 6 or a similar well accessing the center of

the cavern, but they would require the removal of a very large volume of salt (at least 200 feet thick at the center), and the development of a football-shaped roof to alleviate casing strain concerns.

Question 1: Estimate of Oil Volume

Prior to the execution of sonars in WH-6, Sandia used its geomechanical analyses to estimate the volume of oil remaining in the cavern resulting from isolation from 6B caused by roof sag. Figure 1 shows the roof sag predicted from the geomechanical analyses, and the cross-sectional areas used to develop estimates of the trapped oil volume in WH-6 have been calculated (Sobolik et al., 2014). The area hatched in green is the cross-sectional area of oil-filled volume predicted to be in the cavern. When this area is integrated around the cavern (using an axisymmetric integration), the predicted volume of oil is 103 MB. This volume is based on the assumption that the OBI interface is at the point where WH-6B intersects the cavern roof, and that the flat roof geometry as shown by the 1980 sonar is the true original geometry on the cavern. Because of the uncertain knowledge of the actual roof geometry, a potential maximum oil volume was calculated based on the area formed by a straight line between the maximum sag point and the top of the outer perimeter of the cavern (the gray region in Figure 4). This volume is estimated to be 170 MB.

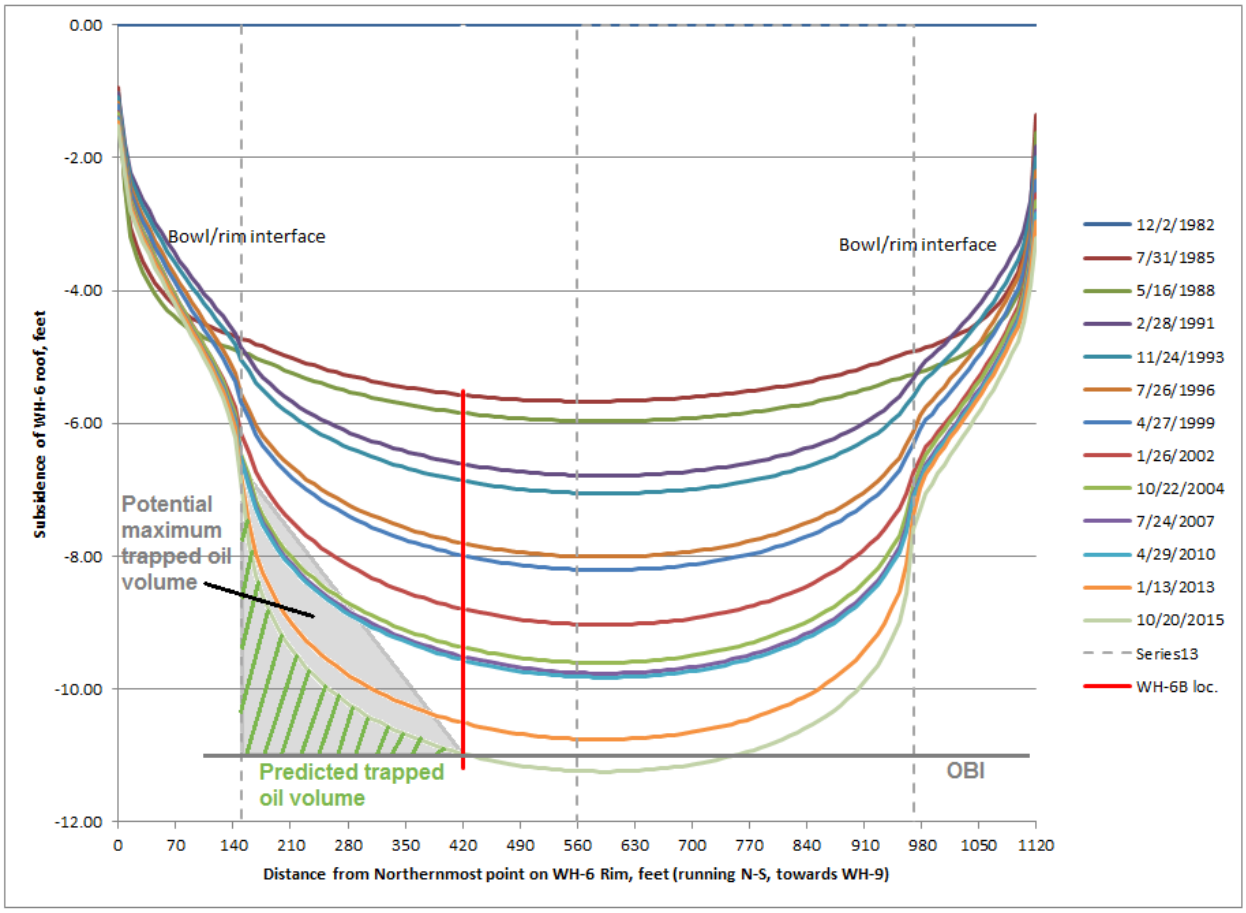

Figure 1. Predicted and potential maximum volumes of trapped oil in WH-6.

Prior to 2014, the most recent sonar of WH-6 was performed in 1981. Figure 2 shows a cross-section of this sonar, which was taken from well 6 near the center of the cavern. The 1981 sonar shows the rim that had formed around the cavern; it is believed that this rim did indeed exist, and

closed sometime in the 1990s, based on cavern pressure and OBI data (Sobolik & Ehgartner, 2009). Sonarwire performed the new sonar measurement of the geometry of WH-6 on 10/19/2014. The sonar for WH-6 was shot from the 6B borehole, which enters the cavern off-center in the NE quadrant. There were several sets of desired data from these sonars: the chimney geometry from the casing shoe down to where it opens up into the roof; the roof itself, including where it may be below the OBI in the vicinity of the bottom of WH-6B; and back into the rim, if it exists. Assuming 10-foot stations, it was also desired to see the walls at every station, and some upward shots of the roof for a more complete perspective and perhaps use the multiple angles for verification. It was known *a priori* that the roof geometry measured from the sonars may in fact turn out to be a map of the OBI, as sonar technology is not usually capable of effectively penetrating oil to give a reflection of a cavern surface behind it.

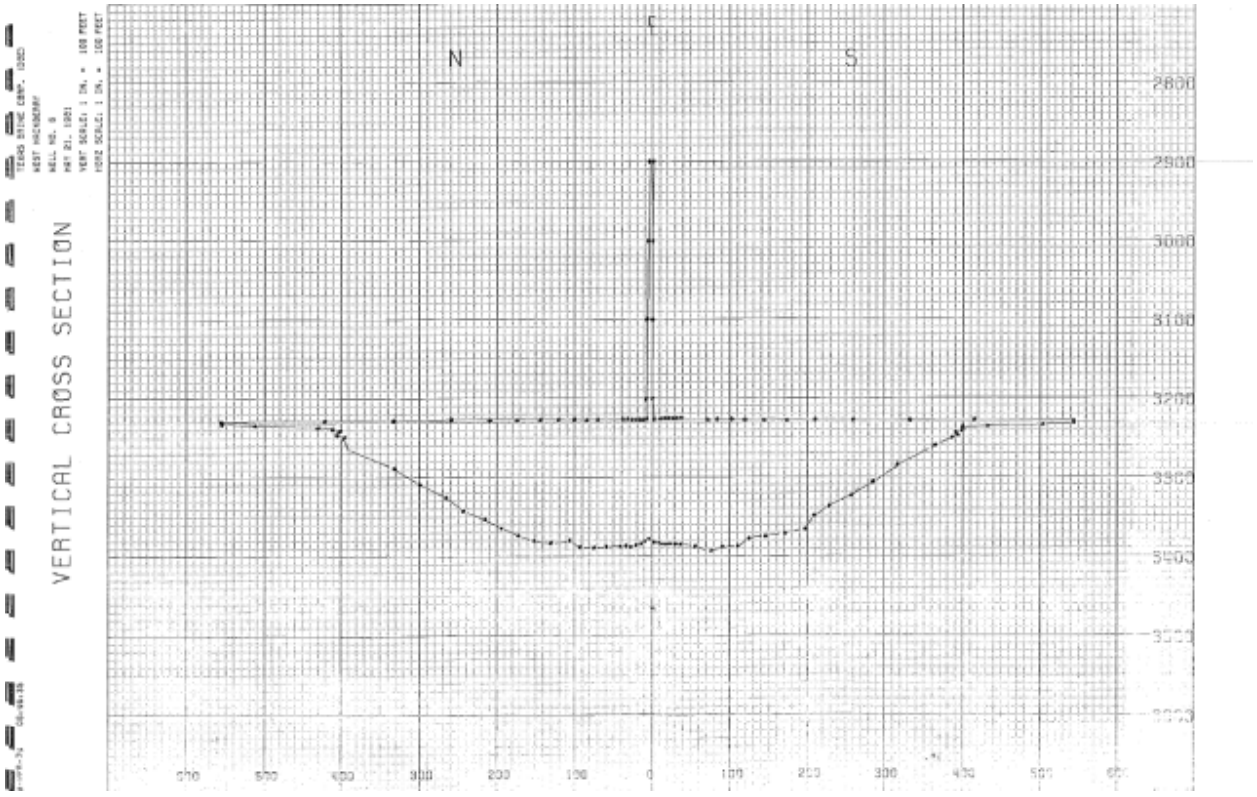

Figure 2. Vertical slice of 1981 WH-6 sonar through Well 6.

Figures 3 and 4 show North-South and West-East vertical slices of the measured shaped of WH-6 from the October, 2014 sonar. Several observations can be made from these images and others to follow:

- The sonar was unable to detect the existence of an outer rim of the cavern.
- The roof appears lower than in the 1981 survey.
- The roof at the bottom of 6B is as much as 15 feet lower than the measured cavern perimeter.
- A large area around 6B looks relatively flat, with 6B being approximately the low point in the roof.
- The roof profile appears higher toward the South and West.
- The presence of oil was definitively detected near the location of Borehole 6.
- The chimney was successfully captured through the brine string.

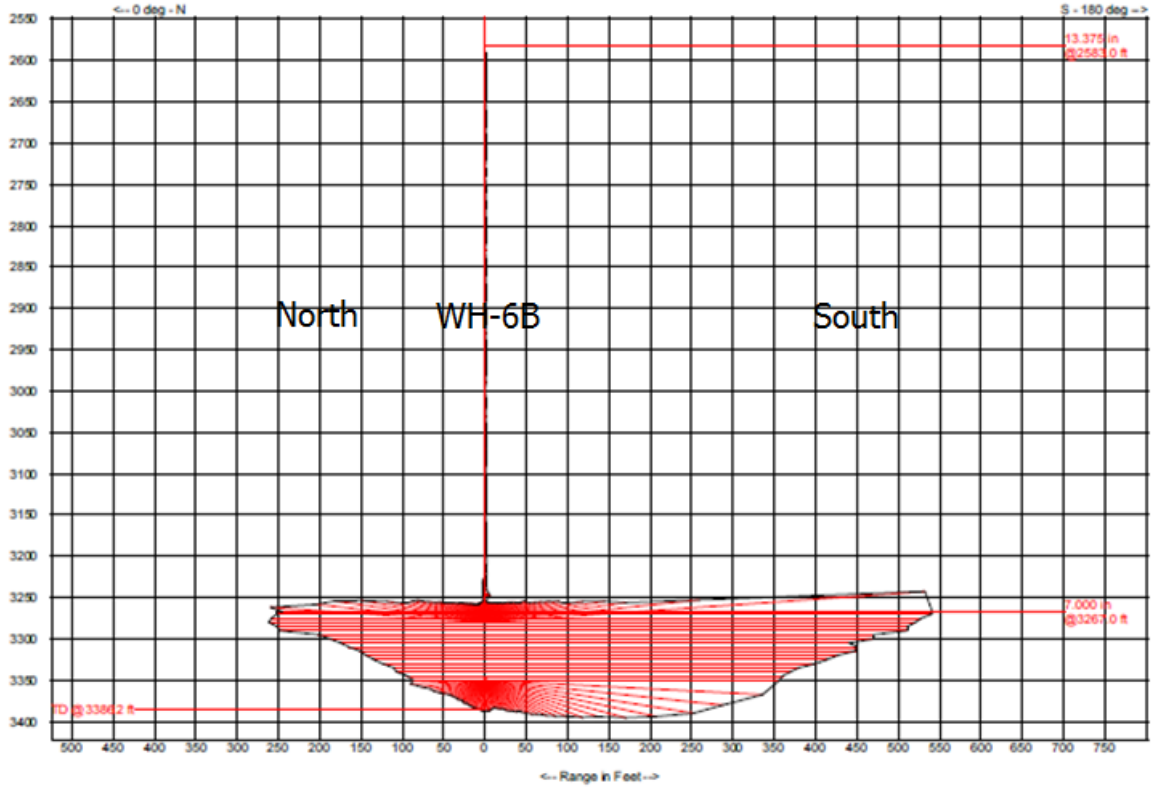

Figure 3. North-South vertical slice of WH-6 sonar (10/19/2014) through Well 6B.

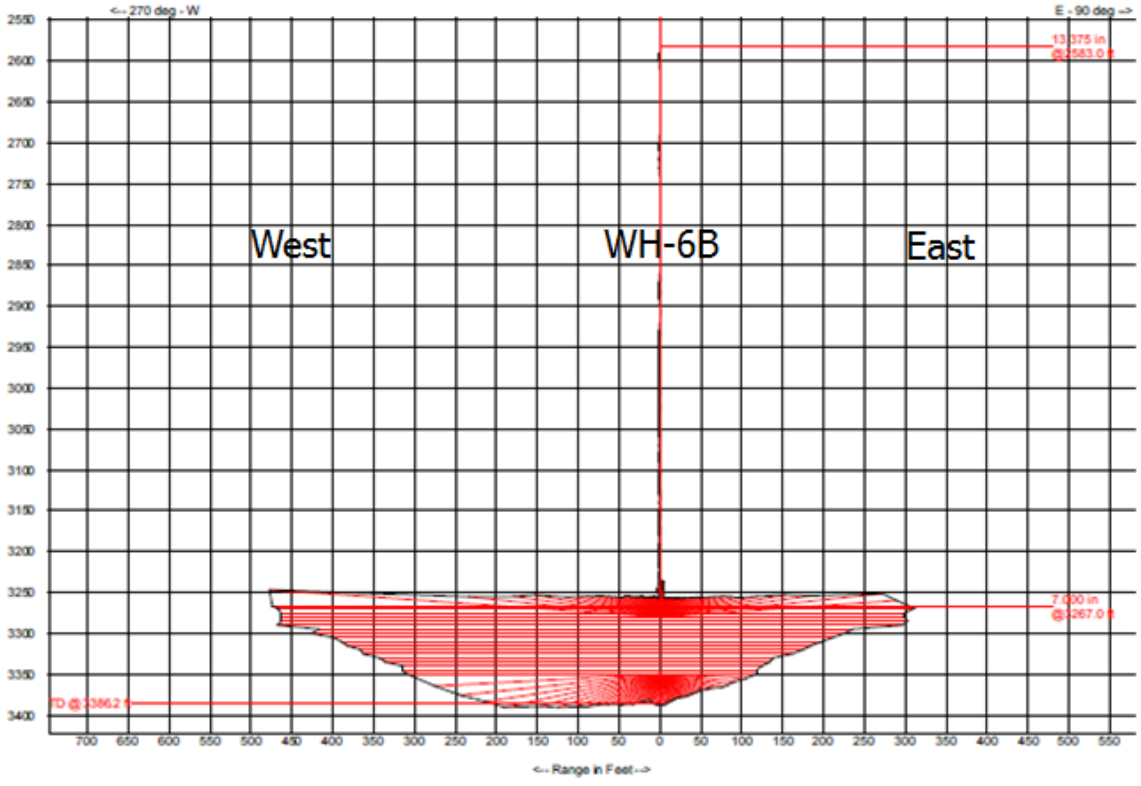

Figure 4. West-East vertical slice of WH-6 sonar (10/19/2014) through Well 6B.

An estimate of the potential oil remaining in WH-6 was computed from the October, 2014 cavern sonar data using a technique which divides the potential storage area into horizontal slices. The area of these slices is then computed and this, along with the thickness of the slice, is used to compute the slice volume. Summation of all the slices then gives the final total volume.

The horizontal slices used in the volume calculation included all areas above and disconnected from the WH-6B well borehole. These are the areas believed to potentially contain trapped oil as they have no continuous pathway to the WH-6B borehole. Figure 5 shows an example of the plan-view extent of one of the horizontal slices which is disconnected from the borehole.

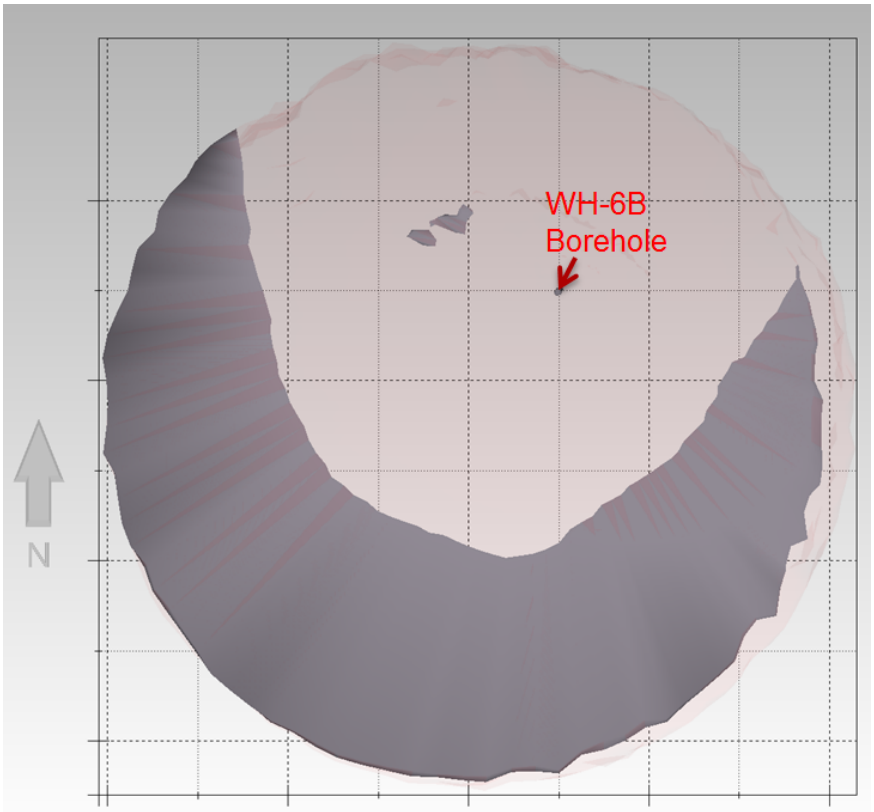

Figure 5. Example horizontal slice of area above base of borehole WH-6B. Dark gray indicates area which might contain trapped oil.

The total potential oil trapped would be the summation of all the horizontal slice volumes above the point at which the trapped oil is low enough to enter the WH-6B borehole. Figure 6 shows the extent of area disconnected from the borehole at a depth of -3255 feet. At this depth, any oil located in the gray areas would be trapped, with no continuous pathway to the borehole. Figure 7 shows the extent of area above a depth of -3256 feet; one foot below the previous figure. At this depth, the gray area has a very narrow connection to the borehole. Based on the sonar data, it appears that the critical depth for connection to the borehole is close to -3256 feet. Using -3256 as the summation base, the total volume of oil potentially isolated from the WH-6B borehole is on the order of 523,000 BBL, as shown in Figure 8.

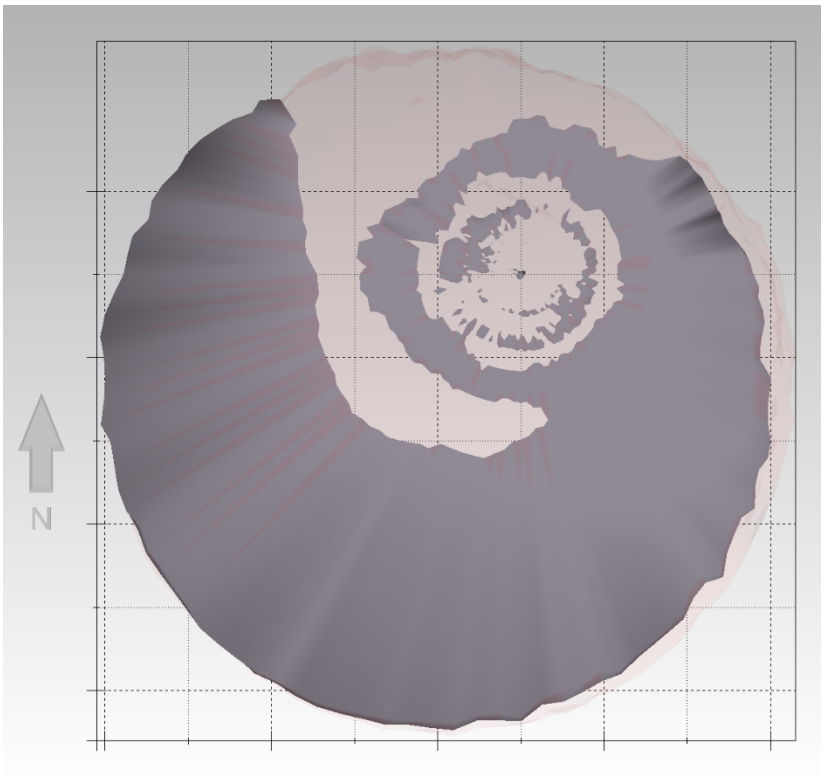

Figure 6. Area above -3255 foot depth.

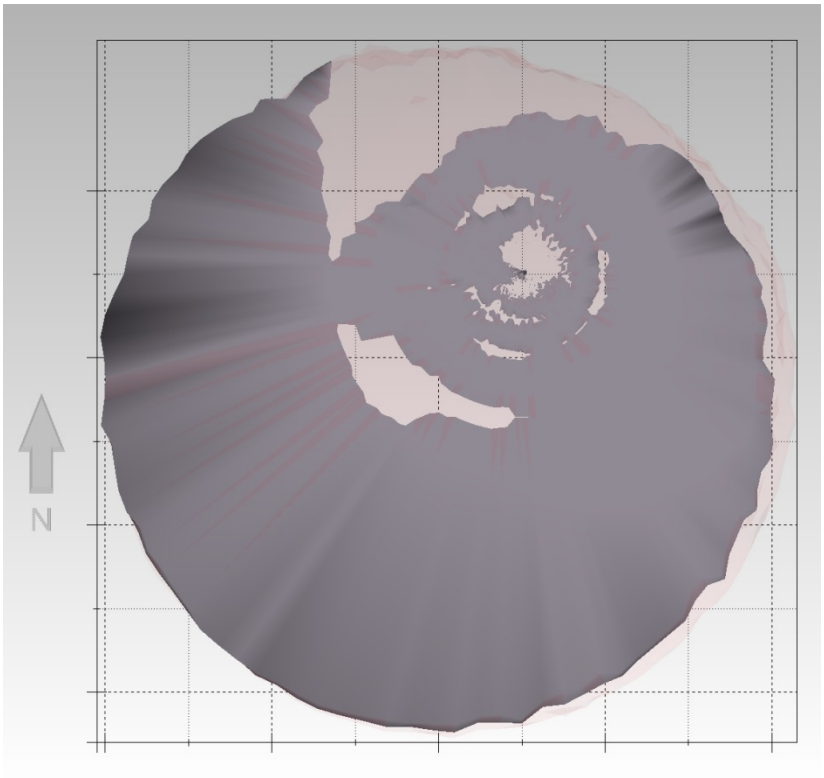

Figure 7. Area above -3256 foot depth.

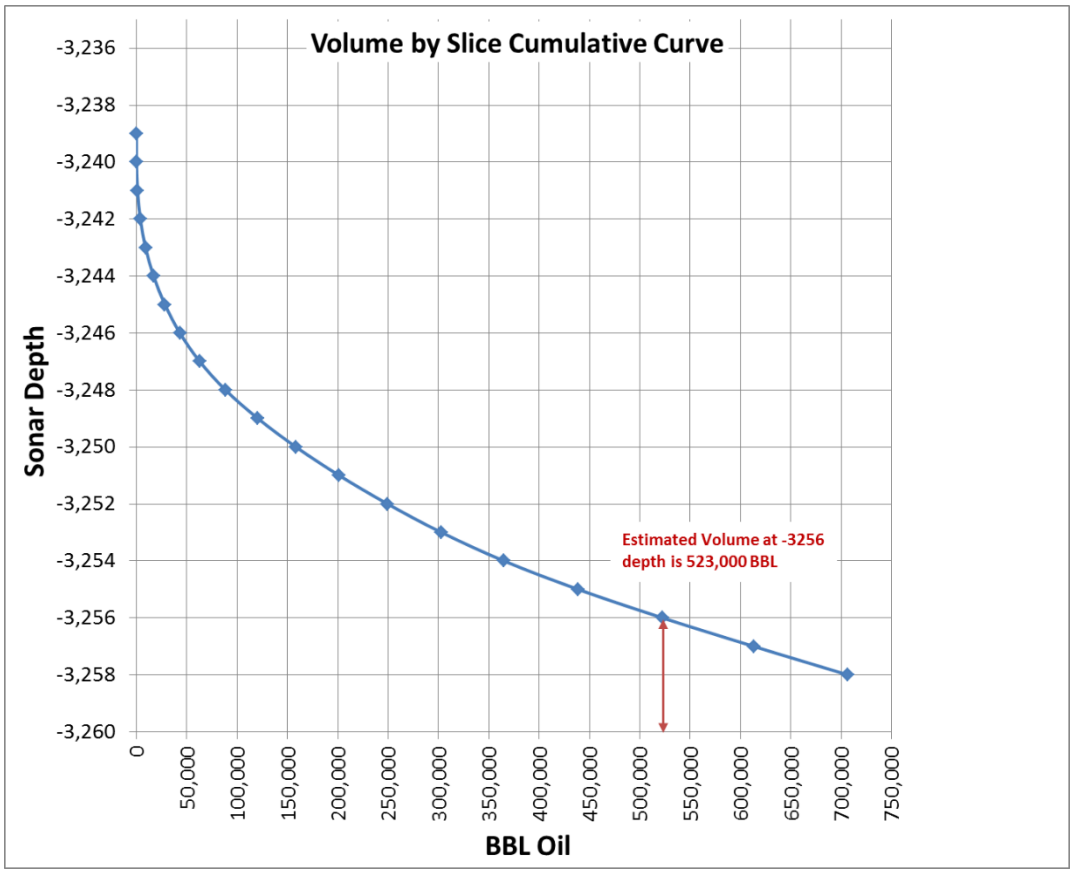

Figure 8. Cumulative trapped volume curve computed from volume slice calculations

This estimate of trapped oil volume is based on a direct use of the cavern sonar data for critical area and depth values; errors and uncertainty in the sonar data will have a significant impact on the final volume calculation. The primary reasons for this extreme sensitivity is the low vertical relief of the roof sag (about 15 feet over a distance of about 600 feet), and the large horizontal extent of the cavern. The low vertical relief (low roof slope angle), means that small changes in picking a contour value on the roof (as used in the horizontal slicing), will have dramatic changes in the lateral extent of the contoured area. This makes the volume calculations highly sensitive to uncertainty in the sonar data. In addition, it is difficult to ascertain if the sonar signal is returning off of the cavern roof, or from the OBI. Figure 9 shows the raw sonar data from two angular shots, where the presence of oil has been identified by regions of large spreads in return signals. In an email correspondence with Sean McCool of Sonarwire, these regions to the west and northwest of 6B are the only locations that are explicitly interpreted as having oil; other locations may also have it, but are not obvious from the data. Therefore, significant uncertainty still exists in identifying all the locations of oil from the sonar. The most likely case is that the vast majority of the roof as seen from the data is actually from the OBI, in which case, the above volume estimate is a minimum bound as the true cavern roof is above what we see from the sonar data. The uncertainty in the measured radius at the perimeter of the cavern also affects the confidence in the calculated volume of 523 MB above the bottom of 6B.

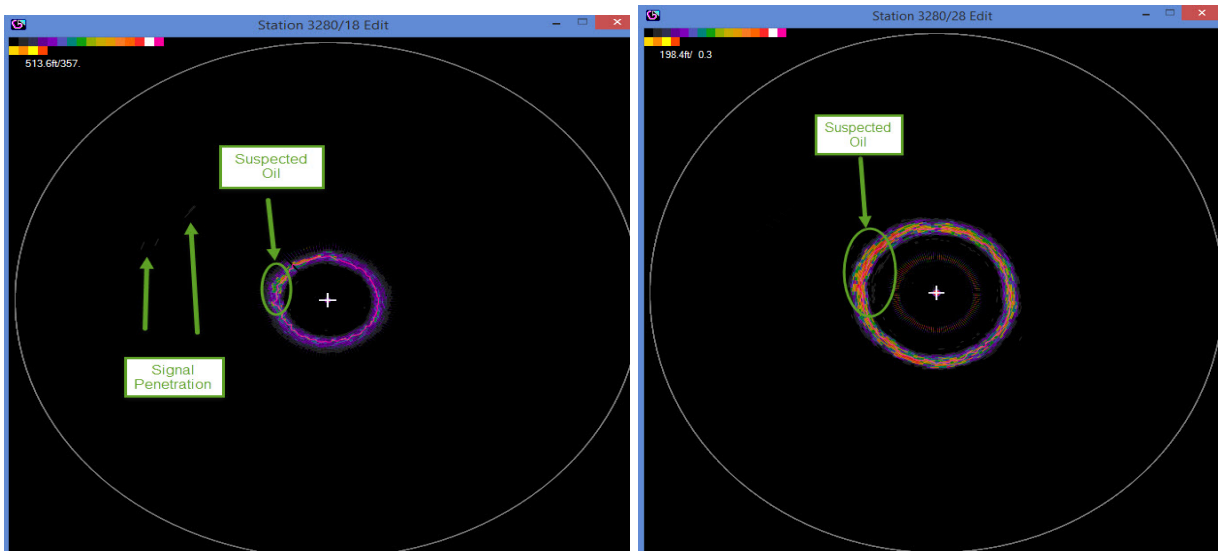

Figure 9. Locations of suspected oil from 2014 sonar data.

Question 2: Estimate of Roof Sag

Figure 1 plots the predicted roof sag of WH-6 at several dates (Sobolik et al, 2014). The simulations predict as much as 11 feet of roof subsidence near the center of the cavern. The roof depression is nearly axisymmetric, but slightly biased in the direction of nearby WH-9; that is, the point of maximum subsidence is about 30 feet off-center of WH-6 on a line pointed toward the center of WH-9. The location of wellbore WH-6B where it intersects the ceiling is shown in the figure. The difference in elevation between the 6B entry point and the point of maximum sag is about 0.25 feet (3 inches).

The predicted sag of the WH-6 roof was plotted against the sag actually measured from the sonar data. Figure 10 compares the predicted and measured roof shapes at two vertical west-east cross-sections of WH-6, with the displacement from the predictions indexed to the bottom of 6B from the sonar. The sonar (in blue) shows the roof at the bottom of 6B is as much as 15 feet lower than the cavern perimeter (primarily in the south and west highest locations). The geomechanical analyses (in red) predicted the bottom of 6B about 5 feet lower than the cavern perimeter.

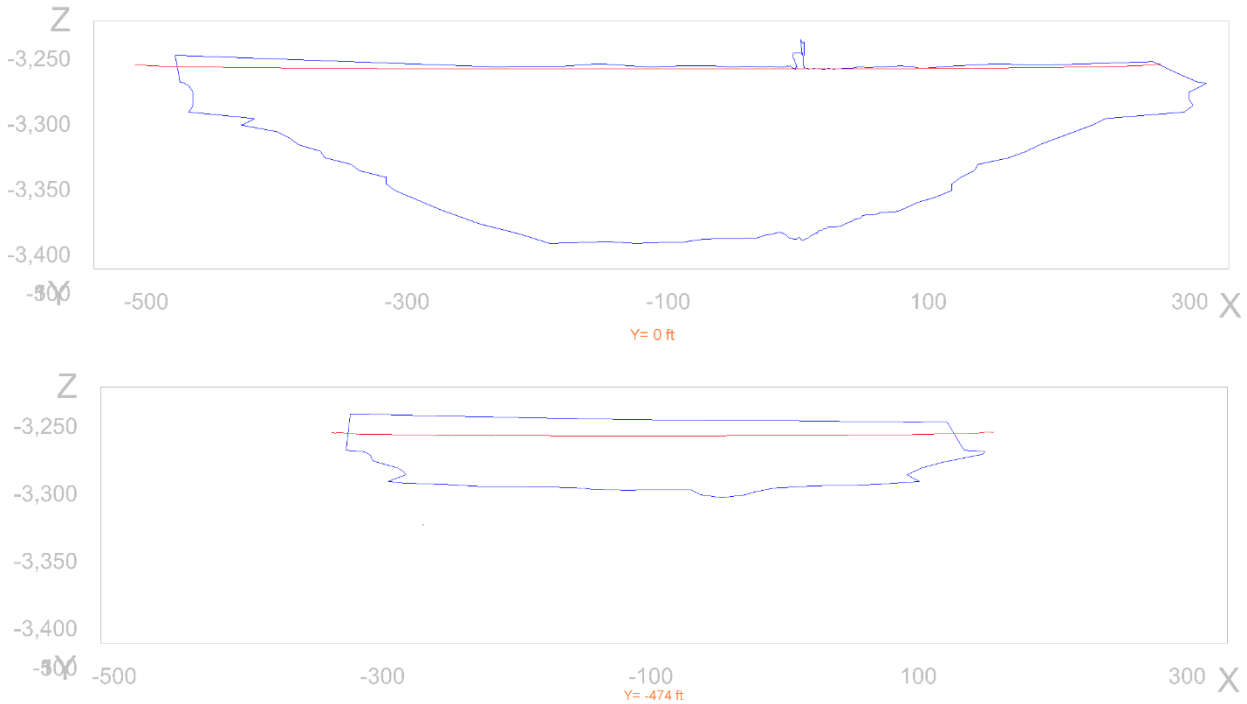

Figure 10. Comparison between predict and measured roof shape of WH-6.

Figure 11 shows the bottom of the 6B borehole from the sonar data. The bottom of 6B is estimated to be between 3256 and 3257 feet deep. This depth actually reflects depth along the borehole, and not true vertical depth; the well 6B deviates nearly 400 feet to the north from wellhead to cavern roof. The following information regarding the depth of the casing shoe and the cavern roof were obtained from sonar data and technical drawings:

- 1981 sonar from Well 6

- Depth at top of cavern 3228 feet (assumed to be true vertical depth)
- No more than 2 feet variation along top of cavern; sonar also included rim

- 2002 drawing of Well 6B
  - Depth to bottom of 13-3/8" casing 2583 feet; assumed to be casing length, true vertical depth 2569 feet
  - Depth to bottom of borehole 3249 feet; assumed to be borehole length, true vertical depth 3232 feet
- 2014 sonar from Well 6B
  - Beginning of sonar file 2591 feet (bottom of casing?); assumed to be casing length, true vertical depth 2577 feet
  - Depth to bottom of borehole 3257 feet; assumed to be borehole length, true vertical depth 3240 feet

Based on this information, the sag of the roof of WH-6 from 1981 to 2014 is approximately 12 feet.

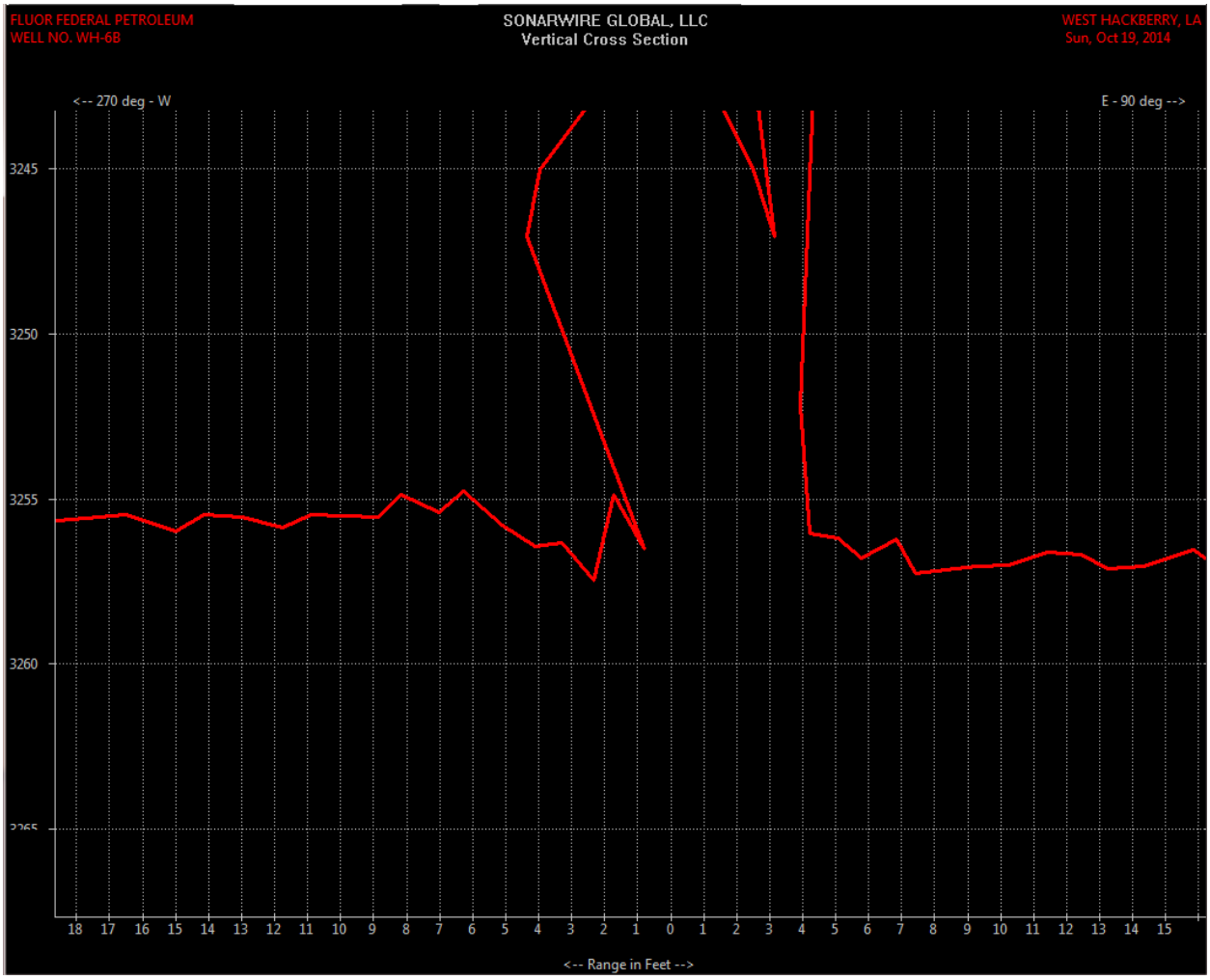

Figure 11. Bottom of Well 6B from the 2014 sonar data.

Question 3: Brine Gradient Operations

During a roof leaching process, the brine strings will likely have to be pulled. Because there is now a brine gradient rather than an oil gradient in the borehole, there are concerns about any technical issues with lowering the cavern to a brine gradient long enough to change strings. For standard operating conditions, before and after oil removal, the pressure at the roof of WH-6 would be equal for the following conditions:

Oil: Wellhead pressure 900 psi + (0.37 psi/ft)*3240 ft = 2098.8 psi
Brine: Wellhead pressure 414 psi + (0.52 psi/ft)*3240 ft = 2098.8 psi

Under current brine conditions, a purely brine gradient (i.e., wellhead pressure of zero) would be equivalent to an oil wellhead pressure of 486 psi, making the roof pressure 1684.8 psi. Earlier analyses to determine a repressurization rate after a full workover of WH-6 favored slowing that rate when wellhead pressure reached 700 psi, as shown in Figure 12. The brine gradient is equivalent to starting at an oil wellhead pressure of 484 psi, so the concerns about causing stress problems under a zero-wellhead pressure brine gradient are greatly reduced. However, it is still advised to continue previous repressurization rate recommendations after the work is completed.

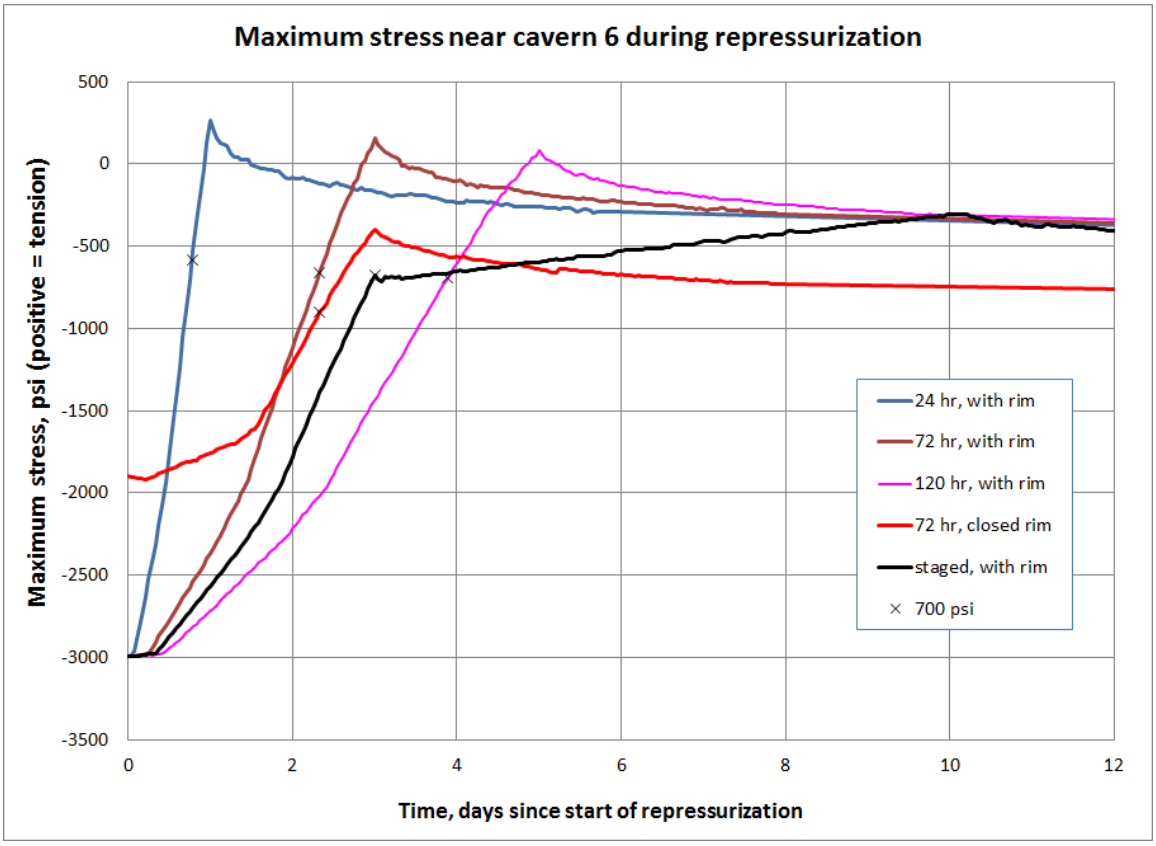

Figure 12. Effect of repressurization of WH-6 on maximum stress at perimeter of the cavern (Sobolik, 2012).

Regarding axial (vertical) well casing strain, earlier analyses have not modeled strain response when the wellhead pressure is lowered by only ~400 psi (instead of the previous usual 900 psi, as shown in Figure 13). However, a smaller pressure reduction would certainly result in smaller strain accumulation rate because the stress state of the salt is less perturbed. Furthermore, string changing operations are much shorter than the typical workover duration of 60 days. Therefore, based on these results, the only technical issues with lowering the cavern to a brine gradient for changing strings are the current standard operation procedures for WH-6: repressurize the cavern at the recommended slow rate, and keep low pressure time as short as possible.

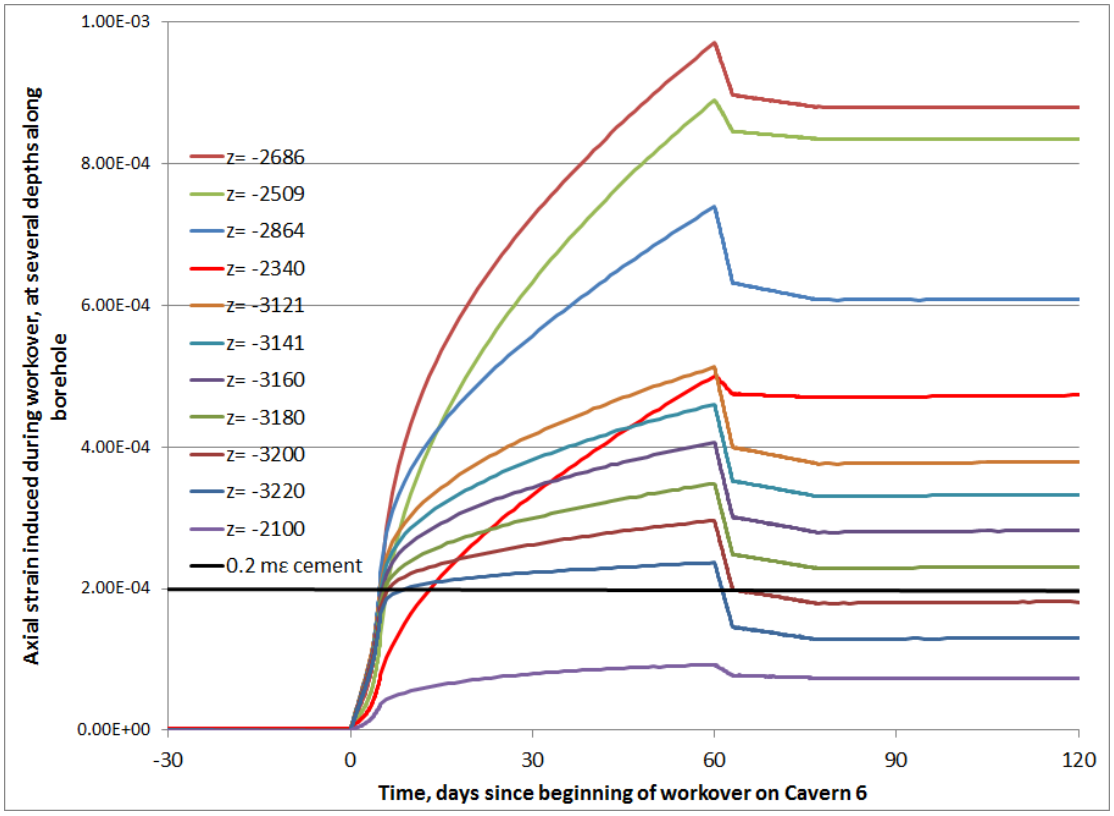

Figure 13. Predicted axial strain as a function of depth for WH-6 casings during a standard workover (Sobolik, 2012).

Question 4: Dome Leaching Options

DOE has been discussing "doming" the roof of WH-6 to add structural stability, specifically how much doming would be required to get any structural benefit. There are several potential goals that might be obtained from additional leaching of the roof of WH-6:

- Removal of just enough material to recover most of the remaining oil in the cavern as outlined in the Sabine Storage proposal (2014).
    - There is a good possibility of successful oil removal; however, the leaching program SANSMIC was created with certain flow and dissolution assumptions that are incongruent with the leaching scenario proposed by Sabine.
    - The potential effect on long-term cavern stability would be dependent on the amount and geometry of salt removed; this would require some additional geomechanical analysis.
- Removal of enough material to achieve a cavern shape with greater structural integrity.
    - The primary current concern about cavern stability is regarding fast repressurization, and its effect on perimeter stress conditions; an axisymmetric doming of the cavern would alleviate this to a modest extent.
- Removal of enough material to significantly decrease the amount of strain on the borehole casings.
    - This would require a substantial removal from the roof, done axisymmetrically and with a football-style curvature.

As shown in Figure 13, the location of peak axial strain on the casings occurs at around 2500-2700 feet depth, or approximately midway between the top of cavern and the top of salt. This location has been found to be due primarily to the assumed flat shape of the cavern roof, particularly because it is a large-diameter roof. In the Bryan Mound geomechanical analyses, all of the caverns were meshed to sonar-based shapes; therefore all the BM Phase 2 caverns have rounded tops, whereas caverns such as BM-2 has a flat top. In the previous West Hackberry analyses, the Phase 1 caverns and WH-103 were modeled sonar shapes and have either round or flat tops based on the sonars, whereas the other Phase 2 caverns were modeled with flat-topped frustums. Figures 14 and 15 show axial strain as a function of depth for two Bryan Mound caverns, one with a rounded roof and one with a flat roof. For the rounded roof, the maximum strain is predicted to occur at the roof itself, below the casing shoe. For the flat roof, the maximum strain is predicted to occur at some distance above the roof, and larger diameter roofs push the maximum strain point higher above the roof. This pattern has been observed for all the caverns in the Bryan Mound and West Hackberry models. Therefore, the shape of the top of the cavern influences the location of the maximum casing vertical strain in salt.

Based on these observations, there is a potential gain in cavern and well casing integrity to be gained from leaching out a significant portion of the roof from WH-6. This would require a substantial removal from the roof (at least 200 feet) done axisymmetrically and with a football-style curvature. However, these gains are almost certainly only available by leaching from the center of the cavern, and not from well 6B. Performing such a leaching operation from 6B is not

recommended because the resulting highly asymmetric shape would likely have adverse effects on cavern stability.

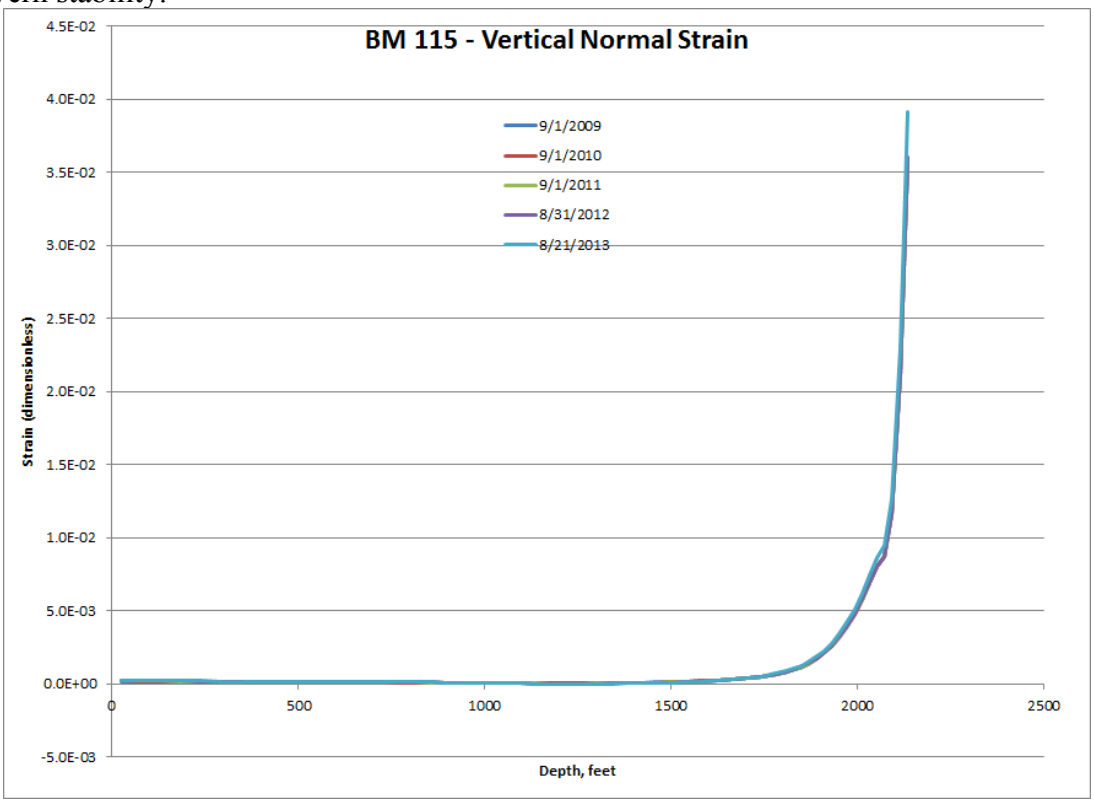

Figure 14. Vertical strain as a function of depth for a cavern with a rounded roof.

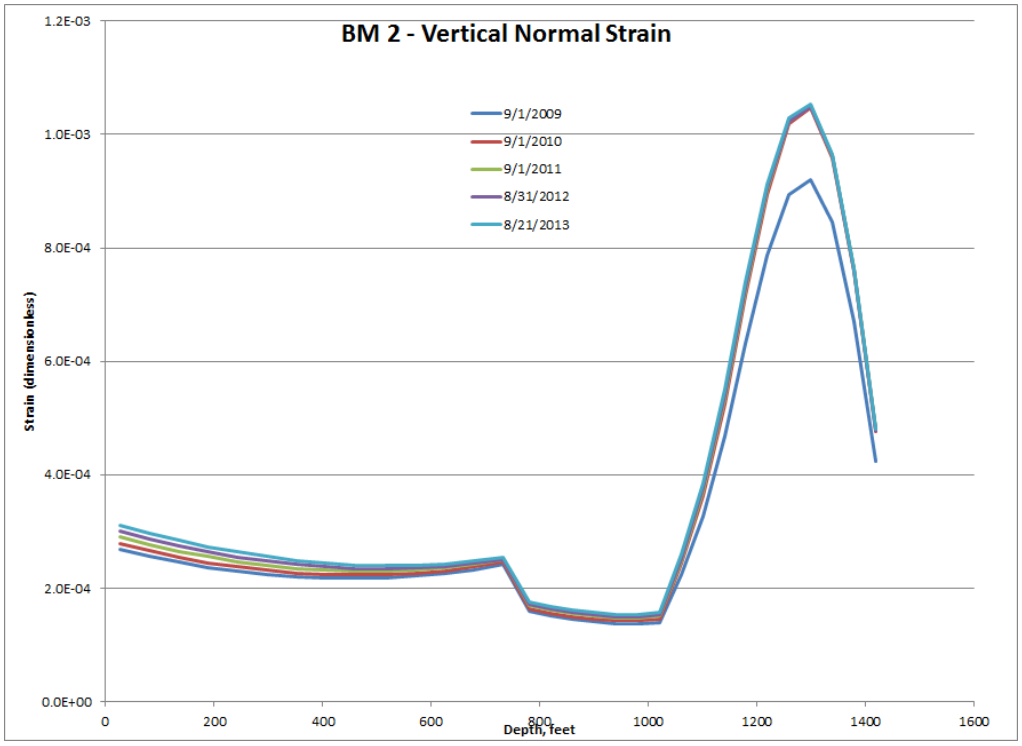

Figure 15. Vertical strain as a function of depth for a cavern with a flat roof.

A potential leaching operation of WH-6 for long-term stability would need to be performed from a centrally-located well such as the existing Well 6 or a newly-drilled well. This operation can be simulated using SANSMIC, a solution mining software package that was developed at Sandia in the early 1980s by A. J. Russo. It allows for variable injection, production, and OBI (oil-brine interface) depths and uses a combination of 1D advection/diffusion and a complete mixing assumption in the injection plume region to model the raw water, brine, and salt wall interactions within an axisymmetric cavern domain. The jet length is dependent on injection rates and string geometry and the plume region is dependent upon the relative location of the OBI, injection, and production depths and injection rate. Leaching is only in the radial direction and varies with depth – SANSMIC does not model vertical leaching.

Excluding withdrawal leach, a leach operation with the goal of controlled final geometry requires a controlled OBI, injection string depth, and production string depth. The injection string is used to inject raw water within the cavern; the production string is used to remove saturated or partially saturated brine; the controlled OBI requires an oil annulus or second slick well with which to inject or remove oil thus setting the OBI depth. When the injection string is deeper than the production string the leach is called a direct leach or bottom leach. A reverse leach, or top leach, occurs when the injection string is higher than the production string. A direct or reverse leach is possible in a one well cavern and uses concentric strings like those used during the development of the Phase II caverns at WH (West Hackberry). Questions remain regarding the level of control of the OBI for the leaching of WH-6 as leaching the regions near the trapped OBI may increase the connectivity of the trapped oil to the well. This may result in a large influx of oil volume that is unaccounted for and could result in unplanned for changes to the leach geometry if not removed in a timely fashion.

A proposal to remove the oil remaining in WH-6 by leaching has been presented by Sabine Storage (2014) as it is assumed that variation in the roof height has trapped a significant volume of oil. SANSMIC is not currently capable of explicitly modeling this leach activity because it requires vertical leaching. It is also important to note that SANSMIC is not validated for Phase I SPR cavern geometries such as WH-6. In spite of the short comings, a qualitatively reasonable prediction of the development of a new, geomechanically stable domed roof for WH-6 has been performed. Results presented below assume the injection and production locations are given at the center of the cavern and, if implemented, would require remediation of well 6 or a new well to be drilled into the center of WH-6. The geometry utilized in the following leach scenarios is taken from the recent sonar conducted by Sonarwire in October 2014 and is shown in Figure 16 overlaid with the results from the prior sonars. Vertical offsets in the figure are likely due to different reference depths for sonars taken in different wells. Absolute roof depth is not a critical parameter for leach modeling.

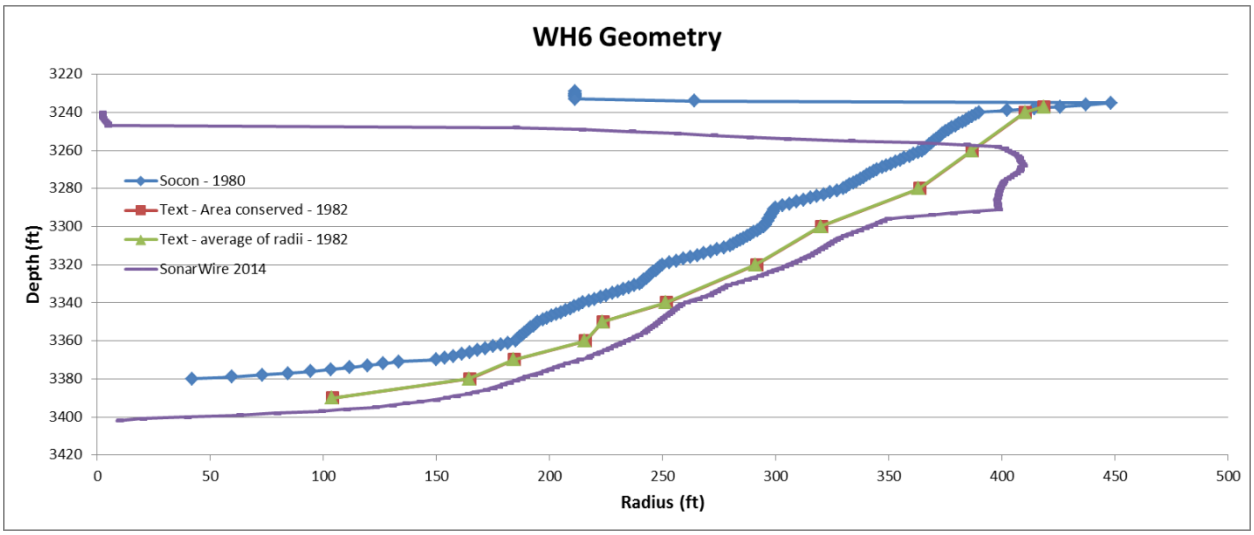

Figure 16. Axisymmetric geometry of WH6 taken from available sonars. Utilized "Sonarwire 2014" in this investigation.

Improving the geomechanical stability of WH-6 requires a domed roof rather than an inverted cone (or inverted collapsed cone) as currently assumed in this analysis. The peak of the new roof depth is taken to be approximately 100 ft above what appears to the current roof depth which is here assumed to be 3247 ft. Three leach cases were conducted for this exercise using the reverse leach configuration:

1.) The injection depth is held constant at 3225 ft and the raw water injection rate is set at 80,000 BPD (barrels per day);
2.) The injection depth is held constant at 3225 ft and the raw water injection rate is reduced to 60,000 BPD;
3.) The injection depth begins higher in the cavern at 3170 ft and is then lowered to 3220 ft during the leach operation. Injection rate is 80,000 BPD. The purpose of the third case is to minimize radial expansion at the current roof elevation.

The initial geometry and the final predicted geometry of case 1 is shown in Figure 17. The leach operation is predicted to take approximately 860 days. Note that the large radial expansion at the elevation of the current roof may not actually be realized. Note also, that scenario 3 was conducted to minimize this expansion effect, but it showed little difference from the other two cases in this regard. It is possible that the large expansion at the current roof elevation may be due to the SANSMIC wall angle enhancement model, mixing assumptions, lack of vertical leaching, or by a combination of effects. The second case was run for approximately the same duration as the other two but results in a more cone-shaped roof which is not as desirable for geomechanical purposes. If the slower rate is preferred, the duration of the leach will need to be lengthened.

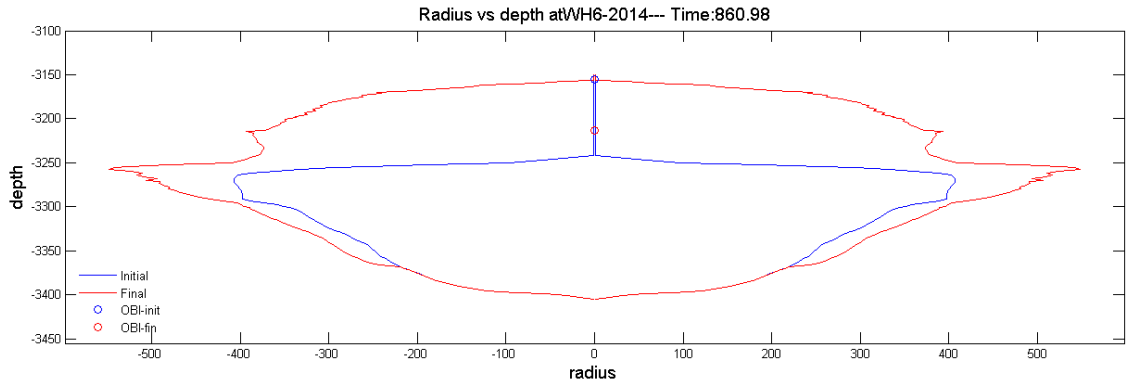

Figure 17. The initial geometry and final predicted geometry of WH-6 for the first case. It is unknown at this time if the expansion of the current roof's radius by approximately 100 ft. should be expected or is due to model assumptions.

The analysis shown here is preliminary and should not be used as a leach plan. In addition, there remain a number of open questions and potential problems that should be addressed if the large scale leach option is to be pursued.

1. The depth of the penetrating jet and leach potential is unknown especially with regard to the extension of the current maximum radius.
2. Tools that are available for monitoring the leach progress should be evaluated against the given the string size(s) and pressurization requirements for effectiveness and cost-benefit.
3. It is possible that an emulsion could be created if the OBI is near the jet depth. In addition, unknown vertical leaching could occur.
4. Leaching the upper portion of the dome may result in a temporary ledge formation of the salt directly above the current roof depth as salt is removed above this depth. As the ledge thins it is possible that large blocks of salt may fall modifying the geometry and sting depths and require a modification to the leach plan.
5. The current string configuration (using WH-6B) is not recommended as this may result in asymmetrical cavern roof geometry which will likely not improve the stability of the cavern.
6. If the current string is used as a production string in conjunction with a new centered well, as the injection string, asymmetrical leaching may occur with more leaching occurring near 6B and little or no leaching occurring at the opposite wall.
7. There is no existing data for Phase I cavern geometries with which to validate SANSMIC (see Figure 18). Also, there is no data for leach scenarios with similar relative distances between the OBI, injection, and production depths. Thus, predictive capability of SANSMIC for the WH6 geometry is not known.

An overlay of the SANSMIC predicted geometry for the first case leach of WH-6 (blue dashed) is shown below in Figure 18 with the SANSMIC predicted geometry for the first reverse of WH-103 (orange dotted) and the actual observed geometry for the first reverse of WH-103 (green solid). The planned roof for WH-6 is almost 3 times as large as a typical SPR developed cavern. The comparison of the geometries highlight the difference in the validated Phase II and Phase III caverns and the unvalidated Phase I caverns such as WH-6.

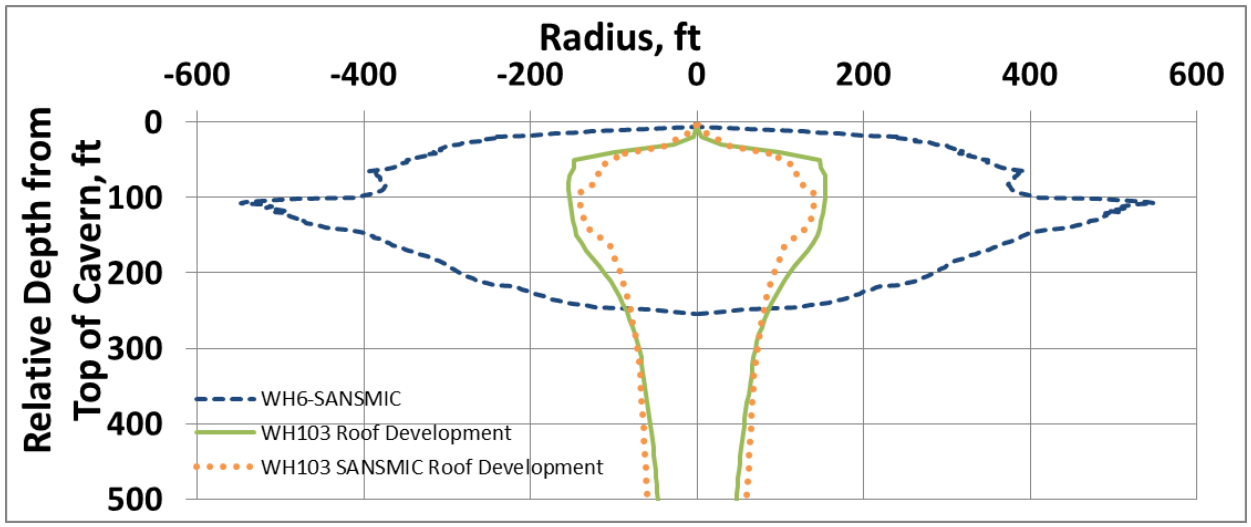

Figure 18. Comparison of geometries for roof development of Phase I and Phase II or Phase III caverns.

No analysis has been conducted concerning the Sabine proposal to leach a small region in the hopes of allowing trapped oil an avenue to the current well. This proposal requires vertical leaching and SANSMIC is not capable of modeling such leaching. It is NOT recommended to utilize the current well (WH-6B) for substantial leaching. Substantial leaching from WH-6B would likely not result in an improvement of cavern stability. Leaching from a newly constructed centered well would likely improve the stability of WH-6. Leaching of this kind has been modeled using SANSMIC and looks to be possible given a long enough leach duration, careful OBI control and by close monitoring because of the unknown predictive capability of SANSMIC.

In summary, the only leaching operation that should be considered from well 6B is an operation to remove enough salt to access and remove as much remaining oil as possible. There would be geomechanical consequences from the creation of an asymmetric hump by leaching from 6B, and a specific geomechanical analysis would need to be performed on such a geometry to evaluate those consequences. There are potential long-term integrity gains from an axisymmetric leach from Well 6 or a similar well accessing the center of the cavern, but they would require the removal of a very large volume of salt (at least 200 feet thick at the center), and the development of a football-shaped roof to alleviate casing strain concerns.

References

- Sabine Storage & Operations, 2014. *Cavern WH-6 Oil Removal*, Letter to Robert Murray, FFPO, September 5, 2014, Houston, TX.
- Sobolik, S.R. and B.L. Ehgartner, 2009. *Analysis of Cavern Stability at the West Hackberry SPR Site.* SAND2009-2194, Sandia National Laboratories, Albuquerque, New Mexico.

- Sobolik, S.R., 2012. *Sandia Technical Recommendations for Continued Operation of West Hackberry Cavern 6.* Letter Report to Robert Myers, DOE-SPR, November 20, 2012, Sandia National Laboratories, Albuquerque, New Mexico.
- Sobolik, S.R., D.L. Lord, and B.L. Roberts, 2014. *Recommendations Regarding the Sonars to be Performed on West Hackberry Cavern 6 for Evaluation of Final Oil Removal*, Letter to Lionel Gele, DOE-SPR, September 30, 2014.

6.5 UPDATE OF SANDIA ANALYSIS OF WEST HACKBERRY CAVERN 6 – REMAINING OIL VOLUME AND LEACHING OPTIONS

This letter serves as an update to the December 15, 2014 formal response to several questions regarding the remaining oil in West Hackberry Cavern 6 (Sobolik et al, 2014b). The update concerns the first question addressed in the earlier letter:

5. Use the latest sonar data, along with geomechanical predictions, to update the estimate of oil remaining in WH-6, which based on geomechanical analyses is currently 100 to 170 thousand barrels (MB).

The answer Sandia provided to this particular question was:

7. Based on strapping calculations from the Sonarwire sonar data, the volume of WH-6 located above the bottom of the 6B borehole is approximately 523 MB. However, there are several significant uncertainties regarding that volume, including: how much of this volume is actually oil; are the far-radius data points reflections from the actual cavern roof, or the oil-brine interface (OBI); what is the accuracy of the far-radius data points; and are the interpreted regions of oil the only oil in the cavern. Additional correspondence with Sonarwire (specifically, Sean McCool) is required to develop a more definitive answer.

Sandia has further evaluated the results of the October 2014 sonar, along with the comments from Sean McCool of Sonarwire (McCool, 2014a and 2014b), and geomechanical analyses (Sobolik et al, 2014a), to refine the estimate of remaining volume. This letter repeats the description of the methodology for obtaining the original estimate from the December 15, 2014 letter, and then describes the additional work to refine this estimate. Note that it was known *a priori* that the roof geometry measured from the October 2014 sonar may in fact turn out to be a map of the OBI, as sonar technology is not usually capable of effectively penetrating oil to give a reflection of a cavern surface behind it. This assumption contributes significantly to the additional work to compute the final revised estimates. Several values characterizing the remaining volume of oil are presented at the end of the letter; unfortunately, because of the large uncertainties involved, it is not feasible to come up with a singular volume estimate with a high degree of confidence.

Estimate of Oil Volume from December 15, 2014 letter

Prior to the execution of sonars in WH-6, Sandia used its geomechanical analyses to estimate the volume of oil remaining in the cavern resulting from isolation from 6B caused by roof sag. Figure 1 shows the roof sag predicted from the geomechanical analyses, and the cross-sectional areas used to develop estimates of the trapped oil volume in WH-6 have been calculated (Sobolik et al., 2014). The area hatched in green is the cross-sectional area of oil-filled volume predicted to be in the cavern. When this area is integrated around the cavern (using an axisymmetric integration), the predicted volume of oil is 103 MB. This volume is based on the assumption that the OBI interface is at the point where WH-6B intersects the cavern roof, and that the flat roof geometry as shown by the 1980 sonar is the true original geometry on the cavern. Because of the uncertain knowledge of the actual roof geometry, a potential maximum oil volume was calculated based on the area formed by a straight line between the maximum sag point and the

top of the outer perimeter of the cavern (the gray region in Figure 4). This volume is estimated to be 170 MB.

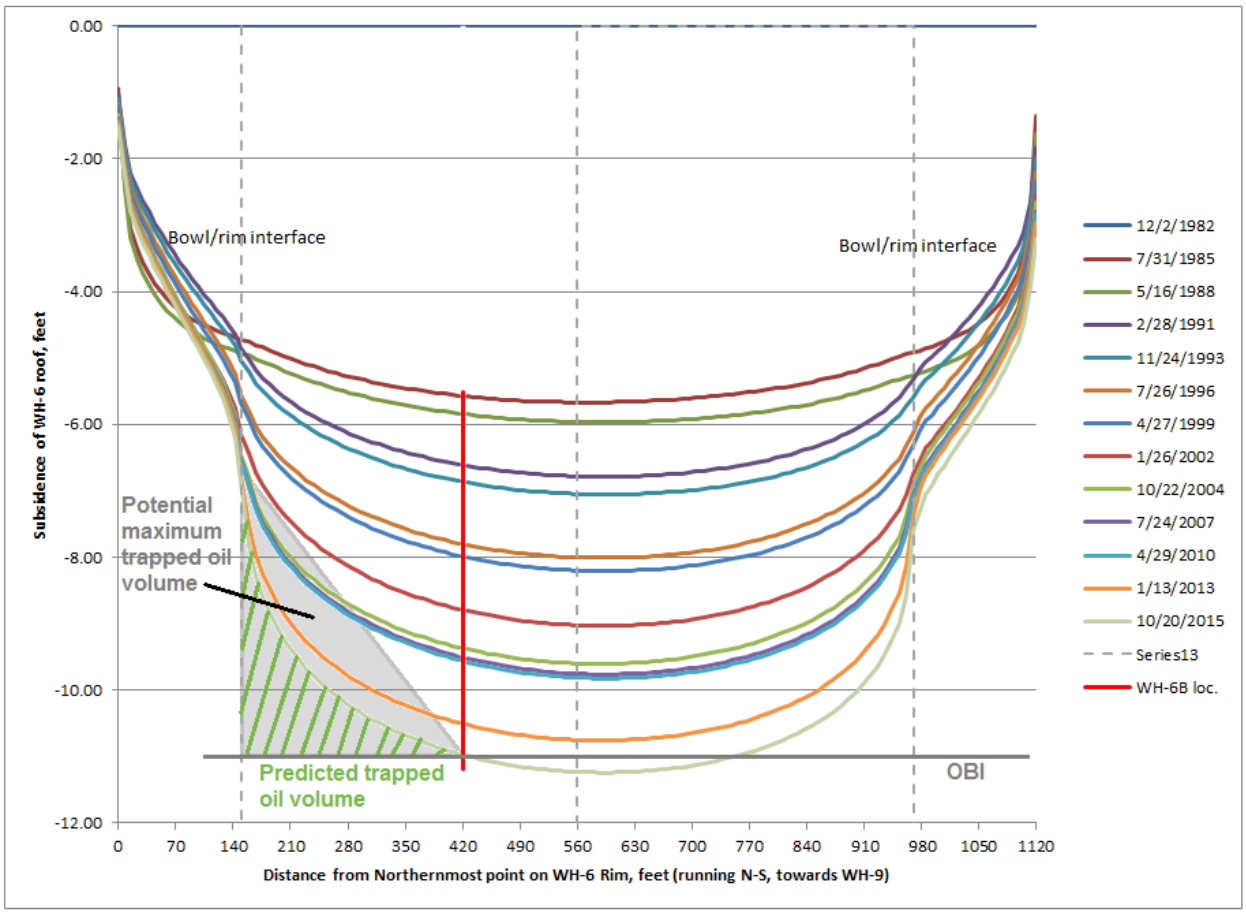

Figure 1. Predicted and potential maximum volumes of trapped oil in WH-6.

Prior to 2014, the most recent sonar of WH-6 was performed in 1981. Figure 2 shows a cross-section of this sonar, which was taken from well 6 near the center of the cavern. The 1981 sonar shows the rim that had formed around the cavern; it is believed that this rim did indeed exist, and closed sometime in the 1990s, based on cavern pressure and OBI data (Sobolik & Ehgartner, 2009). Sonarwire performed the new sonar measurement of the geometry of WH-6 on 10/19/2014. The sonar for WH-6 was shot from the 6B borehole, which enters the cavern off-center in the NE quadrant. There were several sets of desired data from these sonars: the chimney geometry from the casing shoe down to where it opens up into the roof; the roof itself, including where it may be below the OBI in the vicinity of the bottom of WH-6B; and back into the rim, if it exists. Assuming 10-foot stations, it was also desired to see the walls at every station, and some upward shots of the roof for a more complete perspective and perhaps use the multiple angles for verification. It was known *a priori* that the roof geometry measured from the sonars may in fact turn out to be a map of the OBI, as sonar technology is not usually capable of effectively penetrating oil to give a reflection of a cavern surface behind it.

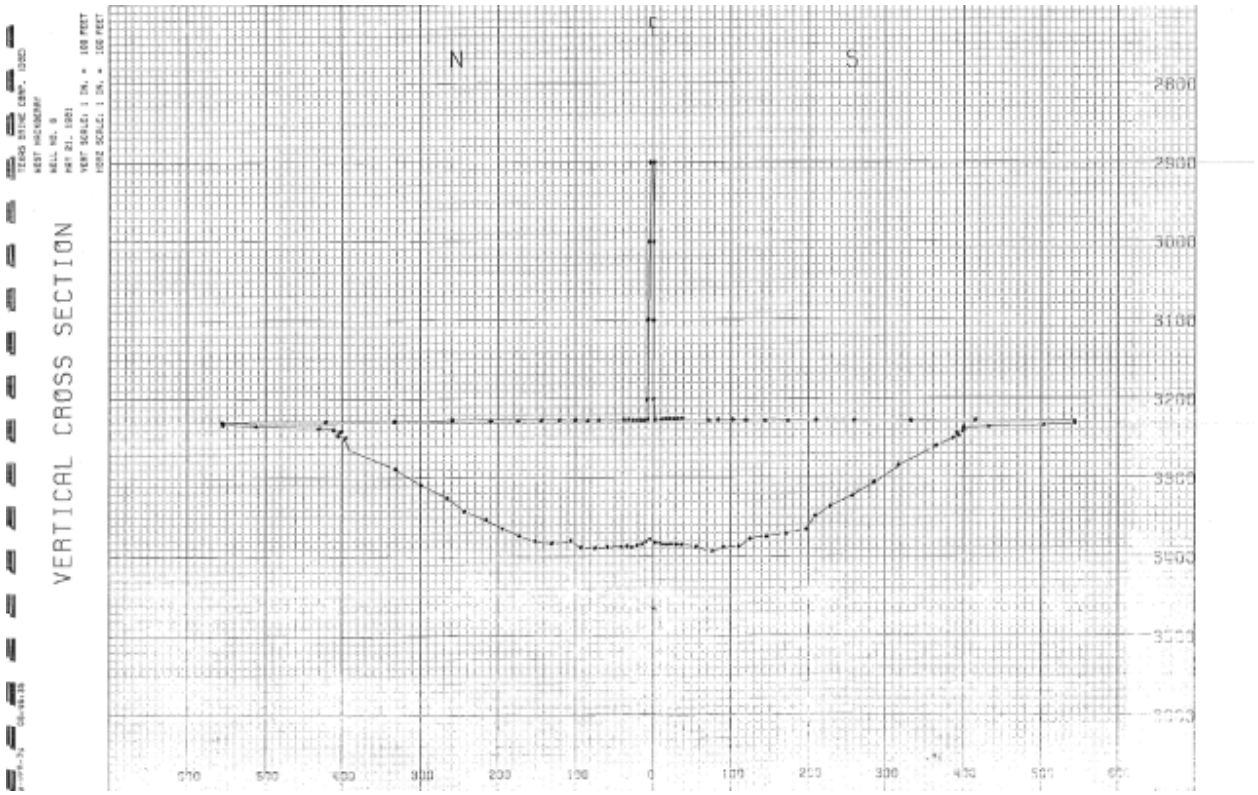

Figure 2. Vertical slice of 1981 WH-6 sonar through Well 6.

Figures 3 and 4 show North-South and West-East vertical slices of the measured shaped of WH-6 from the October, 2014 sonar. Several observations can be made from these images and others to follow:

- The sonar was unable to detect the existence of an outer rim of the cavern.
- The roof appears lower than in the 1981 survey.
- The roof at the bottom of 6B is as much as 15 feet lower than the measured cavern perimeter.
- A large area around 6B looks relatively flat, with 6B being approximately the low point in the roof.
- The roof profile appears higher toward the South and West.
- The presence of oil was definitively detected near the location of Borehole 6.
- The chimney was successfully captured through the brine string.

An estimate of the potential oil remaining in WH-6 was computed from the October, 2014 cavern sonar data using a technique which divides the potential storage area into horizontal slices. The area of these slices is then computed and this, along with the thickness of the slice, is used to compute the slice volume. Summation of all the slices then gives the final total volume.

The horizontal slices used in the volume calculation included all areas above and disconnected from the WH-6B well borehole. These are the areas believed to potentially contain trapped oil as they have no continuous pathway to the WH-6B borehole. Figure 5 shows an example of the plan-view extent of one of the horizontal slices which is disconnected from the borehole.

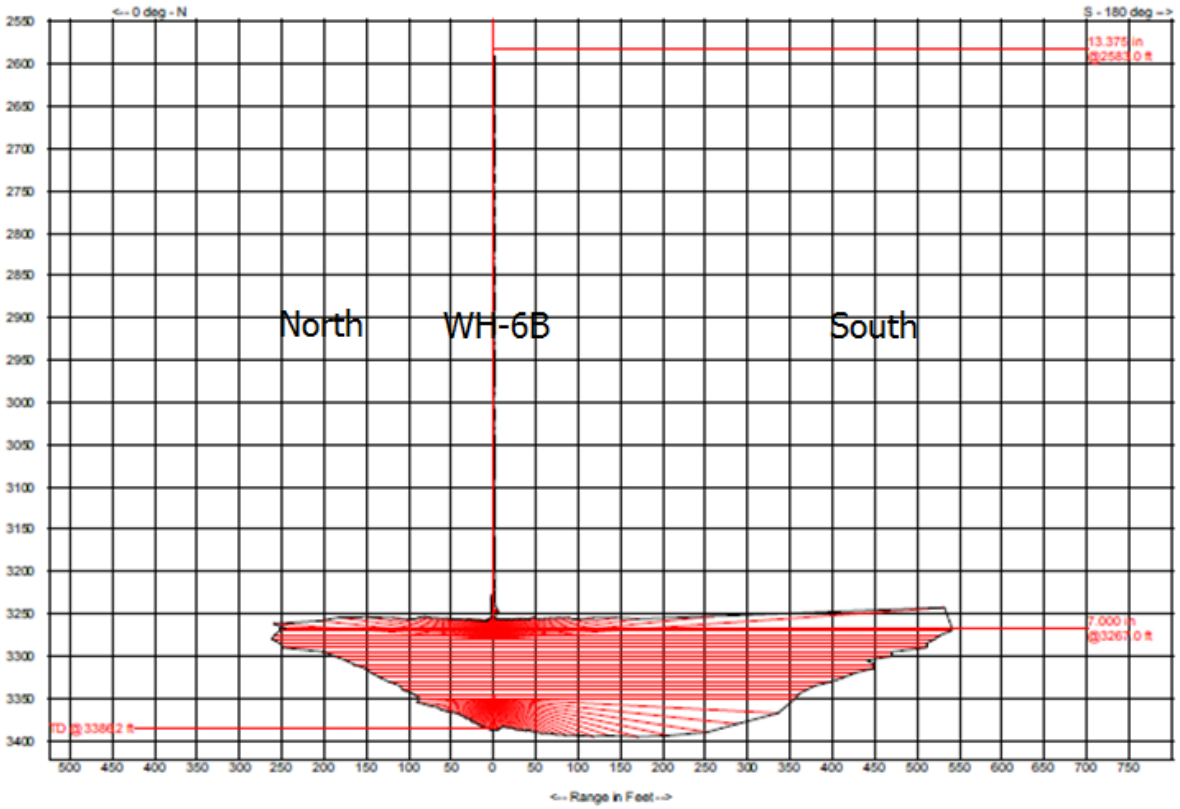

Figure 3. North-South vertical slice of WH-6 sonar (10/19/2014) through Well 6B.

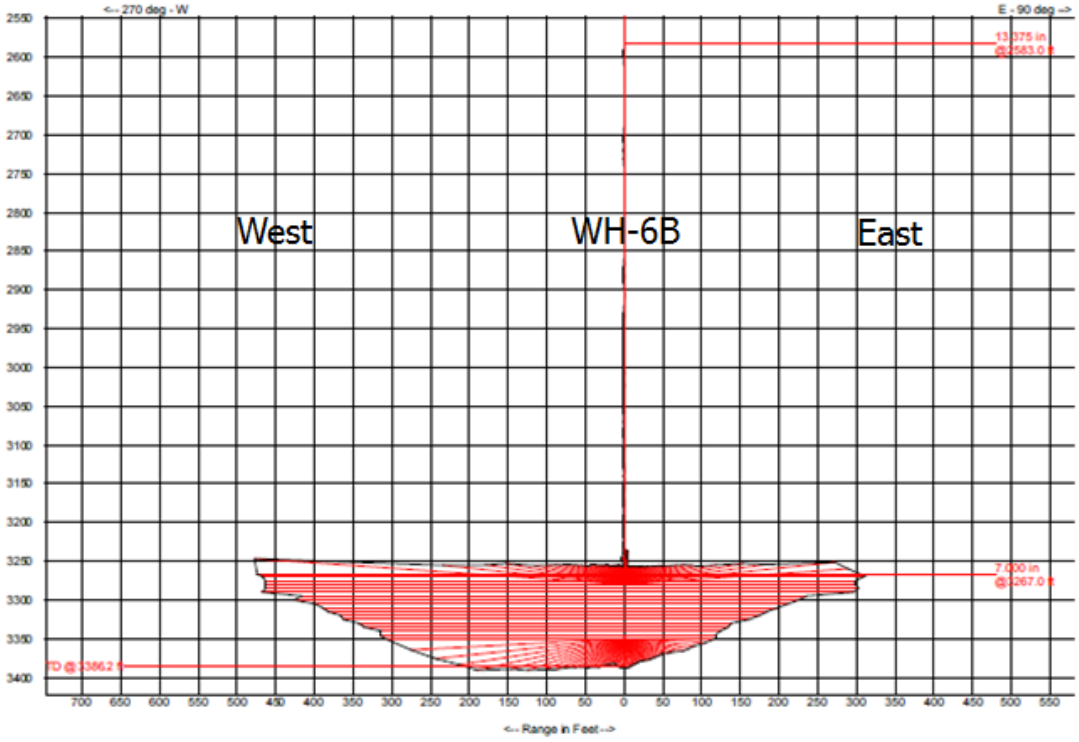

Figure 4. West-East vertical slice of WH-6 sonar (10/19/2014) through Well 6B.

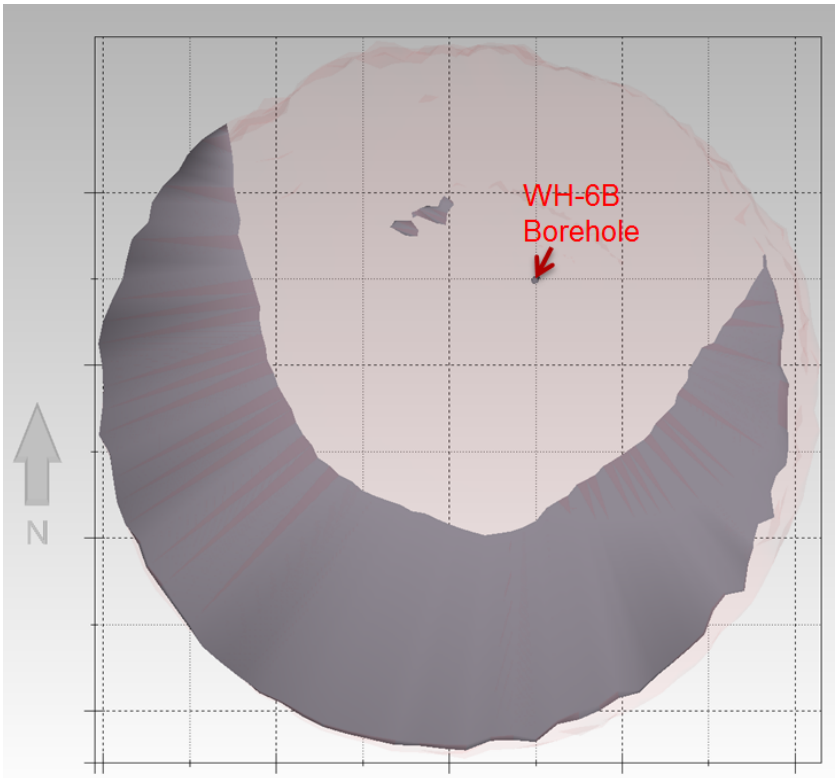

Figure 5. Example horizontal slice of area above base of borehole WH-6B. Dark gray indicates area which might contain trapped oil.

The total potential oil trapped would be the summation of all the horizontal slice volumes above the point at which the trapped oil is low enough to enter the WH-6B borehole. Figure 6 shows the extent of area disconnected from the borehole at a depth of -3255 feet. At this depth, any oil located in the gray areas would be trapped, with no continuous pathway to the borehole. Figure 7 shows the extent of area above a depth of -3256 feet; one foot below the previous figure. At this depth, the gray area has a very narrow connection to the borehole. Based on the sonar data, it appears that the critical depth for connection to the borehole is close to -3256 feet. Using -3256 as the summation base, the total volume of oil potentially isolated from the WH-6B borehole is on the order of 523,000 BBL, as shown in Figure 8.

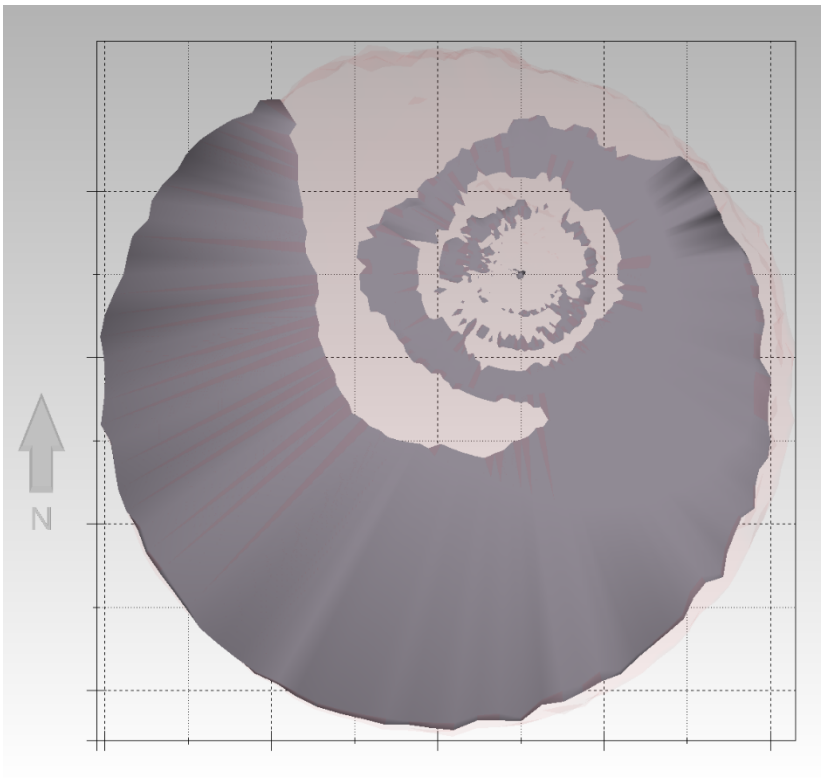

Figure 6. Area above -3255 foot depth.

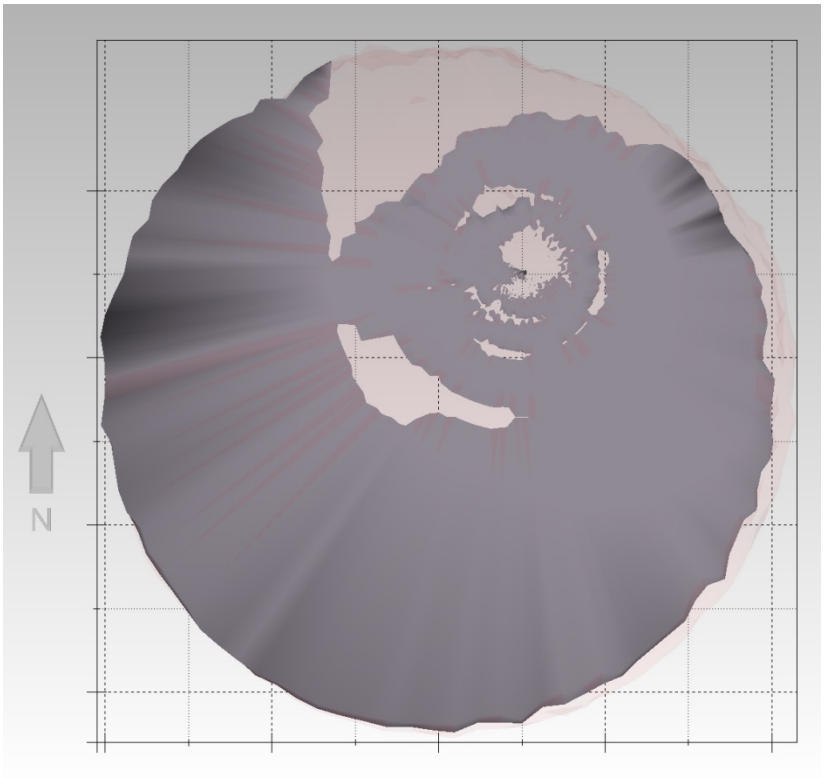

Figure 7. Area above -3256 foot depth.

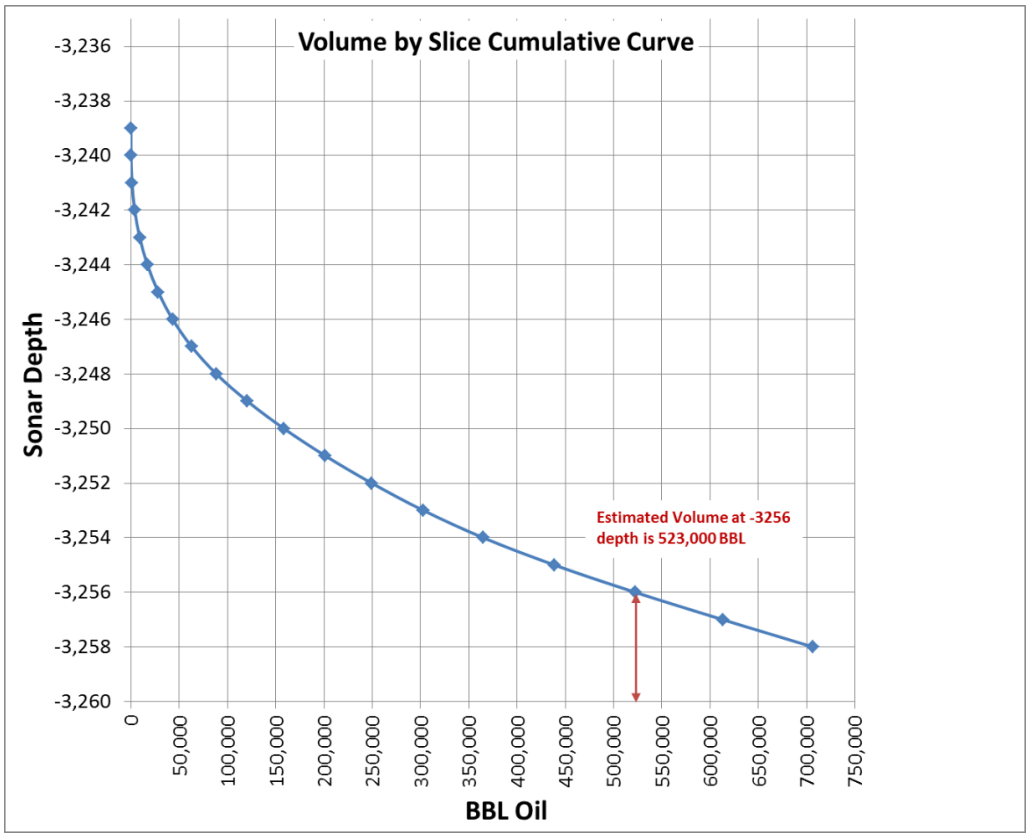

Figure 8. Cumulative trapped volume curve computed from volume slice calculations

This estimate of trapped oil volume is based on a direct use of the cavern sonar data for critical area and depth values; errors and uncertainty in the sonar data will have a significant impact on the final volume calculation. The primary reasons for this extreme sensitivity is the low vertical relief of the roof sag (about 15 feet over a distance of about 600 feet), and the large horizontal extent of the cavern. The low vertical relief (low roof slope angle), means that small changes in picking a contour value on the roof (as used in the horizontal slicing), will have dramatic changes in the lateral extent of the contoured area. This makes the volume calculations highly sensitive to uncertainty in the sonar data. In addition, it is difficult to ascertain if the sonar signal is returning off of the cavern roof, or from the OBI. Figure 9 shows the raw sonar data from two angular shots, where the presence of oil has been identified by regions of large spreads in return signals. In an email correspondence with Sean McCool of Sonarwire, these regions to the west and northwest of 6B are the only locations that are explicitly interpreted as having oil; other locations may also have it, but are not obvious from the data. Therefore, significant uncertainty still exists in identifying all the locations of oil from the sonar. The most likely case is that the vast majority of the roof as seen from the data is actually from the OBI, in which case, the above volume estimate is a minimum bound as the true cavern roof is above what we see from the sonar data. The uncertainty in the measured radius at the perimeter of the cavern also affects the confidence in the calculated volume of 523 MB above the bottom of 6B.

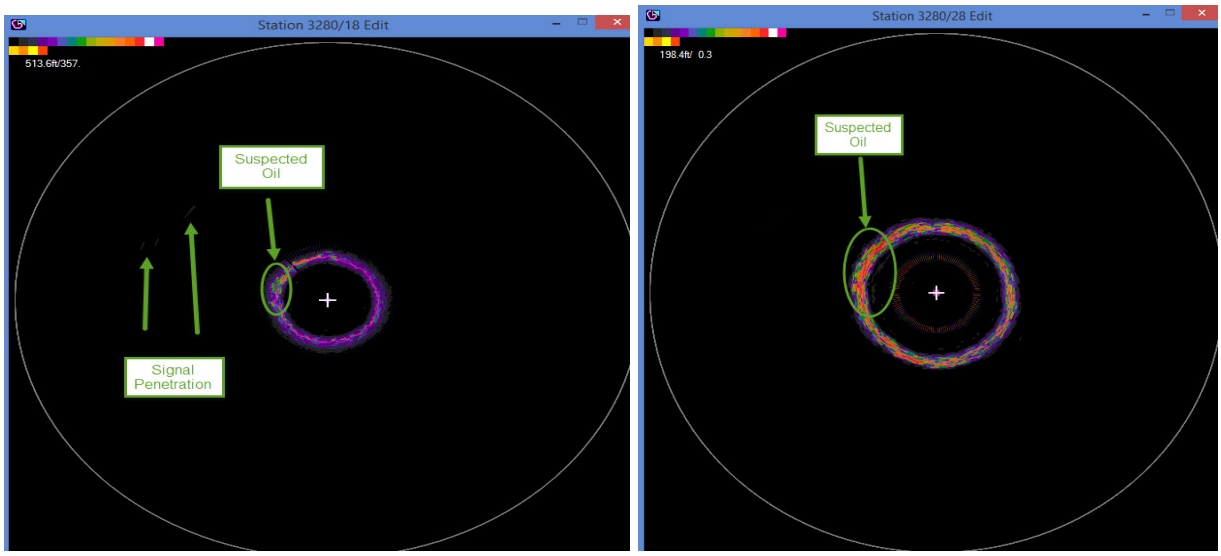

Figure 9. Locations of suspected oil from 2014 sonar data.

Updated Estimate for Remaining Volume of oil in WH-6

For the additional evaluation of the WH-6 sonar, two pieces of correspondence from Sean McCool, Operations Manager of Sonarwire Global LLC, are pertinent. In the first email correspondence dated October 22, 2014 (McCool, 2014a), which refers to the scattered reflected data shown in Figure 9 (underlined section emphasizes the oil-bearing region):

> "… there was trapped oil detected in the roof of 6B. Upon analyzing the data from the angle shots taken at depth 3280, there is the common signature associated with a echo bouncing off product. There appears to be oil from 261 degrees to 310 degrees. The oil was only seen on angle shots 20-44 degrees off [horizontal]. I cannot determine how much oil is present, only that there appears to be oil in this area of the roof."

The second correspondence occurred between Steven Sobolik and Sean McCool (McCool, 2014b) on December 7, 2014, in which Sobolik stated the following:

> "We are currently estimating somewhere between 387k and 522k barrels of oil above the bottom of the 6B borehole, based on your sonar measurements. We are trying to determine how much of that volume is oil. You noted a region to the west of 6B that was definitely oil because of the scatter in the reflected data. Is that the only location you KNOW there to be oil, or is that the ONLY location where oil exists? Also, on the long-angled shots, would we expect to see the roof through the oil-brine interface? It is difficult to interpret from the vertical sonar slices which volumes may be oil-bearing."

Sean McCool's response to the questions was:

> "The area to the west is the only area I believe to have oil based on the reflections I saw coming back to the sonar tool. I saw no other indications in the roof of oil, just to the west. We would not be able to penetrate the oil from the brine to get a determination of the shape of the roof in those areas."

Finally, the authors had a phone conversation with Sean McCool on December 17, 2014, in which the following points were clarified:

- Regarding the oil-bearing region described in the October 2014 email, Sean expressed high confidence that the scattered reflective signals he observed indicate the presence of oil. Furthermore, for those same angle shots for the remainder of the circumference, he expressed high confidence that the measured roof points are indicative of a reflection off of salt, meaning he doubts oil exists in that region.
- For the shots angled at about 12° with the horizontal and lower, he advised that there is no confidence one way or the other about the presence of oil in those regions because of the length and angle of the signal. Furthermore, he agreed that there are greater amounts of error in the measured roof elevation at the farthest set of measurements (the 4°-angle shot ring) defining the roof at the perimeter of the cavern.

Using the information from these correspondences, and other assumptions that can be made about the sonar data, the following steps have been used refine the earlier oil volume estimate. Figure 10 shows a horizontal slice of the WH-6 sonar at the depth of 3255 feet. Each ring of points represents a set of sonar shots taken at a particular angle, and the rays emanating from Well 6B show the azimuth lines along which those shots were taken. The region identified by McCool's October 2014 email was determined to identify the location of the OBI; this region is highlighted by the blue data points. The elevations from the data points in this region ranged from 3253.5 to 3257.5 feet, and the average value of 3255.0 feet was chosen as the depth of the OBI. From this, the volume of WH-6 identified by the sonar above this depth (the OBI at 3255 feet) was calculated to be 439 MB, smaller than the 523 MB above the bottom of Well 6B.

The area of the oil-bearing region identified by Sonarwire (blue points in Figure 10) was calculated to be 1765 square feet. For this region to produce the characteristic response of reflection off of an OBI, the oil is probably at least one foot thick; thus, a 1-ft thick volume of oil with 1765 square feet in area results in 314 *barrels* of oil. Because the sonar cannot transmit through oil, it is unknown how thick this patch of oil may be. The oil-bearing region is within a circular region, as shown in Figure 10, in which Sean McCool has high confidence in where oil exists (the blue region), and importantly, where it does not exist (the remainder of the circular zone), because of the non-scattered reflective data received there. This circular region has a radius of about 77 feet; therefore, the sonar indicates that within 77 feet of Well 6B, oil is only found in the region to the west of the well as described the October 2014 email (blue region in Figure 10).

For regions past the 77-foot radius circle, the uncertainty in the sonar data and interpretation increases as a function of radius. Regions A and B in Figure 10 are representative of this problem. There is both an uncertainty about the measured elevation of the roof at the largest radii in A & B, and also whether the reflected surface is the salt roof or the OBI. Because the sonars are not expected to be able to transmit a roof reflection through oil, the previous assumption that the outer regions of WH-6 where the roof is measured to be at or above the oil-bearing region near 6B are in fact the OBI is maintained. These regions represent a very large area of potential oil, but again, the thickness between the OBI and the roof cannot be measured. Region C in Figure 10 is interesting, in that it appears as a "hook" that occurs beneath the OBI around the west side of Well 6B. Sean McCool indicated a higher degree of confidence in these points because their radius from 6B is smaller. If this hooked ridge in the roof of WH-6 is in fact real, it may partially explain the existence of the oil-bearing region, and may also act as a shadow preventing detection and access to oil to the west of the ridge. A calculation of a volume of the oil in Regions A and B assuming an average thickness of oil of 1 foot resulted in a volume estimate of 100 MB. This assumption is based somewhat on the geomechanical prediction of roof geometry, but again there is significant uncertainty in this estimate. All of the volume values described above are summarized in Table 1.

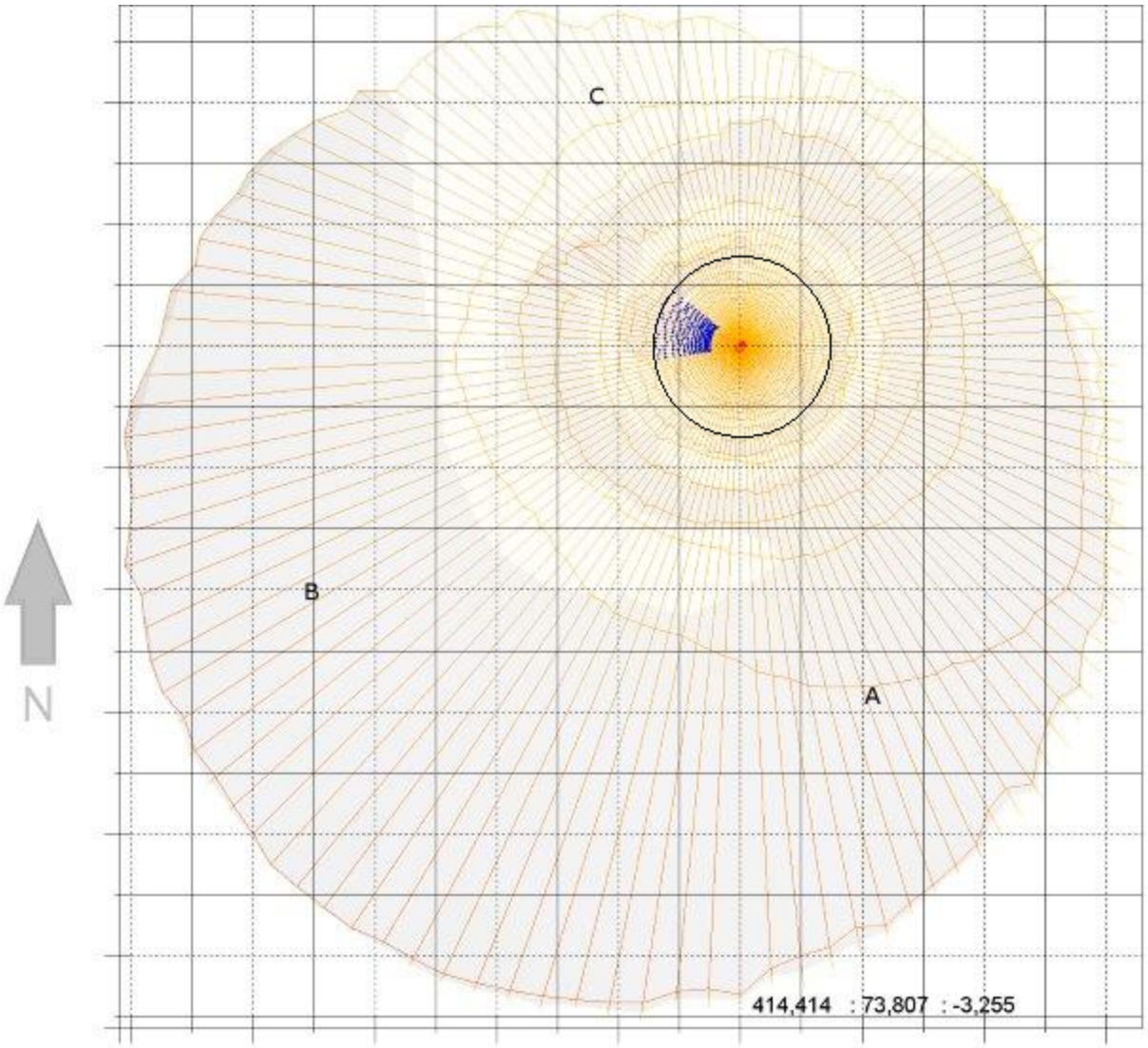

Figure 10. Sonarwire image of WH-6 at a depth of 3255 feet.

Table 1. Summary of computed remaining volumes of oil in WH-6 for several scenarios.

Scenario	Volume (barrels)
Cavern volume computed from October 2014 sonar above the bottom of Well 6B (3256 feet depth)	523,000
Cavern volume computed from October 2014 sonar above average depth of OBI (3255 feet) based on Sean McCool's interpretation of oil-bearing region near Well 6B	439,000
Volume of confirmed oil-bearing region near Well 6B (area of 1765 sq. ft.), assuming thickness of oil = 1 ft	314
Estimated oil volume of Regions A & B (Figure 10), assuming OBI at 3255 depth, assuming average thickness of oil = 1 ft	100,000

References

- McCool, Sean, 2014a. "Hackberry 6B", email from Sean McCool, Operations Manager, Sonarwire Global LLC, to John Kyle, Sabine Storage, October 22, 2014.
- McCool, Sean, 2014b. "Re: WH6 Questions", email from Sean McCool, Operations Manager, Sonarwire Global LLC, to Steven Sobolik, Sandia National Laboratories, December 7, 2014.
- Sobolik, S.R. and B.L. Ehgartner, 2009. *Analysis of Cavern Stability at the West Hackberry SPR Site.* SAND2009-2194, Sandia National Laboratories, Albuquerque, New Mexico.
- Sobolik, S.R., 2012. *Sandia Technical Recommendations for Continued Operation of West Hackberry Cavern 6.* Letter Report to Robert Myers, DOE-SPR, November 20, 2012, Sandia National Laboratories, Albuquerque, New Mexico.
- Sobolik, S.R., D.L. Lord, and B.L. Roberts, 2014a. *Recommendations Regarding the Sonars to be Performed on West Hackberry Cavern 6 for Evaluation of Final Oil Removal*, Letter to Lionel Gele, DOE-SPR, September 30, 2014.
- Sobolik, S.R., B.L. Roberts, and P. Weber, 2014b. *Sandia Analysis of West Hackberry Cavern 6 – Remaining Oil Volume and Leaching Options*, Letter to Paul Malphurs, DOE-SPR, December 15, 2014.

6.6 *SANDIA ANALYSIS OF THE SAFE OPERATION CAPABILITY OF WEST HACKBERRY CAVERNS 8 AND 9 FROM A GEOMECHANICAL PERSPECTIVE*

This letter is a summation of the current knowledge of the geomechanical stability of West Hackberry caverns 8 and 9. These caverns have been identified by the Louisiana Department of Natural Resources (LADNR) as being within 200 feet of each other, thus requiring additional documentation of their suitability for continued safe operation as oil storage caverns. This letter discusses the results of several geomechanical analyses of the West Hackberry caverns conducted beginning in 2009 as they pertain to safe operating criteria for an underground storage cavern in a salt dome. This letter does not cover any other issues that may pertain to safe cavern operations, such as internal casing pressures, surface operating procedures, and so on.

In order to show that a cavern is stable and capable of safe operations, there are some basic operational criteria that must be identified, and then shown to be met. Most of these potential criteria are concerned with the actual operations of a storage cavern, and thus are not discussed in this letter. However, some criteria are based upon the physical conditions of the cavern itself, and how the geomechanical forces on the cavern and its wellbore casings affect its safe operation. From a geomechanical perspective, these criteria may be used to determine if a cavern may be operated safely:

1. Under normal expected operating conditions, the salt surrounding the cavern is not expected to experience a fracture that would connect it (i.e., create a flow path) to another cavern or region where fluid may transport. From a geomechanical standpoint, this can be illustrated by the absence of tensile forces in the salt surrounding the cavern.
2. Under normal expected operating conditions, the salt above and surrounding the cavern is not expected to fail in such a way as to create a cavern collapse and/or sinkhole. From a geomechanical standpoint, this can be shown using predicted stresses above and around the cavern to show no tensile conditions, and no large-scale, long time-period conditions of high shear or deviatoric stress ("salt damage factor").
3. Under normal operating conditions, a wellbore casing in the caprock or overburden is not predicted to fail, thus releasing fluids to the environment. (This does not include casing failure in the salt; by the nature of salt formation creep, it is both expected that casing issues will occur in the salt at some point in the cavern lifetime, and assumed that fluid release into the salt still equals containment). This can also be evaluated with geomechanical analyses.

Several geomechanical analyses of the behavior of WH-8 and 9 have been performed, beginning with a large-scale three-dimensional analysis in 2009 (Sobolik and Ehgartner, 2009). The close proximity of WH-8 and 9 has previously been identified as an issue of concern, and as a result additional analyses have been performed to evaluate the effect of specific non-standard cavern operations of WH-8 and 9 on each other (Sobolik, 2013 and 2014). These analyses have shown that for standard operating procedures, the performance of WH-8 and 9 satisfy the criteria stated above; in addition, the caverns' performance also satisfies the criteria for the identified non-standard procedures. The analysis results that explain this performance are summarized below.

Figure 1 shows the predicted maximum stresses in the salt around WH-8 and WH-9 as a function of time. (In this plot, tensile stress in positive, compressive stress is negative.) The in situ

stresses around the entirety of the caverns remain compressive due to natural overburden, but are changed due to pressure changes in the oil stored in the caverns. Because of salt creep, there is a transient response in the stress of the salt as it adjusts to pressure changes in the cavern. The major peaks in the predicted stress histories occur during workovers for the specific caverns; the minor wiggles usually indicate workovers being performed on nearby caverns. Because of unusual geometries of some caverns, there may be isolated areas where the salt stress may become tensile for short periods of time. The historic maximum stress plots shown in Figure 1 are the maximum stress at any point in the salt in the salt immediately around the cavern as well as a circular column of salt surrounding the cavern going to the salt/caprock interface. For both WH-8 and WH-9, the stress is predicted to have remained compressive throughout the history of the caverns, and should continue to do so. Figure 2 is a plot showing the geometries of caverns WH-8 and WH-9. The location of the least compressive stress around WH-8 is at near the base of the cavern, where there is a sudden increase in diameter. For WH-9, the location of the least compressive stress is in the circumferential ledge that occurs at about mid-height in the cavern. Figure 1 indicates that the maximum compressive stress in this ledge in WH-9 steadily increases over time. It is expected that the ledge will eventually fracture, causing salt falls in the cavern. While this is an operational issue that requires future monitoring, it is not an issue that affects safe operation of the cavern, as it will not result in loss of oil from the cavern to the surrounding rock. Therefore, Figure 1 satisfies the first criterion and partially satisfies the second criterion for geomechanical stability, in that the prediction of no tensile stresses both around and above the caverns result in no expected tensile cracking and no saltback failure resulting in cavern collapse.

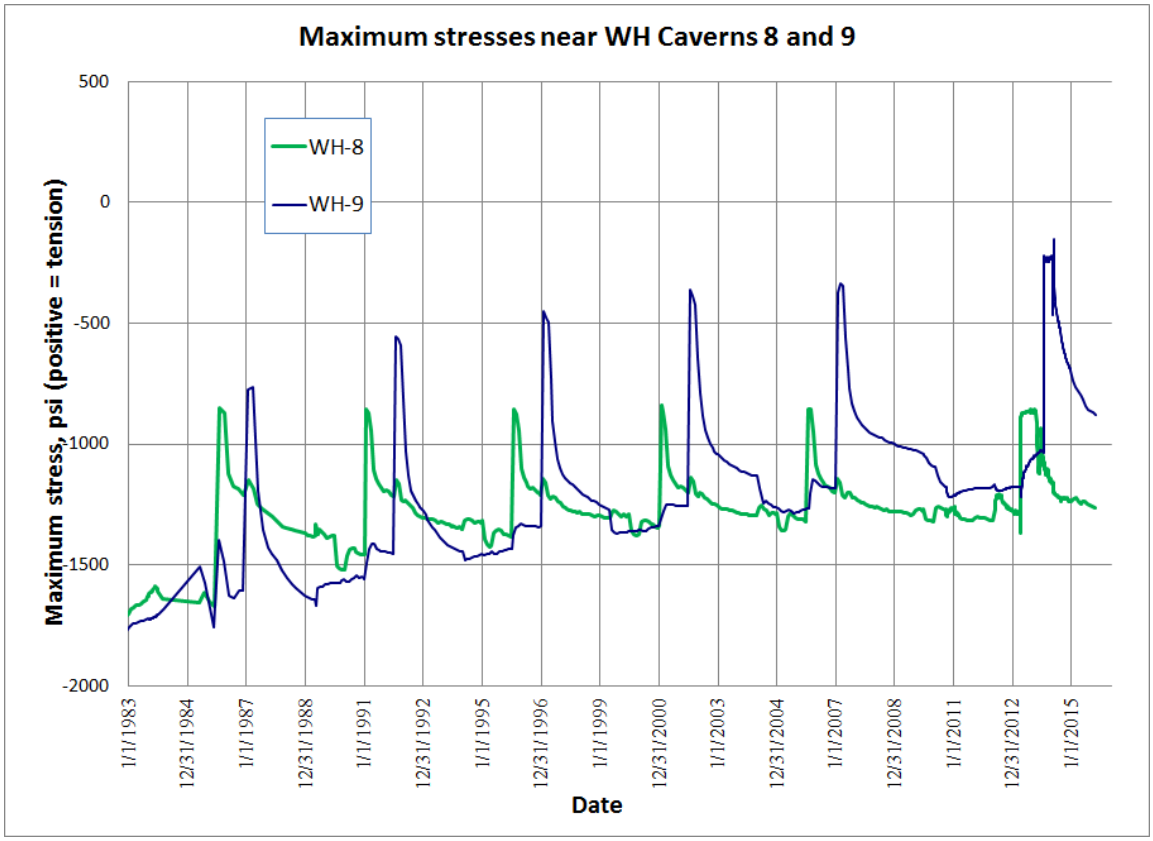

Figure 1. Predicted maximum stresses in WH-8 and WH-9.

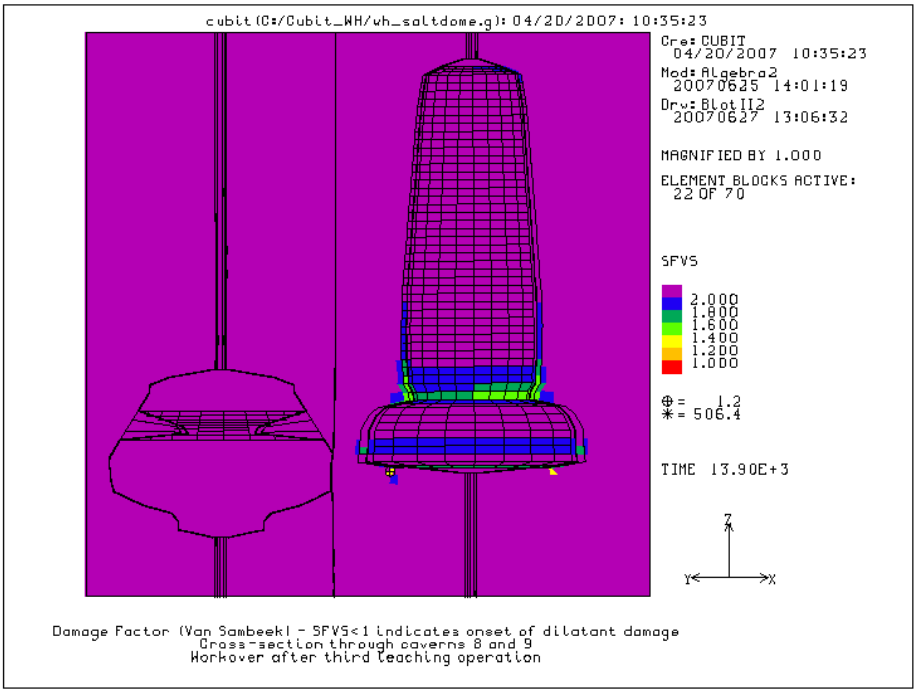

Figure 2. Dilatant safety factor around caverns WH-9 and WH-8 during a workover on WH-8.

Figure 3 is similar to Figure 1, but instead plots the minimum salt damage factor to the salt around and above the two caverns. The salt damage factor is a measure of the potential for deviatoric stresses to cause microcracking in the salt, thus increasing salt permeability and eventually leading to the formation of larger-scale fractures. The well-known dilatancy criterion of Van Sambeek et al. (1993) was used to calculate a salt damage factor, which is based on a ratio of shear stress to average normal stress in the salt. A value of the salt damage factor less than 1 indicates that salt damage is occurring; it is not indicative of any immediate failure of the salt, but can indicate long-term damage if values less than 1 occur over a long period of time. Figure 3 shows that the salt around and above WH-8 and WH-9 maintain damage factors above 1, with the minimum value occurring during workovers, and in the same locations as the maximum stress values. Figure 3 completes the satisfaction of the second geomechanical criterion, in that damage sufficient to cause large-scale salt dilatancy or saltback failure will not occur.

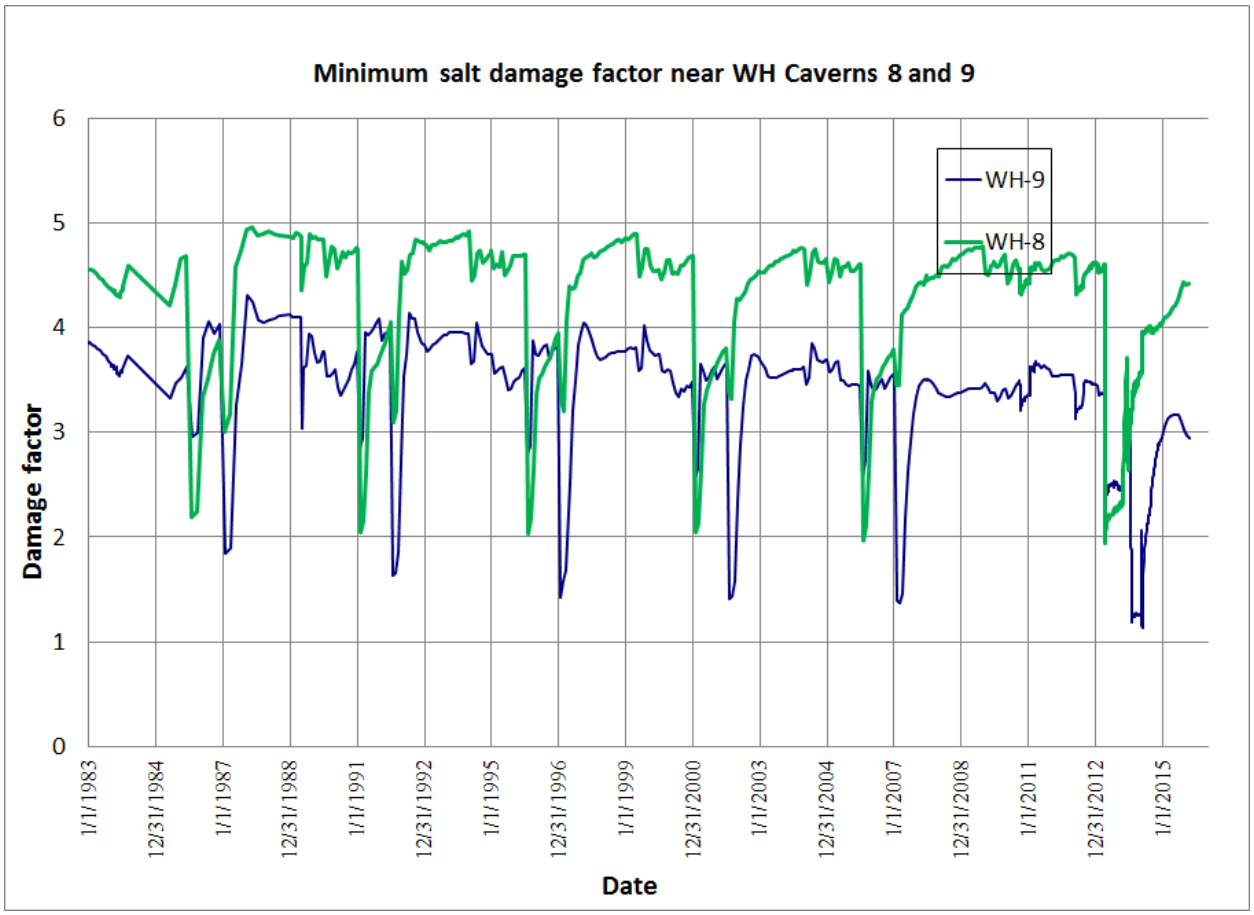

Figure 3. Predicted minimum salt damage factor in WH-8 and WH-9.

The third criterion involves the cavern's effect on the wellbore casings above the salt, primarily in the caprock. Geomechanical analyses of another SPR site, Bryan Mound in Texas, indicate that a caprock that has been significantly altered due to large-scale sulfur mining can create nonhomogeneous stress conditions which can damage some casings (Sobolik and Ehgartner, 2012). Evidence of this has been found at that site. The known history of the West Hackberry site indicates that there is little evidence of wide-scale caprock mining at the site, and geological mapping of the caprock reveals little in the way of significant features that would suggest irregular distribution of stresses. Therefore, the caprock at West Hackberry has been modeled as a homogeneous medium, and the resulting calculations predict that the stresses applied from the caprock to the wellbore casings are very small compared to criteria for steel such as collapse pressure of the steel casings and plastic deformation of steel. There have been no historic casing issues in the caprock at West Hackberry, so the history of the site seems to support the results of the analyses. Therefore, the third geomechanical criterion is satisfied.

The geomechanical analyses of the West Hackberry site, which have taken into account the close proximity of caverns WH-8 and WH-9, show that the caverns present no geomechanical safety concerns when operated under normal operating conditions, and even under some specific nonstandard conditions. Additional geomechanical analyses have been and will continue to be

used to evaluate other nonstandard procedures involving WH-8 and WH-9 to advise DOE on safe operations of the caverns.

References

- Sobolik, S.R. and B.L. Ehgartner, 2009. *Analysis of Cavern Stability at the West Hackberry SPR Site.* SAND2009-2194, Sandia National Laboratories, Albuquerque, New Mexico.
- Sobolik, S.R., & B.L. Ehgartner, 2012. *Structural Integrity of Oil Storage Caverns at a Strategic Petroleum Reserve Site with Highly Heterogeneous Salt and Caprock*, ARMA 12-189, 46th US Rock Mechanics Symposium, held in Chicago, IL, USA, June 24–27, 2012.
- Sobolik, S.R., 2013. *Preliminary Recommendations Regarding the Maximum Length of Workover of West Hackberry Cavern 8 on Cavern 9 during Cavern 6 Oil Removal Process.* Letter Report to Robert Myers, DOE-SPR, July 25, 2013, Sandia National Laboratories, Albuquerque, New Mexico.
- Sobolik, S.R., 2014. *Recommendations Regarding the Maximum Length of Workovers of West Hackberry Caverns 6, 8, and 9 during Cavern 6 Oil Removal Process.* Letter Report to Robert Myers, DOE-SPR, January 15, 2014, Sandia National Laboratories, Albuquerque, New Mexico.
- Van Sambeek, L.L., J.L. Ratigan, and F.D. Hansen, 1993. Dilatancy of Rock Salt in Laboratory Tests, Int. J. Rock Mech. Min. Sci. & Geomech. Abstr. Vol. 30, No. 7, pp 735-738.

7. CONCLUSIONS

These analyses evaluated the geomechanical behavior of the caverns at the West Hackberry SPR site for the current condition of the caverns and their wellbores, the effect of the caverns on surface facilities, and for potential enlargement in the form of drawdowns. The analyses examined the overall performance of the West Hackberry site by evaluating surface subsidence, horizontal surface strains, and axial well strains. Finally, the analyses evaluated the possibility of nonlinear dilatancy behavior of the West Hackberry salt, and its possible ramifications on cavern performance. The following conclusions were obtained from the results of the analyses:

- The transition from JAS3D to Adagio has been completed. The property set used for the M-D model for West Hackberry was reexamined in comparisons between measured and predicted surface subsidence and cavern closure, with the result that higher values of the secondary creep coefficient were required to better match predictions to results.
- The new predictions of surface subsidence compared very well to the historical measured data.
- The new predictions of cavern volume closure compared reasonably well to the cavern volume values derived from cavern pressure data using the CAVEMAN software. The predicted rates of cavern closure during steady state closure (i.e., between workovers) tend to be less than the rates supplied through CAVEMAN, but the predicted change of volume during workovers usually made up the difference. The procedure used by CAVEMAN to calculate cavern volume as a function of wellhead pressure will be examined and compared to the calculation of cavern volume from Adagio will determine if the two processes are consistent; any inconsistencies or potential changes in material creep properties will then be addressed.
- The safety parameters used to evaluate cavern and wellbore integrity (salt dilatant/tension stresses, wellbore axial strain) indicate that caverns WH-6, 8, and 9 have ongoing integrity concerns that have been addressed (e.g., the removal of oil from WH-6), or can be addressed with limits on caverns operations and drawdowns. Some other caverns, including WH-110 and 113, are predicted to experience very localized dilatant stress points at the bottom of the caverns; these points may be merely due to a stress concentration resulting from the mesh construction, or may be indicative of a true condition that due to its location may be of minimal consequence.
- Based on a preliminary assessment of the mechanical behavior of the caverns through five drawdown cycles, there is not expected to be any significant downgrade to the number of available drawdowns for the WH caverns compared to the numbers reported in 2014 (Sobolik et al., 2014), and in fact many of the Phase 2 caverns will probably see an increase in their number of available drawdowns.
- In addition to the new analyses conducted for this report, previous letter reports of analyses concerning WH caverns 6, 8, and 9 have been included in this report for completeness.
- A follow-up report to this work is planned for 2016. The follow-up report will include further examination of the results of these calculations as they pertain to three items: 1) a new assessment of the number of available drawdowns for all the WH caverns; 2) an evaluation of the methods used to calculate cavern volume closure in both CAVEMAN and Adagio to make sure the methods are reasonably consistent and can be used for effective comparison; and 3) a further evaluation of the plastic strain experienced by the casing materials similar to that performed by Park (2013, 2014) for the Big Hill site, to provide a more complete

understanding of the effect of creep on the WH boreholes. The results in the follow-up report will also be used as input to the West Hackberry well integrity grading matrix used to prioritze wellbore remediation (Roberts et al., 2015).

8. REFERENCES

- Arguello, J.G. & Rath, J.S. 2012. SIERRA Mechanics for Coupled MultiPhysics Modeling of Salt Repositories. CRC Press/Balkema. *SaltMech7 - 7th International Conference on the Mechanical Behavior of Salt*, Paris, France, April 2012.
- Ballard, S. and B. L. Ehgartner, 2000. *CaveMan Version 3.0: A Software System for SPR Cavern Pressure Analysis*, SAND2000-1751, Sandia National Laboratories, Albuquerque, New Mexico.
- Blanford, M.L., M.W. Heinstein, and S.W. Key, 2001. *JAS3D. A Multi-Strategy Iterative Code for Solid Mechanics Analysis*. ***User's Instructions****, Release 2.0*. SEACAS Library, JAS3D Manuals, Computational Solid Mechanics / Structural Dynamics, Sandia National Laboratories, Albuquerque, New Mexico.
- Checkai, D., G. Osborne, L. Eldredge, and D. Lord, 2014. Pressure Trending Analysis to Support Cavern Integrity Monitoring at the U.S. Strategic Petroleum Reserve. Solution Mining Research Institute Spring Technical Conference, San Antonio, Texas, May 5-6, 2014.
- Edwards, H. C., & Stewart, J. R. 2001. *SIERRA: A Software Environment for Developing Complex MultiPhysics Applications*. Amsterdam : Elsevier, 2001. In K. J. Bathe (ed.), First MIT Conference on Computational Fluid and Solid Mechanics.
- Ehgartner, B.L. and S.R. Sobolik, 2002. *3-D Cavern Enlargement Analyses*, SAND2002-0526, Sandia National Laboratories, Albuquerque, New Mexico.
- Fossum, A.F., G.D. Callahan, L.L. Van Sambeek, and P.E. Senseny, 1988. How Should One-Dimensional Laboratory Equations be Cast in Three-Dimensional Form?, Key Questions in Rock Mechanics: Proceedings of the 29th U.S. Symposium. Brookfield, MA: McGraw-Hill Book Company.
- Gerstle, W., T. McCarty-Glenn, S.F. Dwyer, and J.H. Gerstle, 2014. Leakage from drill pipe casing subject to shear deformation, *Int. J. Petroleum Engineering*, Vol. 1, No. 1, pp 49-61.
- Lama, R.D. and V.S. Vutukuri, 1978, *Handbook on Mechanical Properties of Rocks – Testing Techniques and Results* -, Series on Rock and Soil Mechanics, Vol. 3, No.2, Trans Tech Publications.
- Lord, D.L., S.R. Sobolik, B.Y. Park and D.K. Rudeen (2013), "Impacts of First Water Drawdown on SPR Low P/D Caverns", Letter Report to Gilbert Shank DOE PMO dated December 20, 2013. Geotechnology & Engineering, Sandia National Laboratories. U.S. Strategic Petroleum Reserve.
- Magorian, T.R., J.T. Neal, S. Perkins, Q.J. Xiao, and K.O. Byrne. 1991. *Strategic Petroleum Reserve Additional Geologic Characterization Studies West Hackberry Salt Dome, Louisiana*, SAND90-0224, Sandia National Laboratories, Albuquerque, New Mexico.
- Moriarty, D., 2014. August 2014 West Hackberry Subsidence Analysis, Letter Report to Diane Willard, Strategic Petroleum Reserve, December 8, 2014.
- Munson, D.E., 1979. Preliminary Deformation-Mechanism Map for Salt (with Application to WIPP), SAND70-0079, Sandia National Laboratories, Albuquerque, NM.

- Munson, D.E. and P.R. Dawson, 1979. *Constitutive Model for the Low Temperature Creep of Salt (With Application to WIPP)*. SAND79-1853, Sandia National Laboratories, Albuquerque, New Mexico.
- Munson, D.E. and P.R. Dawson. 1982. *A Transient Creep Model for Salt during Stress Loading and Unloading.* SAND82-0962, Sandia National Laboratories, Albuquerque, New Mexico.
- Munson, D.E. and P.R. Dawson, 1984. Salt Constitutive Modeling using Mechanism Maps. *1st International Conference on the Mechanical Behavior of Salt, Trans Tech Publications*, 717-737, Clausthal, Germany.
- Munson, D.E., A.F. Fossum, and P.E. Senseny. 1989. *Advances in Resolution of Discrepancies between Predicted and Measured in Situ WIPP Room Closures*. SAND88-2948, Sandia National Laboratories, Albuquerque, New Mexico.
- Munson, D.E., 1998. *Analysis of Multistage and Other Creep Data for Domal Salts*, SAND98-2276, Sandia National Laboratories, Albuquerque, New Mexico.
- Munson, D.E., 2006. *Features of West Hackberry Salt Caverns and Internal Structure of the Salt Dome*, SAND2006-5409, Sandia National Laboratories, Albuquerque, New Mexico.
- Notz, P.K., et al. 2007**.** *Aria 1.5: User Manual.* SAND2007-2734, Sandia National Laboratories, Albuquerque, New Mexico.
- Park, B.Y., 2013. Interface Modeling to Predict Wellbore Damage for Big Hill Strategic Petroleum Reserve. In *Proceedings of the 47th US Rock Mechanics Symposium, San Francisco, CA, June 23–26, 2010,* ARMA No. 13-223.
- Park, B.Y., 2014. *Geomechanical Analysis to Predict the Oil Leak at the Wellbores in Big Hill Strategic Petroleum Reserve*, SAND2014-0669, Sandia National Laboratories, Albuquerque, New Mexico.
- Peng, S.S., 1985. Coal Mine Ground Control. 2nd Ed., John Wiley and Sons, New York, New York.
- Preece, D.S. and J.T. Foley, 1984. *Long-Term Performance Predictions for Strategic Petroleum Reserve (SPR) Caverns*, SAND83-2343, Sandia National Laboratories, Albuquerque, New Mexico.
- Rautman, C.A., J.S. Stein, and A.C. Snider, 2004. *Conversion of the West Hackberry Geological Site Characterization Report to a Three-Dimensional Model*, SAND2004-3981, Sandia National Laboratories, Albuquerque, New Mexico
- Rautman, C.A. and A.C. Snider, 2007. *Sonar Atlas of Caverns Comprising the U.S. Strategic Petroleum Reserve Volume 4: West Hackberry Site, Louisiana*, SAND2007-6051, Sandia National Laboratories, Albuquerque, New Mexico
- Roberts, B.L., D.L. Lord, A.S. Lord, G. Bettin, S.R. Sobolik, D.K. Rudeen, L.L. Eldredge, K. Wynn, D. Checkai, G. Osborne and D. Moore, 2015. *2015 Strategic Petroleum Reserve West Hackberry Well Integrity Grading Report*, SAND2015-3072, Sandia National Laboratories, Albuquerque, New Mexico
- Rudeen, D.K. and D.L. Lord (2013). "SPR Cavern Pillar-to-Diameter 2013 Update," Letter Report to Gilbert Shank, DOE PMO dated October 1, 2013. Geotechnology & Engineering, Sandia National Laboratories. U.S. Strategic Petroleum Reserve.
- SIERRA Solid Mechanics Team, 2010. Adagio 4.18 User's Guide. SAND2010-6313, Sandia National Laboratories, Albuquerque, New Mexico.

- SIERRA Solid Mechanics Team, 2011. Sierra/Solid Mechanics 4.22 User's Guide. SAND2011-7597, Sandia National Laboratories, Albuquerque, New Mexico.
- Sobolik, S.R. and B.L. Ehgartner, 2009a. *Analysis of Cavern Stability at the West Hackberry SPR Site*, SAND2009-2194, Sandia National Laboratories, Albuquerque, New Mexico.
- Sobolik, S.R. and B.L. Ehgartner, 2009b. *Analysis of Cavern Stability at the Bryan Mound SPR Site.* SAND2009-1986, Sandia National Laboratories, Albuquerque, New Mexico.
- Sobolik, S.R., J.E. Bean, and B.L. Ehgartner, 2010. Application of the Multi-Mechanism Deformation Model for Three-Dimensional Simulations of Salt Behavior for the Strategic Petroleum Reserve. In *Proceedings of the 44th US Rock Mechanics Symposium and 5th U.S.-Canada Rock Mechanics Symposium, Salt Lake City, UT June 27–30, 2010,* ARMA No. 10-403.
- Sobolik, S.R. & B.L. Ehgartner, 2012. Analyzing Large Pressure Changes on the Stability of Large-Diameter Caverns Using the M-D Model. In *Mechanical Behavior of Salt VII: Proceedings of the 7th Conference on the Mechanical Behavior of Salt, Paris, France, 16-19 April 2012,* eds. Berest, Ghoreychi, Hadj-hassen & Tijani, 321-330. London: CRC Press, Taylor & Francis Group.
- Sobolik, S.R. 2013a. Analyzing the Effect of Large Pressure Changes on the Operational Stability of Large-Diameter Caverns for the Strategic Petroleum Reserve. In *Proceedings of the 47th US Rock Mechanics Symposium, San Francisco, CA, June 23–26, 2010,* ARMA No. 13-226.
- Sobolik, S.R. 2013b. Verification of the Transition from JAS3D to ADAGIO for the Bryan Mound Geomechanical Model, Letter Report to Robert Myers, Strategic Petroleum Reserve, March 21, 2013.
- Sobolik, S.R., B.Y. Park, D.L. Lord, B.L. Roberts, and D.L. Rudeen, 2014. Current Recommendations Regarding ECP PM-00449, Baseline Remaining Drawdowns for all SPR Caverns, Letter Report to Lisa Nicholson, Strategic Petroleum Reserve, May 8, 2014.
- Sobolik, S.R. & A.S. Lord, 2015. Operation, Maintenance, and Monitoring of Large-Diameter Caverns in Oil Storage Facilities in Domal Salt. In *Mechanical Behavior of Salt VIII: Proceedings of the 8th Conference on the Mechanical Behavior of Salt, Rapid City, South Dakota, USA, 25-27 May 2015,* eds. Roberts, Mellegard, & Hansen. London: CRC Press, Taylor & Francis Group.
- Thorton, C.H and I.P. Lew, 1983. *Concrete and Design Construction. Standard Handbook for Civil Engineers*, Chapter 8, 3rd ed., F.S. Merritt, editor, McGraw-Hill, New York, NY.
- Van Sambeek, L.L., J.L. Ratigan, and F.D. Hansen, 1993. *Dilatancy of Rock Salt in Laboratory Tests*, Int. J. Rock Mech. Min. Sci. & Geomech. Abstr. Vol. 30, No. 7, pp 735-738.
- Weber, P.D., D.K. Rudeen, & D.L. Lord, 2014. *SANSMIC Validation*, SAND2014-16980, Sandia National Laboratories Albuquerque, New Mexico.
- Whiting, G. H., 1980. *Strategic Petroleum Reserve (SPR): Geological Site Characterization Report, West Hackberry Salt Dome*, SAND80-7131, Sandia National Laboratories Albuquerque, New Mexico.

- **DISTRIBUTION:**

External Distribution

Electronic copies to:

Wayne Elias (wayne.elias@hq.doe.gov)
for distribution to DOE SPR Program Office, Washington, D.C.
U.S. Department of Energy
Office of Fossil Energy
Forrestal Building
1000 Independence Ave., SW
Washington, DC 20585

Diane Willard (diane.willard@spr.doe.gov)
for distribution to DOE and FFPO SPR Project Management Office, New Orleans, LA.
U.S. Department of Energy
Strategic Petroleum Reserve Project Management Office
900 Commerce Road East
New Orleans, LA 70123

Sandia Distribution

Print copies to:

5	MS0750	Carolyn Kirby
1	MS0751	B. Y. Park
1	MS0751	Steven R. Sobolik

Electronic Copies:

Borns, David	djborns@sandia.gov
Halloran, Amy Randolph	arhallo@sandia.gov
Kirby, Carolyn	clkirby@sandia.gov
Lee, Moo	mylee@sandia.gov
Sobolik, Steven R.	srsobol@sandia.gov
Webb, Erik K	ekwebb@sandia.gov
Technical Library	


Sandia National Laboratories